NUREG/CR-6551
MCS 970501

Improved Embrittlement Correlations for Reactor Pressure Vessel Steels

Prepared by
E.D. Eason, J.E. Wright, MCS
G.R. Odette, Univ. CA

Modeling and Computing Services

University of California

Prepared for
U.S. Nuclear Regulatory Commission

AVAILABILITY NOTICE

Availability of Reference Materials Cited in NRC Publications

NRC publications in the NUREG series, NRC regulations, and *Title 10, Energy,* of the *Code of Federal Regulations,* may be purchased from one of the following sources:

1. The Superintendent of Documents
   U.S. Government Printing Office
   P.O. Box 37082
   Washington, DC 20402–9328
   <http://www.access.gpo.gov/su_docs>
   202–512–1800

2. The National Technical Information Service
   Springfield, VA 22161–0002
   <http://www.ntis.gov/ordernow>
   703–487–4650

The NUREG series comprises (1) technical and administrative reports, including those prepared for international agreements, (2) brochures, (3) proceedings of conferences and workshops, (4) adjudications and other issuances of the Commission and Atomic Safety and Licensing Boards, and (5) books.

A single copy of each NRC draft report is available free, to the extent of supply, upon written request as follows:

Address: Office of the Chief Information Officer
Reproduction and Distribution
Services Section
U.S. Nuclear Regulatory Commission
Washington, DC 20555–0001
E–mail: <GRW1@NRC.GOV>
Facsimile: 301–415–2289

A portion of NRC regulatory and technical information is available at NRC's World Wide Web site:

<http://www.nrc.gov>

All NRC documents released to the public are available for inspection or copying for a fee, in paper, microfiche, or, in some cases, diskette, from the Public Document Room (PDR):

NRC Public Document Room
2121 L Street, N.W., Lower Level
Washington, DC 20555–0001
<http://www.nrc.gov/NRC/PDR/pdr1.htm>
1–800–397–4209 or locally 202–634–3273

Microfiche of most NRC documents made publicly available since January 1981 may be found in the Local Public Document Rooms (LPDRs) located in the vicinity of nuclear power plants. The locations of the LPDRs may be obtained from the PDR (see previous paragraph) or through:

<http://www.nrc.gov/NRC/NUREGS/SR1350/V9/lpdr/html>

Publicly released documents include, to name a few, NUREG-series reports; *Federal Register* notices; applicant, licensee, and vendor documents and correspondence; NRC correspondence and internal memoranda; bulletins and information notices; inspection and investigation reports; licensee event reports; and Commission papers and their attachments.

Documents available from public and special technical libraries include all open literature items, such as books, journal articles, and transactions, *Federal Register* notices, Federal and State legislation, and congressional reports. Such documents as theses, dissertations, foreign reports and translations, and non-NRC conference proceedings may be purchased from their sponsoring organization.

Copies of industry codes and standards used in a substantive manner in the NRC regulatory process are maintained at the NRC Library, Two White Flint North, 11545 Rockville Pike, Rockville, MD 20852–2738. These standards are available in the library for reference use by the public. Codes and standards are usually copyrighted and may be purchased from the originating organization or, if they are American National Standards, from—

American National Standards Institute
11 West 42nd Street
New York, NY 10036–8002
<http://www.ansi.org>
212–642–4900

NUREG/CR-6551
MCS 970501

Improved Embrittlement Correlations for Reactor Pressure Vessel Steels

Manuscript Completed: September 1998
Date Published: November 1998

Prepared by
E.D. Eason, J.E. Wright, Modeling and Computing Services
G.R. Odette, University of California

Modeling and Computing Services
6560 Gunpark Drive, Suite B
Boulder, CO 80301

University of California
Santa Barbara, CA 93106

A.L. Lund, NRC Project Manager

Prepared for
Division of Engineering Technology
Office of Nuclear Regulatory Research
U.S. Nuclear Regulatory Commission
Washington, DC 20555-0001
NRC Job Code W6878

ABSTRACT

The reactor pressure vessels of commercial nuclear power plants are subject to embrittlement due to exposure to high energy neutrons from the core. Irradiation embrittlement of RPV beltline materials is currently evaluated using Regulatory Guide 1.99 Revision 2 (RG1.99/2), which presents methods for estimating the shift in Charpy transition temperature at 30 ft-lbs (TTS) and the drop in Charpy upper shelf energy (ΔUSE). The purpose of the reported work was to improve on the correlation models in RG1.99/2 using the broader data base now available and current understanding of embrittlement mechanisms.

The embrittlement data base used for this analysis was derived primarily from the Power Reactor Embrittlement Data Base (PR-EDB) developed at Oak Ridge National Laboratory. Shifts in transition temperature and drops in upper shelf energy were calculated on a consistent basis from individual fits to unirradiated and irradiated raw Charpy data. The independent variables considered in the analysis include material chemistries, irradiation time and temperature, fluence, flux, product form (i.e., weld, plate or forging), material, type of reactor, vessel manufacturer and designer, specimen orientation, plus weld flux and weld wire for welds. Chemistries, Charpy data, and irradiation parameters were reviewed by a subcommittee of ASTM E10.02, which recommended additions and revisions of the data base to ensure that the calibration data reflected the best available information. The main revisions were changes in chemical composition to update data or correct reporting errors and substitution of coolant temperatures for melt-wire irradiation temperatures from the PR-EDB. In addition, the fluences reported in the PR-EDB were revised by the vendors during the project, at NRC request, to reflect more current fluence calculation methodology.

The final TTS and USE models include fluence, copper, nickel, phosphorous content, and product form; the TTS model also includes coolant temperature and irradiation time. The models were developed using multivariable surface-fitting techniques, based on pattern recognition, understanding of the TTS mechanisms, and engineering judgement. The models were evaluated by overall measures such as standard error and standard deviation of subset residuals, review of overall and subset residual plots, and comparison with other data not used for fitting. The key variable trends, such as the copper-nickel dependence in the new TTS model, are much improved over RG1.99/2 and are well supported by independent data and current understanding of embrittlement mechanisms. The improved TTS model reduces scatter significantly relative to RG1.99/2 on the currently-available data base for plates, forgings, and welds.

TABLE OF CONTENTS

LIST OF FIGURES

Figure **Page**

LIST OF TABLES

Table **Page**

ACKNOWLEDGMENTS

The authors appreciate the advice and encouragement received from M. Vassilaros, A. Taboada, and A. L. Hiser, current and former project managers at the U. S. Nuclear Regulatory Commission. Advice and support from other U. S. NRC staff is also appreciated, including E. Hackett and M. Mayfield. The staff at Oak Ridge National Laboratory have provided data and advice which is appreciated, especially F. Kam, J. A. Wang, and R. Stoller. Helpful discussions and productive collaboration with G. Lucas at U.C. Santa Barbara are also gratefully acknowledged. Finally, the extensive efforts of W. Pavinich and other members of ASTM E10.02.02 in reviewing the analysis data base and providing revisions and additional data contributed to the success of this effort. This work was performed under U. S. NRC contract 04-92-048.

1 INTRODUCTION

1.1 Background

The beltline region of a reactor pressure vessel (RPV) surrounding the core in a commercial nuclear power plant is subject to embrittlement from exposure to neutrons. Current methods of estimating embrittlement of RPV beltline materials in the U. S. are described in Regulatory Guide 1.99 Revision 2 (RG1.99/2). In RG1.99/2, embrittlement is characterized by the 30 ft-lb transition temperature shift (TTS) and by the drop in the upper shelf energy (ΔUSE) due to irradiation, using data from Charpy impact energy-temperature tests. The TTS model in RG1.99/2 was based on analysis of Charpy data available in 1984. Since then, a large body of additional Charpy surveillance data have become available, and the understanding of embrittlement mechanisms has advanced.

1.2 Objectives and Scope of Work

The primary objective of this work was to develop improved irradiation embrittlement correlations using advanced data analysis techniques, results from mechanistic research, and the large body of U. S. embrittlement data that has become available in recent years in the Power Reactor Embrittlement Data Base (PR-EDB: NUREG/CR-4816) compiled at Oak Ridge National Laboratory. Correlations for estimating embrittlement recovery due to annealing were also developed under this contract; these have been previously reported (NUREG/CR-6327, Eason et al., 1995).

The terms "correlation" and "model" are sometimes used to distinguish statistical curve fits from mechanistic models. In this report, the terms are used interchangeably.

The first task was the development of a working data base. Raw Charpy data were extracted from the PR-EDB and fitted on a consistent basis. The fitted curves for unirradiated and irradiated specimens of the same heat tested in the same orientation were matched, and Charpy transition temperature shifts and upper shelf energy drops were computed. Other associated independent variables such as material composition and type, irradiation variables, product form, etc. were also extracted from the PR-EDB. Some data extracted from the PR-EDB required assessment and further processing, as described in Section 2. A preliminary version of the analysis data base was reviewed by the ASTM E10.02.02 Task Group on Embrittlement Correlations, resulting in some revisions and additions to the data base, detailed in Section 2.

The second task was the data analysis. Pattern recognition and transformation analyses were used in conjunction with mechanistically-motivated analyses of embrittlement data to define the variables and candidate functional forms. The variables considered in the analysis included irradiation time and melt-wire temperature, coolant temperature, fluence, flux, chemical composition, product form (i.e., weld, plate, or forging), weld flux and weld wire, and combinations of these variables. Hundreds of candidate model forms were evaluated to varying degrees, leading to the results presented in later sections.

The final task was calibration and evaluation of correlation models. Pattern recognition, least squares fitting of candidate models, and residual analysis were the primary tools for developing the USE model. For the TTS model, results of pattern recognition provided some guidance in early stages of the analysis. However, the current understanding of embrittlement, based on controlled experiments, microstructural studies, and theoretical considerations, was used to identify and select appropriate functional forms and variable sets and to build candidate models. Nonlinear least squares techniques, minimizing the sum of squared residuals about the model, were the primary tools used to screen a large number of physically-motivated candidate models. Extensive residual analysis was performed on the candidate models, both for the overall data set and data subsets, such as welds, forgings, and plates. Engineering judgement and comparison with other data from mechanistic experiments also played a key role, particularly when choosing between model forms that were statistically comparable for the surveillance data.

1.3 Previous Embrittlement Models

Substantial effort to model embrittlement trends preceded the present work, both in the USA and abroad. In the USA, irradiation embrittlement is typically characterized by the TTS at 30 ft-lbs and by ΔUSE, measured according to relevant ASTM standards, while some other countries use somewhat different indexing levels and Charpy test procedures. The TTS model in Regulatory Guide 1.99 Revision 1 was

$$TTS = [40 + 5000(P - 0.008) + 1000(Cu - 0.08)](\phi t)^{0.5} \quad \textbf{(1-1)}$$

with TTS in °F, fluence (ϕt) in units of 10^{19} n/cm^2 (E > 1 MeV), and chemical contents *P* and *Cu* in wt%. Both the P and Cu effects were subject to threshold values (0.008 for P and 0.08 for Cu). There was no nickel term or Cu-Ni interaction term in this model - an increasingly apparent weakness by the early 1980's.

The TTS formulation in RG1.99/2 was based on results reported by two separate investigators working independently (Odette et al., 1984; Guthrie, NUREG/CR-3391 Volume 2). TTS is calculated as the product of a chemistry factor and a fluence function:

$$TTS = CF(\phi t)^{(0.28 - 0.1 \log \phi t)} \quad \textbf{(1-2)}$$

The chemistry factor (*CF*) depends on Cu and Ni and is represented by separate tables for welds and base metals. The reason for the tabular form is that the chemistry factor was taken as the higher of the Guthrie and Odette estimates at each combination of Cu and Ni, as described elsewhere (Randall, 1984, 1987). Note that the phosphorous term in Revision 1 was not included in the Revision 2 model.

The drop in Charpy upper shelf energy is estimated in RG1.99/2 as a percentage of the original, unirradiated upper shelf energy. The percentage depends on Cu, fluence, and whether the material is a weld or base metal.

There are many other correlations in the literature for estimating the transition temperature shift. Some early physically-motivated model forms are discussed by Odette et al. (1984). The principal correlations developed in the USA, France, Germany, Japan, and Russia are described and compared by Petrequin (1996). All of these correlations contain Cu and fluence; most also consider product form, P, and Ni (especially the interaction of Cu and Ni), and in some cases Si. These formulas can be described in the form

$$TTS = CF \times FF \; . \quad \textbf{(1-3)}$$

where *CF* is a chemistry factor and *FF* is a fluence factor. The majority of model forms do not fully reflect the basic mechanisms of embrittlement.

1.4 Current Mechanistic Understanding

In the manganese-molybdenum steels used in U. S. RPVs, the transition temperature shifts upward and the upper shelf energy drops as the yield strength increases. The increase in yield strength, or hardening, is related to ultra-fine-scale microstructural features introduced by irradiation. Much of the research work on embrittlement mechanisms has focussed on the yield strength increase, which provides a useful surrogate for TTS (see Odette and Lucas, 1996 and 1998 for recent reviews).

For surveillance conditions, three features contribute to hardening and TTS:

- stable matrix defects (SMD)
- phosphide precipitates (PP)
- copper-rich precipitates (CRP)

These general categories may contain multiple features with a range of characteristics. It is common to lump SMD and PP together with other features that are independent of CRP contributions (Williams and Phythian, 1996). The relative numbers and volume fractions of these features and their detailed character (e.g., CRP composition) depend on the *combination* of metallurgical and irradiation variables, including first order effects of copper content (Cu), nickel content (Ni), fluence (ϕt), irradiation temperature (T_i), and flux (ϕ). Second order variables may include, for example, phosphorous and manganese contents (P and Mn), heat treatment, product form, and neutron spectrum. Interactions among the variables are common and important in mediating embrittlement.

The effects of these variables have been studied in some detail in controlled, single-variable experiments (e.g., Odette and Lucas, 1989, 1996). It has been possible to study separately the SMD and CRP mechanisms of embrittlement by using low-copper (Cu < 0.1 wt%) and high-copper heats as well as post-irradiation annealing (Mader et al., 1993). Hence, much is known about the mechanisms that can be used to develop physically-motivated models.

A major contribution from the mechanistic research to the present effort is the recognition that a single model of the form given in Equation 1-3 is inadequate for characterizing the two dominant forms of damage - matrix defects and copper-rich precipitates. The SMD damage increases with increasing fluence and P and with decreasing irradiation temperature and is weakly dependent on Cu and Ni. The relatively athermal CRP damage saturates at high values of fluence and strongly depends on Cu and Ni. The TTS model described in Section 4 reflects these mechanisms in two major terms, each of which can be represented as a product of chemistry and fluence factors as in Equation 1-3. In this regard, the work presented here is more physically-

motivated than previous modeling efforts.

It is important to point out that statistical modeling of embrittlement data trends based on the concept of independent CRP and SMD contributions has been successfully used for some time by a number of workers, beginning in the mid-1980s (Odette and Lucas, 1986a, 1986b; Fisher et al., 1985, 1987; Williams et al., 1988; Bolton et al., 1996; McElroy and Lowe, 1986; Williams and Phythian, 1996). Indeed, such models are a key element in the UK Nuclear Electric/Magnox and Rolls Royce Associates methods of predicting embrittlement in their pressure vessels. The strategy used in most of these studies has been to fix a temperature-dependent SMD term, which increases with the square root of fluence, by fits to low-copper data, while attributing the remaining effects to a more athermal CRP contribution that saturates at high fluence. Additional contributions to the SMD term from nickel (Odette and Lucas, 1986a, 1986b, 1990) and phosphorous (Jones and Buswell, 1988; Williams and Phythian, 1996) have also been proposed. Other studies have suggested: (a) adding a phosphorous term to the CRP as an additional saturating precipitate (Odette and Lucas, 1986a) and (b) recognizing the synergistic role of nickel and copper mediated by increasing the volume fraction of CRPs with the addition of manganese and nickel (Odette and Lucas, 1990, 1997a, 1998; Odette, 1995) and an indirect effect by increasing the copper in solution following heat treatment (Odette and Lucas, 1986a, 1986b, 1990, to be published; Williams and Phythian, 1996).

2 DATA BASE

Development of an analysis data base was a major part of this project, using the PR-EDB (NUREG/CR-4816) as the primary source. The term "analysis data base" is used to denote the data actually used for analysis, model development, and calibration, reproduced in Appendix A. By comparison, the PR-EDB is an archival data base that includes multiple entries in many cases and other information not used in the analysis. Version 2 of the PR-EDB, including Updates 4 and 5, was the source of data for most preliminary analysis, including updated fluences reported to the NRC during the course of the project. The analysis data base includes data from welds, plates, and forgings; heat-affected-zone data are not included. This section discusses the development of the analysis data base.

2.1 Independent Variables

The independent variables in the data base with sufficient data for analysis include chemistries, irradiation time, melt-wire irradiation temperature, reactor coolant temperature, neutron fluence and flux (E > 1 MeV), reactor type, vessel manufacturer and designer, specimen orientation, type of material, product form, weld flux and weld wire, pre- and post-irradiated transition temperature (TT) at 30 ft-lb (41 J), pre- and post-irradiated upper shelf energy (USE), and changes in TT and USE due to irradiation. All the independent variables considered in the analysis and their units are shown in Table 2.1.

2.2 Dependent Variables

Several algebraically-related measures of embrittlement were investigated as potential dependent variables for modeling. The generic types of dependent variables considered were:

- actual quantity after irradiation (TT_i or USE_i)
- shift or drop due to irradiation (TTS or ΔUSE)

In the current RG1.99/2, means of computing TTS and ΔUSE are provided; these quantities are added to unirradiated transition temperature and upper shelf energy, respectively, with prescribed margins to estimate the irradiated values. There was a preference for maintaining this approach, but the alternatives were investigated. The best fits were obtained by using USE_i and TTS.

2.3 Development of Charpy TTS and ΔUSE Data

The PR-EDB includes a file containing transition temperature shifts and upper shelf energy drops taken directly from surveillance reports. However, multiple entries appear for many heats. In addition, the shifts and drops reported were determined using various techniques over many years, including visual inspection of raw Charpy plots and various fitting techniques. In a few cases, especially where data showed a large amount of scatter, the reported shifts or drops in the PR-EDB appear to be bounding values or other conservative estimates rather than best estimates. While a bounding approach may be suitable for regulatory purposes, it is not consistent with the objectives of this project, which were to predict the mean trends with greater fidelity and less scatter.

To eliminate the confusion caused by the multiple entries in the PR-EDB and to ensure that mean estimates of shift and drop (determined on a consistent, repeatable basis) were used, a computer program FITCV was written to fit all the raw Charpy data sets from the PR-EDB and to compute TTS and ΔUSE based on those fits. The general approach was to fit a modified hyperbolic tangent (*tanh*) curve to each set of raw Charpy data from the same heat of material tested at the same orientation and with the same neutron exposure. Then unirradiated and irradiated curves for the same heat and orientation were matched and shifts and drops were computed. The detailed approach is described below.

The general *tanh* model form often used for modeling Charpy curves (e.g., Oldfield, 1982) is:

$$C_v = a_3 \tanh\left(\frac{T - a_1}{a_2}\right) + \left(a_3 + LSE\right) \qquad \textbf{(2-1)}$$

where

C_v = Charpy impact energy
a_3 = fitting parameter equal to *(USE - LSE)/2*
T = test temperature
a_1 = fitting parameter equal to temperature at the inflection point of the fitted curve
a_2 = fitting parameter related to the slope of the transition region
LSE = lower shelf energy; LSE = 1.28 ft-lbs, based on the logarithmic average of low temperature Charpy data (see Appendix B)

Table 2.1 Independent variables considered in embrittlement analysis

Variable	Symbol	Units
Neutron Fluence, E > 1 MeV	ϕt	n/cm^2
Neutron Flux, E > 1 MeV	ϕ	$n/cm^2/s$
Coolant temperature (PWR: cold leg temperature; BWR: recirculation temperature)	T_c	°F
Irradiation time	t_i	hours
Transition temperature at 30 ft-lbs before and after irradiation	TT_{u30} & TT_{i30}	°F
Shift in transition temperature at 30 ft-lbs due to irradiation, defined as TT_{i30} - TT_{u30}	TTS	°F
Upper shelf energy before and after irradiation	USE_u & USE_i	ft-lb
Drop in upper shelf energy due to irradiation, defined as USE_u - USE_i	ΔUSE	ft-lb
Chemical composition: Copper (Cu), Nickel (Ni), Phosphorus (P), Sulfur (S), Silicon (Si), Chromium (Cr), Manganese (Mn), Molybdenum (Mo), Carbon (C)		weight %
Product form (weld, plate, forging)		(Categorical)
Material (A508, A533B1, A302B, A336)		(Categorical)
Reactor type (PWR, BWR, "non-characteristic BWR")		(Categorical)
Vessel manufacturer (see Appendix A)		(Categorical)
Plant designer (see Appendix A)		(Categorical)
Specimen orientation (TL, LT, TS, LS)		(Categorical)
Weld flux (see Appendix A)		(Categorical)
Weld wire (see Appendix A)		(Categorical)

There were a number of data sets, however, for which an upper shelf was not established by the raw Charpy data. In these cases, an exponential model form was used instead of a *tanh*, so that the transition temperature at 30 ft-lbs could be established without the upper shelf energy. The exponential model form was

$$C_v = LSE \exp\left(b_1 T^{b_2}\right) \qquad (2\text{-}2)$$

where b_1 and b_2 were fitting parameters.

The *tanh* form in Equation 2-1 did not do a good job of fitting the Charpy data for sets of data that exhibited an abrupt transition from the lower shelf and a more gradual transition to the upper shelf. In such sets, the symmetric *tanh* curve did not "go through" the data well in the lower transition region, near the 30 ft-lb temperature. Several examples are shown in Figure 2.1. An asymmetric form of the *tanh* model, which fits the data better than the usual *tanh* model in these cases, is also shown in the Figure 2.1.

The form of the asymmetric *tanh* is:

$$C_v = c_3 \tanh\left(\frac{T - c_1}{c_4 T + c_2}\right) + \left(c_3 + LSE\right) \qquad (2\text{-}3)$$

where c_1, c_2, and c_3 are analogous to a_1, a_2, a_3 in Equation 2-1, and c_4 is a positive fitting parameter causing the hyperbolic tangent fit to have a more sharply curved transition in the lower region than the upper region. The examples in Figure 2.1 show that the asymmetric *tanh* is able to come closer to the data than the symmetric *tanh* fit

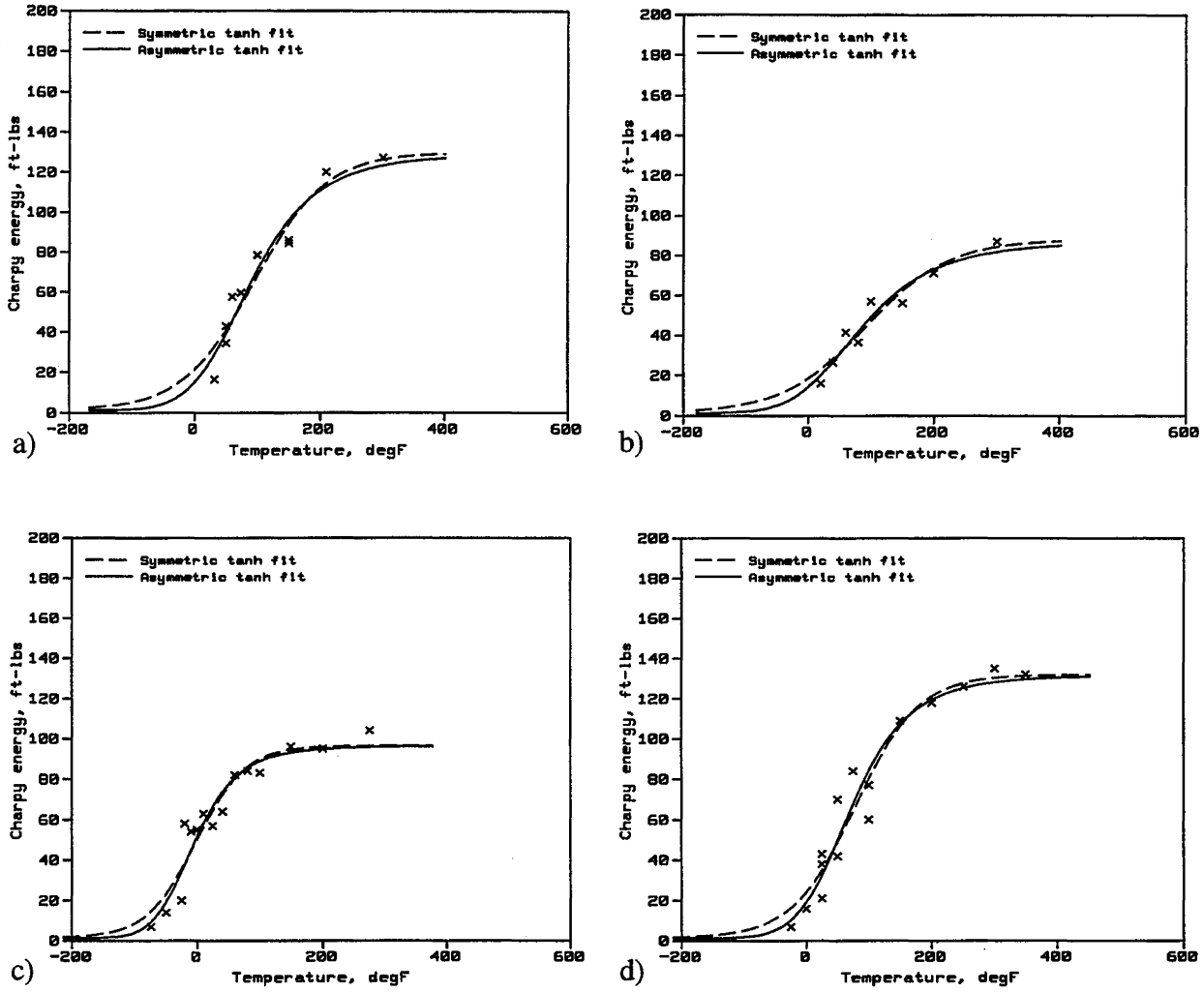

Figure 2.1 Examples of symmetric and asymmetric *tanh* curve fits

in the lower transition region. However, the symmetric *tanh* usually provided a better fit to sets with limited upper shelf data; therefore, the value of c_3 in Equation 2-3 was fixed to the value of a_3 determined by Equation 2-1. Note that Equation 2-1 is a special case of Equation 2-3 where $c_4 = 0$; hence, given sufficient data, Equation 2-3 always fits the lower transition at least as well as Equation 2-1. All the forms of Equations 2-1, 2-2, and 2-3 are shown graphically in Figure 2.2.

The FITCV computer program automatically fitted Equations 2-1 through 2-3 to each set of raw data and determined which fitting form provided a better fit. In addition to the three fitting forms, FITCV used two different algorithms for performing the fits. The computer code SURFIT, previously developed at Modeling & Computing Services (M&CS), was called by FITCV to perform a conventional nonlinear least squares fit, and the computer code ODRPACK (Boggs et al., 1992) was called to fit the data using orthogonal distance regression (ODR) techniques. The SURFIT code minimized the squared residuals in Charpy energy (i.e., the vertical direction), while the ODR code minimized squared residuals perpendicular to the fitted curve.

The FITCV computer program generated plots showing the raw data, along with the best of the three fitted SURFIT models and the best of the three fitted ODR models, for every set of unirradiated and irradiated data in the PR-EDB (270 unirradiated and 845 irradiated sets). The displayed models were best in the sense of minimum sum of squared residuals. Examples are shown in Figure 2.3. In most cases, the best fits by SURFIT and ODR used the same form and were nearly coincident. Where they were not, the ODR fit was usually better than the conventional least squares fit, because of the steep slope in the transition region. So ODR fits were used for computing shifts and drops, unless visual inspection

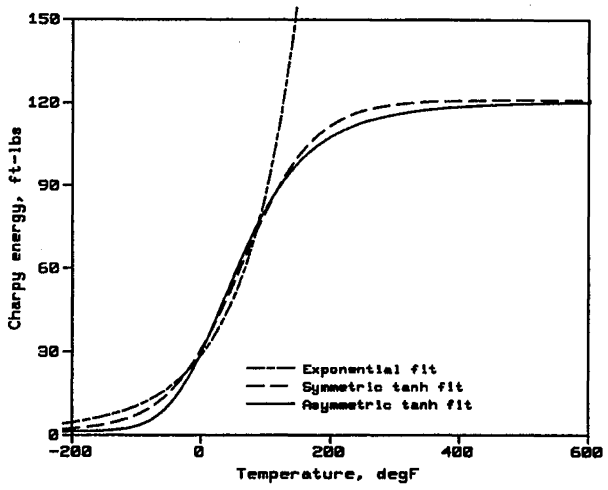

Figure 2.2 Model forms for Charpy curve fits

revealed a better fit from SURFIT. All plots were reviewed individually to ensure that the best fit was chosen in each case.

Most sets of raw Charpy data included specimens of the same heat and orientation that were irradiated in the same capsule at the same plant. But in the case of unirradiated standard reference materials, raw Charpy data associated with different plants were pooled together, so that one unirradiated C_v versus T curve was fitted for each standard reference material in the PR-EDB. The basis for this approach is that the unirradiated standard reference materials were the same heats, regardless of which plant they were sent to, so combining the data from all plants gives the best characterization *of the heat* in the unirradiated condition. No attempt was made to match up like heats of unirradiated data from different plants for materials other than standard reference materials.

2.4 Chemical Composition Data

In the PR-EDB, chemical compositions are given for each heat in the data base. However, in many cases, the PR-EDB contains multiple entries for a single heat, especially for Cu, Ni, and P contents. The multiple entries seem to have occurred for a variety of reasons: (a) different test methods, (b) different results (or duplicate results) from different source documents, and (c) multiple measurements by the same test method. For the preliminary analysis data base, the averages of the multiple entries from the PR-EDB were entered for chemical composition. Critical composition elements received closer attention during the industry review of the data base, discussed in Section 2.7.

2.5 Strength Data

There was some interest in determining whether the tensile properties (yield and ultimate strength) in the PR-EDB could be used as modeling variables, especially for applications where unirradiated Charpy data are unavailable. However, these data presented challenges that led to early abandonment of the effort. As in the Charpy and chemistry data, there were often multiple entries with no clear way to choose the best estimate. In some cases, the data were given at various temperatures, including room temperature (50-100°F) and high temperature (550-610°F), but in other cases the data were at either one or the other temperature range. Choosing either temperature would reduce the size of the available data base. But the insurmountable problem was that the PR-EDB was missing a substantial amount of tensile data. If the analysis data base were restricted to only those observations which had available strength data, either at low or high temperature, the data base would be only about half as large. Consequently, to avoid a major loss of data, a decision was made early in the project not to use strength data in modeling.

2.6 Updated Fluence Data

Early in the project, it was recognized that the fluences in the PR-EDB were not calculated on a consistent basis. The values were reported over a time span of nearly 30 years, during which time cross-section libraries and evaluation methods changed substantially. Therefore, in response to an NRC staff request, the major U. S. RPV manufacturers provided updated fluence values in early 1994.

Westinghouse re-evaluated fluences for all its plants on a consistent basis using cross-sections from the ENDF/B-V dosimetry file and documented the changes in detail (Lippincott, 1994). Nearly all of the updated fluences for irradiations ending after 1980 were within ± 20% of the old values; much larger differences occurred for some earlier evaluations, as might be expected.

The Babcock and Wilcox Owner's Group (BWOG) Materials Committee also provided documentation of their updated fluences (DeVan, 1994). The BWOG report presents updated fluence values along with references to source documents for details; the published dates of the source documents range from 1975 to 1990.

Combustion Engineering and General Electric each provided tables containing their most recent fluence values. Specific references for the method of calculation were not provided.

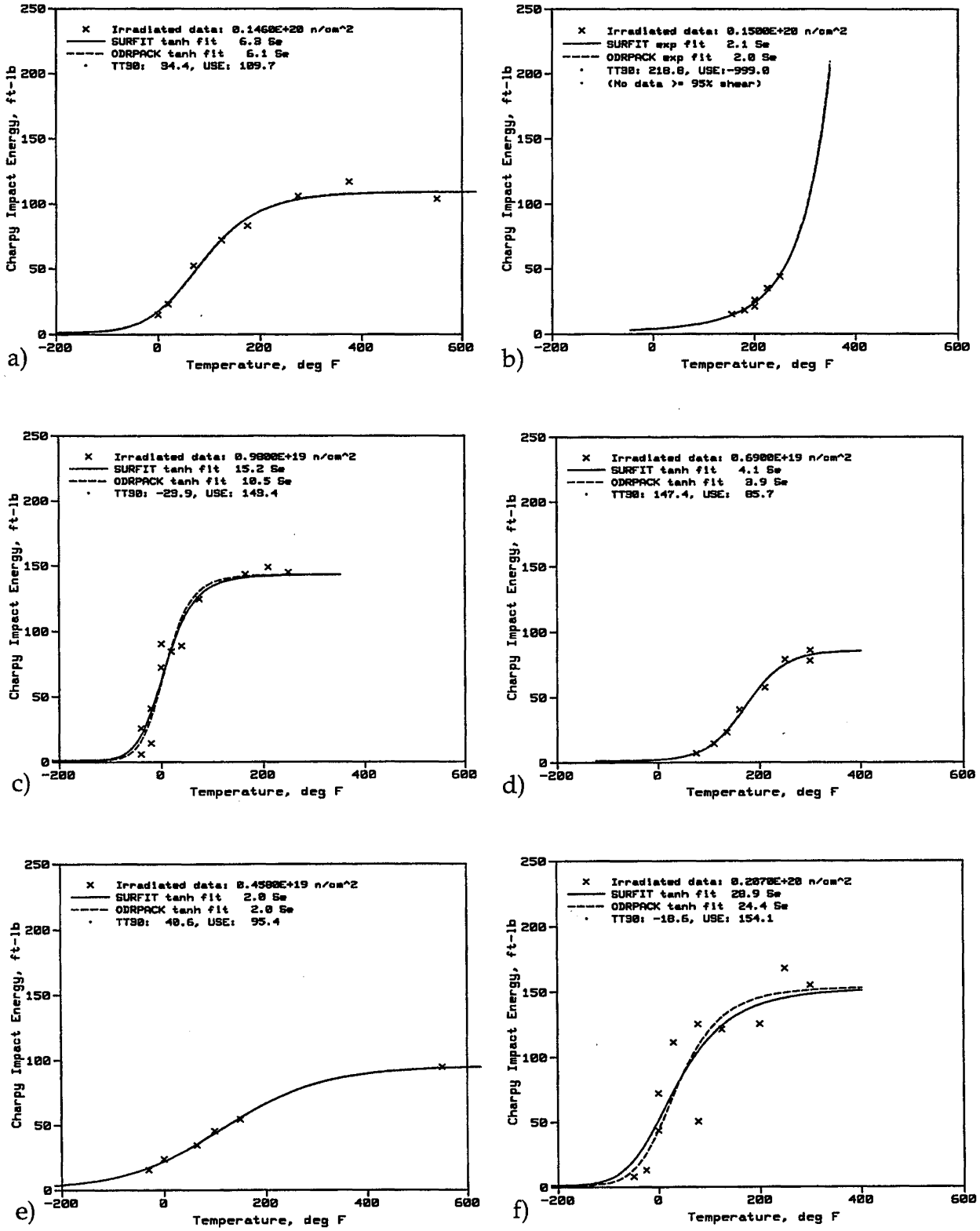

Figure 2.3 Sample Charpy data fits

2.7 Industry Review of the Analysis Data Base

Once a preliminary analysis data base had been developed, as described above, the data base was delivered to the ASTM E10.02.02 Task Group on Embrittlement Correlations for review and verification of entries for copper, nickel, fluence, material identification, weld wire heat numbers and weld flux types, and the Charpy properties. The plots of each Charpy data set, developed as described in Section 2.3, were produced for review by the ASTM Task Group. Phosphorous values were also scanned by Task Group members for obvious errors. Some corrected or updated values for these variables were provided by Task Group members. Some additional surveillance data not yet in the PR-EDB were also provided. All new or revised data were documented with the NRC and entered into the analysis data base used for final analysis.

The ASTM E10.02.02 Task Group also provided (and documented) coolant temperatures for the final analysis data base. The reason for this addition was that the irradiation temperatures in the PR-EDB were melt-wire data. The melt-wire data were considered unreliable for modeling by the ASTM E10.02.02 Task Group because they reflect the highest temperature over a period of time, which can be quite different from the average. This study confirmed that melt-wire data were not useful indicators of irradiation temperature in preliminary pattern recognition runs, where they were found to have no predictive value, contrary to considerable research on the effect of irradiation temperature. Coolant temperatures are believed to provide better estimates of the average temperature during irradiation. The coolant temperatures provided by the Task Group members were cold leg temperatures for pressurized water reactors (PWRs) and recirculation temperatures for boiling water reactors (BWRs).

The consistently-calculated Charpy shifts and drops were compared to tabulated values in the Electric Power Research Institute's PREP4 data base (Griesbach and Burgos, 1996), with special attention given to shift data. Most recalculated shifts agreed closely with PREP4 values, which were also consistently determined, using symmetric *tanh* fits to raw Charpy data. Discrepancies of more than 10°F received closer examination. In almost all cases with discrepancies greater than 10°F, the data appeared from the plots to have been fitted well using the current methods. There were several cases where the asymmetric *tanh* provided a noticeably better fit to the data than the symmetric *tanh* fits used in PREP4. In one case, it was determined that the irradiated transition temperature could not be well established from the data, and the TTS for that point was omitted. This was the only data base change resulting from the PREP4 comparison and review of Charpy data set plots.

2.8 Characterization of the Analysis Data Base

The analysis data base contains 758 irradiated data points, including 752 shifts and 692 drops. This is more than three times the size of the data base (177 to 216 points) that was available when RG1.99/2 was developed. The current analysis data base is attached as Appendix A. As in most data bases composed of data from various sources, there are cases of missing data; some independent variables are missing, and in many cases only one of the quantities to be modeled - TTS or ΔUSE - is available. Missing values are indicated by "-999" in Appendix A, except for missing categorical variables, which are blank.

The distribution of data useable for modeling by product form is shown in Tables 3.1 and 4.1. Summarizing the results presented there, about half of the useable data are for plates, a third for welds, and the remainder (101 - 105 points) for forgings. The total number of points used in the upper shelf and shift models are 662 and 609 points, respectively.

The ranges of values in the data base for the modeling variables are given in Tables 5.1 and 5.2, together with a discussion of the estimated validity ranges of the models. But it should be noted that the coverage of the multi-dimensional space is relatively sparse and non-uniform in the independent variables. There are many combinations of conditions that are not well represented in the data base, such as high Cu - high Ni. These limitations should be considered in some applications, as discussed in Section 5.

2.9 Correlations Among "Independent" Variables

Correlations among the supposedly independent variables were investigated using the TACMVS computer code previously developed at M&CS. This code identifies monotonic, not necessarily linear, relationships between variables and computes an R^2 value, which is interpreted as a linear correlation coefficient ($R^2 = 1$ for a strong relationship, $R^2 = 0$ for no relationship). The significance of the identification of correlations among "independent" variables is that correlated variables ideally should not be used in the same model, since their effects are at least partially confounded. When it is necessary to use correlated variables, the modeling and interpretation require greater care. Figure 2.4 shows the correlations among independent variables in the analysis data base.

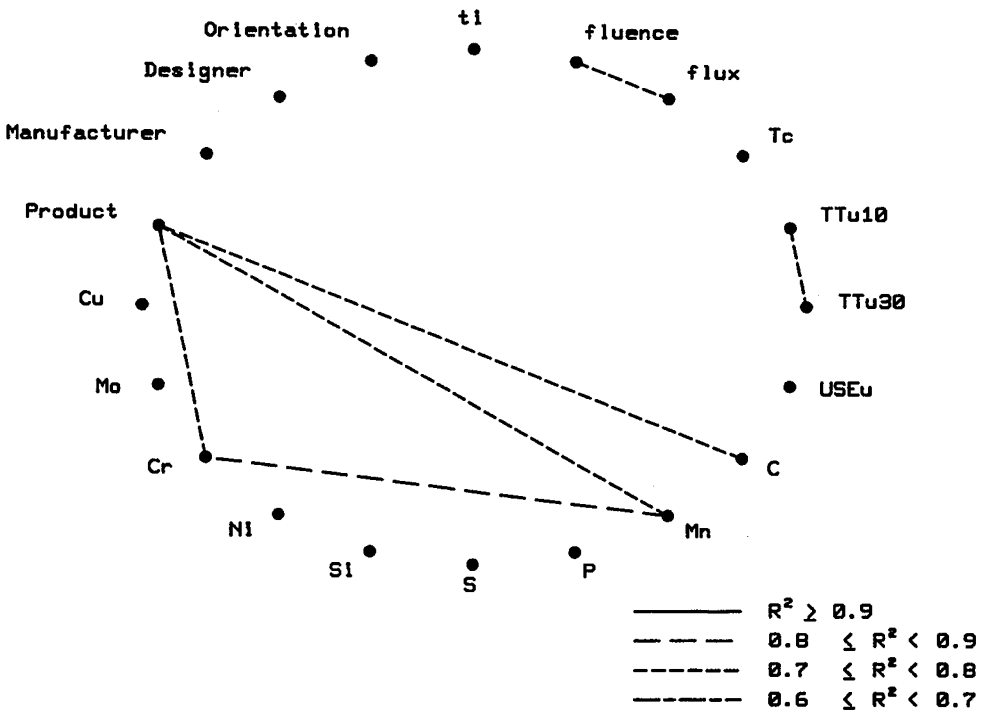

Figure 2.4 Correlations among "independent" variables

among selected independent variables in the analysis data base. A relatively strong correlation is shown between Cr and Mn; moderate correlations between product form and chemical components, between fluence and flux, and between TT_{u10} and TT_{u30} are also shown. The major modeling variables fluence, Cu, Ni, P, T_c, and product form are reasonably independent.

None of these correlations proved troublesome. None of the correlated pairs are present in the USE model. The only pair of correlated variables in the final TTS model is fluence and irradiation time. This is a well-understood, physical relationship that is unavoidable.

3 UPPER SHELF ENERGY MODEL

3.1 USE Analysis Methodology

The schematic diagram in Figure 3.1 shows the methodology used in developing a model for Charpy upper shelf energy (USE). As illustrated, the data base development, pattern recognition, model development, and calibration of final models is an iterative process. One reason is that outliers, regions of poor fit, and other anomalies are discovered throughout the analysis, right up to the point where final normalized plots are produced. Each time an anomaly is discovered, it requires modifying the data base or the fitting form and recalculating all affected results.

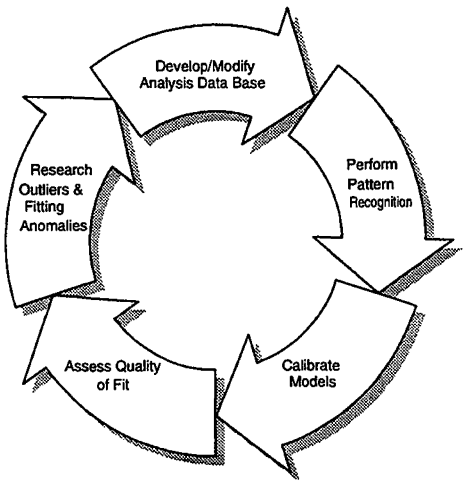

Figure 3.1 Schematic of analysis methodology for USE model

Little guidance was available from embrittlement mechanism research to help with formulation of the upper shelf model. Thus statistical analysis played the dominant role in developing the upper shelf energy model.

The overall approach taken in this part of the project was similar to that used in several previous characterizations of materials behavior (Eason and Nelson, 1994; NUREG/CR-5356; NUREG/CR-5729). Having identified correlations among potential modeling variables, as discussed in Section 2.9, the next step in the analysis process was pattern recognition.

All available variables and many combinations of variables were considered in the pattern recognition phase of analysis to ensure the best possible chance of identifying secondary variables or combinations of variables. The M&CS Transformation Analysis Code (TAC) was applied, first to identify key variables (or variable combinations) and then to help determine optimal functional forms.

The basic tool for model calibration was the nonlinear least squares code SURFIT. This code has been used continually by the Principal Investigator since he developed it in 1976; it has proven to be robust and convenient for calibrating nonlinear multivariable models. It allows complete flexibility in the specification of the function to be fitted. Note that nonlinear least squares is a minimization-based procedure, for which it is always necessary to solve a problem at least twice using different starting estimates - to assure that a minimum has been found and to explore the sensitivity of the minimum to changes in the parameters.

Data with fluence greater than or equal to approximately 10^{16} n/cm^2 were used for model calibration. For some data records in the analysis data base (see Appendix A), not all independent variables or dependent variables were available from the information given in the PR-EDB or provided by the ASTM E10.02.02 Task Group. A data point could be included for model calibration only if all variables required by the model being calibrated were present in the data base.

Great caution was exercised in the removal of outlier points during calibration. The reluctance to ignore potentially-valid data had to be balanced with the need to omit data that could bias the fits in an unrealistic fashion. For this reason, an objective rule-of-thumb referred to as Chauvenet's criterion was applied (Young, 1962; Taylor, 1982). Chauvenet's criterion calls for rejection of a data point if the probability of obtaining it is less than 1/(2N) based on a normal distribution of residuals about the model, where N is the total number of points. This technique is discussed in more detail in Appendix C, and the three USE outlier points identified by this criterion are listed there. Application of Chauvenet's criterion usually results in rejection of very few points, if any; i.e., only the extreme outliers that could potentially bias a least squares fit are removed using this procedure.

The quality of each candidate model was assessed by evaluating the standard error of estimate of the measured data about the model prediction, reviewing plots of each of the independent variables versus the dependent

variable (normalized relative to the variables not shown), analyzing residual plots for all independent variables, and reviewing a plot showing measured versus predicted values of the dependent variable. The standard error of estimate is computed by

$$S_e = \sqrt{\frac{\sum_{i=1}^{npts} \left(Y_{predicted} - Y_{actual}\right)^2}{npts - nparam}} \qquad (3\text{-}1)$$

where Y is the dependent variable, *npts* is the number of data points used, and *nparam* is the number of fitting parameters.

3.2 USE Model

Preliminary pattern recognition results for upper shelf energy indicated that the irradiated value, USE_i, could be predicted better than ΔUSE using the independent variables in the analysis data base. For this reason, USE_i was chosen as the dependent variable for studying the drop in Charpy upper shelf energy. Drop in upper shelf energy can be obtained algebraically from $\Delta USE = USE_u - USE_i$.

Several independent variables and some combinations of variables were found to be potentially important for modeling USE_i, using the transformation analysis code. Complex interactions among variables involved in the embrittlement process were expected, and specific combinations of variables were inputs for the transformation analysis. Variables identified as potentially important were USE_u, fluence, Cu, and some combination of Cu, Ni, and fluence. Irradiation temperature was not an important variable. But at the time of the pattern recognition work, the data base included only melt-wire temperature, which was not important for the TTS model either. The USE model was later checked to determine if coolant temperature should have been included, with the result that it should not. The strongest predictor variable for irradiated USE was unirradiated USE. There was some indication that the effects of Cu and fluence saturate for Cu greater than about 0.3 wt%, which was consistent with the preliminary work on the TTS model. Hence a saturating (*tanh*) form was chosen for the candidate models.

The best correlation found for predicting USE_i was:

$$USE_i = 0.0570\,USE_u^{1.456} + \begin{Bmatrix} 55.4, \text{ welds} \\ 61.0, \text{ plates} \\ 66.3, \text{ forgings} \end{Bmatrix} - \left[17.5 f(Cu)\left(1 + 1.17 Ni^{0.8894}\right) + 305P\right]\left(\frac{\phi t}{10^{19}}\right)^{0.2223} \qquad (3\text{-}2a)$$

$$f(Cu) = \left[\frac{1}{2} + \frac{1}{2}\tanh\left(\frac{Cu - 0.138}{0.0846}\right)\right] \qquad (3\text{-}2b)$$

where all upper shelf energies are in ft-lb, *Cu*, *Ni*, and *P* are in wt%, and ϕt is in n/cm^2. This model has a standard error of 11.2 ft-lb, with 662 points used in the calibration, not including the three outlier points that were omitted (see Appendix C).

The goodness of fit of Equation 3-2 is demonstrated graphically in Figure 3.2. Figure 3.2a shows the predicted USE_i versus the actual USE_i with bounds that enclose 90% of the data. For Figures 3.2b through 3.2f, the USE data were normalized to median values of the independent variables, as if all tests were conducted at the same conditions. To obtain these plots, the data were adjusted using Equation 3-2 to minimize the "scatter" about the model arising from other variables that are not plotted. For example, the normalized plot of ϕt versus USE_i, Figure 3.2c, was obtained by the following formula:

$$USE_{norm} = USE_{data} + \left(USE_{median} - USE_{model}\right) \qquad (3\text{-}3)$$

where

USE_{norm} = the plotted (normalized) value of USE_i
USE_{data} = the actual value of USE_i
USE_{median} = the model value of USE_i for plates at the measured value of ϕt and median values of USE_u, *Cu*, *Ni*, and *P*
USE_{model} = the model value of USE_i for plates at the measured values of ϕt, USE_u, *Cu*, *Ni*, and *P*

Median values of the independent variables for the calibration data set are:

ϕt = 8.06×10^{18} n/cm^2
USE_u = 121 ft-lb
Cu = 0.135 wt%
Ni = 0.594 wt%
P = 0.011 wt%

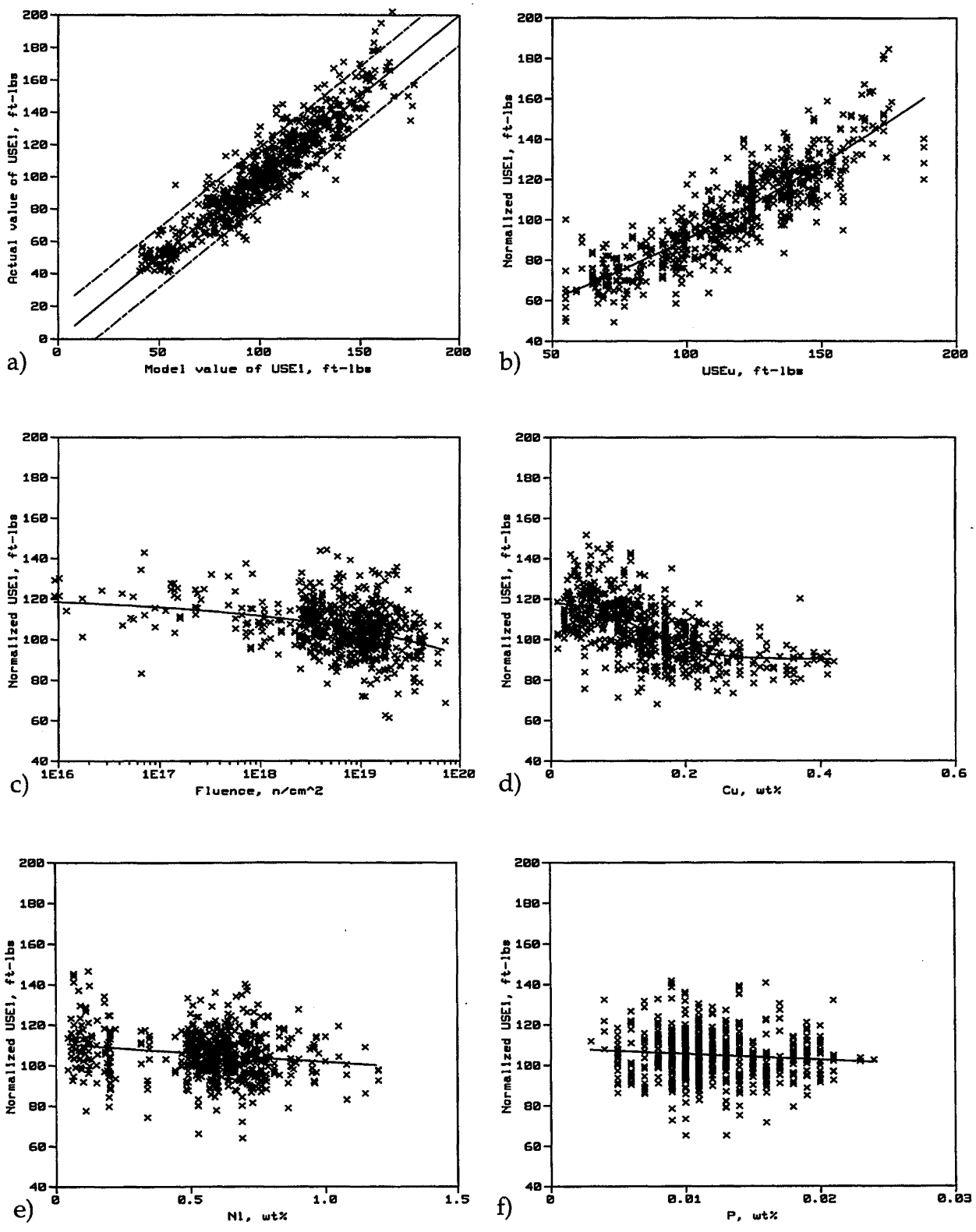

Figure 3.2 Predicted versus actual and normalized plots for USE model variables

The value of the constant for plates (61.0) was used for normalization. The normalization procedure makes it possible to visually assess the trends and the quality of fit to a multivariable model. Without such a procedure, the apparent scatter arising from different test conditions of variables not being plotted makes any assessment of trends difficult. Normalized plots show the functional forms of the variables in the model, and a comparison of the vertical ranges of the model lines provides an indication of the relative importance of each variable at the median values of other variables.

The quality of fit can also be assessed using the residual plots shown in Figure 3.3. The plots show the difference between the actual and predicted values of USE_i for each calibration data point versus all the independent variables in the model. If a variable were modeled improperly, a trend in the residual data distribution about the zero line would be apparent. No such trends are evident in Figure 3.3.

3.3 Discussion of USE Model

The quality of fit of the calibration data about the model is excellent. The standard error of 11.2 ft-lb is not much greater than the experimental error one would expect in repeated tests of the same material at various laboratories.

The standard error, calculated according to Equation 3-1, is an appropriate measure for comparing models on the data base used for fitting, but it is inappropriate for showing the quality of fit of the model to a subset of the calibration data or to other data not used for calibration.

To facilitate comparison of the quality of fit of Equation 3-2 to selected subsets of data, a standard deviation (S_d) of the subset residuals about the model prediction was defined as

$$S_d = \sqrt{\frac{\sum_{i=1}^{npts} \left(Y_{predicted} - Y_{actual} \right)^2}{npts - 1}} \qquad (3\text{-}4)$$

where *npts* is the number of points in the subset. This formula treats the model as fixed for evaluation purposes.

Standard deviations for selected subsets of the calibration data are shown in Table 3.1. Predicted versus actual plots for the plate, forging, weld, and Linde 80 subsets are shown in Figure 3.4, where the bounds are based on ± 1.645 S_d for each subset, thus they should enclose 90% of the data for each subset. The model does a reasonably good job in each subset. Indeed, the S_d values in Table 3.1 are 10% (or less) of the average USE_u values in all product forms.

Table 3.1 USE_i model: S_d for subsets of data

Data set	Number of points	S_d about Equation 3-2
Base Metals	443	11.6 ft-lbs
Plates	338	10.9 ft-lbs
Forgings	105	13.7 ft-lbs
Welds	219	10.1 ft-lbs
Linde 80	66	7.18 ft-lbs
All Materials	662	S_e = 11.2 ft-lbs (12 DOF)

Note that Equation 3-2 allows negative drops in upper shelf energy with irradiation, which did appear frequently in the data base (113 observations). It is not clear what would cause an increase in the unirradiated USE with irradiation; one hypothesis is measurement error in the original USE_u value. But increases in USE_u happen often enough, and clearly enough, that they are believed to be a real effect.

The unirradiated value of USE is needed to estimate USE_i using Equation 3-2. If the actual USE_u is not known, an estimate must be used. Table 3.2 shows averages and standard deviations of the raw USE_u data from the analysis data base for various subsets of data, depending on product form and specimen orientation.

Table 3.2 Average USE_u and S_d

Data set	Orient	Avg USE_u (ft-lb)	S_d USE_u (ft-lb)	S_d about Eq.3-2 (ft-lb)
Plates	LT/LS	127	18	18.1
	TL/TS	100	16	15.1
Forgings	LT/LS	155	17	20.8
	TL/TS	119	28	23.5
Welds	TL/TS	98	28	21.0

Also shown is the standard deviation of each subset of data about Equation 3-2 using the corresponding average USE_u. The scatter about the predicted USE_i is always greater when using an average USE_u, compared to using point-by-point actual USE_u values, as one would expect.

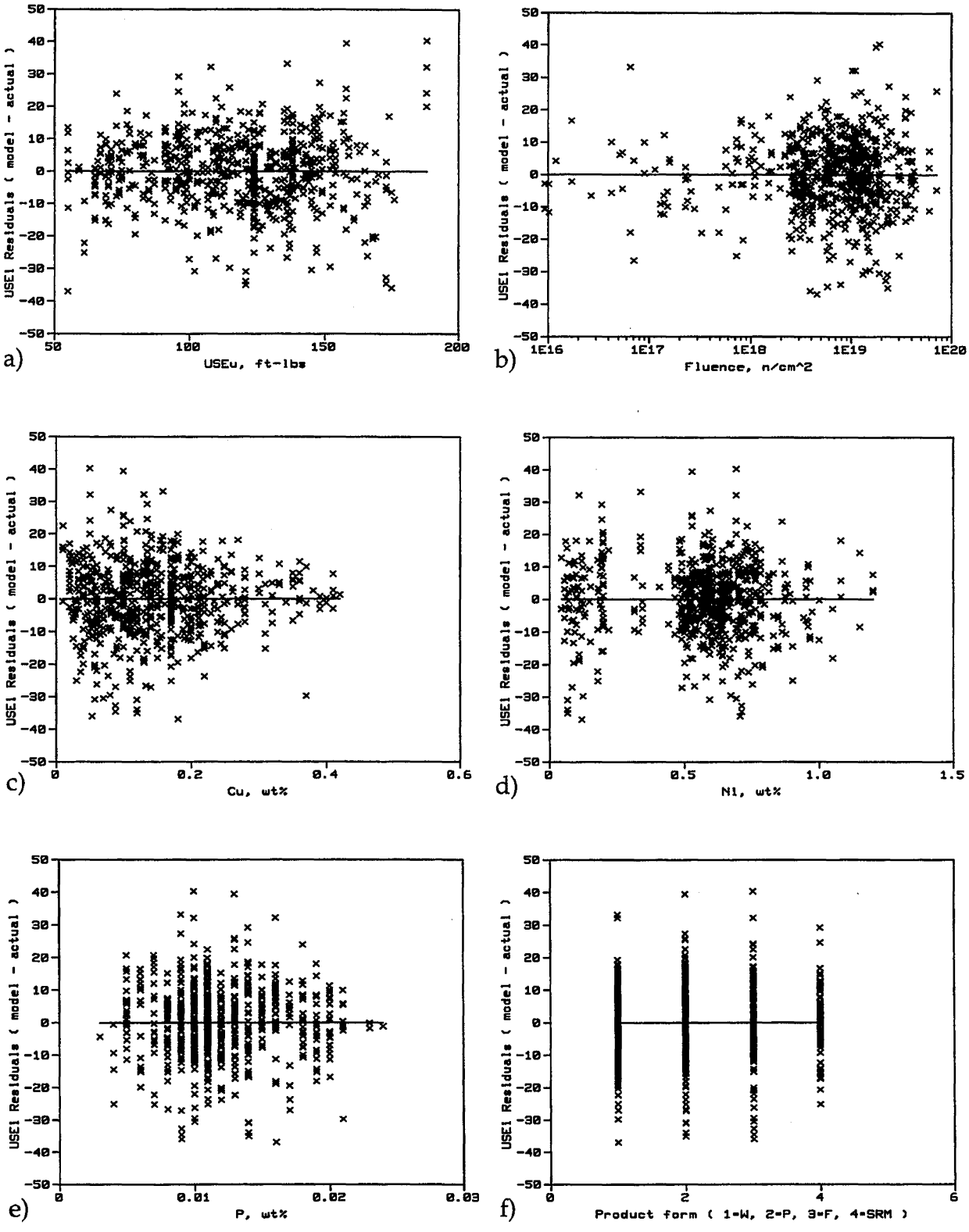

Figure 3.3 Residual plots for USE model variables

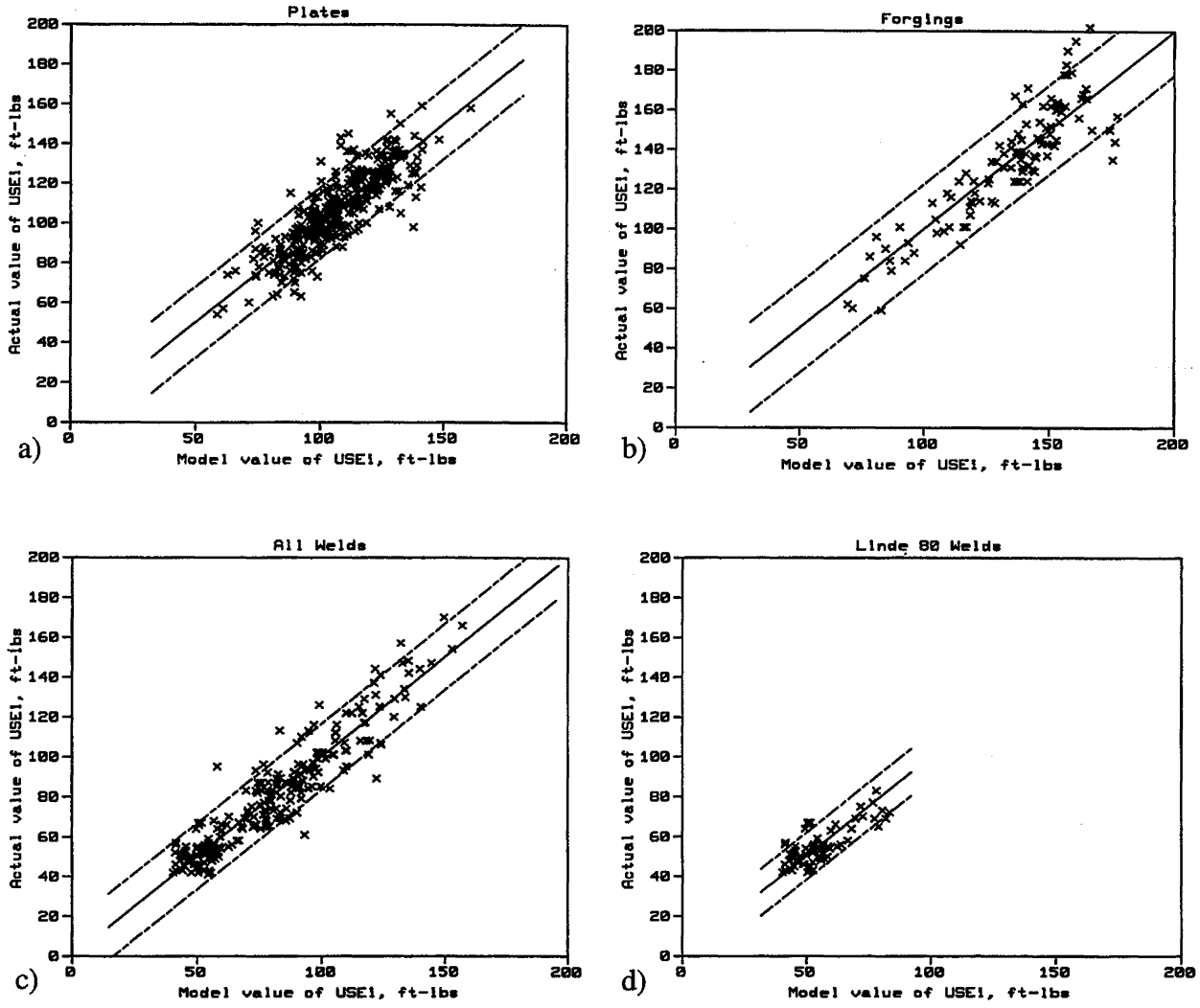

Figure 3.4 Predicted versus actual plots for subsets of USE data

Like Equation 3-2, the TTS correlation presented in Section 4 depends primarily on ϕt, Cu, Ni, P, and product form. But the TTS correlation also depends on T_c and irradiation time, although these are relatively small effects. Since TTS and ΔUSE are correlated, the authors re-evaluated the final USE_i model with respect to T_c and t_i, after completing the TTS model, to ensure that important variable effects were not missed. Plots showing residuals about Equation 3-2 versus T_c and t_i are shown in Figure 3.5. The effects of T_c and t_i on USE_i, if any, appear to be accounted for reasonably well, based on Figures 3.5a and 3.5b, respectively.

3.4 Alternative USE Models

Several other USE model forms were investigated during this project. Not all of these models have been investigated in as much detail as Equation 3-2, and none of them fit the data as well as Equation 3-2, based on their standard errors. The differences among the better alternative models are not statistically significant. For example, an alternative model without product form dependence is

$$USE_i = 0.0185\,USE_u^{1.674} + 24.7 + 35.4\left\{\frac{1}{2} - \frac{1}{2}\tanh\left[\frac{0.0652\log(\phi t) + CuNi^{0.1007} + 2.42P - 1.42}{0.0803}\right]\right\} \quad (3\text{-}5)$$

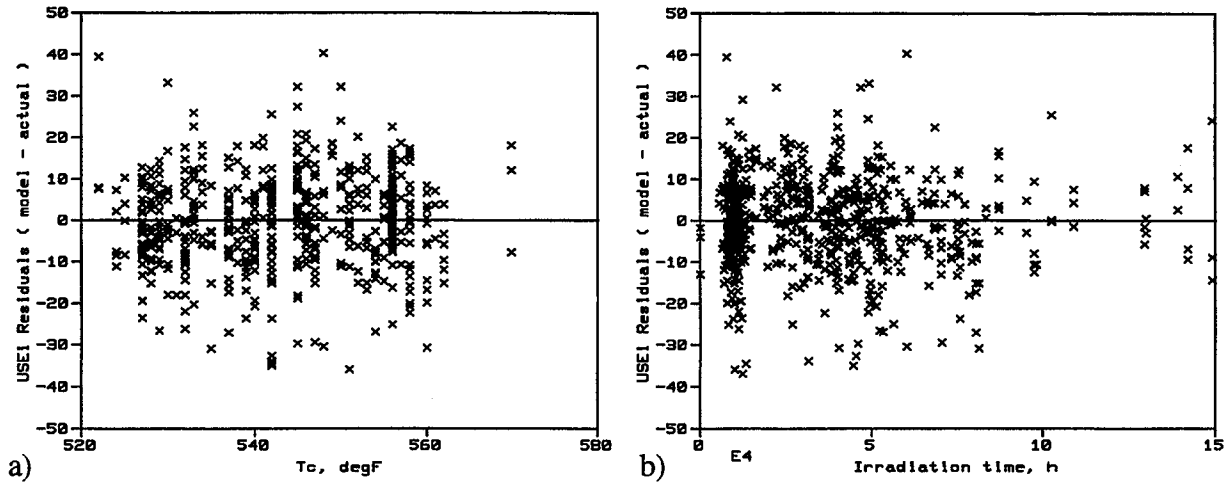

Figure 3.5 Residual plots for variables in TTS model but not in USE_i model

In this equation and throughout the report, logarithms are base 10. The standard error of this model is 11.7 ft-lb for the 662 calibration points. The residual plots for model variables are shown in Figure 3.6, and predicted versus actual plots for subsets of the calibration data set are shown in Figure 3.7. The residual plots at high Cu (> 0.35 wt%) and high Ni (> 1.0 wt%) are not as well centered about the zero residual line for this model compared to Equation 3-2.

Another alternative model form derives from the fact that ΔUSE and TTS are correlated. Because of this correlation, it is possible to predict ΔUSE directly from actual values of TTS, by

$$\Delta USE = 2.51 + 0.147\,TTS \qquad (3\text{-}6)$$

This form has a standard error of 12.9 ft-lb and is based on 682 points. But it is even better to combine some aspects of Equation 3-2a with the final TTS correlation presented in Section 4:

$$USE_i = 0.126\,USE_u^{1.317} + \begin{Bmatrix} 44.7, \text{ welds} \\ 49.7, \text{ plates} \\ 53.7, \text{ forgings} \end{Bmatrix} - 0.170\,TTS_{Eq.4\text{-}1} \qquad (3\text{-}7)$$

The standard error is 11.3 ft-lb for the 562 calibration points. Residual plots for model variables, which include irradiation time and coolant temperature from the TTS model, are shown in Figure 3.8. The residuals at high Cu (> 0.35 wt%) are not as well centered for this model compared to Equation 3-2.

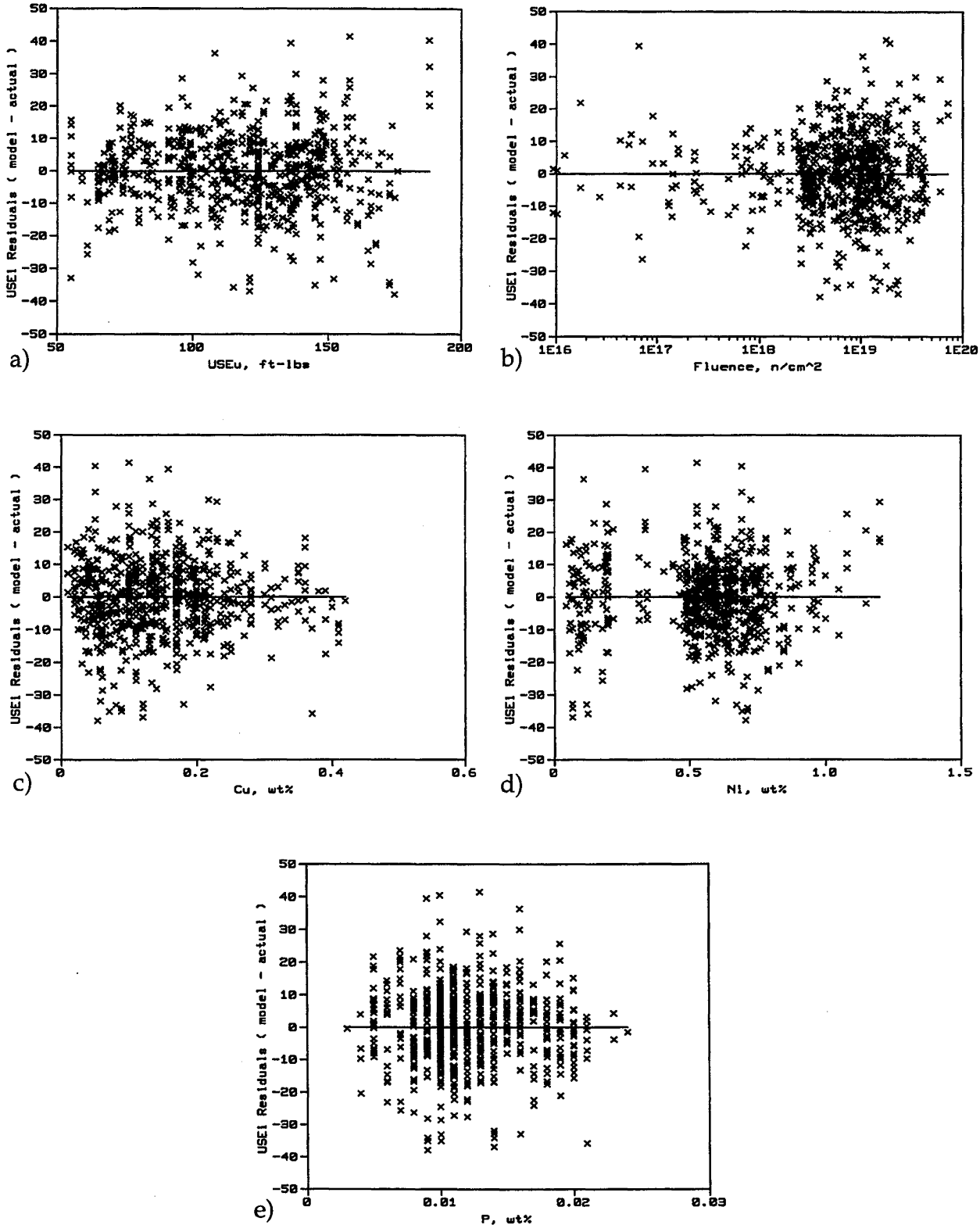

Figure 3.6 Residual plots for model variables in Equation 3-5

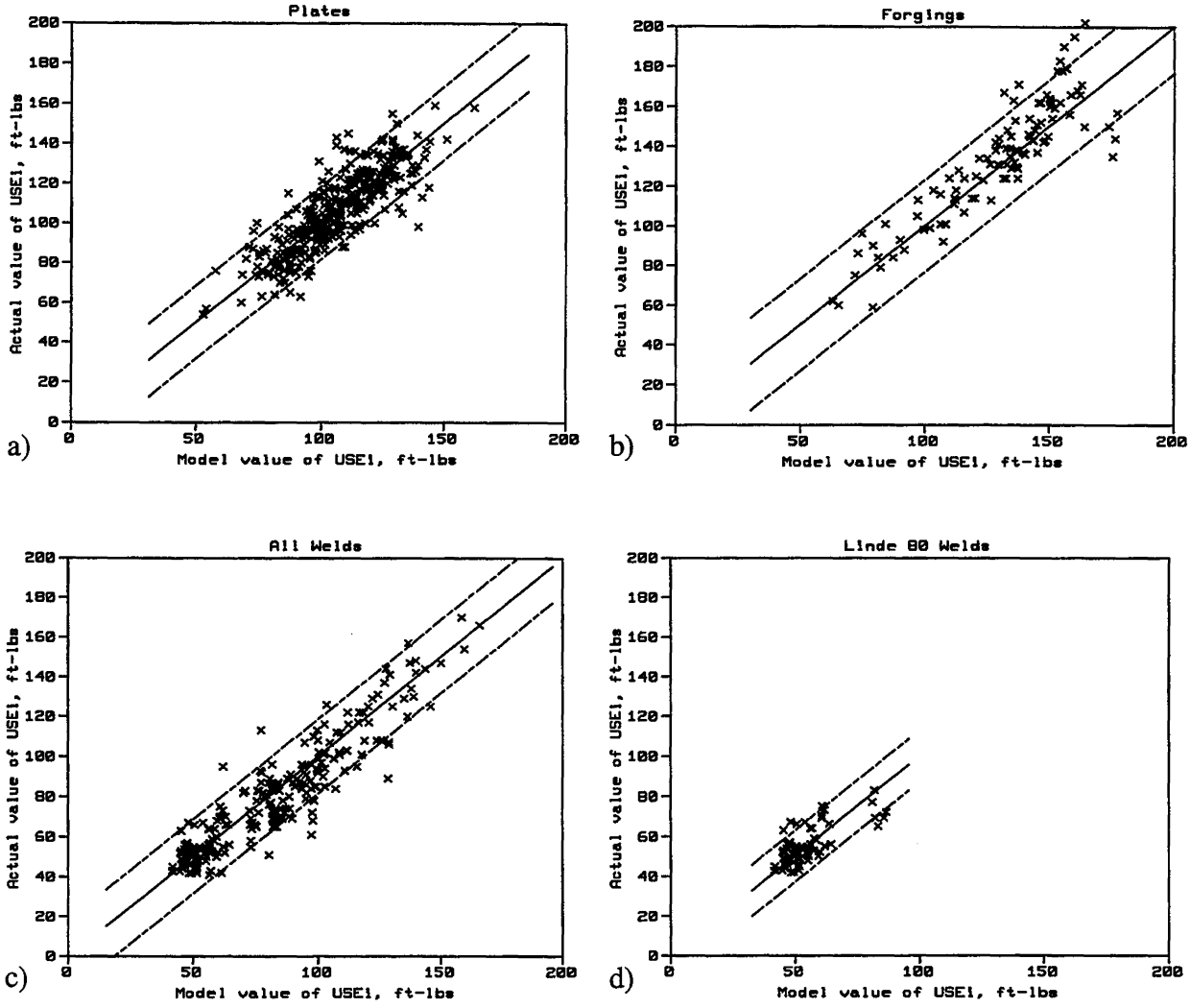

Figure 3.7 Predicted versus actual plots for subsets of data for Equation 3-5

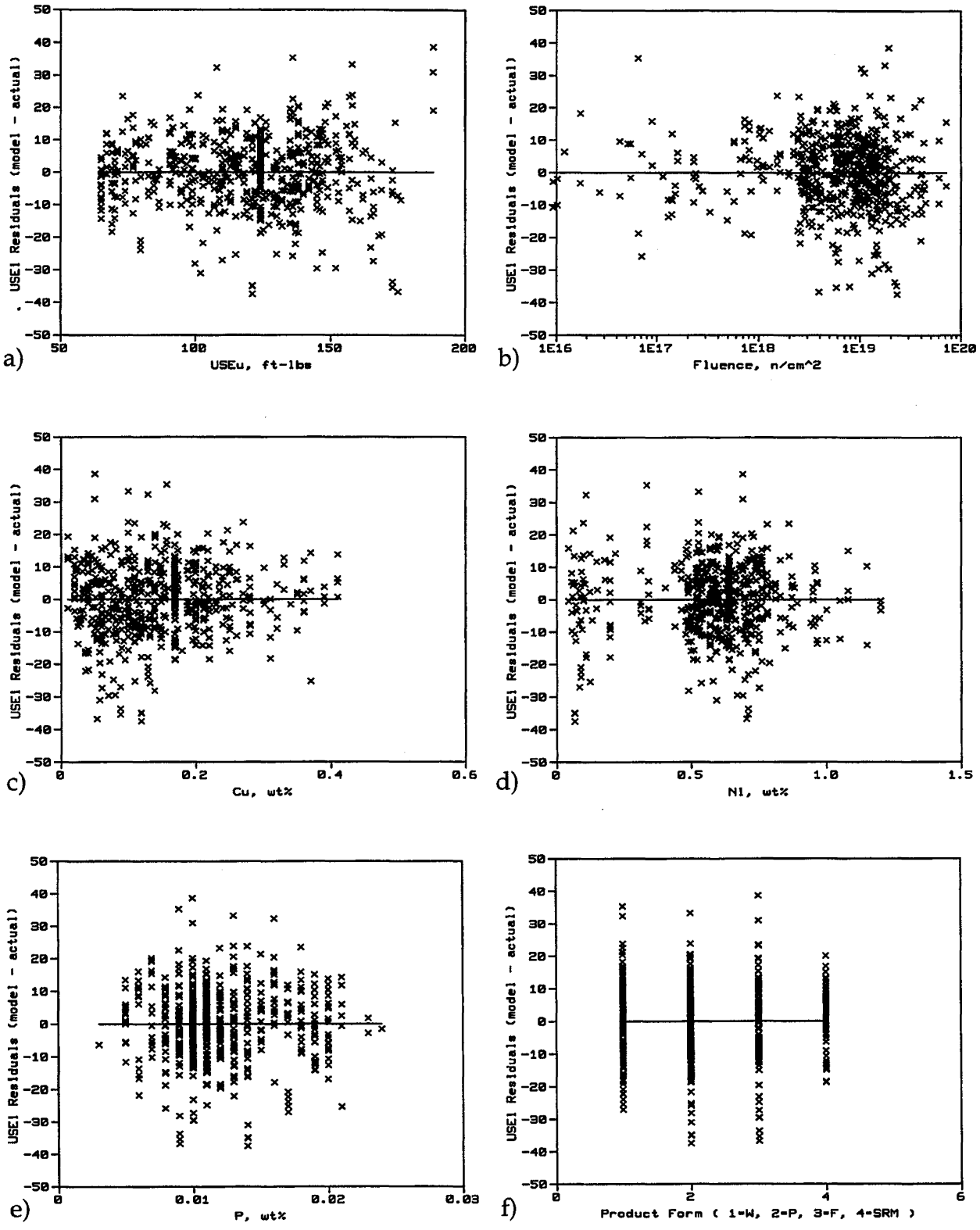

Figure 3.8 Residual plots for model variables in Equation 3-7

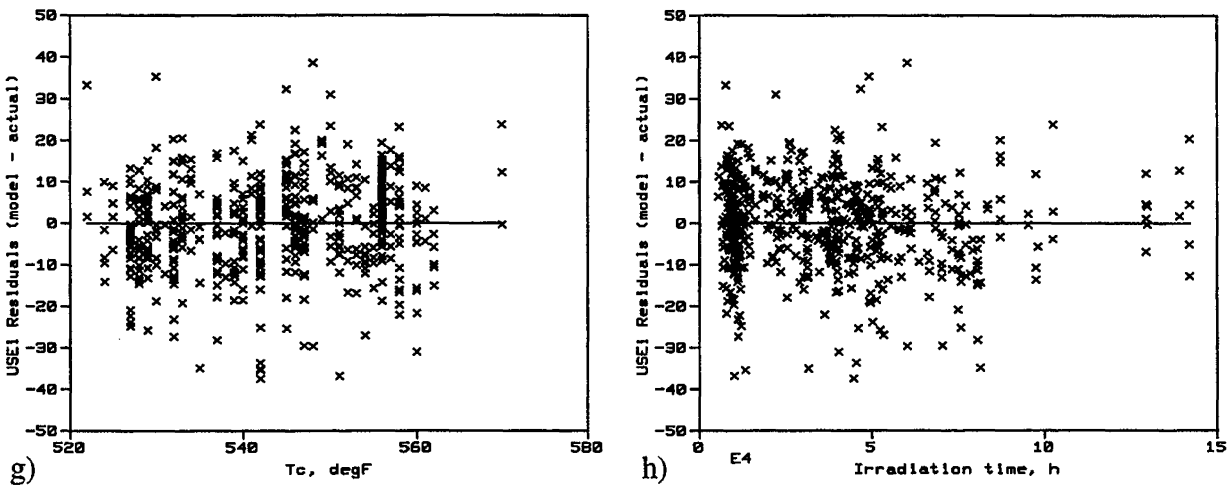

Figure 3.8 Residual plots for variables in Equation 3-7, cont'd

4 TRANSITION TEMPERATURE SHIFT MODEL

4.1 TTS Analysis Methodology

The analysis methodology used in developing the transition temperature shift (TTS) models was similar to that used for USE. The TTS model development was enhanced, however by the greater understanding of the TTS mechanisms from previous and ongoing research. The enhanced schematic of the analysis methodology is shown in Figure 4.1, illustrating the incorporation of the current understanding of embrittlement mechanisms into various stages of the analysis process. Pattern recognition results were used initially to identify correlations among "independent" variables, to guide the development of the data base and preliminary models, and to verify effects (or lack of effect) of some potential modeling variables. For instance, the lack of an effect of melt-wire temperature was clear in the preliminary pattern recognition work, as was the lack of strong chemistry effects other than those involving Cu, Ni, and P. Model refinement relied more on an understanding of embrittlement mechanisms and classical data analysis such as residual analysis in subsets.

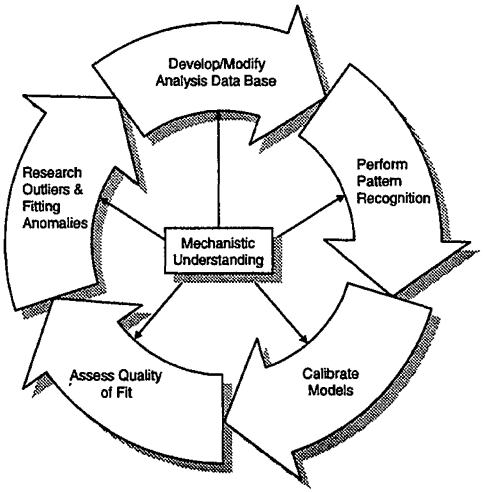

Figure 4.1 Schematic of analysis methodology for TTS model

As mentioned in Section 1.4, the primary mechanisms contributing to TTS produce stable matrix defects (SMD), phosphide precipitates (PP), and copper-rich precipitates (CRP). Based on prior work, including single-variable experiments, the SMD term should be independent of flux, scale approximately with $\sqrt{\phi t}$, and include an irradiation temperature effect, such as $(1\text{-}CT_i)$, where C is a constant. The CRP term should be approximately independent of flux in the intermediate surveillance data range but depend on flux above about 10^{12} n/cm^2/s and below about 10^{10} n/cm^2/s (depending on irradiation temperature). There should be no effect of copper for Cu < ~0.1 wt%, and the Cu effect should saturate at about 0.3 wt% (depending on heat treatment). The form of the Cu effect should be approximately $\sqrt{Cu - 0.1}$. There should also be a strong interaction of copper with nickel and/or manganese. The effect of fluence for the CRP term should saturate, and the saturation fluence should increase with increasing Ni and decreasing Cu. The PP contribution is not well understood. It is known that the detrimental effect of phosphorous on embrittlement decreases with increasing Cu.

Model development began by constructing mathematical functions of independent variables to reflect each of the three embrittlement mechanisms described above. Pattern recognition suggested some convenient forms, such as *tanh* for the saturating fluence effect, but many other functional forms suggested by prior studies were also considered. Hundreds of candidate models were investigated, with various functional forms for each proposed variable effect and interaction. Nonlinear least squares surface fitting techniques were applied to calibrate candidate models using all available data in the analysis data base. The final model form evolved through exhaustive analysis of the calibration data base, including analysis of residuals in key subsets and comparisons with other data not used for fitting.

Model refinements were made based on fits to the overall calibration data set as well as calculation of residuals and standard deviations in subsets of interest. Normalized and residual plots were used to evaluate possible bias and consequences of data base limitations. In addition to the calibration data set, the best models were compared to data from independent single-variable experiments in the literature and unpublished work at the University of California at Santa Barbara (UCSB). The candidate models and their individual terms were also evaluated relative to detailed microstructural studies and physical models developed by other investigators.

4.2 Negative Shifts in the Data Base

Of the 752 data points in the data base for which TTS was known, negative values of TTS were computed for 37 cases. Unlike the negative drops in USE, which were

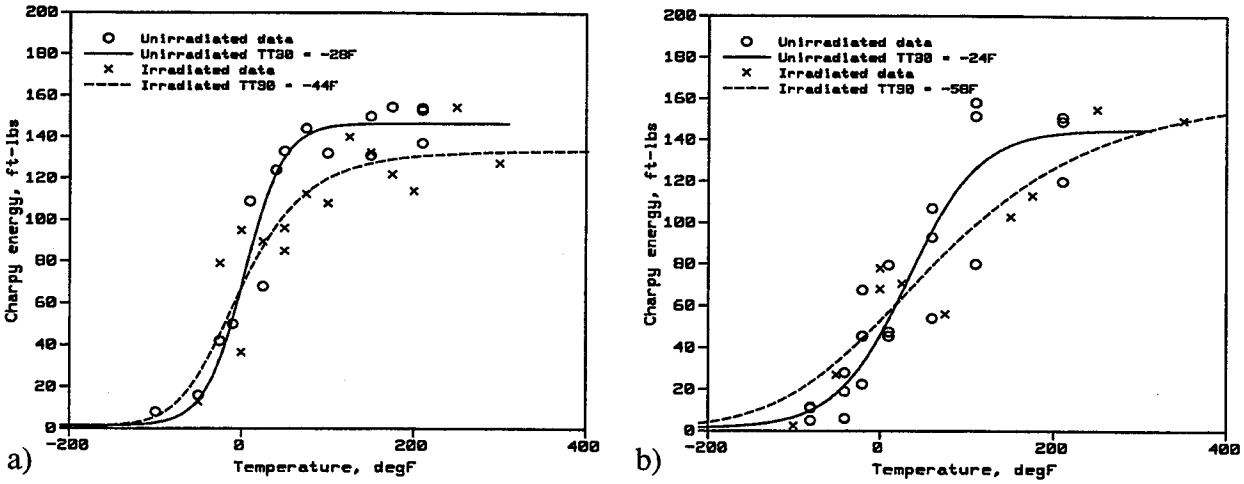

Figure 4.2 Examples where negative shifts were computed

considered credible (though not well understood), the negative shifts are questionable, since there is no reason to expect negative shifts from a mechanistic point of view. The examples in Figure 4.2 show two typical cases where computed negative shifts appear to be artifacts of Charpy data-fits; i.e., the raw Charpy data near 30 ft-lb show little or no shift, but the fitted *tanh* functions produce negative shifts.

There are two schools of thought on how to deal with negative shifts during model calibration. The first is to use the negative shifts - as computed - in the calibration data set. Arguments for this approach include 1) negative shifts are observed when testing low shift materials, 2) failing to consider residuals from negative shift data in the same way as the residuals from positive shift data would introduce a bias in the least squares fitting procedure, and 3) even if the negative shifts are not physically meaningful, they reflect the uncertainty in the data analysis procedure, which also affects the computation of positive shifts and the overall measures of quality of fit of the models (S_e).

The other school of thought is to set the negative shifts to zero during model calibration. Arguments for this approach are 1) negative shifts are not credible on a mechanistic basis, 2) the negative shifts appear to be data-fitting artifacts, since comparisons of raw irradiated and unirradiated Charpy data in these cases do not support the negative shift values computed (as shown in Figure 4.2); thus, the best estimate for these shifts is zero, 3) any bias introduced by reducing (not ignoring) residuals corresponding to negative shift data only affects near-zero shifts, which are of no practical consequence, and 4) the resulting nonconservative estimate of standard error, acknowledged as a drawback of this approach, could be addressed by calculating the standard error for high fluence or high shift subsets of data, rather than using the number for the overall calibration set.

During this project, models were calibrated using both approaches. The final models presented in this section were calibrated using the negative shifts as computed. Other models were calibrated with negative shifts set to zero, as in Appendix D (last entry) and Eason, et al., 1997. The differences in model predictions from the two approaches are small, as shown in Appendix D, and primarily evident in the low shift regime, as expected. The difference in overall standard error is less than 1°F; the difference in standard error is larger for forgings than for the other product forms.

4.3 TTS Model

In developing the TTS model, pattern recognition was used in the preliminary stages of analysis for analyzing variable independence and for preliminary models and guidance while developing the data base. Fluence, Cu, and Ni and two- and three-way interactions of these variables were found to be important for predicting TTS, consistent with prior research. Phosphorous showed weaker effects, with less certainty as to how important it would be in a model. Product form was found to be possibly important. The most interesting result from the transformation analysis is the plot for fluence shown in Figure 4.3. This plot should be interpreted as the effect of fluence on TTS, in non-dimensional standard deviation units. The expected effect of fluence is shown, given that average effects of Cu, Ni, P, product form, and T_c are approximately accounted for simultaneously. Figure 4.3 indicates that the shape of the trend with fluence is consistent with the mechanistic understanding; i.e., the

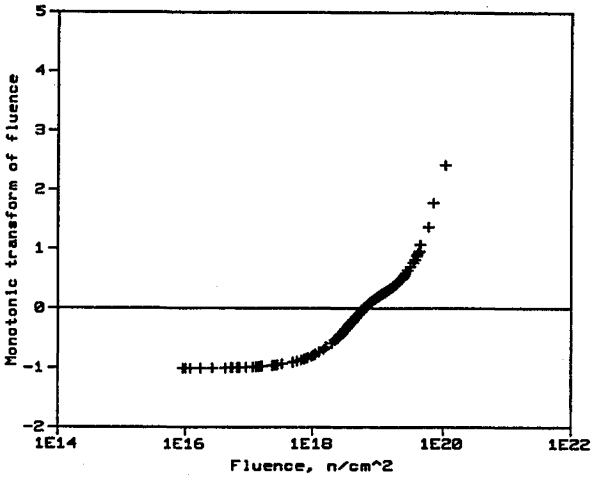

Figure 4.3 TAC plot for fluence effect on TTS

fluence effect is the sum of a saturating term (the "bump") and a term that increases with fluence.

Based on the two major hardening mechanisms, SMD and CRP, and the qualitatively consistent results from pattern recognition, the TTS model was constructed with two major terms. The first term, corresponding to SMD features, contains fluence to a power and no Cu effects, while the second term corresponding to CRP features reflects Cu and Ni effects and a saturating (*tanh*) form for fluence. Note that the *tanh* function is roughly equivalent to a Johnson-Mehl-type function $f(\phi t) = 1 - \exp[-k(\phi t)^n]$. With such a function, for normal diffusion-controlled growth of a fixed number of CRPs, the value of n is 1.5. The effect of phosphorus is incorporated in the SMD term for reasons discussed below.

Calibration of the model was carried out by fitting the entire data base. However, a separate analysis was carried out for low Cu (≤ 0.1 wt%) alloys to verify the presence of an independent SMD effect. In general, the function fitted to the low Cu data was close to that found for the matrix defect term using the entire data base. However, analysis of the low copper data and subsets of low copper data with the same heat irradiated to different fluences tended to yield a lower effective fluence exponent for the SMD term (~0.34) than found in the final data analysis (range from about 0.35 at 10^{18} n/cm^2 to 0.5 at 10^{20} n/cm^2). The reasons for this difference warrant further investigation.

At various stages of the analysis, the SMD term was held fixed while fitting the CRP term. This effort established that the presence of two terms, each involving fluence, did not lead to significant numerical difficulties. The potential difficulty would be trade-offs between fitting parameters in the fluence terms, where neither could be well-defined numerically. This occurred only to a limited extent; the power on fluence in the SMD term was reasonably stable whether fixed or allowed to vary as the second term was calibrated. This fortunate situation was not found with temperature or phosphorous in both terms. In this case, numerical trade-offs and unstable calibrations were observed. Thus, these variables were ultimately included only in the SMD term, where they appeared to be better determined and, in the case of irradiation temperature, better established by prior mechanistic studies.

Hundreds of different modeling forms were considered in the two-term form. The following TTS model was the best under the combined statistical, mechanistic, and engineering criteria used by the project team. It was calibrated to all available data with fluence greater than $9\text{x}10^{15}$ n/cm^2, considering all product forms together:

$$TTS = A\exp\left(\frac{1.906\text{x}10^4}{T_c+460}\right)(1+57.7P)f(\phi t) + B(1+2.56Ni^{1.358})\,h(Cu)\,g(\phi t) \qquad \textbf{(4-1a)}$$

where

$$f(\phi t) = \left(\frac{\phi t}{10^{19}}\right)^{\left[0.4449+0.0597\log\left(\frac{\phi t}{10^{19}}\right)\right]} \qquad \textbf{(4-1b)}$$

$$g(\phi t) = \frac{1}{2}+\frac{1}{2}\tanh\left[\frac{\log\left(\phi t+5.48\text{x}10^{12}t_i\right)-18.290}{0.600}\right] \qquad \textbf{(4-1c)}$$

$$h(Cu) = \begin{cases} 0, & Cu \le 0.072\ \text{wt\%} \\ (Cu-0.072)^{0.678}, & 0.072 < Cu < 0.300\ \text{wt\%} \\ 0.367, & Cu \ge 0.300\ \text{wt\%} \end{cases} \qquad \textbf{(4-1d)}$$

For welds $A = 1.10\text{x}10^{-7}$, $B = 209$; for plates $A = 1.24\text{x}10^{-7}$, $B = 172$; for forgings $A = 8.98\text{x}10^{-8}$, $B = 135$. *TTS* and T_c are in °F; *Cu*, *Ni*, and *P* are in wt%; ϕt is in n/cm^2 (E > 1 MeV), and t_i is in hours. All of the non-integer constants in Equation 4-1 were fitting parameters, determined by least squares. In this equation and throughout the report, logarithms are base 10. The standard error of the calibration data about Equation 4-1 is 23.0°F, using the 609 data points for which TTS and all

independent variables in the model were known; two outlier points which were greater than $4S_e$ from the model were omitted from the calibration data set, based on Chauvenet's criterion (see Appendix C). The goodness of fit of Equation 4-1 is shown graphically in Figures 4.4 through 4.6.

Figure 4.4 shows the predicted TTS versus actual TTS for the calibration data. Normalized plots are shown in Figure 4.5, using the same normalization procedure described in Section 3. (Note that there is no normalized plot for irradiation temperature, since a plot showing the variation in irradiation time at constant fluence is not realistic and could be misleading.) For the normalization procedure, the values of A and B were set to the plate values (the most common category, with $A = 1.23 \times 10^{-7}$, $B = 172$), and the median values for the independent variables were:

ϕt = 7.50×10^{18} n/cm^2
T_c = 545.0°F
t_i = 31861 h
Cu = 0.140 wt%
Ni = 0.600 wt%
P = 0.011 wt%

Residual plots for all modeling variables are shown in Figure 4.6. If any of these plots showed a trend, rather than a horizontal band of residuals, the authors should question the adequacy of the corresponding model term. But there are no indications of trends in the residual plots.

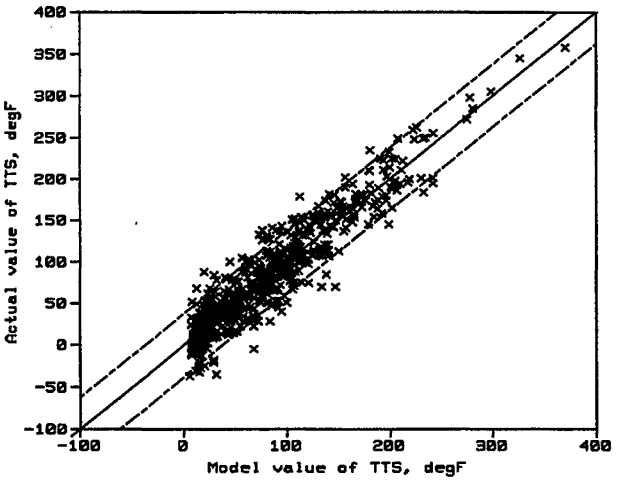

Figure 4.4 Predicted versus actual plot for TTS model

4.4 Discussion of TTS Model

4.4.1 TTS Model Form

The improved TTS model includes two major terms, with coefficients A and B, which correspond to the primary mechanisms occurring in the embrittlement process. The first term in Equation 4-1 is the stable matrix defect (SMD) term (which also includes the phosphide precipitation, PP, contribution), and the second term is the copper-rich precipitate (CRP) term. The SMD term is active regardless of Cu content, whereas the CRP term is zero for Cu below 0.072 wt%. The Cu effect also saturates for Cu above 0.300 wt%, a value determined by calibration but equal to the expected copper in solution following typical post-weld heat treatment. There is a term for an independent contribution of Cu plus a term describing a strong Cu-Ni synergism. The fluence effect on copper precipitation saturates, but the fluence effect in the SMD term continues to increase with increasing fluence. The model also accounts for the effects of irradiation time (and, indirectly, flux, as discussed below), coolant temperature, and product form. The treatment of these variables is in reasonable accord with current understanding of embrittlement mechanisms.

The form of the model appears somewhat complex, in large part because it treats both overall trends and trends that are only important in subsets of the data. For instance, the power on fluence in the matrix defect term depends on fluence, because if a constant power is used instead, the fit is biased in the unconservative direction at high fluence ($\geq 5 \times 10^{19}$ n/cm^2). The irradiation time term has almost no effect overall, but it does affect the estimated shift of data with flux less than 10^{10} n/cm^2/s, as discussed in Subsection 4.4.5. Another example is the product form effect. The overall fit is similar for plates and welds, but the forging data are overpredicted if product form effects are ignored. These effects are discussed in greater detail in Appendix D, where simpler models without these terms are described.

The relative contributions of the SMD and CRP terms, and the interaction of fluence and chemistry variables according to Equation 4-1, are illustrated in Figures 4.7 and 4.8. The figures show the overall embrittlement versus fluence (solid curves) along with the SMD (long dash) and CRP (long-short dash) contributions for various levels of Cu, Ni, P, and T_c. To generate these curves, the values of A and B for plates and median values of all model variables not specified in the plot titles were used.

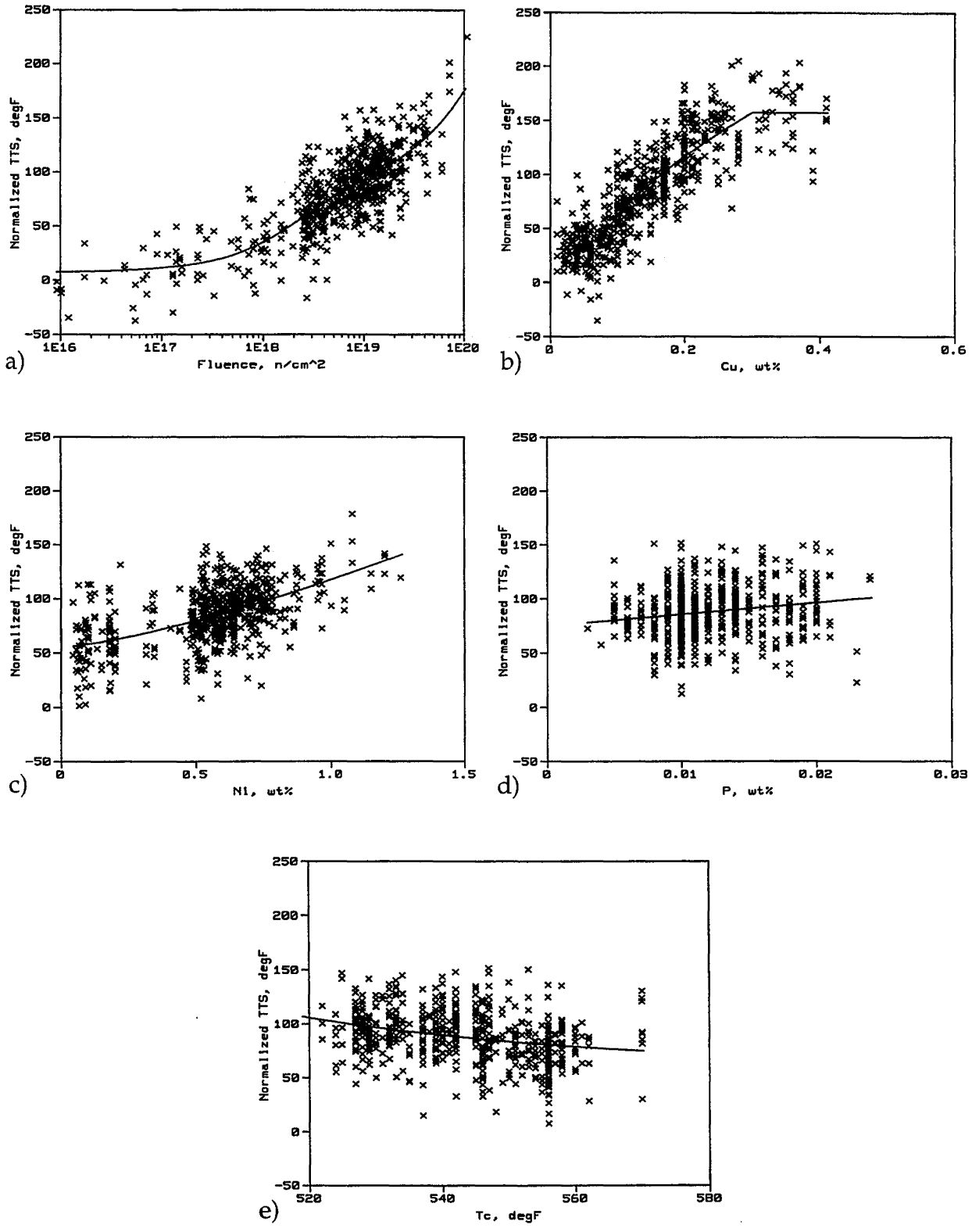

Figure 4.5 Normalized plots for TTS model variables

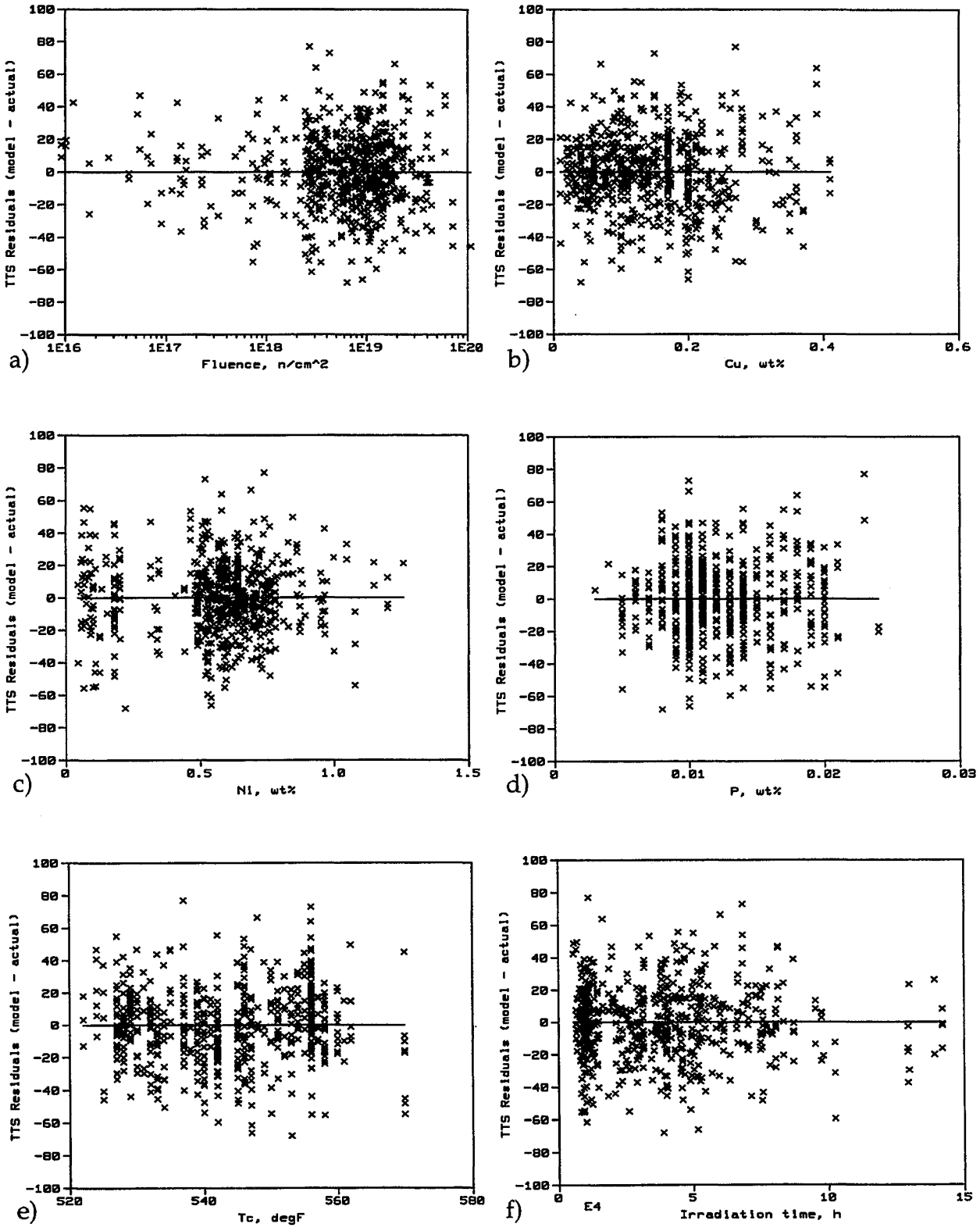

Figure 4.6 Residual plots for TTS model variables

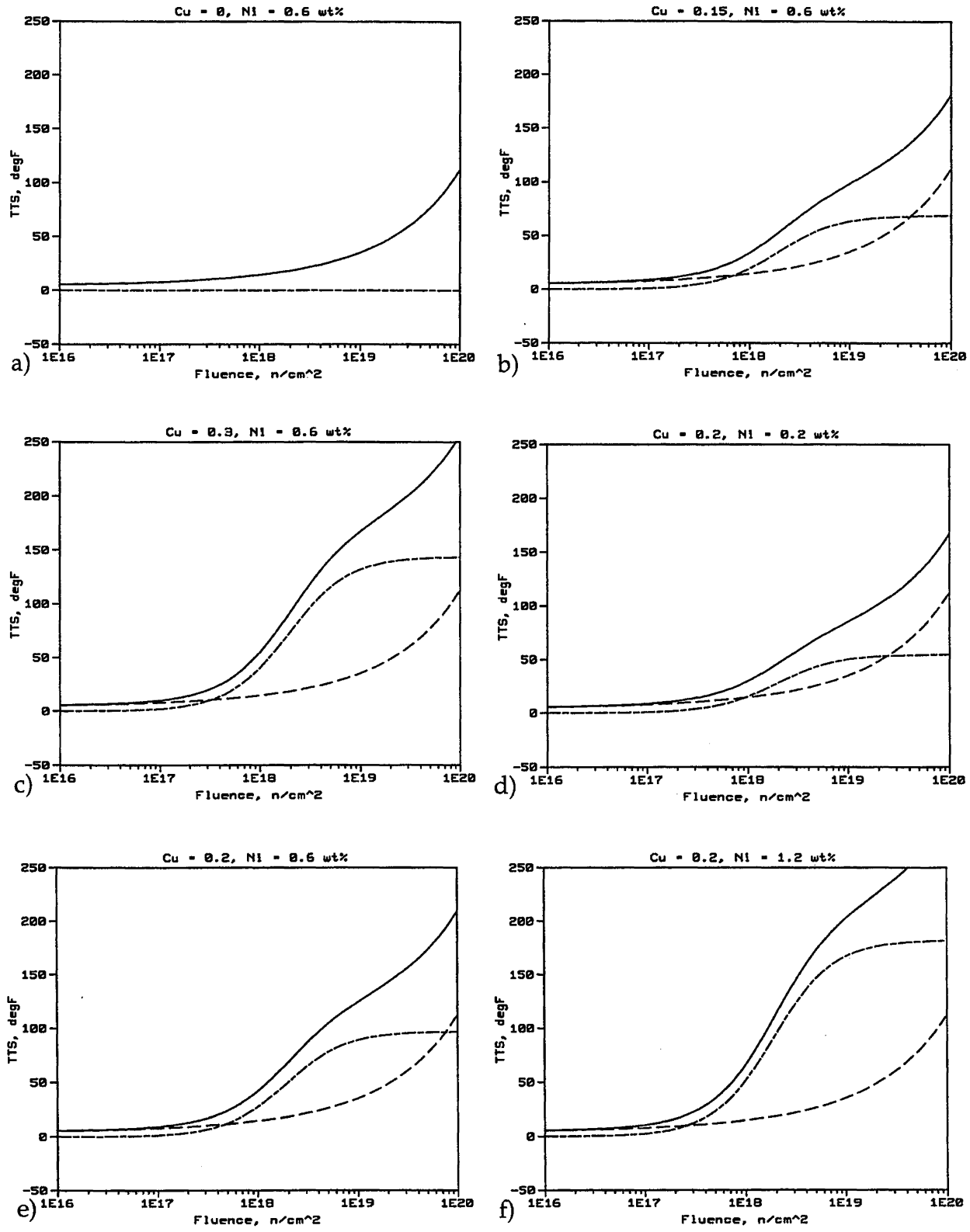

Figure 4.7 Contributions of SMD and CRP terms of TTS model to overall embrittlement for various Cu and Ni values

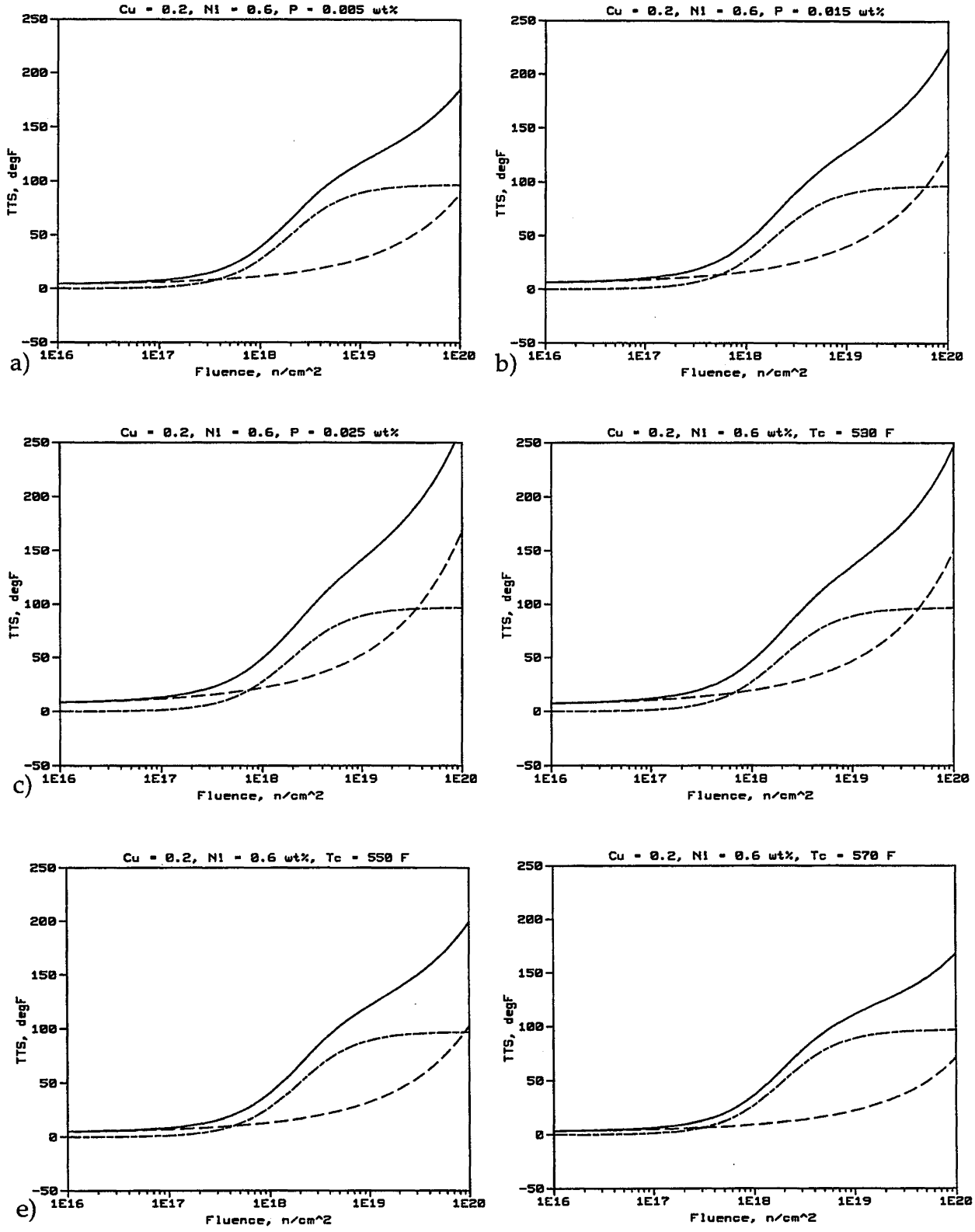

Figure 4.8 Contributions of SMD and CRP terms of TTS model to overall embrittlement for various P and T_c values

4.4.2 Product Form Effects and Comparison to RG1.99/2

The current RG1.99/2 contains separate models for welds and base metals. The present analysis suggests that plates and welds are similar but different from forgings. Plate and weld materials exhibit the same trends in the independent variables, with a somewhat different magnitude and relative importance of matrix defect and copper-rich precipitation mechanisms. Forgings also exhibit similar variable trends (within the rather limited range of composition), again with a different relative importance of the two mechanisms. But forgings also exhibit an overall offset (lower shifts) relative to welds and plates. It should not be surprising that the three types of materials would exhibit some differences, since their microstructures and, particularly in the case of forgings, their compositions (e.g., lower Mn, higher Cr) are different.

Because of the observed differences in importance of the two mechanisms and the overall consistency in variable trends, Equation 4-1 contains two coefficients (A and B) that depend on product form (plate, forging, or weld), but the overall trends in other variables were determined by the combined data set. Figure 4.9 shows predicted versus actual plots for subsets of the calibration data containing plates, forgings, all welds, and Linde 80 welds; residual plots for plates, forgings, and welds are shown in Figures 4.10, 4.11, and 4.12, respectively.

The SMD coefficient A is larger for plates than welds, while the CRP coefficient B is smaller for plates than welds. Thus, while the overall relative sensitivity depends on both metallurgical and irradiation variables, these offsetting effects generally produced slightly higher shifts for welds versus plates. However, both the SMD and CRP coefficients for the forgings were much less than for plates and welds, indicating an overall reduced irradiation sensitivity for forgings. While a number of factors may be responsible for the lower sensitivity of forgings, including limitations of the data base itself, one important factor is believed to be the lower manganese content (~0.7% versus ~1.4%).

The new model is a significant improvement over the RG1.99/2 model, as indicated by reduced scatter about the model. Standard deviations of selected data subsets about Equation 4-1 are compared to standard deviations about the RG1.99/2 model in Table 4.1. These standard deviations were used to construct the bounds in Figure 4.9 so that 90% of the data in each subset should be inside the bounds, assuming a normal distribution of residuals. In all cases except forgings, the improvement in standard deviation for the new model relative to RG1.99/2 is statistically significant at $p \leq 0.02$ in F tests. The difference in standard deviations for forgings is significant at $p \leq 0.09$.

It may seem that the fit to the subsets could be improved further if other fitting parameters in Equation 4-1 were recalibrated for each subset of data. However, that approach is not practical given the limited ranges in variables for all subsets except welds. An alternative model is given in Appendix D where the upper limit on copper was allowed to be different for Linde 80 welds and all other welds. For forgings, the small range in Ni and Cu is illustrated in Figure 4.11b and 4.11c; one could not expect to calibrate credible Cu and Ni effects using that subset of data. And none of the plate materials have high copper. Yet Figures 4.10 through 4.12 show that the model calibrated to all data correctly captures trends in all modeling variables for the plate, forging, and weld subsets, so that recalibration to subsets is not needed.

Table 4.1 TTS model: S_d for subsets of data

Data set	#pts	S_d about Eq. 4-1	S_d about RG1.99/2
Base Metals	424	21.6°F	25.5°F
Plates	323	22.1°F	26.4°F
Forgings	101	19.9°F	22.8°F
Welds	185	25.0°F	29.1°F
Linde 80	53	23.5°F	36.1°F
All Materials	609	S_e = 23.0°F (18 dof)	26.6°F

4.4.3 Effect of Cu, Ni, and P

The treatment of Cu and Ni has several features worth noting. First, the lower limit on Cu might be attributed to an effective nucleation limit for producing CRPs capable of significant hardening (Odette, 1995). In addition, the subtraction of this threshold level at all Cu levels is likely due to a combination of (a) sequestering Cu in sulphides prior to irradiation (Fisher et al., 1985; Williams and Phythian, 1996) and (b) the effect of non-equilibrium solubility limits of Cu due to three contributions, including the interface, crystal structure, and coherency strains to the free energy, which are important for the nanoscale CRPs (Odette, 1995). The fitted lower limit of 0.072 wt% is close to the nominal value of about 0.1 wt% established by both microanalytical studies and other mechanical property trends (Odette and Lucas, 1988, 1996).

The effective upper limit on Cu of around 0.3 wt% is primarily due to pre-precipitation of Cu during stress relief treatments at around 600 to 630°C. This effect has

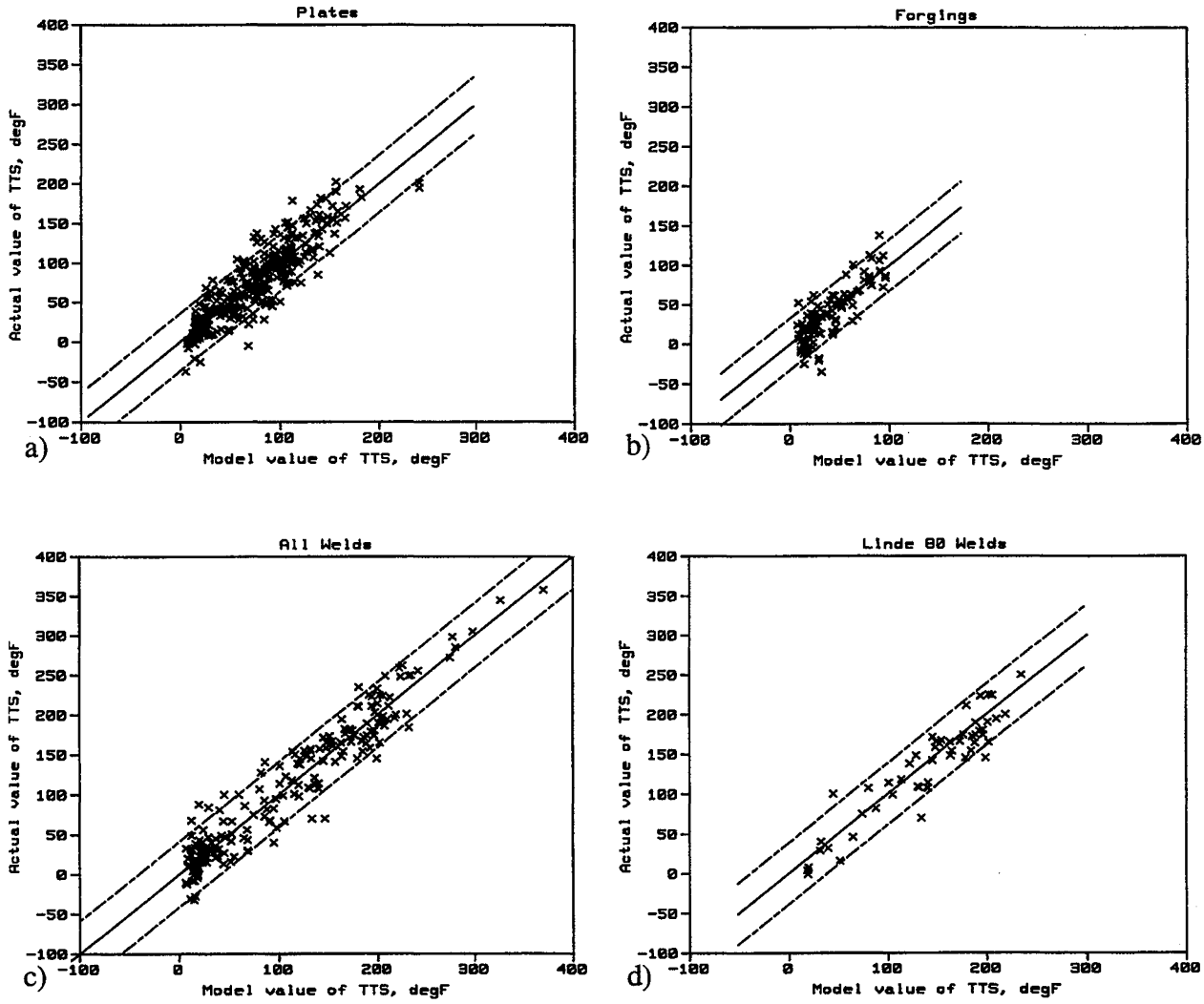

Figure 4.9 Predicted versus actual plots for subsets of TTS data

been established by both microanalytical studies and mechanical property trends (Odette, 1983, 1995, 1997; Odette and Lucas, 1986b, 1988, 1996, 1997; Buswell et al., 1993; Williams and Phythian, 1996; McElroy and Lowe, 1996). Indeed, some of these results suggest even lower limits of about Cu = 0.25 wt%, and a few atom probe studies yield even lower values of less than 0.15% (Miller et al., 1992). Some of the differences may be due to factors such as the effect of higher Ni keeping more Cu in solution during heat treatments (Odette and Lucas, 1986b, 1988, 1990, to be published; Williams and Phythian, 1996) and differences in stress relief times, temperatures, and cool-down rates. Heterogeneous Cu distributions and effective resolution limits may be responsible for the lower values found in some of the atom probe studies. Overall, the upper limit on Cu of 0.3 wt% as found in the data fit, appears to be the most credible value at this time. However, use of this limit for nominally higher bulk levels of Cu should be justified based on demonstration of typical post-weld heat treatments and alloy nickel content less than around 0.8 wt%.

Inclusion of a phosphorous contribution to the matrix defect term did not result in a large reduction in the overall standard error. However, this term helped to center the data and removed an apparent bias in the P residuals. Further, a phosphorous effect has been found in many other data correlations as well as in single-variable experiments (Petrequin, 1996; Jones and Buswell, 1988; Williams and Phythian, 1996; Odette et al., to be published). The phosphorous contribution found in this study is well within the range of the P effects in a recent compilation of published TTS correlation equations (Petrequin, 1996).

The absolute contribution of P in Equation 4-1 is not

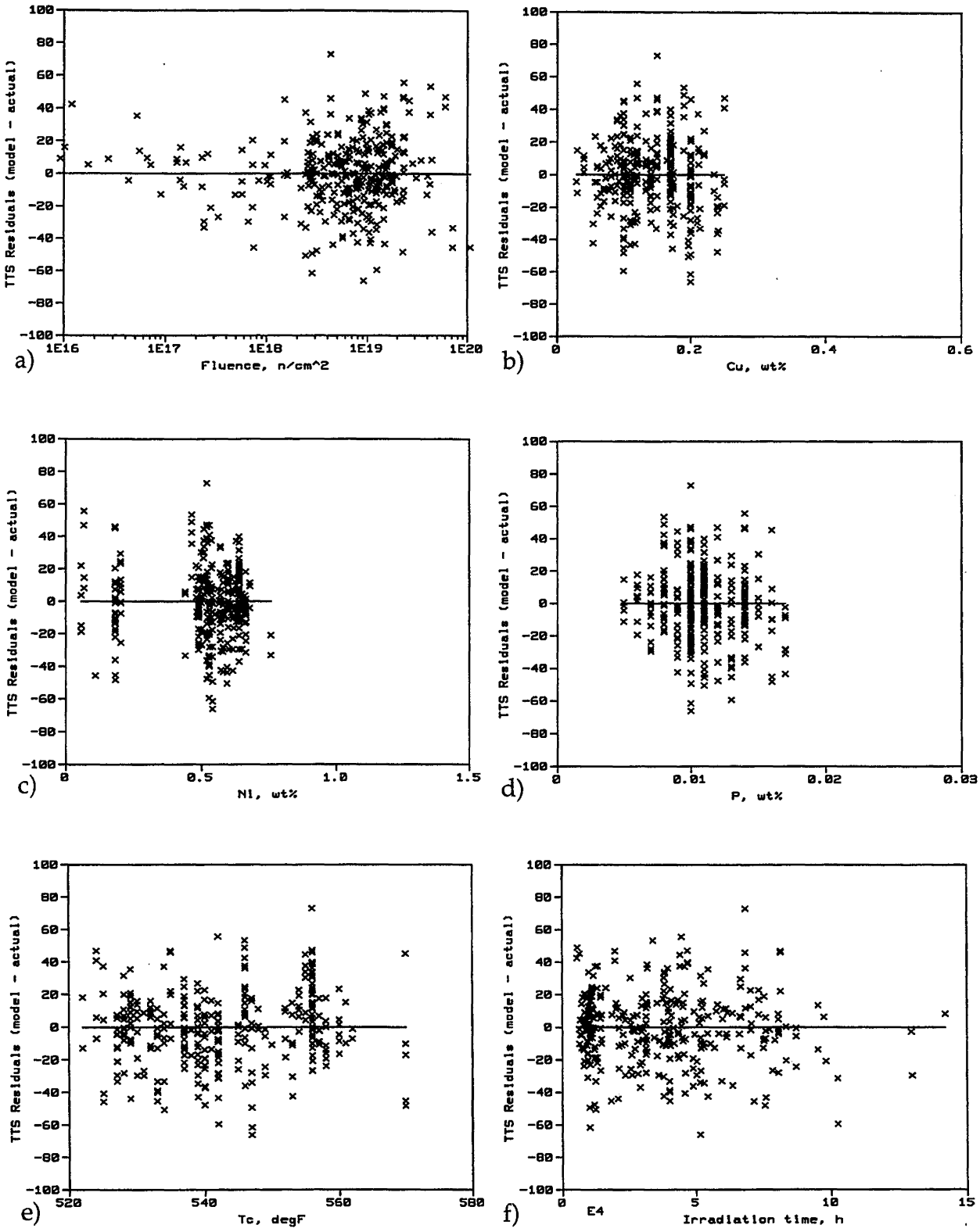

Figure 4.10 Residual plots for plate subset of TTS calibration data

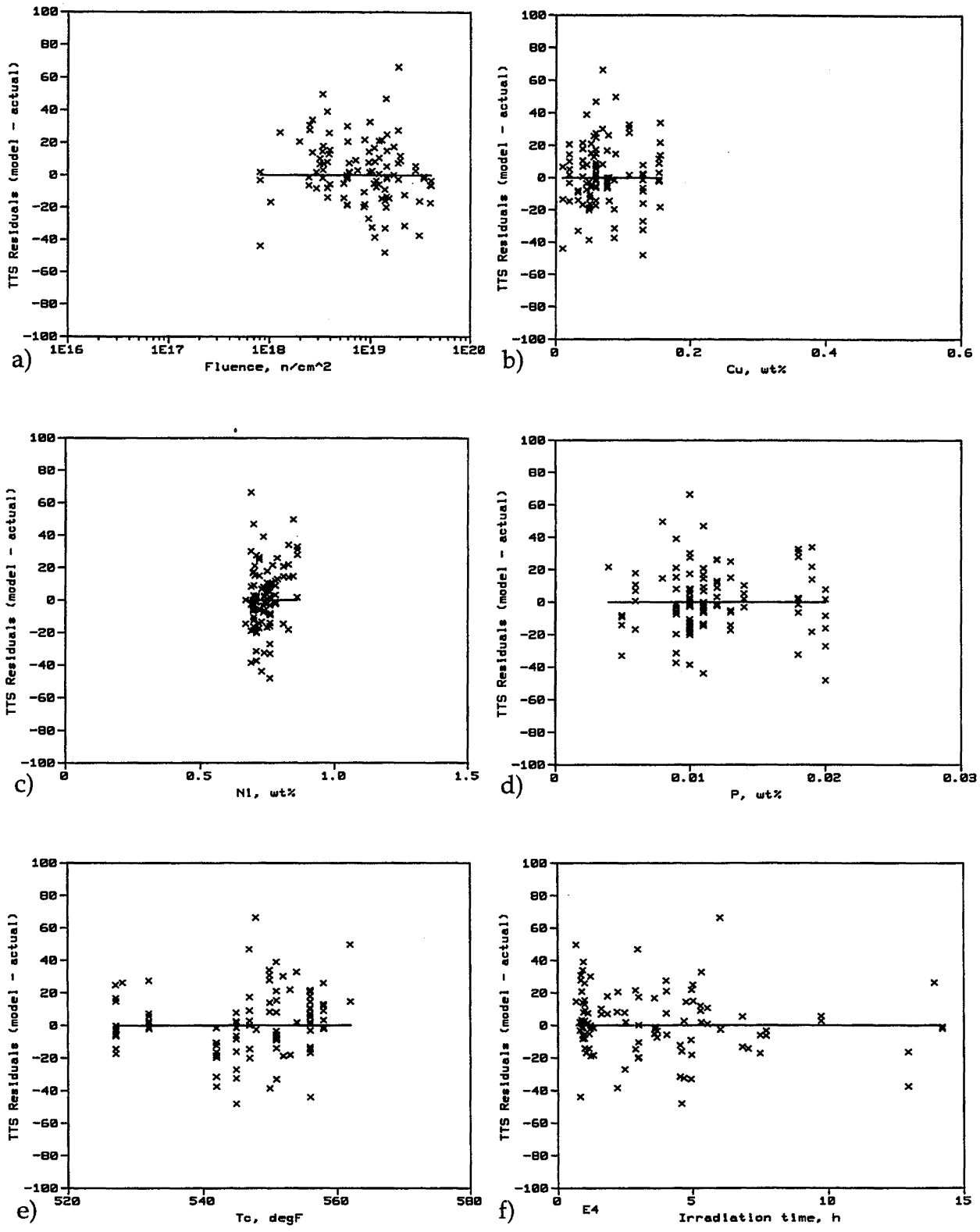

Figure 4.11 Residual plots for forging subset of TTS calibration data

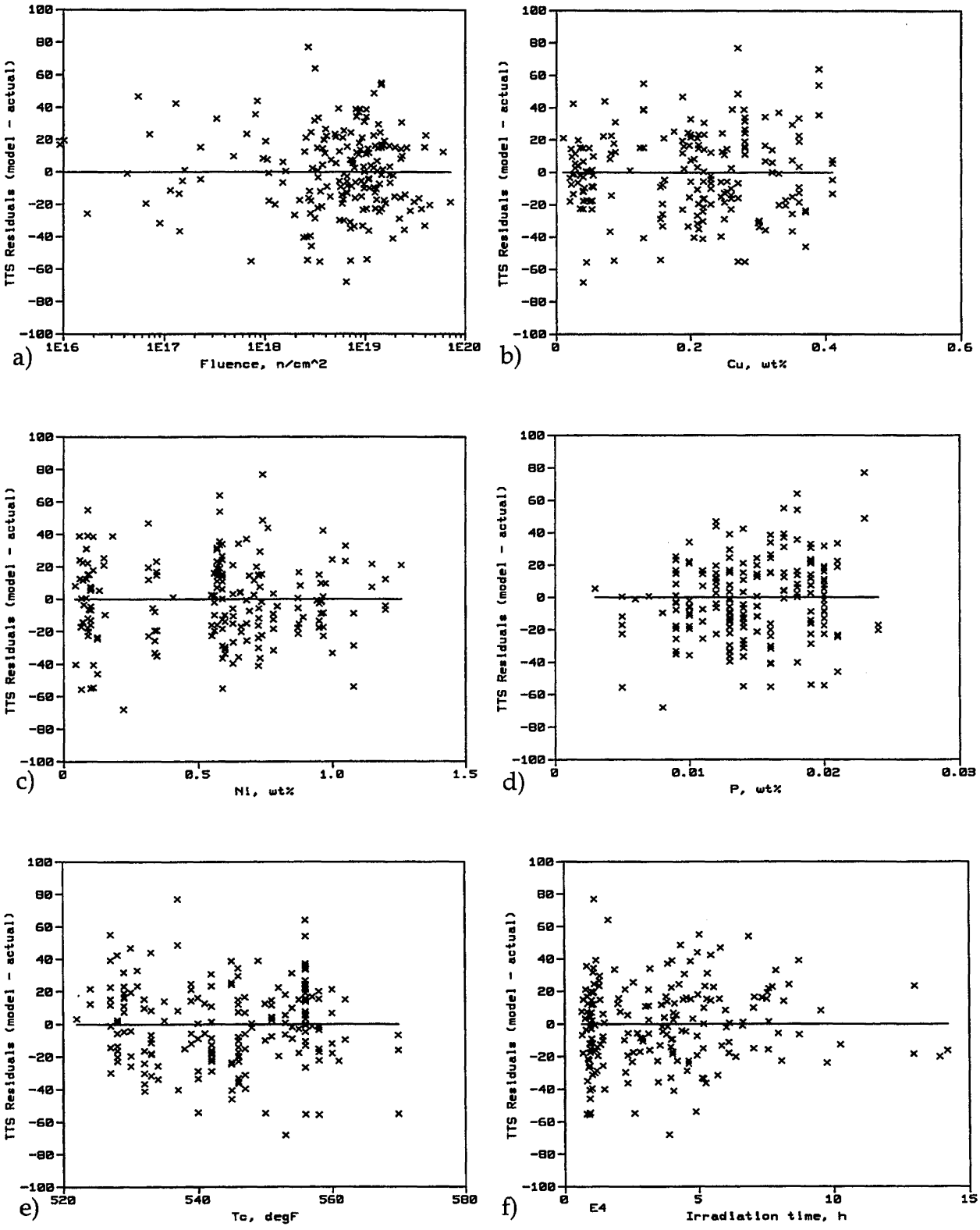

Figure 4.12 Residual plots for weld subset of TTS calibration data

reduced at high Cu, as other studies have suggested (Jones and Buswell, 1988). Further, the basis for treating the fluence and temperature dependence of the PP contribution as part of the SMD term is not apparent. However, this approach provided stable numerical solutions in the nonlinear least squares fits. An alternative model including an explicit interaction between Cu and P was considered, as discussed in Appendix D.

The Cu, Ni, and P effects calibrated to the surveillance data are strongly supported by other data not used in fitting. Comparisons against test reactor data, French surveillance data, and single-variable mechanistic experiments indicate good agreement, as discussed in detail in Section 5.1.

4.4.4 Effect of Irradiation Temperature

Test reactor studies have clearly established an increase in TTS with decreasing irradiation temperature on the order of 0.4 to 1 degree per degree (Odette and Lucas, 1986a, 1986b, 1996; Jones and Williams, 1996). It was determined during preliminary analysis that the melt-wire irradiation temperatures reported in the PR-EDB showed no correlation to TTS. However, coolant temperatures provided by members of the ASTM E10.02.02 subcommittee did have the expected effect. Figure 4.5e shows that the effect of reactor coolant temperature in Equation 4-1 is approximately 0.6 degrees more shift per degree lower T_c at median values of the variables. The TTS correlation attributes the temperature dependence to the stable matrix defect term, consistent with current understanding. At higher phosphorous and fluence the temperature effect is larger, and at lower values the effect is smaller. The calibrated temperature effect is in very good overall agreement with correlations based on independent test reactor data, as discussed in Section 5.1.

4.4.5 Effect of Irradiation Time (and Neutron Flux)

A time-at-temperature effect has been incorporated into Equation 4-1, yielding an "effective fluence" that is the actual fluence plus $5.48 \times 10^{12} t_i$, where t_i is in hours. Given the relationship among fluence, irradiation time, and neutron flux, the irradiation time effect can also be represented approximately as a flux effect, yielding an adjusted fluence equal to $\phi t(1+1.52 \times 10^9/\phi)$, where ϕ is in $n/cm^2/s$. The effect of irradiation time is only apparent at low flux, where it increases the estimated TTS by about 7.5°F, as shown in Figure 4.13. This effect (whether represented in terms of flux or irradiation time) produces a statistically insignificant reduction in terms of the overall standard error (from 23.02 to 22.95°F). However, its inclusion does provide an improvement in the centering of the residuals at the low flux levels ($<10^{10}$ $n/cm^2/s$) that are characteristic of BWR surveillance irradiations.

It is known that at flux levels greater than about 10^{12} $n/cm^2/s$, hardening and embrittlement may increase or decrease with flux depending on the combination of Cu and Ni, irradiation temperature and other variables (Odette et al., 1993). This effect is mediated by thermally unstable matrix defects, which act both as point defect sinks, retarding CRP evolution, and as weak hardening features (Odette et al., 1993; Odette, 1995, 1997; Odette and Lucas, 1997a, 1997b). The effect of flux is expected to be small in the regime between 10^{10} and 10^{12} $n/cm^2/s$ (Odette, 1995, 1997; Odette and Lucas, 1986a, 1986b, 1997a, 1997b; Williams et al., 1988; Williams and Phythian, 1996), consistent with the present results. However, at much lower fluxes the possibility of time-at-temperature thermal aging contributions to hardening and embrittlement has been proposed (Fisher et al., 1985, 1987; Williams et al., 1988; Odette and Lucas, 1997c).

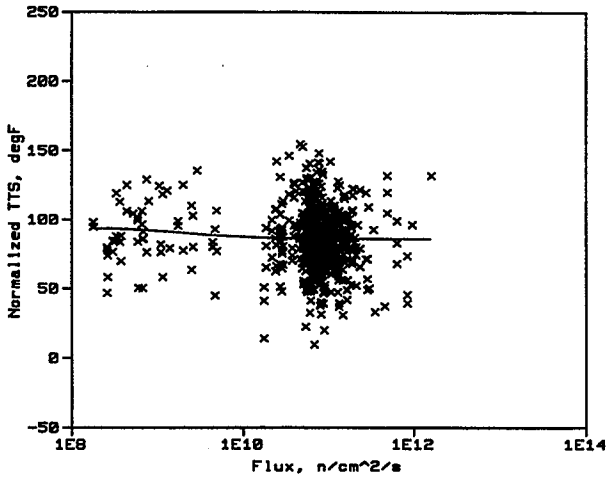

Figure 4.13 "Flux effect" for TTS model

It must be noted that the irradiation time (or flux) effect is partly confounded with fluence, since all of the low-flux data are also low fluence. It is not likely that this effect is strongly confounded with reactor type, although all the low flux points are from BWRs, because the high flux data include some BWR data as well as PWR data. (See discussion in Sub-section 4.4.7.)

Note that the effect of irradiation time or flux may be more important than is evident from the current data base. Although a weak effect overall, flux may be more important as the low-flux plants reach higher fluences

and for subsets, such as high Cu - high Ni data, which are not well represented in the data base (Odette and Lucas, 1997b).

4.4.6 Effect of Neutron Fluence

The fluence effect in the CRP term saturates, while the fluence effect in the SMD term continues to increase with fluence. In fact, the power on fluence in Equation 4-1 increases with fluence. As discussed above, results of most previous research indicated that a constant power on fluence should be about 0.5, while analysis of low Cu data from the current analysis data base yielded a value closer to 0.34 wt%, as discussed further in Appendix D. The fluence-dependent power in Equation 4-1 ranges from 0.27 to 0.50 over the fluence range 10^{16} - 10^{20}, which is quite consistent with the range of 0.34 to 0.5 from low Cu data and the other research results.

The tendency for the exponent on fluence to increase with fluence, and for a single exponent fitted to the whole set to be lower than expected, may be unique to this data base. The increase in the exponent on fluence could in part be due to confounding with flux, since high fluence generally correlates with higher flux. However, TTS in the low-Cu French surveillance data increases with the square root of fluence (Petrequin, 1996). This half-power fluence dependence has also been found for a wide range of mild and low alloy steels (Fisher et al., 1985; Jones and Williams, 1996), and it is also predicted by simple hardening models if the number of dispersed obstacles increases in proportion to fluence. Thus it is perhaps most surprising that the fitted exponent is less than 0.5 at low fluence. A complication in some cases is that various studies and data sets sample different fluence regimes; hence, the increase in exponent with fluence may reflect a real underlying physical effect that was not seen over limited fluence ranges. For example, new hardening features may develop only at high flux or high fluence or after a prolonged incubation period. There are other possibilities, and the issue remains to be fully resolved. However, as a practical matter, an exponent in the range of about 0.5 is consistent with a wide range of data and is required in the correlation model to avoid nonconservative bias for fluence greater than about $5x10^{19}$ n/cm^2. The present model provides this exponent of 0.5 at high fluence by allowing the exponent to vary with fluence.

Test reactor data trends and microstructural data (Williams and Phythian, 1996; Odette and Lucas, to be published) suggest that the fluence dependence of the CRP contribution is a function of the Ni content. When normalized by the saturation contribution (which is, of course, much larger for high Ni), addition of Ni has the effect of shifting the saturating function up in fluence and perhaps broadening it, producing a more gradual approach to saturation. Theoretical considerations and test data suggest that high Cu has the opposite effect in shifting the saturating function to lower fluence (Odette and Lucas, 1986a, 1986b, 1997; Lucas et al., 1985). Correlations with a Ni term in the fluence function did indeed produce a small, statistically insignificant effect in the right direction, although similar agreement could not be found in the case of Cu. Model variations incorporating a Ni term inside the fluence *tanh* function are discussed in Appendix D along with the reasons for not including the effect in Equation 4-1 at this time.

4.4.7 Effects of Variables Not in Equation 4-1

The normalized and residual plots (Figs. 4.5 and 4.6) show how well the TTS model accounts for effects of the variables that are used in the model. Residual plots for variables not included in the model also may be used to help assess whether or not the model is missing some variable effects. Such plots are discussed in this section for variables of potential interest.

Both BWR and PWR data were used in model calibration, so an important question is whether there is a difference between the two reactor types that is not reflected in Equation 4-1. As discussed above, flux is indirectly accounted for in the model by the irradiation time term; this is confirmed in Figure 4.14, which shows no trend in the residuals about zero when plotted against neutron flux. Figure 4.14a shows residuals about Equation 4-1 versus flux for the BWR data used in calibration; "typical BWR data" are shown with different symbols than "non-representative BWR data." The latter term, used by Tom Caine (GE Nuclear Energy), refers to data from high flux locations on the core shroud in Dresden and Quad Cities plants and data from high flux BWR/1 reactors, e.g., Big Rock Point and Humboldt. Because of these unusual situations, there are both high and low flux data for BWRs. Figure 4.14b shows residuals for the PWR data. Statistics on the residuals were computed, and they verify that BWR and PWR data are equally well represented by the TTS model. The average offset of the residuals for BWR data is 0.59°F and the average offset for PWR data is 0.12°F, with standard deviations of 25°F and 22°F, respectively. The average difference is less than 0.5°F, neither statistically nor practically significant. Based on these statistics and the reasonable distribution of residuals, the authors conclude that the model in Equation 4-1 adequately captures embrittlement-related differences, if any, between BWR and PWR data.

The increase in hardening and embrittlement due to manganese (Mn) is apparently accounted for by the dependence of the SMD and CRP coefficients on product

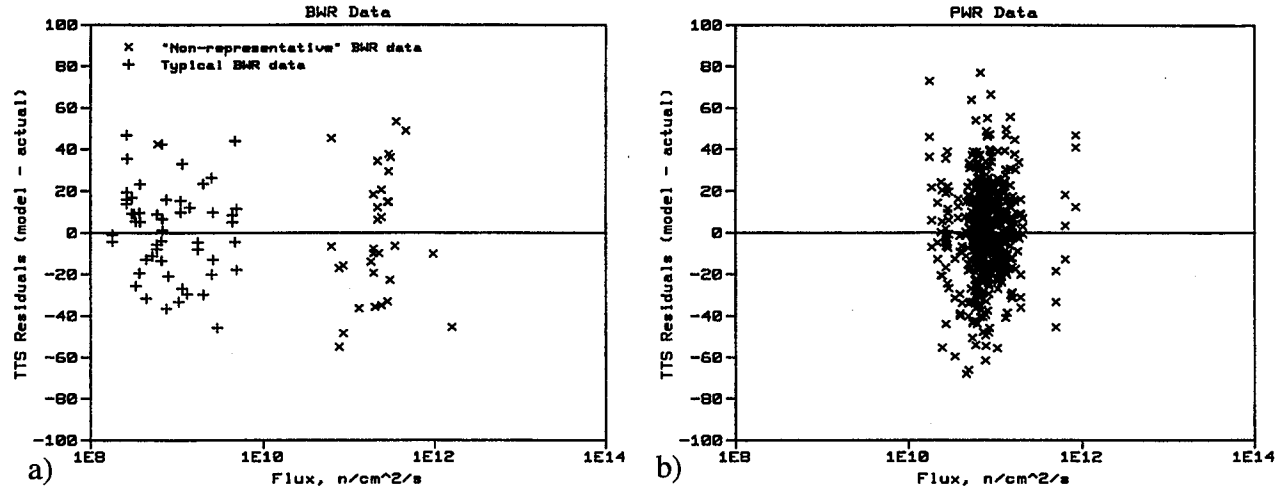

Figure 4.14 BWR and PWR data versus flux for TTS model

form. Figure 4.15 shows the residuals of the calibration data about Equation 4-1 plotted versus Mn. The residuals arising from low Mn points, which are from forgings, are evenly distributed for the final TTS model, suggesting that the Mn effect is implicit in Equation 4-1. However, a similar model with no dependence on product form shows a poor fit to the low Mn data. Attempts to account for the product form effect using Mn in the model were less successful, exhibiting unstable numerical tradeoffs with the Ni and P terms. Thus in practice it appears better to model the product form, rather than a manganese effect directly.

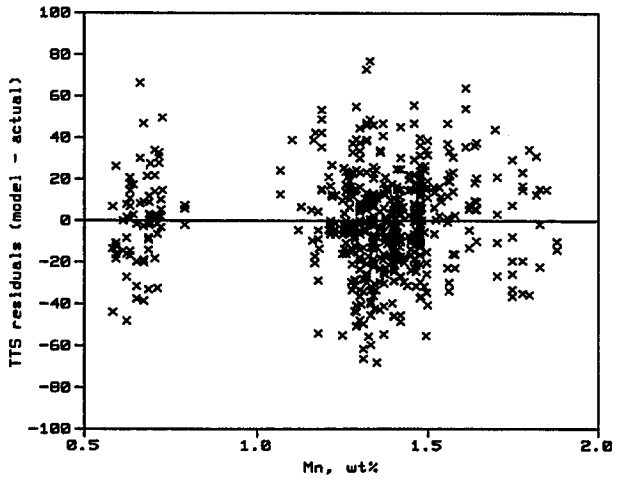

Figure 4.15 Mn residual plot for TTS model

4.4.8 Alternative Model Forms

It would be impractical to list all the model forms considered during this project. Instead, several alternative model forms that were considered to varying degrees while making the final selection of the TTS model are shown in Appendix D. Many different TTS models provided essentially the same standard error; the various models agreed in data-rich regions, differed somewhat in subsets and at the extremes of variable ranges and, in some cases, extrapolated quite differently.

The primary purpose of listing the models in Appendix D is to show the effects of simplifying or increasing the complexity of Equation 4-1 and to discuss the reasons for the choices that were made. It should be emphasized, however, that the authors recommend using Equation 4-1 wherever possible (i.e., wherever Cu, Ni, P, T_c, ϕt, and t_i are known). *The models in Appendix D have not been investigated and checked to the same extent as Equation 4-1 with respect to convergence from alternative initial estimates, robustness over the range of variables, reasonableness compared to other data not used for fitting, and quality of fit within subsets.*

The alternative models and their strengths and weaknesses are discussed in Appendix D, to the extent they have been investigated. The model equations and selected plots are presented, with comments on the regions of the data base where differences from Equation 4-1 are noted. None of the models is significantly different statistically from Equation 4-1, based on overall measures of goodness of fit such as S_e, but there are differences in subsets or local regions of the data base.

4.4.9 Estimating Irradiated TT_{30} When Unirradiated TT_{30} is Unknown

Transition temperature shift is related to the final, irradiated transition temperature by the simple mathematical equation:

$$TT_{i30} = TT_{u30} + TTS \quad (4\text{-}2)$$

If the actual TT_{u30} is not known, an estimate must be used in order to estimate the irradiated TT_{i30}. Table 4.2 shows averages and standard deviations of the raw TT_{u30} data from the analysis data base for various subsets of data, depending on product form and specimen orientation. Also shown is the standard deviation of each subset of data about Equation 4-2 using the corresponding average TT_{u30} and TTS estimated from Equation 4-1. Attempts were unsuccessful to model TT_{u30} as a function of other variables, such as chemistry components, to improve on the use of simple average estimates.

Table 4.2 Average TT_{u30} and S_d

Data set	Orient	Avg TT_{u30}	S_d TT_{u30}	S_d about Eq. 4-2
Plates	LT/LS	6°F	34°F	36.2°F
	TL/TS	15°F	21°F	34.9°F
Forgings	LT/LS	-42°F	24°F	25.8°F
	TL/TS	-8°F	29°F	31.3°F
Welds	TL/TS	-34°F	33°F	38.1°F

For reference, when the actual TT_{u30} values are used in Equation 4-2, the standard error of TT_{i30} over the full calibration data set is 23.0°F; standard deviations for subsets of the data are 22.1°F for plates, 19.8°F for forgings, and 25.1°F for welds. Thus the uncertainty is always larger if the averages are used for TT_{u30}, than if the actual point by point values are used, as expected.

5 VALIDITY OF MODELS

5.1 Comparisons with Other Data

The validity of the model can be tested by comparing it to independent data not used in the statistical fit. For example, comparisons against surveillance data from other countries or test reactor data are useful. The effect of key variables predicted by the model also can be tested by comparison with experimental results involving well established conditions, precise measurements, and controlled changes in the variable or variables in question while all other conditions are kept constant. Finally, comparisons of the model with mechanical property data that can be interpreted in terms of the irradiation-induced nanostructures and nanostructural evolution processes provide a very strong fundamental basis for confidence in the model. This section presents several comparisons with data not used for fitting. In carrying out such comparisons, the independent data generally have been restricted to the applicability limits of the model; this restriction is particularly important for flux.

Figure 5.1 compares the model to the result of the NRC-sponsored Pool Side Facility (PSF) Experiment conducted at the core face of the Oak Ridge Research Reactor (Hawthorne and Menke, 1984). This study involved 290°C irradiations of six steels in prototypical surveillance positions, as well as quarter and half thickness locations in a simulated pressure vessel wall at fluxes less than about 10^{12} n/cm^2. The fluences are based on displacements-per-atom converted to equivalent fluence (E > 1 MeV) values for a typical surveillance spectrum. The Cu, Ni, and P contents and alloy type and product form are given in Figures 5.1a - f. Agreement is reasonable for the ASTM A302B and A533B HSST03 reference plates, an EPRI weld (EC) and a low-Cu A508 Class III forging (Figures 5.1a, b, d, and f). For the limited range of data, the fluence dependence is well represented by the model. Agreement is not good in the case of a very high, 1.58% Ni weld (Figure 5.1c), where the model significantly underpredicts the high fluence shifts. Note that in this case the PSF data have been supplemented with a data point from another low flux irradiation (Williams et al., 1988). However, this weld had an unusual heat treatment and, in any event, falls outside the Ni limits of applicability of the model. The model significantly overpredicts the shifts in an A508 Class II forging with relatively low Cu and high Ni (Figure 5.1e); however, even in this case, the highest fluence data point is approaching the model prediction. Overall the comparison with the PSF data lends considerable support to the model.

Figure 5.2 compares the SMD part of Equation 4-1 and the UKNE SMD model predictions to French low-Cu (<0.07%) plate and weld surveillance data, for irradiations at 286°C (Petrequin, 1996). The data have been adjusted to a common P level of 0.008%. This was done by using linear least squares to fit the P dependence of measured TTS divided by the square root of fluence. The P coefficient found in this analysis was 870°C/%P, reasonably close to the value from Equation 4-1 of about 600°C/%P for plate and 540°C/%P for welds. The model predictions fall towards the lower side of the data scatter. This may be due in part to the higher energy level (41 ft-lb or 56 J) of Charpy indexing in the French data (Brillaud et al., 1996). However, Figure 5.2 shows that the fitted model predictions for the SMD term of Equation 4-1 also fall somewhat below a recent SMD curve based on analysis of a variety of steels and irradiation conditions (Jones and Williams, 1996). Nevertheless, the similarity of the predictions and the independent data trends generally support the treatment of the SMD term in Equation 4-1.

Figure 5.3 compares the model predictions for the effect of irradiation temperature (shown as solid lines over the range of the data base) to the results of an analysis of test reactor data (Odette and Lucas, 1996). The model predictions are for 0.0125%P at 10^{19} n/cm^2. The various treatments of temperature have been normalized to 286°C for Cu = 0.05 and Cu = 0.3 wt%. At low Cu, the agreement is excellent, supporting the temperature dependence of the SMD term in Equation 4-1. At high Cu, the straight line is an interpolation of test reactor results between 260 and 316°C, which suggests a somewhat greater temperature sensitivity. The trilinear curve is based on additional low flux data at intermediate temperatures between 260 and 316°C. These results suggest a minimal temperature sensitivity in the temperature interval between about 275 and 305°C. Over the temperature range of the surveillance data base, the model in Equation 4-1 essentially splits the difference, yielding an average effect of about 0.6 degrees per degree. Other recent work yields very similar results (Jones and Williams, 1996).

Figure 5.4 compares the fitted coefficient of the P term in the model to results from controlled test reactor irradiations of split melt A533B plate-type alloys with P levels from 0.005 to 0.04 wt% at Cu contents of both 0.0 and 0.1 wt% (Odette and Lucas, to be published). The irradiations were carried out at a flux of 7×10^{11} n/cm^2/s at 290°C, to a fluence of 10^{19} n/cm^2. The measured yield stress increases were converted to TTS using procedures described elsewhere (Odette et al., 1985). The

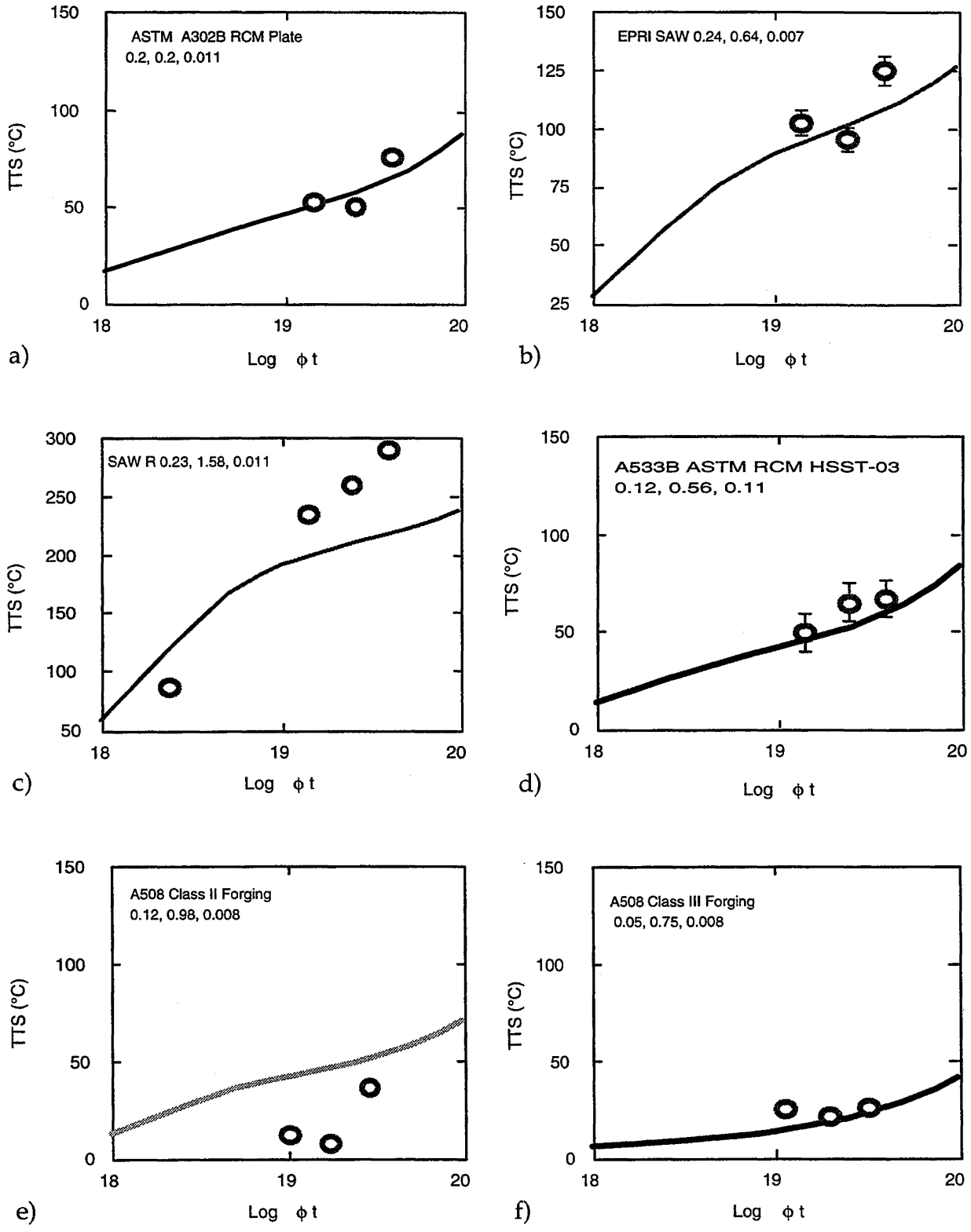

Figure 5.1 Comparison of Equation 4-1 with PSF data

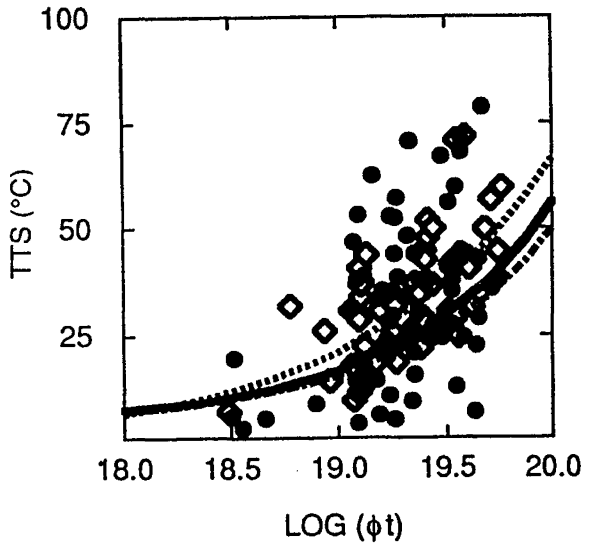

Figure 5.2 Comparison with French surveillance data (UKNE MD Term is dotted curve; Equation 4-1 MD Term is solid curve for plates, dot-dash for welds; plate data are circles, weld data are diamonds)

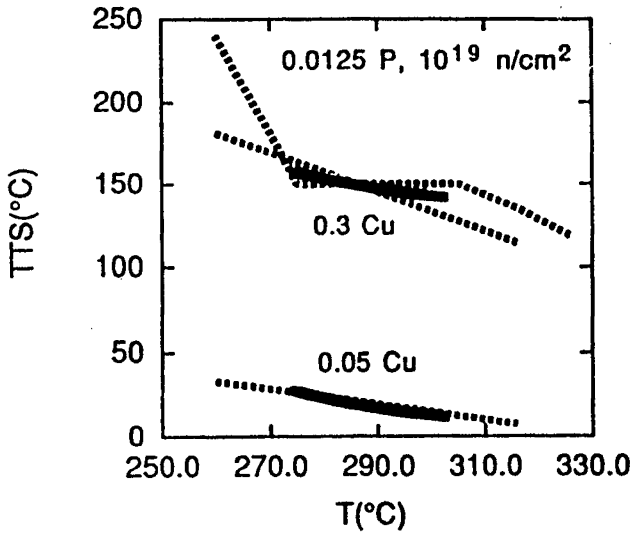

Figure 5.3 Comparison of Equation 4-1 (solid lines) with other irradiation temperature correlations (dotted lines)

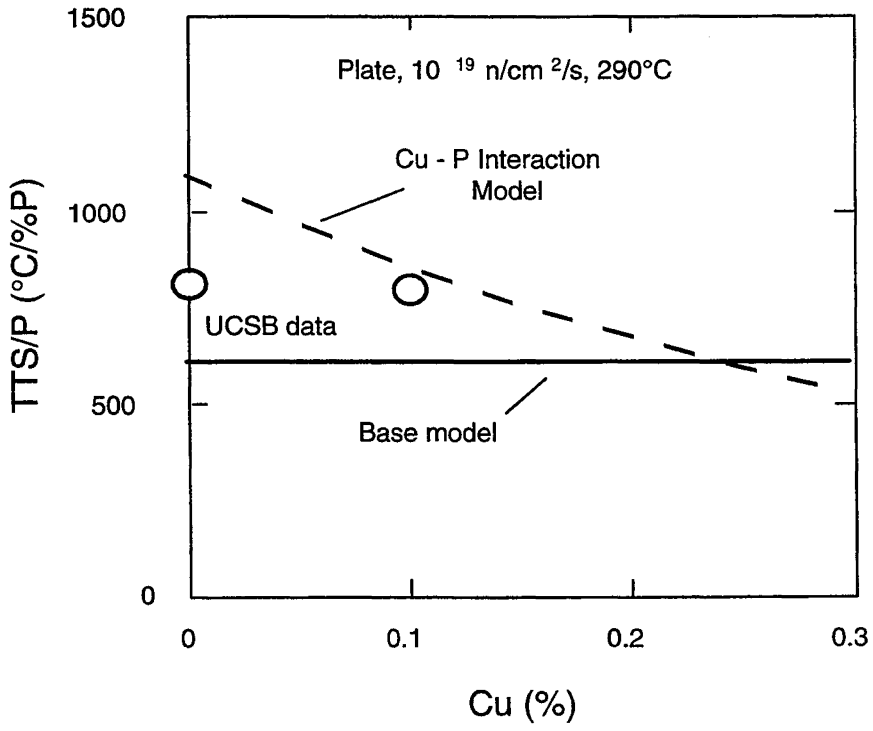

Figure 5.4 Comparison of Cu-P effects in the MD term of Equation 4-1 (Base model) and the Cu-P model in Appendix D with UCSB test reactor data

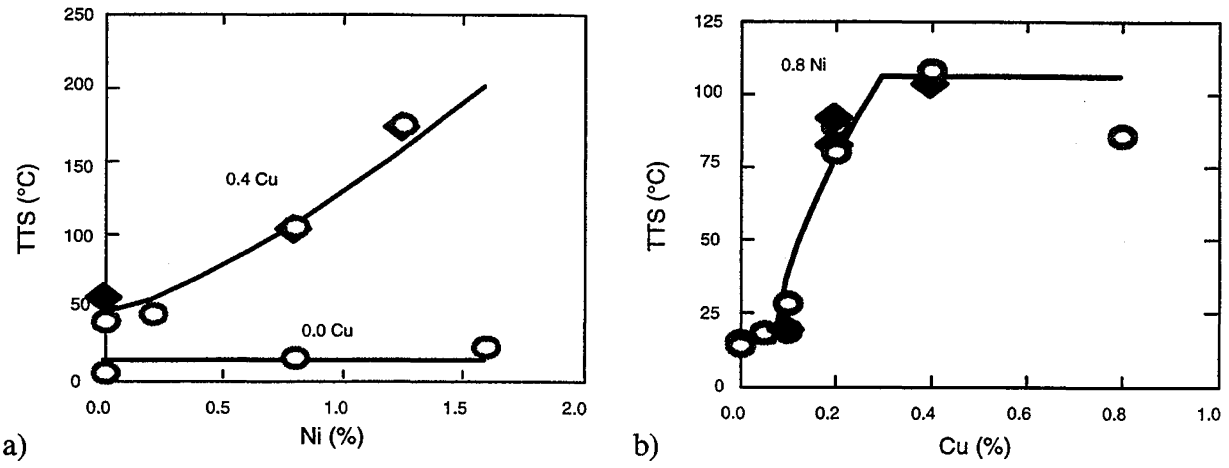

Figure 5.5 Comparison of Cu and Ni effects in Equation 4-1 to split melt heats of the same material (SANS data shown as diamonds, change in yield strength data shown as circles)

corresponding experimental coefficients, shown as circles, are the slopes of a linear least squares fit to the converted TTS versus P data. The horizontal line is the P coefficient of the SMD term in Equation 4-1 for plates ("Base model") for the irradiation conditions of the experiment. The dashed curve is the prediction of an alternative model featuring a Cu-P interaction term (see Appendix D). The data, which show only a slight effect of Cu on the P sensitivity, are bounded by the fitted models. A higher P coefficient at low Cu (more than 2000°C/%P) decreasing to around 600°C/%P at about 0.2% Cu has been reported, based on analysis of data on a variety of Mn-Mo steels irradiated over a range of generally high fluences (Jones and Buswell, 1988). This is consistent with the increasing P contribution with fluence in the base model (Equation 4-1). The P coefficient in the base model is within the range of the corresponding coefficients from other correlations (Petrequin, 1996). Thus the overall phosphorous sensitivity in Equation 4-1 is reasonably well supported by these independent observations.

Figures 5.5a and 5.5b show similar comparisons of the effects of Cu and Ni variations predicted by the model to split melt data from the same experiment described above. Once again, the measured yield stress increases have been converted to TTS estimates, shown as circle symbols. Figure 5.5a shows the effect of Ni variations at 0.0 and 0.4 wt% Cu (bulk nominal). Figure 5.5b shows the effect of Cu variations at 0.8 wt% Ni. The solid lines are absolute predictions of Equation 4-1 for these compositions and irradiation conditions. The large filled diamonds are corresponding estimates of the TTS shifts made using small angle neutron scattering (SANS) measurements of the CRP nanostructure. The SANS data were converted to estimates of the CRP contribution to yield strength increases, as described elsewhere (Odette and Lucas, to be published). Experimental estimates of the SMD contribution have been added to the CRP contribution to obtain the total yield stress increase. As previously described, the computed yield stress increases were then converted to TTS estimates. The agreement is remarkable and lends very strong independent and fundamental support to the treatment of Cu and Ni effects and Cu-Ni interactions in Equation 4-1.

5.2 Ranges of Data, Limits of Applicability

The models presented in this report are curve fits, strictly valid only within the ranges of data used to create them. While substantial effort has been made to consider the underlying mechanisms, other data, and what is known about variable combinations that are not represented in the data base, the quality of prediction outside the range of the variables remains largely unknown. Caution appropriate to engineering extrapolation must be exercised when using these models for conditions outside the ranges used for calibration, as shown in Tables 5.1 and 5.2. Table 5.1 also shows estimated limits of applicability for the TTS model; they are approximately the same as the ranges of data, unless theory, data base coverage, or other data suggested that the range could be expanded (e.g., T_c, Cu) or should be limited (e.g., ϕt). Table 5.2 shows the same information for the USE model.

Table 5.1 Estimated limits of applicability for TTS model

Variable	Range in Calibration Set	Estimated Limits of Applicability
Fluence, n/cm^2	$9.26x10^{15}$ - $1.07x10^{20}$	10^{16} - $7.5x10^{19}$
t_i, h	5556 - 142000	5550 - 142000
Cu, wt%	0.01 - 0.41	0 - 0.5(0.3*)
Ni, wt%	0.044 - 1.26	0 - 1.3
P, wt%	0.003 - 0.024	0 - 0.025
T_c, °F	522 - 570	500 - 570
Flux, $n/cm^2/s$	$1.8x10^8$ - $1.6x10^{12}$	$2x10^8$ - 10^{12}

*See discussion below.

Table 5.2 Estimated limits of applicability for USE_i model

Variable	Range in Calibration Set	Estimated Limits of Applicability
USE_u, ft-lb	55 - 188	50 - 180
Fluence, n/cm^2	$9.26x10^{15}$ - $7.13x10^{19}$	10^{16} - $7.0x10^{19}$
Cu, wt%	0.01 - 0.42	0 - 0.5
Ni, wt%	0.044 - 1.20	0 - 1.3
P, wt%	0.003 - 0.024	0 - 0.024

Some combinations of variables within the limits specified in Tables 5.1 and 5.2 were not well represented in the data base, so caution is also required *within* the range of individual variables at unusual combinations of variables. For example, in the TTS calibration data set, the data at Cu ≥ 0.3 wt% corresponded to 0.092 ≤ Ni ≤ 0.78 wt%, so the quality of the model prediction at the combination of high Cu (≥ 0.3 wt%) and high Ni (> 0.78 wt%) is unknown. Further, the maximum effective Cu level of ~0.3 wt% is believed to be associated with prototypical post-weld heat treatments. Therefore, use of the 0.3 wt% limit for alloys containing higher levels of bulk Cu should be restricted to materials with Ni levels ≤ ~0.8 wt% and supported by demonstration of appropriate heat treatments. In general, for any application of the model that involves one or more variables that are near the limits shown in Tables 5.1 and 5.2, the data base given in Appendix A should be examined to determine whether or not there were sufficient data in that region to support the model. If not, the combination of conditions should be treated as an extrapolation, even though each variable is within the range found in the calibration set.

5.3 Future Use of Improved Measures of Fluence and Irradiation Temperature

In this study, coolant temperature was used because it was the best estimate of irradiation temperature that could be added easily to the analysis data base. As discussed above, coolant temperature was found to be important for predicting TTS, whereas melt-wire irradiation temperature was not. Discussions have already begun concerning more accurate estimates of irradiation temperatures. While accurate determination of irradiation temperature is encouraged, it must be emphasized that only coolant temperatures - cold leg temperatures for PWRs and recirculation temperatures for BWRs - should be used for T_c in Equation 4-1. If a better method of estimating irradiation temperature is developed, and the resulting estimates differ substantially from coolant temperature, Equation 4-1 must be recalibrated before the revised temperatures are used for estimating TTS; otherwise, the predictions may be biased relative to the data.

Similarly, values of fluence determined using methods other than those used for the calibration data base should not be used in Equation 4-1. The updated fluences used for calibration were presumably consistent with the state of the art in the 1980's and early 1990's, as discussed in Section 2.6. Since methods of determining fluence are continually under development, caution must be exercised when estimating TTS to ensure that compatible fluence estimates are used. If a revision in the method of calculating fluence makes a large change in fluences in the calibration set, the model should be recalibrated using the re-evaluated fluences before revised fluence values are used in Equation 4-1. If this recalibration is not performed, there may be a bias in the predictions due to the inconsistency of fluences used for calibration and later evaluation.

To illustrate the potential magnitude of such a bias, Table 5.3 shows the sensitivity of calculated TTS to increases in fluence over a range of conditions. If a revised method of calculating fluence causes a 20% increase in the recorded value of fluence, the increase in TTS is less than 8°F over the range of conditions shown (at median values of variables not shown). This table can be used to estimate the expected effect of revised fluence estimation methods on the bias in calculated TTS. If the fluences used in Equation 4-1 are revised upwards by 20% relative to those in Appendix A, the model will overestimate the actual shifts by the amounts shown (a conservative bias). If the fluence calculation procedure changes such that fluences are revised downwards, the model will underestimate the actual shifts.

Table 5.3 Increase in calculated TTS (Equation 4-1) with 20% increase in fluence

	Cu, wt%		
ϕt	0.05	0.15	0.30
10^{17}	0.3°F (3.9%)	0.7°F (6.4%)	1.2°F (7.4%)
$7.5x10^{18}$	2.3°F (8.3%)	4.4°F (4.3%)	6.6°F (3.7%)
$5x10^{19}$	7.0°F (10.2%)	7.2°F (4.7%)	7.4°F (3.0%)

5.4 Stability of Model Relative to Initial Estimates

For any nonlinear least squares calibration, as was used for the models developed here, it is necessary to begin the solution iteration from an initial estimate of the solution. The initial estimate is refined by a minimization algorithm operating on the residuals. Because it is a nonlinear minimization process, neither global convergence nor uniqueness of the result is guaranteed. Thus, it is standard practice to begin the calibration from various initial estimates of the solution and monitor convergence to determine how sensitive the solution is to initial estimates and to ensure that a credible minimum over the region of interest has been found.

In the case of the TTS model, the surface described by the sum of squared residuals in the multi-dimensional domain appears relatively flat with respect to several fitting parameters near the optimum. Changes in initial estimates produced small variations, up to a few percent, in most of the parameters, with no change in the standard error (to at least four places). Although the sensitivity of the fitting parameters in the TTS model to starting estimates was greater than in the USE model and in other previous projects performed by the authors, it was not unreasonable. The small variations in the parameters caused no visible changes in TTS model trends, quality of fit as measured by S_e, or conclusions drawn.

In order to ensure that a stable solution had been found, the final TTS model was calibrated using five different sets of initial estimates, determined randomly in each case. For each parameter, the solutions from the five fits were averaged to produce a final set of initial estimates. Equation 4-1 is the result of a final calibration using the final set of initial estimates chosen using this procedure. The standard errors of the five intermediate fits and the final fit were identical to four digits.

5.5 Stability of Model Relative to Randomly Selected Subsets, Rounding

Because of the uneven distribution of data over the range in each variable, the effective size of the data base is somewhat less than it appears. In effect, some points are nearly replicates of other points, at similar values of all variables. Because of this fact, and the sparsity of coverage over the rather large, multi-dimensional domain, the entire analysis data base was used for calibration. This approach did not leave surveillance data for validation that were not used in calibration, a difficulty that was addressed by comparison with other data (Section 5.1) and by analyzing random subsets, reported in this section.

The sensitivity of the models to changes in the calibration data set was explored by recalibrating to ten subsets of the data used for calibration, each including 90% of the calibration set. The data were randomized, then a different 10% sample of data was excluded from each of the ten subsets. When the same model form was recalibrated to each of the 10 subsets, some fitting parameters varied while others were stable.

The fitting parameters that varied most in the subset analyses were strongly correlated to other fitting parameters with very different sensitivities. For example, one such correlated pair is the coefficient A of the matrix defect term and the fitting parameter inside the exponential ($1.906x10^4$). Because of the exponential function and the correlation between these fitting parameters, a small increase in the fitting parameter inside the exponential corresponds to a large decrease in A. The net effect on both the absolute value of the TTS prediction and the slope of the temperature effect is small, because the *product* of the coefficient and the exponential term (which is all that matters to the model) is reasonably stable.

There are other pairs of fitting parameters that are reasonably uncorrelated, but one parameter is much more sensitive than the other and only the combination matters. For example, the two parameters in the power on fluence in the matrix defect term (0.4449 and 0.0597 in Equation 4-1b) combine to establish the power on fluence, but with unequal effect. Over the 10 subsets examined, the variation (standard deviation) in the first constant was 3.8% of the average value while the variation in the second constant was 17.3%. But a 17.3% change in the second constant has less effect on the overall power on fluence than a 3.8% change in the first constant over the range containing most of the data (10^{18} - 10^{20} n/cm^2). Thus the higher apparent uncertainty of the second constant is just a reflection of the lower sensitivity of that constant.

After performing analyses of the type outlined above, considering both the correlated fitting constants and uncorrelated constants with large differences in

sensitivity, the following conclusions were reached. First, several of the fitting parameters in Equation 4-1 are correlated to some extent with other fitting parameters; *one should not change or delete any parameters in Equation 4-1 without re-fitting.*

Second, the key fitting parameters and key combinations of related parameters appear to be established with an uncertainty (1 standard deviation) of a few percent over ten subsets of data. This level of uncertainty would normally correspond to representing the fitting constants in Equation 4-1 to two significant digits, but generally three or four digits are given instead. The reason is that the usual rounding rules do not respect the correlations among parameters, the nonlinear functions, and the highly variable sensitivities of the parameters. Equation 4-1 should be evaluated using the number of digits given for the fitting parameters; then the result can be rounded to the nearest °F (typically two or three digits) if desired. It would also be appropriate to round to the nearest °C if results are presented in metric units. Note that the results in this report (S_e, S_d, plots, etc.) were generated with constants represented to six digits or machine double precision, depending on the analysis; results generated with the rounded constants in Equation 4-1 should be expected to vary slightly.

Third, the uncertainty associated with data scatter about the model is larger than the variation due to fitting ten data subsets or the uncertainty due to rounding. The standard deviation of residuals (scatter) about the model is 19.9 to 25.0°F (see Table 4.1), which corresponds to uncertainties greater than 10% for shifts less than 200°F. The overall uncertainty in the model fitting parameters (or combinations of parameters) implied by our subset analysis is less than that, as would be typical two-digit rounding errors on the final calculated result.

6 CONCLUSIONS

The U. S. embrittlement data base has been substantially improved during this project, with a focus on the variables used in the models.

An improved upper shelf energy model has been developed, based on the improved analysis data base. The standard error of the model (11.2 ft-lb) is not much larger than the basic error in determining USE for a single heat.

An improved transition temperature shift model has been developed, based on analysis of the improved data base and the current understanding of embrittlement phenomena. The improved TTS model differs from the Regulatory Guide 1.99 Revision 2 model in form and by the inclusion of phosphorous, coolant temperature, and irradiation time in addition to copper, nickel, fluence, and product form. The new model has two terms, corresponding to stable matrix defect and copper-rich precipitation mechanisms. The improved TTS model reduces scatter significantly relative to RG1.99/2 for base metal and weld subsets and the combined data set. The standard error (23.0°F) is not much larger than the expected experimental error in determining unirradiated transition temperature at 30 ft-lb for a single heat.

The RG1.99/2 treatment of product form, providing separate model forms for base metals and welds, was found to be unnecessary. The trends relative to the independent variables used for modeling are the same regardless of product form, but there are apparent differences in the relative importance of the two major model terms for welds, plates, and forgings and a significantly lower shift magnitude for forgings. These effects are incorporated into the model. The scatter is significantly higher for welds than for base metals.

The TTS model development was a combined statistical, mechanistic, and engineering analysis effort, with the result that not all terms in the model are justified solely by statistical significance. However, all the variable effects that are included did improve the standard error on the surveillance data and are supported by (a) visible trends in the data used for calibration, (b) consistent trends in other data, such as single-variable experiments and surveillance data from other countries, and/or (c) the current understanding of embrittlement mechanisms.

The treatments of key variable trends, such as the copper-nickel dependence, in the new TTS model are much improved over RG1.99/2 and are well supported by independent data and current understanding of the mechanisms.

7 REFERENCES

Boggs, P. T., R. H. Byrd, J. E. Rogers, and R. B. Schnabel, *User's Reference Guide for ODRPACK Version 2.01 Software for Weighted Orthogonal Distance Regression*, NISTIR 4834, June 1992.

Bolton, C. J., J. T. Buswell, R. B. Jones, R. Moskovic, and R. H. Priest, "Modeling of Irradiation Embrittlement in Submerged-Arc Welds," *Effects of Irradiation on Materials: 17th International Symposium, ASTM STP 1270*, (D. S. Gelles, R. K. Nanstad, A. V. Kumar, and E. A. Little, eds.), American Society for Testing and Materials, West Conshohoken, PA, 19428-2959, 1996, p. 103.

Brillaud, C., H. Augendre, and M. Bethmont, "Uncertainty Evaluation in Transition Temperature Measurements," *Effects of Radiation on Materials: 17th International Symposium, ASTM STP 1270*, (D. S. Gelles, R. K. Nanstad, A. S. Kumar, and E. A. Little, eds.), American Society for Testing and Materials, Philadelphia, PA, 1996.

Buswell, J. T. and R. B. Jones, "The Modeling of Radiation Hardening and Embrittlement in Magnox Mild Steel Submerged-Arc Welds, *The Effects of Radiation on Materials: 16th International Symposium, ASTM STP 1175*, (D. S. Gelles, R. K. Nanstad and E. A. Little, eds.), American Society for Testing and Materials, Philadelphia, PA, 1993, p. 424.

DeVan, M. J., *Reactor Vessel Surveillance Program Charpy Data for B&W Designed Nuclear Plant*, BAW-2218, February 1994.

Eason, E. D. and E. E. Nelson, "Correlations between Grain Boundary Composition and IASCC Susceptibility in Austenitic Stainless Steel," EPRI Report TR-103508, Electric Power Research Institute, Palo Alto, CA, April 1994.

Eason, E. D., J. E. Wright, and G. R. Odette, "An Improved Embrittlement Correlation for Reactor Pressure Vessel Steels," *8th International Symposium on Environmental Degradation of Materials in Nuclear Power Systems - Water Reactors*, NACE International, August 1997, pp 889-896.

Eason, E. D., J. E. Wright, and E. E. Nelson, "Improved Irradiation Embrittlement and Annealing Correlations," 21st Water Reactor Safety Information Meeting, Bethesda, MD, October 1993.

Eason, E. D. et. al. "Embrittlement Recovery Due to Annealing of Reactor Pressure Vessel Steels," *7th International Symposium on Environmental Degradation of Materials in Nuclear Power Systems - Water Reactors*, NACE International, 1995, pp. 759-770.

Fisher, S. B. and J. T. Buswell, "A Model for PWR Pressure Vessel Embrittlement," *International Journal of Pressure Vessels and Piping, Volume 27*, 1987, p. 91.

Fisher, S. B., J. E. Harbottle and N. Aldridge, "Radiation Hardening in Magnox," *Phil. Trans. Roy Society*, London, A315, 1985, p. 301.

Griesbach, T. J. and B. N. Burgos, *User's Guide to PREP4*, EPRI CM-106726, October 1996.

Hawthorne, J. R. and B. H. Menke, "Light Water Rector Dosimetry Improvement Program: Post Irradiation Notch Ductility and Tensile Strength Determinations for PSF Simulated Surveillance through Wall Specimen Capsules," NUREG/CR-3295-2, Nuclear Regulatory Commission, 1984.

Jones, R. B. and J. T. Buswell, "A Model for PWR Pressure Vessel Embrittlement," *International Journal* of *Pressure Vessels and Piping, 27*, 1987, p. 91.

Jones, R. B. and T. J. Williams, "The Dependence of Radiation Hardening and Embrittlement on Irradiation Temperature," *Effects of Irradiation on Materials: 17th International Symposium, ASTM STP 1270*, (D. S. Gelles, R. K. Nanstad, A. V. Kumar, and E. A. Little, eds.), American Society for Testing and Materials, West Conshohoken, PA, 19428-2959, 1996, p. 569.

Kampmann, et al., "SANS Analysis of Reactor Vessel Materials in Neutron Irradiated, Annealed and Re-Irradiated Conditions," *Proceedings of the 5th International Symposium on Environmental Degradation of Materials in Nuclear Reactors - Water Reactors*, (D. Cubiciotti, E. P. Simonen, and R. Gold, eds.), ANS, 1992, p 679.

Lippincott, E. P., *Westinghouse Surveillance Capsule Neutron Fluence Reevaluation*, WCAP-14044, Westinghouse Electric Corporation, April 1994.

Lucas, G. E., G. R. Odette, P. M. Lombrozo, and J. W. Sheckherd, "Effects of Composition, Microstructure and Temperature on Irradiation Hardening of Pressure Vessels Steels," *Effects of Radiation on Materials: 12th*

International Symposium, ASTM STP 870, (F. A. Garner and J. S. Perrin, eds.), American Society for Testing and Materials, 1985, p. 900.

Lucas, G. E., G. R. Odette, R. Maiti, and J. W. Sheckherd, "Tensile Properties of Irradiated Pressure Vessel Steels," *Effects of Radiation on Materials: 12th International Symposium, ASTM STP 956*, (F. A. Garner, C. H. Henager and N. Igata, eds.), American Society for Testing and Materials, Philadelphia, PA, 1988, p. 379.

Mader, E., G. R. Odette, and G. E. Lucas, "The Effects of Irradiation and Metallurgical Variables on Post Irradiation Annealing at 343°C," *Proceedings of the 6th International Symposium on Environmental Degradation of Materials in Nuclear Power Systems - Water Reactors*, (R. Gold and E. Simonen, eds.), The Metallurgical Society, Warrendale, PA, 1993, p. 739.

McElroy, R. J. and A. L. Lowe, "Irradiation Embrittlement Modeling of Linde 80 Welds," *Effects of Irradiation on Materials: 17th International Symposium, ASTM STP 1270*, (D. S. Gelles, R. K. Nanstad, A. V. Kumar, and E. A. Little, eds.), American Society for Testing and Materials, West Conshohoken, PA, 19428-2959, 1996, p. 68.

Miller, M. K. and M. G. Burke, "An Atom Probe Field Ion Microscopy Study of Neutron Irradiated Pressure Vessel Steels," *Journal of Nuclear Materials, 195*, 1992, p. 68.

Odette, G. R., "On the Dominant Mechanism of Irradiation Embrittlement in Pressure Vessel Steels," *Scripta Met., 11*, 1983, p. 1183.

Odette, G. R., "Radiation Induced Microstructural Evolution in Reactor Pressure Vessel Steels," *MRS Society Symposium Proceedings 373*, 1995, p. 137.

Odette, G. R., P. M. Lombrozo, J. S. Perrin, and R. A. Wullaert, "Physically-Based Regression Correlations of Embrittlement Data from Reactor Pressure Surveillance Programs," EPRI NP-3319, Final Report, January 1984.

Odette, G. R., P. M. Lombrozo, and R. A. Wullaert, "The Relationship between Irradiation Hardening and Embrittlement of Pressure Vessel Steels," *Effects of Radiation on Materials: 12th International Symposium, ASTM STP 870*, (F. A. Garner and J. S. Perrin, eds.), American Society for Testing and Materials, 1985, p. 840.

Odette, G. R. and G. E. Lucas, "Irradiation Embrittlement of Reactor Pressure Vessel Steels: Mechanisms, Models and Data Correlations," *Radiation Embrittlement of Nuclear Reactor Pressure Vessel Steels: An International Review - Volume II*, ASTM STP 909, (L. E. Steele, ed.), American Society for Testing and Materials, 1986a, p. 206.

Odette, G. R. and G. E. Lucas, "Recent Advances in Predicting Embrittlement of Reactor Pressure Vessel Steels," *Proceedings of the 2nd International Symposium on Environmental Degradation of Materials in Nuclear Reactors - Water Reactors*, (J. T. A. Roberts, J. R. Weeks and G. J. Theus, eds.), American Nuclear Society, LeGrange Park, IL, 1986b, p. 345.

Odette, G. R. and G. E. Lucas, "The Effect of Heat Treatment on Irradiation Hardening of Pressure Vessel Steels," *Proceedings of the 3rd International Symposium on Environmental Degradation of Materials in Nuclear Reactors - Water Reactors*, (G. J. Theus and J. R. Weeks, eds.), The Metallurgical Society, Warrendale, PA, 1988, p. 95.

Odette, G. R. and G. E. Lucas, "Irradiation Embrittlement of LWR Pressure Vessel Steels," EPRI Report NP-6114, Electric Power Research Institute, Palo Alto, CA, 1989.

Odette, G. R. and G. E. Lucas, "The Effect of Nickel on Irradiation Hardening of Pressure Vessel Steels," *The Effects of Radiation on Materials: 14th International Symposium, ASTM STP 1046*, (N. H. Packan, R. E. Stoller, and A. S. Kumar, eds.), American Society for Testing and Materials, Philadelphia, PA, 1990, p. 323.

Odette, G. R. and G. E. Lucas, "Current Understanding of the Effects of Environmental and Metallurgical Variables on Reactor Pressure Vessel Embrittlement," *Proceedings of the U.S. Nuclear Regulatory Commission 24th Water Reactor Safety Information Meeting, 2*, NUREG/CR-0157-2, 1997a, p. 1.

Odette, G. R. and G. E. Lucas, "Anomalous Hardening in Model Alloys and Steels Aged at 290°C and 350°C: Implications to Low Flux Irradiation Embrittlement," ASTM STP 1325, (R. K. Nanstad, M. L. Hamilton, F. A. Garner, and A. V. Kumar, eds.), American Society for Testing and Materials, West Conshohoken, PA, 1997b.

Odette, G. R. and G. E. Lucas, "Recent Progress in Understanding Reactor Pressure Vessel Steel Embrittlement," *Radiation Effects and Defects in Solids*, 144, 1998, pp. 189-231.

Odette, G. R., G. E. Lucas, and D. K. Klingensmith, "The Influence of Metallurgical Variables on the Temperature Dependence of Irradiation Hardening in

Pressure Vessel Steels," *Effects of Irradiation on Materials: 17th International Symposium, ASTM STP 1270*, (D. S. Gelles, R. K. Nanstad, A. V. Kumar, and E. A. Little, eds.), American Society for Testing and Materials, West Conshohoken, PA, 19428-2959, 1996, p. 606.

Odette, G. R., E. V. Mader, G. E. Lucas, W. J. Phythian and C. A. English, "The Effect of Flux on the Irradiation Hardening of Pressure Vessel Steels," *The Effects of Radiation on Materials: 16th International Symposium, ASTM STP 1175*, (D. S. Gelles, R. K. Nanstad and E. A. Little, eds.), American Society for Testing and Materials, Philadelphia, PA, 1993, p. 323.

Oldfield, W., et al., "Irradiated Nuclear Pressure Vessel Steel Data Base," EPRI NP-2428, Electric Power Research Institute, Palo Alto, CA, June 1982.

Petrequin, P., "A Review of Formulas for Predicting Irradiation Embrittlement of Reactors Vessel Materials," *European Commission, Directorate General - Joint Research Center, Institute for Advanced Materials, DG XI/C/2 AMES Report No. 6, EUR 16455 EN*, November 1996.

Randall, P. N., "Basis for the Calculative Procedures for Adjustment of Reference Temperature Given in Revision 2 of Regulatory Guide 1.99," U. S. Nuclear Regulatory Commission, Washington, D. C., 1984.

Randall, P. N., "Basis for Revision 2 of the U.S. Nuclear Regulatory Commission's Regulatory Guide 1.99," *Radiation Embrittlement of Nuclear Pressure Vessel Steels: An International Review (Second Volume), ASTM STP 909*, (L. E. Steele, ed.), 1987, p. 149.

Taylor, J. R., *An Introduction to Error Analysis*, University Science Books, Mill Valley, CA, 1982.

Williams, T. J., P. R. Burch, C. A. English, and P. H. N. de la cour Ray, "The Effects of Dose Rate and Temperature and Copper and Nickel Content on the Irradiation Shift of Low Alloy Submerged-Arc Welds," *Proceedings of the 3rd International Symposium on Environmental Degradation of Materials in Nuclear Reactors - Water Reactors*, (G. J. Theus and J. R. Weeks, eds.), The Metallurgical Society, Warrendale, PA, 1988, p. 121.

Williams, T. J. and P. J. Phythian, "Electron Microscopy and Small Angle Neutron Scattering Study of Precipitates in Low-Alloy Submerged-Arc Welds," *Effects of Irradiation on Materials: 17th International Symposium, ASTM STP 1270*, (D. S. Gelles, R. K. Nanstad, A. V. Kumar, and E. A. Little, eds.), American Society for Testing and Materials, West Conshohoken, PA, 19428-2959, 1996, p. 191.

Young, H. D., *Statistical Treatment of Experimental Data*, McGraw-Hill Book Company, Inc., New York, 1962.

APPENDIX A
ANALYSIS DATA BASE

The five identifiers shown in the embrittlement data base (material type, plant, capsule, heat, and product form) came from the PR-EDB (NUREG/CR-4816 Rev. 2). The meaning of entries for material type and capsule are self-evident, and the heat identifiers are a combination of the plant identifier and a heat identifier, assigned at ORNL. The product forms are: P for plates, F for forgings, W for welds, and SRM for standard reference materials. A key to the plant identifiers is given in Table A.1.

A value of -999 is shown to indicate an unknown quantity in the numerical fields, and unknown categorical variables are blank.

Table A.1 Key to plant identifiers

ID	Plant	ID	Plant	ID	Plant
AD1	Angra Dos Reis Unit 1	FA1	Joseph M. Farley Unit 1	PL1	Pilgrim Nuclear Power Station Unit 1
AL2	Almarez Unit 2	FA2	Joseph M. Farley Unit 2	PV2	Palo Verde Unit 2
AN1	Arkansas Nuclear One, Unit 1	FC1	Fort Calhoun Station Unit 1	QC1	Quad Cities Nuclear Power Station Unit 1
AN2	Arkansas Nuclear One, Unit 2	FTZ	James A. Fitzpatrick	QC2	Quad Cities Nuclear Power Station Unit 2
AS1	Asco Unit 1	GAR	Garigliano	RI2	Ringhals Unit 2
AS2	Asco Unit 2	GIN	Robert E. Ginna Nuclear Plant Unit 1	RS1	Rancho Seco Unit 1
BD1	Braidwood Unit 1	HA1	Edwin I. Hatch Unit 1	SA1	Salem Unit 1
BD2	Braidwood Unit 2	HB2	H. B. Robinson Unit 2	SA2	Salem Unit 2
BF3	Browns Ferry Unit 3	HM3	Humbolt Bay Power Plant Unit 3	SB1	Seabrook Unit 1
BR	Big Rock Point Reactor	IP2	Indian Point Unit 2	SH1	Susquehanna Unit 1
BV1	Beaver Valley Unit 1	IP3	Indian Point Unit 3	SH2	Susquehanna Unit 2
BV2	Beaver Valley Unit 2	KO1	Korea Nuclear Unit 1	SL1	St. Lucie Unit 1
BW1	Brunswick Unit 1	KWE	Kewaunee Nuclear Power Plant	SL2	St. Lucie Unit 2
BW2	Brunswick Unit 2	LAC	Lacrosse Boiling Water Reactor	SO1	San Onofre Unit 1
BY1	Byron Unit 1	LM2	Lemoniz Unit 2	SO2	San Onofre Unit 2
BY2	Byron Unit 2	MC1	W. B. McGuire Unit 1	SO3	San Onofre Unit 3
BZ1	Beznau Unit 1	MC2	W. B. McGuire Unit 2	SQ1	Sequoyah Unit 1
BZ2	Beznau Unit 2	MD1	Midland Unit 1	SQ2	Sequoyah Unit 2
CAB	Jose Cabrera-Zorita Reactor	MD2	Midland Unit 2	SR1	Shearon Harris Unit 1
CB1	Catawba Unit 1	ML1	Millstone Nuclear Power Station Unit 1	ST1	South Texas Unit 1
CB2	Catawba Unit 2	ML2	Millstone Nuclear Power Station Unit 2	SU1	Surry Unit 1
CC1	Calvert Cliffs Unit 1	ML3	Millstone Nuclear Power Station Unit 3	SU2	Surry Unit 2

ID	Plant	ID	Plant	ID	Plant
CC2	Calvert Cliffs Unit 2	MON	Monticello Nuclear Generating Plant	TA1	Tarapur Unit 1
CK1	Donald C. Cook Unit 1	MY	Maine Yankee Nuclear Plant	TA2	Tarapur Unit 2
CK2	Donald C. Cook Unit 2	NA1	North Anna Unit 1	TM1	Three Mile Island Nuclear Station Unit 1
CL1	Callaway Unit 1	NA2	North Anna Unit 2	TM2	Three Mile Island Nuclear Station Unit 2
CP2	Comanche Peak Unit 2	NM1	Nine Mile Point Unit 1	TP3	Turkey Point Nuclear Power Station Unit 3
CPR	Cooper	OC1	Oconee Nuclear Station Unit 1	TP4	Turkey Point Nuclear Power Station Unit 4
CR3	Crystal River Unit 3	OC2	Oconee Nuclear Station Unit 2	TRO	Trojan Reactor
CTY	Haddam Neck	OC3	Oconee Nuclear Station Unit 3	VO2	Vogtle Unit 2
DAC	Duane Arnold Energy Center Unit 1	OYS	Oyster Creek Nuclear Generating Station	VS1	Virgil C. Summer Unit 1
DB1	Davis-Beese Nuclear Power Station Unit 1	PAL	Palisades Nuclear Plant	VY	Vermont Yankee Nuclear Power Station
DC1	Diablo Canyon Unit 1	PB1	Point Beach Nuclear Plant Unit 1	WB1	Watts Bar Unit 1
DC2	Diablo Canyon Unit 2	PB2	Point Beach Nuclear Plant Unit 2	WC1	Wolf Creek Unit 1
DR1	Dresden Nuclear Plant Station Unit 1	PH2	Peach Bottom Atomic Power Station Unit 2	WF3	Waterford Generating Station Unit 3
DR2	Dresden Nuclear Plant Station Unit 2	PH3	Peach Bottom Atomic Power Station Unit 3	YR	Yankee-Rowe
DR3	Dresden Nuclear Plant Station Unit 3	PI1	Prairie Island Unit 1	ZN1	Zion Nuclear Plant Reactor Unit 1
ERR	Elk River	PI2	Prairie Island Unit 2	ZN2	Zion Nuclear Plant Reactor Unit 1

Embrittlement Analysis Data Base

Material ID	Plant ID	Capsule	Heat ID	Product ID	Specimen Orientation	Irradiation time hr	Fluence n/cm^2	Flux n/cm^2/s	Tcoolant F	TTu30 F	USEu ft-lb	TTi30 F	USEi ft-lb	dTT30 F	dUSE ft-lb	C wt%	Mn wt%	P wt%	S wt%	Si wt%	Ni wt%	Cr wt%	Mo wt%	Cu wt%
A5082	AD1	V	FAD101	F	LT	8607	4.580E+18	-9.990E+02	-999	-36.	148.	1.	130.	38.	18.	0.210	0.600	0.012	0.009	0.230	0.740	0.320	0.560	0.040
A5082	AD1	V	FAD101	F	TL	8607	4.580E+18	-9.990E+02	-999	-21.	134.	17.	131.	38.	3.	0.210	0.600	0.012	0.009	0.230	0.740	0.320	0.560	0.040
A533B1	AN1	A	PAN101	P	LT	-999	1.030E+19	8.980E+10	556	-19.	135.	28.	109.	47.	26.	0.210	1.320	0.010	0.016	0.200	0.520	0.190	0.570	0.150
A533B1	AN1	A	PAN101	P	TL	-999	1.030E+19	8.980E+10	556	10.	96.	81.	82.	72.	13.	0.210	1.320	0.010	0.016	0.200	0.520	0.190	0.570	0.150
A533B1	AN1	A	SHSS02	SRM	LT	-999	1.030E+19	8.980E+10	556	47.	124.	118.	96.	71.	28.	0.217	1.478	0.011	0.015	0.225	0.640	0.095	0.502	0.170
A533B1	AN1	B	PAN102	P	LT	-999	4.280E+18	1.740E+10	556	-9.	143.	13.	125.	22.	18.	0.210	1.320	0.010	0.016	0.200	0.520	0.190	0.570	0.150
A533B1	AN1	B	PAN102	P	TL	-999	4.280E+18	1.740E+10	556	14.	109.	9.	91.	-5.	17.	0.210	1.320	0.010	0.016	0.200	0.520	0.190	0.570	0.150
A533B1	AN1	B	SHSS02	SRM	LT	-999	4.280E+18	1.740E+10	556	47.	124.	97.	100.	50.	24.	0.217	1.478	0.011	0.015	0.225	0.640	0.095	0.502	0.170
A533B1	AN1	C	PAN101	P	LT	-999	1.460E+19	8.630E+10	556	-19.	135.	34.	110.	53.	25.	0.210	1.320	0.010	0.016	0.200	0.520	0.190	0.570	0.150
A533B1	AN1	C	PAN101	P	TL	-999	1.460E+19	8.630E+10	556	10.	96.	54.	85.	45.	11.	0.210	1.320	0.010	0.016	0.200	0.520	0.190	0.570	0.150
A533B1	AN1	C	SHSS02	SRM	LT	-999	1.460E+19	8.630E+10	556	47.	124.	122.	99.	75.	25.	0.217	1.478	0.011	0.015	0.225	0.640	0.095	0.502	0.170
A533B1	AN1	E	PAN101	P	LT	8281	7.270E+17	-9.990E+02	556	-19.	135.	-1.	117.	18.	18.	0.210	1.320	0.010	0.016	0.200	0.520	0.190	0.570	0.150
A533B1	AN1	E	PAN101	P	TL	8281	7.270E+17	-9.990E+02	556	10.	96.	54.	83.	44.	13.	0.210	1.320	0.010	0.016	0.200	0.520	0.190	0.570	0.150
A533B1	AN1	E	SHSS02	SRM	LT	8281	7.270E+17	-9.990E+02	556	47.	124.	55.	136.	8.	-12.	0.217	1.478	0.011	0.015	0.225	0.640	0.095	0.502	0.170
A533B1	AN2	W97	PAN201	P	LT	14815	3.410E+18	6.400E+10	553	4.	163.	25.	142.	21.	21.	0.220	1.400	0.013	0.011	0.210	0.561	0.150	0.630	0.078
A533B1	AN2	W97	PAN201	P	TL	14815	3.330E+18	6.400E+10	553	12.	142.	51.	123.	38.	19.	0.220	1.400	0.013	0.011	0.210	0.561	0.150	0.630	0.078
A5083	BD1	U	FBD1JW	F	LT	9639	3.700E+18	1.070E+11	551	-66.	173.	-60.	166.	6.	7.	-999.000	-999.000	0.009	-999.000	-999.000	0.736	-999.000	-999.000	0.046
A5083	BD1	U	FBD1JW	F	TL	9639	3.700E+18	1.070E+11	551	-44.	158.	-69.	142.	-25.	16.	-999.000	-999.000	0.009	-999.000	-999.000	0.736	-999.000	-999.000	0.046
A5083	BD1	X	FBD1JW	F	LT	37080	1.144E+19	-9.990E+02	551	-66.	173.	-36.	168.	30.	5.	-999.000	-999.000	0.009	-999.000	-999.000	0.736	-999.000	-999.000	0.046
A5083	BD1	X	FBD1JW	F	TL	37080	1.144E+19	-9.990E+02	551	-44.	158.	-18.	152.	26.	6.	-999.000	-999.000	0.009	-999.000	-999.000	0.736	-999.000	-999.000	0.046
A5083	BD2	U	FBD201	F	LT	10056	3.850E+18	1.060E+11	558	-15.	168.	-27.	179.	-12.	-12.	0.230	1.340	0.012	0.006	0.290	0.787	0.087	0.525	0.057
A5083	BD2	U	FBD201	F	TL	10056	3.850E+18	1.060E+11	558	-21.	154.	-20.	143.	1.	12.	0.230	1.340	0.012	0.006	0.290	0.787	0.087	0.525	0.057
A5083	BD2	X	FBD201	F	LT	-999	1.126E+19	-9.990E+02	558	-15.	168.	-19.	178.	-5.	-10.	0.230	1.340	0.012	0.006	0.290	0.787	0.087	0.525	0.057
A5083	BD2	X	FBD201	F	TL	-999	1.126E+19	-9.990E+02	558	-21.	154.	13.	146.	34.	8.	0.230	1.340	0.012	0.006	0.290	0.787	0.087	0.525	0.057
A302BM	BF2	30D	PBF2JW	P	LT	79299	1.520E+17	5.890E+08	528	-40.	142.	-13.	137.	27.	5.	0.200	1.350	0.007	0.011	0.190	0.550	-999.000	0.490	0.140
A302B	BR	119	PBR_01	P	TL	6578	1.500E+18	6.100E+10	570	5.	91.	-20.	-999.	-25.	-999.	0.300	1.420	0.016	0.018	0.250	0.180	0.130	0.510	0.100
A302B	BR	122	PBR_01	P	TL	6578	2.300E+19	9.600E+11	570	5.	91.	72.	-999.	67.	-999.	0.300	1.420	0.016	0.018	0.250	0.180	0.130	0.510	0.100
A302B	BR	124	PBR_01	P	TL	18290	1.070E+20	1.600E+12	570	5.	91.	156.	-999.	151.	-999.	0.300	1.420	0.016	0.018	0.250	0.180	0.130	0.510	0.100
A302B	BR	125	PBR_01	P	TL	75556	2.270E+19	8.380E+10	570	5.	91.	110.	76.	105.	14.	0.300	1.420	0.016	0.018	0.250	0.180	0.130	0.510	0.100
A302B	BR	127	PBR_01	P	TL	26114	7.100E+18	7.500E+10	570	5.	91.	61.	-999.	56.	-999.	0.300	1.420	0.016	0.018	0.250	0.180	0.130	0.510	0.100
A533B1	BV1	U	PBV101	P	LT	31389	6.530E+18	5.770E+10	547	-2.	136.	116.	108.	117.	28.	0.200	1.310	0.010	0.015	0.180	0.540	0.140	0.550	0.200
A533B1	BV1	U	PBV101	P	TL	31389	6.530E+18	5.770E+10	547	18.	85.	149.	82.	132.	3.	0.200	1.310	0.010	0.015	0.180	0.540	0.140	0.550	0.200
A533B1	BV1	V	PBV101	P	LT	10167	2.810E+18	7.660E+10	547	-2.	136.	125.	120.	126.	16.	0.200	1.310	0.010	0.015	0.180	0.540	0.140	0.550	0.200
A533B1	BV1	V	PBV101	P	TL	10167	2.810E+18	7.660E+10	547	18.	85.	156.	83.	138.	2.	0.200	1.310	0.010	0.015	0.180	0.540	0.140	0.550	0.200
A533B1	BV1	W	PBV101	P	LT	51667	9.130E+18	4.910E+10	547	-2.	136.	145.	117.	147.	19.	0.200	1.310	0.010	0.015	0.180	0.540	0.140	0.550	0.200
A533B1	BV1	W	PBV101	P	TL	51667	9.130E+18	4.910E+10	547	18.	85.	196.	60.	179.	25.	0.200	1.310	0.010	0.015	0.180	0.540	0.140	0.550	0.200
A5082	BY1	U	FBY101	F	LT	10083	3.720E+18	1.020E+11	551	-86.	169.	-60.	166.	26.	3.	0.198	0.684	0.005	0.010	0.256	0.761	0.350	0.562	0.033
A5082	BY1	U	FBY101	F	TL	10083	3.720E+18	1.020E+11	551	-70.	154.	-50.	148.	20.	6.	0.198	0.684	0.005	0.010	0.256	0.761	0.350	0.562	0.033
A5082	BY1	X	FBY101	F	LT	49444	1.390E+19	7.810E+10	551	-86.	169.	-56.	156.	30.	13.	0.198	0.684	0.005	0.010	0.256	0.761	0.350	0.562	0.033
A5082	BY1	X	FBY101	F	TL	49444	1.390E+19	7.810E+10	551	-70.	154.	-16.	143.	54.	11.	0.198	0.684	0.005	0.010	0.256	0.761	0.350	0.562	0.033
A5083	BY2	U	FBY201	F	LT	10111	3.930E+18	1.080E+11	551	-32.	175.	-33.	202.	-1.	-27.	0.124	1.266	0.009	0.011	0.361	0.704	0.072	0.417	0.053
A5083	BY2	U	FBY201	F	TL	10111	3.930E+18	1.080E+11	551	-42.	157.	-22.	162.	20.	-5.	0.124	1.266	0.009	0.011	0.361	0.704	0.072	0.417	0.053
A5083	BY2	W	FBY201	F	LT	40587	1.211E+19	-9.990E+02	551	-32.	175.	-30.	171.	2.	4.	0.124	1.266	0.009	0.011	0.361	0.704	0.072	0.417	0.053
A5083	BY2	W	FBY201	F	TL	40587	1.211E+19	-9.990E+02	551	-42.	157.	-13.	137.	29.	20.	0.124	1.266	0.009	0.011	0.361	0.704	0.072	0.417	0.053
A302B	BZ1	R	SASTM	SRM	LT	-999	5.720E+18	6.820E+10	-999	37.	-999.	147.	-999.	110.	-999.	0.240	1.340	0.014	0.023	0.230	0.180	0.110	0.510	0.200
A302B	BZ1	V	SASTM	SRM	LT	-999	2.770E+18	7.760E+10	-999	37.	-999.	50.	-999.	13.	-999.	0.240	1.340	0.014	0.023	0.230	0.180	0.110	0.510	0.200
A533B1	CAB	K	PCAB01	P	LT	36730	1.400E+19	-9.990E+02	-999	-44.	111.	86.	93.	131.	18.	0.200	1.290	0.013	0.022	0.250	0.500	-999.000	0.490	0.140
A302B	CAB	K	SASTM	SRM	LT	36730	1.400E+19	-9.990E+02	-999	37.	-999.	129.	80.	92.	-999.	0.240	1.340	0.014	0.023	0.230	0.180	0.110	0.510	0.200
A533B1	CAB	N	PCAB01	P	LT	64722	3.680E+19	1.580E+11	-999	-44.	111.	109.	86.	153.	24.	0.200	1.290	0.013	0.022	0.250	0.500	-999.000	0.490	0.140
A302B	CAB	N	SASTM	SRM	LT	64722	3.680E+19	1.580E+11	-999	37.	-999.	179.	57.	142.	-999.	0.240	1.340	0.014	0.023	0.230	0.180	0.110	0.510	0.200
A533B1	CAB	P	PCAB01	P	LT	-999	1.430E+19	-9.990E+02	-999	-44.	111.	79.	94.	123.	17.	0.200	1.290	0.013	0.022	0.250	0.500	-999.000	0.490	0.140
A533B1	CAB	P	PCAB02	P	LT	-999	1.430E+19	-9.990E+02	-999	-32.	126.	34.	130.	66.	-4.	0.210	1.240	0.011	0.020	0.240	0.530	-999.000	0.480	0.110
A302B	CAB	P	SASTM	SRM	LT	-999	1.430E+19	-9.990E+02	-999	37.	-999.	164.	68.	127.	-999.	0.240	1.340	0.014	0.023	0.230	0.180	0.110	0.510	0.200
A5082	CB1	Y	FCB101	F	LT	43611	1.350E+19	8.600E+10	-999	-4.	161.	11.	162.	15.	0.	0.204	0.725	0.008	0.009	0.292	0.845	0.399	0.580	0.090
A5082	CB1	Y	FCB101	F	TL	43611	1.350E+19	8.600E+10	-999	-16.	138.	29.	134.	45.	4.	0.204	0.725	0.008	0.009	0.292	0.845	0.399	0.580	0.090
A5082	CB1	Z	FCB101	F	LT	6944	3.320E+18	1.320E+11	562	-4.	161.	-24.	166.	-21.	-5.	0.204	0.725	0.008	0.009	0.292	0.845	0.399	0.580	0.090
A5082	CB1	Z	FCB101	F	TL	6944	3.320E+18	1.320E+11	562	-16.	138.	-2.	138.	14.	0.	0.204	0.725	0.008	0.009	0.292	0.845	0.399	0.580	0.090
A533B1	CB2	X	PCB201	P	LT	39722	1.220E+19	8.580E+10	562	-19.	144.	26.	133.	45.	10.	0.235	1.393	0.012	0.013	0.285	0.610	0.087	0.580	0.081
A533B1	CB2	X	PCB201	P	TL	39722	1.220E+19	8.580E+10	562	1.	99.	52.	106.	51.	-7.	0.235	1.393	0.012	0.013	0.285	0.610	0.087	0.580	0.081
A533B1	CB2	Z	PCB201	P	LT	0	3.380E+18	1.250E+11	-999	-19.	144.	2.	134.	21.	9.	0.235	1.393	0.012	0.013	0.285	0.610	0.087	0.580	0.081
A533B1	CB2	Z	PCB201	P	TL	0	3.380E+18	1.250E+11	-999	1.	99.	32.	103.	31.	-4.	0.235	1.393	0.012	0.013	0.285	0.610	0.087	0.580	0.081
A533B1	CC1	W263	PCC103	P	LT	25760	6.000E+18	6.490E+10	545	6.	148.	71.	119.	65.	29.	0.260	1.374	0.009	0.032	0.316	0.596	0.033	0.581	0.081
A533B1	CC1	W263	SHSS01	SRM	LT	25760	5.900E+18	6.490E+10	545	30.	138.	131.	113.	101.	25.	0.219	1.465	0.010	0.015	0.186	0.665	0.103	0.548	0.174
A533B1	CC1	W97	PCC103	P	LT	-999	2.380E+19	-9.990E+02	545	6.	148.	118.	105.	111.	43.	0.260	1.374	0.009	0.032	0.316	0.596	0.033	0.581	0.081
A533B1	CC1	W97	PCC103	P	TL	-999	2.470E+19	-9.990E+02	545	21.	114.	131.	93.	110.	21.	0.260	1.374	0.009	0.032	0.316	0.596	0.033	0.581	0.081
A533B1	CC2	W263	PCC202	P	LT	40114	8.060E+18	5.580E+10	545	14.	146.	95.	138.	81.	8.	0.208	1.210	0.005	0.007	0.205	0.590	0.104	0.570	0.133
A533B1	CC2	W263	SHSS01	SRM	LT	40114	8.060E+18	5.580E+10	545	30.	138.	149.	99.	120.	40.	0.219	1.465	0.010	0.015	0.186	0.665	0.103	0.548	0.174
A533B1	CC2	W97	PCC202	P	LT	-999	1.850E+19	-9.990E+02	545	14.	146.	122.	107.	108.	40.	0.208	1.210	0.005	0.007	0.205	0.590	0.104	0.570	0.133
A533B1	CC2	W97	PCC202	P	TL	-999	1.850E+19	-9.990E+02	545	33.	127.	136.	88.	103.	39.	0.208	1.210	0.005	0.007	0.205	0.590	0.104	0.570	0.133
A533B1	CH1	30D	PCH1JW	P	LT	61871	1.300E+17	5.900E+08	531	26.	110.	38.	154.	12.	-44.	0.200	1.420	0.016	0.022	0.300	0.530	-999.000	0.530	0.165
A533B1	CK1	T	PCK101	P	LT	11111	2.690E+18	6.720E+10	537	8.	132.	67.	115.	58.	17.	0.240	1.400	0.009	0.009	0.250	0.490	0.068	0.460	0.140
A533B1	CK1	T	PCK101	P	TL	11111	2.690E+18	6.720E+10	537	20.	100.	81.	97.	60.	3.	0.240	1.400	0.009	0.009	0.250	0.490	0.068	0.460	0.140
A533B1	CK1	T	SHSS02	SRM	LT	11111	2.690E+18	6.720E+10	537	47.	124.	105.	104.	58.	20.	0.217	1.478	0.011	0.015	0.225	0.640	0.095	0.502	0.170
A533B1	CK1	U	PCK101	P	LT	80556	1.770E+19	6.110E+10	537	8.	132.	114.	120.	106.	12.	0.240	1.400	0.009	0.009	0.250	0.490	0.068	0.460	0.140
A533B1	CK1	U	PCK101	P	TL	80556	1.770E+19	6.110E+10	537	20.	100.	115.	115.	94.	-15.	0.240	1.400	0.009	0.009	0.250	0.490	0.068	0.460	0.140
A533B1	CK1	U	SHSS02	SRM	LT	80556	1.770E+19	6.110E+10	537	47.	124.	185.	114.	138.	10.	0.217	1.478	0.011	0.015	0.225	0.640	0.095	0.502	0.170
A533B1	CK1	X	PCK101	P	LT	29722	8.130E+18	7.580E+10	537	8.	132.	94.	117.	86.	15.	0.240	1.400	0.009	0.009	0.250	0.490	0.068	0.460	0.140
A533B1	CK1	X	PCK101	P	TL	29722	8.130E+18	7.580E+10	537	20.	100.	125.	86.	105.	14.	0.240	1.400	0.009	0.009	0.250	0.490	0.068	0.460	0.140
A533B1	CK1	X	SHSS02	SRM	LT	29722	8.130E+18	7.580E+10	537	47.	124.	147.	86.	100.	38.	0.217	1.478	0.011	0.015	0.225	0.640	0.095	0.502	0.170
A533B1	CK1	Y	PCK101	P	LT	43333	1.230E+19	7.860E+10	537	8.	132.	106.	121.	97.	11.	0.240	1.400	0.009	0.009	0.250	0.490	0.068	0.460	0.140
A533B1	CK1	Y	PCK101	P	TL	43333	1.230E+19	7.860E+10	537	20.	100.	130.	84.	110.	15.	0.240	1.400	0.009	0.009	0.250	0.490	0.068	0.460	0.140
A533B1	CK1	Y	SHSS02	SRM	LT	43333	1.230E+19	7.860E+10	537	47.	124.	155.	113.	108.	11.	0.217	1.478	0.011	0.015	0.225	0.640	0.095	0.502	0.170

Material ID	Plant ID	Capsule	Heat ID	Product ID	Specimen Orientation	Irradiation time hr	Fluence n/cm^2	Flux n/cm^2/s	Tcoolant F	TTu30 F	USEu ft-lb	TTi30 F	USEi ft-lb	dTT30 F	dUSE ft-lb	C wt%	Mn wt%	P wt%	S wt%	Si wt%	Ni wt%	Cr wt%	Mo wt%	Cu wt%
A533B1	CK2	T	PCK201	P	LT	9444	2.180E+18	6.400E+10	542	25.	130.	81.	112.	56.	19.	0.215	1.285	0.017	0.014	0.215	0.580	0.072	0.525	0.110
A533B1	CK2	T	PCK201	P	TL	9444	2.180E+18	6.400E+10	542	25.	91.	103.	78.	78.	14.	0.215	1.285	0.017	0.014	0.215	0.580	0.072	0.525	0.110
A533B1	CK2	U	PCK201	P	LT	75833	1.500E+19	5.490E+10	542	25.	130.	121.	136.	96.	-5.	0.215	1.285	0.017	0.014	0.215	0.580	0.072	0.525	0.110
A533B1	CK2	U	PCK201	P	TL	75833	1.500E+19	5.490E+10	542	25.	91.	162.	-999.	137.	-999.	0.215	1.285	0.017	0.014	0.215	0.580	0.072	0.525	0.110
A533B1	CK2	X	PCK201	P	LT	46111	1.030E+19	6.220E+10	542	25.	130.	116.	112.	91.	18.	0.215	1.285	0.017	0.014	0.215	0.580	0.072	0.525	0.110
A533B1	CK2	X	PCK201	P	TL	46111	1.030E+19	6.220E+10	542	25.	91.	137.	81.	112.	10.	0.215	1.285	0.017	0.014	0.215	0.580	0.072	0.525	0.110
A533B1	CK2	Y	PCK201	P	LT	28333	6.620E+18	6.510E+10	542	25.	130.	107.	111.	82.	19.	0.215	1.285	0.017	0.014	0.215	0.580	0.072	0.525	0.110
A533B1	CK2	Y	PCK201	P	TL	28333	6.620E+18	6.510E+10	542	25.	91.	127.	79.	102.	12.	0.215	1.285	0.017	0.014	0.215	0.580	0.072	0.525	0.110
A533B1	CL1	U	PCL101	P	LT	9222	3.470E+18	1.050E+11	558	-2.	130.	-5.	135.	-3.	-5.	0.225	1.395	0.006	0.015	0.235	0.570	0.055	0.530	0.065
A533B1	CL1	U	PCL101	P	TL	9222	3.470E+18	1.050E+11	558	-17.	110.	9.	93.	26.	18.	0.225	1.395	0.006	0.015	0.235	0.570	0.055	0.530	0.065
A533B1	CL1	Y	PCL101	P	LT	40278	1.300E+19	8.970E+10	558	-2.	130.	20.	136.	22.	-6.	0.225	1.395	0.006	0.015	0.235	0.570	0.055	0.530	0.065
A533B1	CL1	Y	PCL101	P	TL	40278	1.300E+19	8.970E+10	558	-17.	110.	28.	101.	45.	10.	0.225	1.395	0.006	0.015	0.235	0.570	0.055	0.530	0.065
A533B1	COF	3D	PCOFJW	P	TL	49646	8.400E+17	4.700E+09	533	-49.	122.	-31.	124.	18.	-3.	-999.000	1.480	0.005	-999.000	0.240	0.600	-999.000	0.580	0.029
A533B1	CP1	U	PCP1JW	P	LT	7972	3.530E+18	1.230E+11	-999	-20.	132.	-12.	121.	8.	11.	-999.000	-999.000	0.006	-999.000	-999.000	0.590	-999.000	-999.000	0.050
A533B1	CP1	U	PCP1JW	P	TL	7972	3.530E+18	1.230E+11	-999	2.	79.	22.	94.	20.	-15.	-999.000	-999.000	0.006	-999.000	-999.000	0.590	-999.000	-999.000	0.050
A533B1	CP2	U	PCP201	P	LT	7924	3.280E+18	-9.990E+02	-999	-8.	120.	-8.	123.	0.	-3.	0.220	1.380	0.014	0.015	0.245	0.620	0.048	0.585	0.065
A533B1	CP2	U	PCP201	P	TL	7924	3.280E+18	-9.990E+02	-999	-12.	87.	11.	96.	24.	-9.	0.220	1.380	0.014	0.015	0.245	0.620	0.048	0.585	0.065
A533B1	CPR	30D	PCPR01	P	LT	59528	2.400E+17	1.050E+09	527	-54.	132.	10.	125.	64.	7.	0.230	1.278	0.009	0.014	0.200	0.758	0.110	0.496	0.214
A533B1	CPR	300D	PCPR01	P	LT	98179	2.800E+17	7.940E+08	527	-54.	132.	8.	127.	62.	5.	0.230	1.278	0.009	0.014	0.200	0.758	0.110	0.496	0.214
A533B1	CR3	B	PCR301	P	TL	6451	1.050E+18	4.510E+10	556	17.	98.	56.	97.	39.	1.	0.230	1.300	0.008	0.016	0.220	0.540	0.110	0.550	0.200
A533B1	CR3	C	PCR301	P	TL	35568	6.560E+18	5.120E+10	556	17.	98.	133.	75.	116.	23.	0.230	1.300	0.008	0.016	0.220	0.540	0.110	0.550	0.200
A533B1	CR3	C	SHSS02	SRM	LT	35568	6.560E+18	5.120E+10	556	47.	124.	129.	108.	82.	16.	0.217	1.478	0.011	0.015	0.225	0.640	0.095	0.502	0.170
A533B1	CR3	D	PCR301	P	TL	41592	7.500E+18	4.960E+10	556	17.	98.	119.	74.	102.	24.	0.230	1.300	0.008	0.016	0.220	0.540	0.110	0.550	0.200
A533B1	CR3	F	PCR301	P	TL	45024	1.080E+19	6.580E+10	556	17.	98.	133.	75.	116.	23.	0.230	1.300	0.008	0.016	0.220	0.540	0.110	0.550	0.200
A302B	CTY	A	PCTY02	P	LT	14806	2.590E+18	4.870E+10	537	-29.	139.	12.	122.	42.	17.	0.200	1.420	0.010	0.014	0.260	0.200	-999.000	0.470	0.100
A302B	CTY	A	SASTM	SRM	LT	14806	2.590E+18	4.870E+10	537	37.	-999.	-999.	-999.	-999.	-999.	0.240	1.340	0.014	0.023	0.230	0.180	0.110	0.510	0.200
A302B	CTY	D	PCTY04	P	LT	95278	2.280E+19	6.660E+10	537	-17.	130.	55.	110.	72.	20.	0.200	1.370	0.010	0.021	0.190	0.200	-999.000	0.470	0.120
A302B	CTY	D	SASTM	SRM	LT	95278	2.280E+19	6.660E+10	537	37.	-999.	169.	66.	132.	-999.	0.240	1.340	0.014	0.023	0.230	0.180	0.110	0.510	0.200
A302B	CTY	F	PCTY02	P	LT	21278	4.630E+18	6.040E+10	537	-29.	139.	9.	127.	38.	12.	0.200	1.420	0.010	0.014	0.260	0.200	-999.000	0.470	0.100
A302B	CTY	F	PCTY04	P	LT	21278	4.630E+18	6.040E+10	537	-17.	130.	59.	126.	76.	4.	0.200	1.370	0.010	0.021	0.190	0.200	-999.000	0.470	0.120
A302B	CTY	F	PCTY07	P	LT	21278	4.630E+18	6.040E+10	537	-24.	125.	30.	122.	54.	3.	0.200	1.460	0.013	0.010	0.220	0.200	-999.000	0.480	0.120
A302B	CTY	F	SASTM	SRM	LT	21278	4.630E+18	6.040E+10	537	37.	-999.	123.	66.	86.	-999.	0.240	1.340	0.014	0.023	0.230	0.180	0.110	0.510	0.200
A302B	CTY	H	PCTY02	P	LT	66667	1.550E+19	6.460E+10	537	-29.	139.	12.	134.	42.	5.	0.200	1.420	0.010	0.014	0.260	0.200	-999.000	0.470	0.100
A302B	CTY	H	PCTY04	P	LT	66667	1.550E+19	6.460E+10	537	-17.	130.	52.	123.	69.	8.	0.200	1.370	0.010	0.021	0.190	0.200	-999.000	0.470	0.120
A302B	CTY	H	PCTY07	P	LT	66667	1.550E+19	6.460E+10	537	-24.	125.	27.	127.	51.	-2.	0.200	1.460	0.013	0.010	0.220	0.200	-999.000	0.480	0.120
A302B	CTY	H	SASTM	SRM	LT	66667	1.550E+19	6.460E+10	537	37.	-999.	156.	-999.	119.	-999.	0.240	1.340	0.014	0.023	0.230	0.180	0.110	0.510	0.200
A533B1	DAC	1	PDAC01	P	LT	52000	4.900E+17	2.600E+09	532	-33.	158.	10.	159.	42.	-1.	-999.000	1.350	0.008	-999.000	0.065	0.667	0.140	0.625	0.150
A5082	DB1	A	FDB101	F	TL	29146	1.290E+19	1.230E+11	556	-30.	142.	-34.	-999.	-4.	-999.	0.260	0.680	0.004	0.006	0.300	0.770	0.380	0.640	0.040
A5082	DB1	A	FDB102	F	TL	29146	1.290E+19	1.230E+11	556	10.	116.	47.	111.	38.	6.	0.220	0.630	0.011	0.011	0.270	0.810	0.320	0.630	0.020
A533B1	DB1	A	SHSS02	SRM	LT	29146	1.290E+19	1.230E+11	556	47.	124.	159.	98.	112.	26.	0.217	1.478	0.011	0.015	0.225	0.640	0.095	0.502	0.170
A5082	DB1	B	FDB102	F	TL	22632	5.920E+18	-9.990E+02	556	10.	116.	6.	113.	-4.	4.	0.220	0.630	0.011	0.011	0.270	0.810	0.320	0.630	0.020
A5082	DB1	D	FDB102	F	TL	47755	9.620E+18	5.600E+10	556	10.	116.	15.	114.	6.	2.	0.220	0.630	0.011	0.011	0.270	0.810	0.320	0.630	0.020
A5082	DB1	F	FDB102	F	TL	8976	1.960E+18	6.080E+10	556	10.	116.	-1.	118.	-10.	-2.	0.220	0.630	0.011	0.011	0.270	0.810	0.320	0.630	0.020
A533B1	DC1	S	PDC103	P	LT	11056	2.840E+18	7.150E+10	539	6.	122.	14.	126.	9.	-4.	0.235	1.445	0.010	0.014	0.225	0.481	0.049	0.475	0.081
A533B1	DC1	S	SHSS02	SRM	LT	11056	2.840E+18	7.150E+10	539	47.	124.	112.	123.	66.	1.	0.217	1.478	0.011	0.015	0.225	0.640	0.095	0.502	0.170
A533B1	DC1	Y	PDC103	P	LT	51389	9.410E+18	5.090E+10	540	6.	122.	51.	119.	46.	4.	0.235	1.445	0.010	0.014	0.225	0.481	0.049	0.475	0.081
A533B1	DC1	Y	SHSS02	SRM	LT	51389	9.410E+18	5.090E+10	540	47.	124.	155.	121.	109.	3.	0.217	1.478	0.011	0.015	0.225	0.640	0.095	0.502	0.170
A533B1	DC2	U	PDC201	P	LT	8694	3.650E+18	1.160E+11	542	6.	145.	73.	124.	68.	21.	0.237	1.255	0.009	0.012	0.164	0.662	0.073	0.438	0.140
A533B1	DC2	U	PDC201	P	TL	8694	3.650E+18	1.160E+11	542	27.	95.	100.	95.	73.	0.	0.237	1.255	0.009	0.012	0.164	0.662	0.073	0.438	0.140
A533B1	DC2	X	PDC201	P	LT	27250	9.160E+18	9.340E+10	541	6.	145.	115.	114.	109.	31.	0.237	1.255	0.009	0.012	0.164	0.662	0.073	0.438	0.140
A533B1	DC2	X	PDC201	P	TL	27250	9.160E+18	9.340E+10	541	27.	95.	125.	85.	98.	10.	0.237	1.255	0.009	0.012	0.164	0.662	0.073	0.438	0.140
A533B1	DC2	Y	PDC201	P	LT	61362	1.320E+19	-9.990E+02	540	6.	145.	117.	118.	111.	27.	0.237	1.255	0.009	0.012	0.164	0.662	0.073	0.438	0.140
A533B1	DC2	Y	PDC201	P	TL	61362	1.320E+19	-9.990E+02	540	27.	95.	136.	89.	109.	6.	0.237	1.255	0.009	0.012	0.164	0.662	0.073	0.438	0.140
A302BM	DR2	2	PDR201	P	LT	20136	2.000E+19	2.760E+11	546	-12.	152.	90.	118.	102.	34.	0.197	1.190	0.008	0.013	0.250	0.465	-999.000	0.435	0.190
A302BM	DR2	3	PDR201	P	LT	-999	1.200E+16	6.000E+08	546	-12.	152.	-49.	137.	-37.	15.	0.197	1.190	0.008	0.013	0.250	0.465	-999.000	0.435	0.190
A302BM	DR2	4	PDR201	P	LT	-999	9.500E+18	4.600E+11	546	-12.	152.	38.	116.	51.	35.	0.197	1.190	0.008	0.013	0.250	0.465	-999.000	0.435	0.190
A302BM	DR2	5	PDR201	P	LT	33984	4.290E+19	3.510E+11	546	-12.	152.	73.	124.	85.	28.	0.197	1.190	0.008	0.013	0.250	0.465	-999.000	0.435	0.190
A302BM	DR2	8	PDR201	P	LT	54623	5.210E+16	2.650E+08	529	-12.	152.	-34.	133.	-21.	19.	0.197	1.190	0.008	0.013	0.250	0.465	-999.000	0.435	0.190
A302BM	DR3	12	PDR301	P	LT	13200	1.360E+19	2.860E+11	546	-5.	136.	44.	121.	49.	14.	0.247	1.645	0.008	0.016	0.253	0.537	0.102	0.493	0.133
A302BM	DR3	13	PDR301	P	LT	8460	0.926E+16	3.040E+08	529	-5.	136.	-8.	141.	-2.	-6.	0.247	1.645	0.008	0.016	0.253	0.537	0.102	0.493	0.133
A302BM	DR3	14	PDR301	P	LT	8460	7.110E+18	2.340E+11	546	-5.	136.	47.	114.	53.	22.	0.247	1.645	0.008	0.016	0.253	0.537	0.102	0.493	0.133
A302BM	DR3	18	PDR301	P	LT	52421	7.100E+16	3.760E+08	529	-5.	136.	2.	155.	8.	-20.	0.247	1.645	0.008	0.016	0.253	0.537	0.102	0.493	0.133
A302BM	DR3	4	PDR301	P	LT	23564	1.860E+19	-9.990E+02	546	-5.	136.	97.	111.	103.	25.	0.247	1.645	0.008	0.016	0.253	0.537	0.102	0.493	0.133
A302BM	DR3	6	PDR301	P	LT	23232	2.700E+16	3.230E+08	529	-5.	136.	-5.	136.	0.	-1.	0.247	1.645	0.008	0.016	0.253	0.537	0.102	0.493	0.133
A533B1	FA1	U	PFA101	P	LT	27056	1.750E+19	1.800E+11	-999	-22.	143.	85.	119.	107.	24.	0.200	1.395	0.015	0.014	0.230	0.560	0.130	0.535	0.100
A533B1	FA1	U	PFA101	P	TL	27056	1.750E+19	1.800E+11	-999	3.	100.	105.	87.	103.	13.	0.200	1.395	0.015	0.014	0.230	0.560	0.130	0.535	0.100
A533B1	FA1	W	PFA101	P	LT	108961	4.040E+19	-9.990E+02	-999	-22.	143.	125.	117.	146.	26.	0.200	1.395	0.015	0.014	0.230	0.560	0.130	0.535	0.100
A533B1	FA1	W	PFA101	P	TL	108961	4.040E+19	-9.990E+02	-999	3.	100.	154.	91.	152.	10.	0.200	1.395	0.015	0.014	0.230	0.560	0.130	0.535	0.100
A533B1	FA1	X	PFA101	P	LT	53611	2.990E+19	1.550E+11	-999	-22.	143.	107.	120.	128.	23.	0.200	1.395	0.015	0.014	0.230	0.560	0.130	0.535	0.100
A533B1	FA1	X	PFA101	P	TL	53611	2.990E+19	1.550E+11	-999	3.	100.	116.	83.	113.	17.	0.200	1.395	0.015	0.014	0.230	0.560	0.130	0.535	0.100
A533B1	FA1	Y	PFA101	P	LT	10111	5.730E+18	1.580E+11	-999	-22.	143.	46.	129.	68.	14.	0.200	1.395	0.015	0.014	0.230	0.560	0.130	0.535	0.100
A533B1	FA1	Y	PFA101	P	TL	10111	5.730E+18	1.580E+11	-999	3.	100.	75.	96.	73.	4.	0.200	1.395	0.015	0.014	0.230	0.560	0.130	0.535	0.100
A533B1	FA2	U	PFA201	P	LT	9750	6.120E+18	1.750E+11	-999	-22.	137.	80.	105.	102.	32.	0.215	1.327	0.005	0.016	0.229	0.597	0.106	0.490	0.195
A533B1	FA2	U	PFA201	P	TL	9750	6.120E+18	1.750E+11	-999	-8.	99.	117.	74.	125.	24.	0.215	1.327	0.005	0.016	0.229	0.597	0.106	0.490	0.195
A533B1	FA2	W	PFA201	P	LT	34722	1.670E+19	1.340E+11	-999	-22.	137.	141.	111.	163.	27.	0.215	1.327	0.005	0.016	0.229	0.597	0.106	0.490	0.195
A533B1	FA2	W	PFA201	P	TL	34722	1.670E+19	1.340E+11	-999	-8.	99.	160.	86.	168.	13.	0.215	1.327	0.005	0.016	0.229	0.597	0.106	0.490	0.195
A533B1	FA2	X	PFA201	P	LT	56389	3.020E+19	1.490E+11	-999	-22.	137.	142.	102.	164.	36.	0.215	1.327	0.005	0.016	0.229	0.597	0.106	0.490	0.195
A533B1	FA2	X	PFA201	P	TL	56389	3.020E+19	1.490E+11	-999	-8.	99.	192.	74.	200.	24.	0.215	1.327	0.005	0.016	0.229	0.597	0.106	0.490	0.195
A533B1	FC1	W225	PFC101	P	LT	22753	5.530E+18	-9.990E+02	527	21.	147.	77.	133.	56.	15.	0.220	1.461	0.011	0.012	0.214	0.483	0.040	0.524	0.101
A533B1	FC1	W225	SHSS01	SRM	LT	22753	5.530E+18	-9.990E+02	527	30.	138.	146.	108.	116.	30.	0.219	1.465	0.010	0.015	0.186	0.665	0.103	0.548	0.174
A533B1	FC1	W265	PFC101	P	LT	51895	7.710E+18	-9.990E+02	534	21.	147.	93.	116.	72.	32.	0.220	1.461	0.011	0.012	0.214	0.483	0.040	0.524	0.101
A533B1	FC1	W265	PFC101	P	TL	51895	7.710E+18	-9.990E+02	534	31.	126.	106.	97.	75.	29.	0.220	1.461	0.011	0.012	0.214	0.483	0.040	0.524	0.101

Embrittlement Analysis Data Base

Material ID	Plant ID	Capsule	Heat ID	Product ID	Specimen Orientation	Irradiation time hr	Fluence n/cm^2	Flux n/cm^2/s	Tcoolant F	TTu30 F	USEu ft-lb	TTi30 F	USEi ft-lb	dTT30 F	dUSE ft-lb	C wt%	Mn wt%	P wt%	S wt%	Si wt%	Ni wt%	Cr wt%	Mo wt%	Cu wt%
A533B1	FC1	W275	PFC101	P	LT	-999	1.280E+19	-9.990E+02	538	21.	147.	83.	116.	62.	32.	0.220	1.461	0.011	0.012	0.214	0.483	0.040	0.524	0.101
A533B1	FC1	W275	PFC101	P	TL	-999	1.280E+19	-9.990E+02	538	31.	126.	108.	96.	77.	29.	0.220	1.461	0.011	0.012	0.214	0.483	0.040	0.524	0.101
A533B1	FC1	W275	SHSS01	SRM	LT	-999	1.280E+19	-9.990E+02	538	24.	138.	186.	111.	162.	27.	0.219	1.465	0.010	0.015	0.186	0.665	0.103	0.548	0.174
A533B1	FTZ	30D	PFTZ01	P	LT	52438	2.600E+17	1.400E+09	532	-29.	138.	-22.	134.	7.	4.	-999.000	1.350	0.011	-999.000	0.065	0.625	0.110	0.490	0.115
A5082	GIN	R	FGIN01	F	LT	22333	1.100E+19	1.360E+11	550	-42.	188.	20.	144.	62.	44.	0.190	0.670	0.010	0.011	0.200	0.690	0.370	0.570	0.050
A5082	GIN	R	FGIN02	F	LT	22333	1.100E+19	1.360E+11	550	-24.	145.	-9.	148.	15.	-3.	0.180	0.660	0.010	0.007	0.230	0.690	0.330	0.580	0.070
A302B	GIN	R	SASTM	SRM	LT	22333	1.100E+19	1.360E+11	550	37.	-999.	133.	62.	97.	-999.	0.240	1.340	0.014	0.023	0.230	0.180	0.110	0.510	0.200
A5082	GIN	S	FGIN01	F	LT	149167	3.510E+19	6.550E+10	-999	-42.	188.	5.	150.	47.	38.	0.190	0.670	0.010	0.011	0.200	0.690	0.370	0.570	0.050
A5082	GIN	S	FGIN02	F	LT	149167	3.510E+19	6.550E+10	-999	-24.	145.	45.	144.	68.	1.	0.180	0.660	0.010	0.007	0.230	0.690	0.330	0.580	0.070
A5082	GIN	T	FGIN01	F	LT	60278	1.910E+19	8.810E+10	548	-42.	188.	-8.	135.	34.	54.	0.190	0.670	0.010	0.011	0.200	0.690	0.370	0.570	0.050
A5082	GIN	T	FGIN02	F	LT	60278	1.910E+19	8.810E+10	548	-24.	145.	-58.	167.	-35.	-22.	0.180	0.660	0.010	0.007	0.230	0.690	0.330	0.580	0.070
A302B	GIN	T	SASTM	SRM	LT	60278	1.910E+19	8.810E+10	548	37.	-999.	127.	74.	90.	-999.	0.240	1.340	0.014	0.023	0.230	0.180	0.110	0.510	0.200
A5082	GIN	V	FGIN01	F	LT	12361	5.850E+18	1.310E+11	552	-42.	188.	-7.	157.	36.	31.	0.190	0.670	0.010	0.011	0.200	0.690	0.370	0.570	0.050
A5082	GIN	V	FGIN02	F	LT	12361	5.850E+18	1.310E+11	552	-24.	145.	-36.	135.	-13.	10.	0.180	0.660	0.010	0.007	0.230	0.690	0.330	0.580	0.070
A302B	GIN	V	SASTM	SRM	LT	12361	5.850E+18	1.310E+11	552	37.	-999.	127.	69.	90.	-999.	0.240	1.340	0.014	0.023	0.230	0.180	0.110	0.510	0.200
A533B1	HA1	30D	PHA101	P	LT	50324	2.400E+17	1.300E+09	530	-64.	144.	-16.	135.	48.	9.	0.240	1.430	0.010	0.013	0.200	0.650	-999.000	0.560	0.113
A533B1	HA2	30D	PHA2JW	P	LT	57692	2.300E+17	1.100E+09	532	-21.	116.	-16.	115.	4.	1.	-999.000	1.390	0.010	-999.000	-999.000	0.630	-999.000	0.600	0.080
A302B	HB2	S	PHB201	P	LT	11222	5.060E+18	1.250E+11	546	-17.	98.	17.	76.	34.	21.	0.190	1.350	0.007	0.019	0.230	0.200	-999.000	0.480	0.120
A302B	HB2	S	PHB202	P	LT	11222	5.060E+18	1.250E+11	546	11.	99.	27.	85.	16.	14.	0.200	1.290	0.010	0.021	0.220	0.200	-999.000	0.460	0.100
A302B	HB2	S	PHB203	P	LT	11222	5.060E+18	1.250E+11	546	27.	113.	41.	96.	13.	17.	0.190	1.320	0.010	0.015	0.190	0.200	-999.000	0.490	0.090
A302B	HB2	S	SASTM	SRM	TL	11222	5.060E+18	1.250E+11	546	65.	-999.	136.	40.	72.	-999.	0.240	1.340	0.014	0.023	0.230	0.180	0.110	0.510	0.200
A302B	HB2	T	PHB203	P	LT	63611	4.420E+19	1.930E+11	546	27.	113.	102.	109.	74.	4.	0.190	1.320	0.010	0.015	0.190	0.200	-999.000	0.490	0.090
A302B	HB2	T	SASTM	SRM	TL	63611	4.420E+19	1.930E+11	546	65.	-999.	232.	37.	167.	-999.	0.240	1.340	0.014	0.023	0.230	0.180	0.110	0.510	0.200
A302B	HB2	V	PHB202	P	LT	28056	6.010E+18	5.980E+10	546	11.	99.	55.	104.	44.	-5.	0.200	1.290	0.010	0.021	0.220	0.200	-999.000	0.460	0.100
A302B	HB2	V	SASTM	SRM	TL	28056	6.010E+18	5.980E+10	546	65.	-999.	132.	40.	68.	-999.	0.240	1.340	0.014	0.023	0.230	0.180	0.110	0.510	0.200
A302B	HM3	01	SHM3	SRM	LT	-999	4.100E+18	-9.990E+02	570	0.	93.	46.	84.	46.	10.	0.200	1.270	0.016	0.036	0.210	-999.000	-999.000	0.470	-999.000
A302B	HM3	4	SHM3	SRM	LT	-999	2.900E+19	7.100E+11	570	0.	93.	68.	79.	68.	14.	0.200	1.270	0.016	0.036	0.210	-999.000	-999.000	0.470	-999.000
A533B1	HOP	30D	PHOPJW	P	LT	52646	1.420E+17	7.500E+08	532	-6.	147.	-8.	126.	-2.	21.	-999.000	1.380	0.012	-999.000	-999.000	0.640	0.120	0.560	0.090
A302B	IP2	T	PIP201	P	LT	12444	2.430E+18	5.420E+10	534	9.	128.	58.	112.	49.	16.	0.200	1.280	0.010	0.019	0.250	0.630	-999.000	0.460	0.211
A302B	IP2	T	PIP202	P	LT	12444	2.430E+18	5.420E+10	534	17.	121.	110.	99.	93.	22.	0.220	1.300	0.014	0.020	0.220	0.441	-999.000	0.500	0.149
A302B	IP2	T	PIP203	P	LT	12444	2.430E+18	5.420E+10	534	16.	122.	147.	96.	131.	26.	0.220	1.290	0.011	0.018	0.250	0.595	-999.000	0.460	0.197
A302B	IP2	T	SASTM	SRM	LT	12444	2.430E+18	5.420E+10	534	37.	-999.	96.	63.	59.	-999.	0.240	1.340	0.014	0.023	0.230	0.180	0.110	0.510	0.200
A302B	IP2	V	PIP202	P	LT	75833	5.060E+18	1.860E+10	524	17.	121.	100.	113.	83.	8.	0.220	1.300	0.014	0.020	0.220	0.441	-999.000	0.500	0.149
A302B	IP2	V	SASTM	SRM	LT	75833	5.060E+18	1.860E+10	524	37.	-999.	131.	73.	94.	-999.	0.240	1.340	0.014	0.023	0.230	0.180	0.110	0.510	0.200
A302B	IP2	Y	PIP203	P	LT	20833	4.530E+18	6.150E+10	529	16.	122.	169.	87.	152.	35.	0.220	1.290	0.011	0.018	0.250	0.595	-999.000	0.460	0.197
A302B	IP2	Y	SASTM	SRM	LT	20833	4.530E+18	6.150E+10	529	37.	-999.	104.	72.	67.	-999.	0.240	1.340	0.014	0.023	0.230	0.180	0.110	0.510	0.200
A302B	IP2	Z	PIP201	P	LT	45833	1.080E+19	6.660E+10	525	9.	128.	121.	106.	113.	22.	0.200	1.280	0.010	0.019	0.250	0.630	-999.000	0.460	0.211
A302B	IP2	Z	PIP202	P	LT	45833	1.080E+19	6.660E+10	525	17.	121.	123.	92.	106.	29.	0.220	1.300	0.014	0.020	0.220	0.441	-999.000	0.500	0.149
A302B	IP2	Z	PIP203	P	LT	45833	1.080E+19	6.660E+10	525	16.	122.	198.	95.	182.	28.	0.220	1.290	0.011	0.018	0.250	0.595	-999.000	0.460	0.197
A302B	IP2	Z	SASTM	SRM	LT	45833	1.080E+19	6.660E+10	525	37.	-999.	125.	73.	88.	-999.	0.240	1.340	0.014	0.023	0.230	0.180	0.110	0.510	0.200
A302BM	IP3	T	PIP301	P	LT	12000	3.120E+18	7.220E+10	540	-6.	135.	87.	134.	93.	2.	0.220	1.410	0.010	0.023	0.280	0.500	0.080	0.460	0.180
A302BM	IP3	T	PIP304	P	LT	12000	3.120E+18	7.220E+10	540	25.	110.	168.	98.	143.	12.	0.220	1.300	0.012	0.024	0.280	0.520	0.080	0.450	0.240
A302BM	IP3	T	PIP304	P	TL	12000	3.120E+18	7.220E+10	540	59.	71.	168.	76.	109.	-4.	0.220	1.300	0.012	0.024	0.280	0.520	0.080	0.450	0.240
A302BM	IP3	Y	PIP304	P	TL	29167	7.240E+18	6.920E+10	540	59.	71.	208.	57.	150.	14.	0.220	1.300	0.012	0.024	0.280	0.520	0.080	0.450	0.240
A533B1	IP3	Y	SHSS02	SRM	LT	29167	7.240E+18	6.920E+10	540	47.	124.	192.	101.	145.	23.	0.217	1.478	0.011	0.015	0.225	0.640	0.095	0.502	0.170
A302BM	IP3	Z	PIP303	P	LT	48889	1.040E+19	5.930E+10	540	-20.	129.	118.	115.	138.	14.	0.200	1.320	0.011	0.025	0.260	0.490	0.080	0.500	0.190
A302BM	IP3	Z	PIP304	P	LT	48889	1.040E+19	5.930E+10	540	25.	110.	199.	87.	174.	23.	0.220	1.300	0.012	0.024	0.280	0.520	0.080	0.450	0.240
A302BM	IP3	Z	PIP304	P	TL	48889	1.040E+19	5.930E+10	540	59.	71.	216.	54.	157.	17.	0.220	1.300	0.012	0.024	0.280	0.520	0.080	0.450	0.240
A533B1	KU1	177D	PKU1JW	P	TL	59968	9.600E+17	4.400E+09	533	-27.	115.	-15.	111.	11.	4.	0.210	1.160	0.008	0.010	0.230	0.600	0.066	0.500	0.060
A533B1	KU2	3D	PKU2JW	P	TL	61223	1.100E+18	4.900E+09	533	14.	104.	29.	92.	15.	12.	0.210	1.330	0.008	0.013	0.250	0.580	0.130	0.500	0.090
A5082	KWE	P	FKWE01	F	LT	97500	2.840E+19	8.090E+10	532	-34.	165.	15.	164.	49.	1.	0.210	0.690	0.010	0.011	0.250	0.710	0.400	0.580	0.060
A5082	KWE	P	FKWE02	F	LT	97500	2.840E+19	8.090E+10	532	-71.	166.	-25.	162.	46.	4.	0.200	0.790	0.010	0.009	0.280	0.750	0.350	0.580	0.060
A533B1	KWE	P	SHSS02	SRM	LT	97500	2.840E+19	8.090E+10	532	47.	124.	198.	106.	151.	18.	0.217	1.478	0.011	0.015	0.225	0.640	0.095	0.502	0.170
A5082	KWE	R	FKWE01	F	LT	40556	1.900E+19	1.300E+11	532	-34.	165.	-19.	154.	15.	11.	0.210	0.690	0.010	0.011	0.250	0.710	0.400	0.580	0.060
A5082	KWE	R	FKWE02	F	LT	40556	1.900E+19	1.300E+11	532	-71.	166.	-36.	159.	35.	7.	0.200	0.790	0.010	0.009	0.280	0.750	0.350	0.580	0.060
A533B1	KWE	R	SHSS02	SRM	LT	40556	1.900E+19	1.300E+11	532	47.	124.	201.	97.	154.	27.	0.217	1.478	0.011	0.015	0.225	0.640	0.095	0.502	0.170
A5082	KWE	S	FKWE01	F	LT	142009	3.450E+19	-9.990E+02	532	-34.	165.	24.	145.	58.	20.	0.210	0.690	0.010	0.011	0.250	0.710	0.400	0.580	0.060
A5082	KWE	S	FKWE02	F	LT	142009	3.450E+19	-9.990E+02	532	-71.	166.	-13.	163.	59.	4.	0.200	0.790	0.010	0.009	0.280	0.750	0.350	0.580	0.060
A533B1	KWE	S	SHSS02	SRM	LT	142009	3.450E+19	-9.990E+02	532	47.	124.	203.	99.	157.	25.	0.217	1.478	0.011	0.015	0.225	0.640	0.095	0.502	0.170
A5082	KWE	V	FKWE01	F	LT	11278	6.080E+18	1.500E+11	532	-34.	165.	-10.	178.	24.	-13.	0.210	0.690	0.010	0.011	0.250	0.710	0.400	0.580	0.060
A5082	KWE	V	FKWE02	F	LT	11278	6.080E+18	1.500E+11	532	-71.	166.	-54.	183.	18.	-17.	0.200	0.790	0.010	0.009	0.280	0.750	0.350	0.580	0.060
A533B1	KWE	V	SHSS02	SRM	LT	11278	6.080E+18	1.500E+11	532	47.	124.	143.	117.	96.	7.	0.217	1.478	0.011	0.015	0.225	0.640	0.095	0.502	0.170
A302B	LAC	1A	PLAC02	P	LT	12472	4.580E+18	1.020E+11	-999	-76.	126.	-28.	106.	48.	21.	0.190	1.250	0.009	0.016	0.200	-999.000	-999.000	0.470	0.140
A302B	LAC	1A	SLAC01	SRM	LT	12472	4.580E+18	1.020E+11	-999	-62.	96.	25.	63.	86.	32.	0.230	1.335	0.014	0.018	0.265	0.195	0.115	0.515	0.135
A302B	LAC	1B	PLAC02	P	LT	12472	4.130E+18	9.200E+10	-999	-76.	126.	-60.	106.	16.	20.	0.190	1.250	0.009	0.016	0.200	-999.000	-999.000	0.470	0.140
A302B	LAC	1B	PLAC03	P	LT	12472	4.130E+18	9.200E+10	-999	21.	61.	68.	85.	47.	-24.	0.210	1.325	0.007	0.020	0.210	0.180	0.060	0.495	0.110
A302B	LAC	1B	SLAC01	SRM	LT	12472	4.130E+18	9.200E+10	-999	-62.	96.	24.	80.	85.	16.	0.230	1.335	0.014	0.018	0.265	0.195	0.115	0.515	0.135
A302B	LAC	2A	PLAC02	P	LT	26912	1.100E+19	1.140E+11	-999	-76.	126.	4.	134.	80.	-8.	0.190	1.250	0.009	0.016	0.200	-999.000	-999.000	0.470	0.140
A302B	LAC	2A	SLAC01	SRM	LT	26912	1.100E+19	1.140E+11	-999	-62.	96.	23.	78.	84.	18.	0.230	1.335	0.014	0.018	0.265	0.195	0.115	0.515	0.135
A302B	LAC	3A	PLAC02	P	LT	49087	1.080E+19	6.150E+10	-999	-76.	126.	-2.	118.	74.	9.	0.190	1.250	0.009	0.016	0.200	-999.000	-999.000	0.470	0.140
A302B	LAC	3A	SLAC01	SRM	LT	49087	1.080E+19	6.150E+10	-999	-62.	96.	21.	80.	83.	16.	0.230	1.335	0.014	0.018	0.265	0.195	0.115	0.515	0.135
A302B	LAC	3B	PLAC02	P	LT	49087	1.080E+19	5.900E+10	-999	-76.	126.	-31.	104.	45.	23.	0.190	1.250	0.009	0.016	0.200	-999.000	-999.000	0.470	0.140
A302B	LAC	3B	PLAC03	P	LT	49087	1.080E+19	5.900E+10	-999	21.	61.	107.	96.	86.	-35.	0.210	1.325	0.007	0.020	0.210	0.180	0.060	0.495	0.110
A302B	LAC	3B	SLAC01	SRM	LT	49087	1.080E+19	5.900E+10	-999	-62.	96.	44.	77.	105.	19.	0.230	1.335	0.014	0.018	0.265	0.195	0.115	0.515	0.135
A302B	LAC	7B	PLAC02	P	LT	26912	1.020E+19	1.050E+11	-999	-76.	126.	-8.	128.	68.	-2.	0.190	1.250	0.009	0.016	0.200	-999.000	-999.000	0.470	0.140
A302B	LAC	7B	PLAC03	P	LT	26912	1.020E+19	1.050E+11	-999	21.	61.	68.	-999.	46.	-999.	0.210	1.325	0.007	0.020	0.210	0.180	0.060	0.495	0.110
A302B	LAC	7B	SLAC01	SRM	LT	26912	1.020E+19	1.050E+11	-999	-62.	96.	17.	80.	79.	15.	0.230	1.335	0.014	0.018	0.265	0.195	0.115	0.515	0.135
A302B	LAC	8A	PLAC02	P	LT	49087	1.080E+19	6.010E+10	-999	-76.	126.	-11.	109.	65.	17.	0.190	1.250	0.009	0.016	0.200	-999.000	-999.000	0.470	0.140
A302B	LAC	8A	SLAC01	SRM	LT	49087	1.080E+19	6.010E+10	-999	-62.	96.	48.	65.	109.	30.	0.230	1.335	0.014	0.018	0.265	0.195	0.115	0.515	0.135
A302B	LAC	8B	PLAC02	P	LT	49087	1.080E+19	6.320E+10	-999	-76.	126.	21.	119.	97.	7.	0.190	1.250	0.009	0.016	0.200	-999.000	-999.000	0.470	0.140
A302B	LAC	8B	PLAC03	P	LT	49087	1.080E+19	6.320E+10	-999	21.	61.	106.	-999.	85.	-999.	0.210	1.325	0.007	0.020	0.210	0.180	0.060	0.495	0.110
A302B	LAC	8B	SLAC01	SRM	LT	49087	1.080E+19	6.320E+10	-999	-62.	96.	53.	75.	114.	21.	0.230	1.335	0.014	0.018	0.265	0.195	0.115	0.515	0.135

Material ID	Plant ID	Capsule	Heat ID	Product ID	Specimen Orientation	Irradiation time hr	Fluence n/cm^2	Flux n/cm^2/s	Tcoolant F	TTu30 F	USEu ft-lb	TTi30 F	USEi ft-lb	dTT30 F	dUSE ft-lb	C wt%	Mn wt%	P wt%	S wt%	Si wt%	Ni wt%	Cr wt%	Mo wt%	Cu wt%
A302B	LAC	9A	PLAC02	P	LT	26912	6.550E+18	6.760E+10	-999	-76.	126.	11.	122.	87.	4.	0.190	1.250	0.009	0.016	0.200	-999.000	-999.000	0.470	0.140
A302B	LAC	9A	SLAC01	SRM	LT	26912	6.550E+18	6.760E+10	-999	-62.	96.	12.	94.	74.	1.	0.230	1.335	0.014	0.018	0.265	0.195	0.115	0.515	0.135
A302B	LAC	9B	PLAC02	P	LT	26912	6.640E+18	6.850E+10	-999	-76.	126.	-19.	119.	57.	7.	0.190	1.250	0.009	0.016	0.200	-999.000	-999.000	0.470	0.140
A302B	LAC	9B	PLAC03	P	LT	26912	6.640E+18	6.850E+10	-999	21.	61.	81.	100.	60.	-39.	0.210	1.325	0.007	0.020	0.210	0.180	0.060	0.495	0.110
A302B	LAC	9B	SLAC01	SRM	LT	26912	6.640E+18	6.850E+10	-999	-62.	96.	-4.	107.	58.	-11.	0.230	1.335	0.014	0.018	0.265	0.195	0.115	0.515	0.135
A533B1	LS1	300D	PLS1JW	P	LT	56979	9.000E+16	4.400E+08	533	-32.	154.	-3.	141.	29.	13.	-999.000	1.290	0.014	-999.000	-999.000	0.540	0.260	0.500	0.140
A533B1	MC1	U	PMC101	P	LT	9556	4.430E+18	1.290E+11	558	9.	146.	45.	134.	36.	12.	0.210	1.260	0.010	0.016	0.230	0.600	0.068	0.570	0.087
A533B1	MC1	U	PMC101	P	TL	9556	4.430E+18	1.290E+11	558	2.	-999.	53.	103.	52.	-999.	0.210	1.260	0.010	0.016	0.230	0.600	0.068	0.570	0.087
A533B1	MC1	X	PMC101	P	LT	37778	1.460E+19	1.070E+11	557	9.	146.	45.	136.	36.	10.	0.210	1.260	0.010	0.016	0.230	0.600	0.068	0.570	0.087
A533B1	MC1	X	PMC101	P	TL	37778	1.460E+19	1.070E+11	557	2.	-999.	66.	108.	64.	-999.	0.210	1.260	0.010	0.016	0.230	0.600	0.068	0.570	0.087
A5082	MC2	U	FMC201	F	LT	53056	2.000E+19	1.050E+11	558	-74.	157.	13.	113.	87.	45.	0.181	0.686	0.012	0.015	0.179	0.780	0.414	0.592	0.154
A5082	MC2	U	FMC201	F	TL	53056	2.000E+19	1.050E+11	558	-19.	99.	65.	90.	84.	9.	0.181	0.686	0.012	0.015	0.179	0.780	0.414	0.592	0.154
A5082	MC2	V	FMC201	F	LT	9000	3.330E+18	1.030E+11	558	-74.	157.	-12.	138.	63.	20.	0.181	0.686	0.012	0.015	0.179	0.780	0.414	0.592	0.154
A5082	MC2	V	FMC201	F	TL	9000	3.330E+18	1.030E+11	558	-19.	99.	39.	93.	58.	6.	0.181	0.686	0.012	0.015	0.179	0.780	0.414	0.592	0.154
A5082	MC2	X	FMC201	F	LT	36389	1.460E+19	1.110E+11	558	-74.	157.	19.	142.	93.	16.	0.181	0.686	0.012	0.015	0.179	0.780	0.414	0.592	0.154
A5082	MC2	X	FMC201	F	TL	36389	1.460E+19	1.110E+11	558	-19.	99.	72.	84.	92.	15.	0.181	0.686	0.012	0.015	0.179	0.780	0.414	0.592	0.154
A302BM	ML1	210D	PML101	P	LT	78470	3.300E+17	1.150E+09	531	15.	114.	73.	-999.	58.	-999.	0.230	1.320	0.010	0.028	0.220	0.490	0.080	0.470	0.210
A302BM	ML1	300D	PML101	P	LT	129823	6.600E+17	2.000E+09	531	15.	114.	94.	102.	79.	12.	0.230	1.320	0.010	0.028	0.220	0.490	0.080	0.470	0.210
A533B1	ML2	W104	PML201	P	LT	87149	8.840E+18	-9.990E+02	549	41.	135.	131.	100.	90.	34.	0.210	1.276	0.007	0.015	0.312	0.603	0.100	0.601	0.141
A533B1	ML2	W104	SHSS01	SRM	LT	87149	8.840E+18	-9.990E+02	549	30.	138.	166.	94.	136.	44.	0.219	1.465	0.010	0.015	0.186	0.665	0.103	0.548	0.174
A533B1	ML2	W97	PML201	P	LT	26298	3.780E+18	3.900E+10	549	41.	135.	108.	100.	67.	35.	0.210	1.276	0.007	0.015	0.312	0.603	0.100	0.601	0.141
A533B1	ML2	W97	PML201	P	TL	26298	3.780E+18	3.900E+10	549	13.	119.	109.	88.	95.	30.	0.210	1.276	0.007	0.015	0.312	0.603	0.100	0.601	0.141
A533B1	MY	A25	PMY_01	P	LT	7714	1.760E+19	-9.990E+02	522	-6.	158.	112.	98.	119.	60.	0.238	1.332	0.013	0.011	0.154	0.528	0.030	0.492	0.100
A533B1	MY	A25	SHSS01	SRM	LT	7714	1.760E+19	-9.990E+02	522	30.	138.	167.	99.	137.	39.	0.219	1.465	0.010	0.015	0.186	0.665	0.103	0.548	0.174
A533B1	MY	A35	PMY_01	P	LT	40167	7.130E+19	-9.990E+02	533	-6.	158.	184.	87.	190.	70.	0.238	1.332	0.013	0.011	0.154	0.528	0.030	0.492	0.100
A533B1	MY	A35	PMY_01	P	TL	40167	7.130E+19	-9.990E+02	533	6.	115.	208.	73.	202.	43.	0.238	1.332	0.013	0.011	0.154	0.528	0.030	0.492	0.100
A533B1	MY	W253	PMY_01	P	LT	102562	1.250E+19	3.410E+10	542	-6.	158.	127.	113.	133.	44.	0.238	1.332	0.013	0.011	0.154	0.528	0.030	0.492	0.100
A533B1	MY	W253	SHSS01	SRM	LT	102562	1.250E+19	3.410E+10	542	30.	138.	185.	109.	156.	29.	0.219	1.465	0.010	0.015	0.186	0.665	0.103	0.548	0.174
A533B1	MY	W263	PMY_01	P	LT	40167	5.670E+18	-9.990E+02	533	-6.	158.	97.	118.	103.	40.	0.238	1.332	0.013	0.011	0.154	0.528	0.030	0.492	0.100
A533B1	MY	W263	PMY_01	P	TL	40167	5.670E+18	-9.990E+02	533	6.	115.	108.	104.	102.	12.	0.238	1.332	0.013	0.011	0.154	0.528	0.030	0.492	0.100
A5082	NA1	U	FNA101	F	LT	49722	8.720E+18	4.880E+10	553	-2.	133.	110.	116.	112.	18.	0.195	0.703	0.019	0.013	0.240	0.828	0.326	0.637	0.156
A5082	NA1	U	FNA101	F	TL	49722	8.720E+18	4.880E+10	553	40.	91.	112.	96.	72.	-5.	0.195	0.703	0.019	0.013	0.240	0.828	0.326	0.637	0.156
A5082	NA1	V	FNA101	F	LT	9444	2.630E+18	7.720E+10	550	-2.	133.	47.	128.	49.	5.	0.195	0.703	0.019	0.013	0.240	0.828	0.326	0.637	0.156
A5082	NA1	V	FNA101	F	TL	9444	2.630E+18	7.720E+10	550	40.	91.	69.	79.	29.	12.	0.195	0.703	0.019	0.013	0.240	0.828	0.326	0.637	0.156
A5082	NA2	U	FNA201	F	LT	53333	9.800E+18	5.090E+10	554	-22.	126.	13.	124.	35.	3.	0.190	0.715	0.018	0.013	0.230	0.860	0.345	0.615	0.110
A5082	NA2	U	FNA201	F	TL	53333	9.800E+18	5.090E+10	554	54.	73.	120.	86.	66.	-13.	0.190	0.715	0.018	0.013	0.230	0.860	0.345	0.615	0.110
A5082	NA2	V	FNA201	F	LT	8722	2.460E+18	7.820E+10	550	-22.	126.	-10.	107.	12.	20.	0.190	0.715	0.018	0.013	0.230	0.860	0.345	0.615	0.110
A5082	NA2	V	FNA201	F	TL	8722	2.460E+18	7.820E+10	550	54.	73.	69.	59.	15.	14.	0.190	0.715	0.018	0.013	0.230	0.860	0.345	0.615	0.110
A302B	OC1	A	POC102	P	LT	38093	8.950E+18	6.530E+10	556	-7.	142.	48.	131.	55.	11.	0.210	1.420	0.015	0.015	0.230	0.500	0.170	0.490	0.100
A302B	OC1	A	POC102	P	TL	38093	8.950E+18	6.530E+10	556	7.	112.	35.	111.	28.	1.	0.210	1.420	0.015	0.015	0.230	0.500	0.170	0.490	0.100
A533B1	OC1	A	SHSS02	SRM	LT	38093	8.950E+18	6.530E+10	556	47.	124.	129.	96.	82.	28.	0.217	1.478	0.011	0.015	0.225	0.640	0.095	0.502	0.170
A302B	OC1	C	POC102	P	LT	51888	9.860E+18	5.270E+10	556	-7.	142.	38.	128.	45.	14.	0.210	1.420	0.015	0.015	0.230	0.500	0.170	0.490	0.100
A302B	OC1	C	POC102	P	TL	51888	9.860E+18	5.270E+10	556	7.	112.	94.	97.	87.	15.	0.210	1.420	0.015	0.015	0.230	0.500	0.170	0.490	0.100
A533B1	OC1	C	SHSS02	SRM	LT	51888	9.860E+18	5.270E+10	556	47.	124.	122.	100.	75.	24.	0.217	1.478	0.011	0.015	0.225	0.640	0.095	0.502	0.170
A302B	OC1	E	POC102	P	LT	14406	1.500E+18	-9.990E+02	556	-7.	142.	49.	137.	55.	4.	0.210	1.420	0.015	0.015	0.230	0.500	0.170	0.490	0.100
A302B	OC1	E	POC102	P	TL	14406	1.500E+18	-9.990E+02	556	7.	112.	36.	-999.	29.	-999.	0.210	1.420	0.015	0.015	0.230	0.500	0.170	0.490	0.100
A533B1	OC1	E	SHSS02	SRM	LT	14406	1.500E+18	-9.990E+02	556	47.	124.	77.	111.	30.	13.	0.217	1.478	0.011	0.015	0.225	0.640	0.095	0.502	0.170
A302B	OC1	F	POC101	P	LT	7303	5.700E+17	-9.990E+02	556	2.	120.	25.	125.	22.	-5.	0.200	1.400	0.012	0.017	0.200	0.630	0.130	0.500	0.110
A302B	OC1	F	POC101	P	TL	7303	5.700E+17	-9.990E+02	556	-1.	126.	29.	111.	30.	15.	0.200	1.400	0.012	0.017	0.200	0.630	0.130	0.500	0.110
A533B1	OC1	F	SHSS02	SRM	LT	7303	5.700E+17	-9.990E+02	556	47.	124.	56.	109.	9.	15.	0.217	1.478	0.011	0.015	0.225	0.640	0.095	0.502	0.170
A5082	OC2	A	FOC201	F	LT	18672	3.370E+18	5.030E+10	556	-26.	146.	-33.	130.	-7.	16.	0.240	0.630	0.006	0.012	0.250	0.750	0.360	0.620	0.040
A5082	OC2	A	FOC201	F	TL	18672	3.370E+18	5.030E+10	556	-30.	127.	-27.	-999.	4.	-999.	0.240	0.630	0.006	0.012	0.250	0.750	0.360	0.620	0.040
A533B1	OC2	A	SHSS02	SRM	LT	18672	3.370E+18	5.030E+10	556	47.	124.	117.	102.	70.	22.	0.217	1.478	0.011	0.015	0.225	0.640	0.095	0.502	0.170
A5082	OC2	C	FOC201	F	LT	10561	1.020E+18	-9.990E+02	556	-26.	146.	-3.	129.	24.	17.	0.240	0.630	0.006	0.012	0.250	0.750	0.360	0.620	0.040
A5082	OC2	C	FOC201	F	TL	10561	1.020E+18	-9.990E+02	556	-30.	127.	-999.	-999.	-999.	-999.	0.240	0.630	0.006	0.012	0.250	0.750	0.360	0.620	0.040
A533B1	OC2	C	SHSS02	SRM	LT	10561	1.020E+18	-9.990E+02	556	47.	124.	89.	-999.	42.	-999.	0.217	1.478	0.011	0.015	0.225	0.640	0.095	0.502	0.170
A5082	OC2	E	FOC201	F	LT	55584	1.210E+19	6.030E+10	556	-26.	146.	-8.	132.	18.	14.	0.240	0.630	0.006	0.012	0.250	0.750	0.360	0.620	0.040
A5082	OC2	E	FOC201	F	TL	55584	1.210E+19	6.030E+10	556	-30.	127.	-22.	114.	8.	13.	0.240	0.630	0.006	0.012	0.250	0.750	0.360	0.620	0.040
A533B1	OC2	E	SHSS02	SRM	LT	55584	1.210E+19	6.030E+10	556	47.	124.	168.	100.	121.	24.	0.217	1.478	0.011	0.015	0.225	0.640	0.095	0.502	0.170
A5082	OC3	A	FOC301	F	LT	8286	8.050E+17	-9.990E+02	556	3.	174.	15.	150.	12.	24.	0.240	0.720	0.014	0.012	0.210	0.760	0.340	0.620	0.020
A5082	OC3	A	FOC301	F	TL	8286	8.050E+17	-9.990E+02	556	-2.	141.	6.	131.	7.	10.	0.240	0.720	0.014	0.012	0.210	0.760	0.340	0.620	0.020
A5082	OC3	A	FOC302	F	TL	8286	8.050E+17	-9.990E+02	556	1.	110.	53.	101.	52.	9.	0.210	0.580	0.011	0.015	0.240	0.730	0.300	0.600	0.010
A5082	OC3	B	FOC301	F	TL	16392	3.120E+18	5.290E+10	556	-2.	141.	2.	124.	4.	17.	0.240	0.720	0.014	0.012	0.210	0.760	0.340	0.620	0.020
A5082	OC3	B	FOC302	F	TL	16392	3.120E+18	5.290E+10	556	1.	110.	8.	101.	6.	10.	0.210	0.580	0.011	0.015	0.240	0.730	0.300	0.600	0.010
A533B1	OC3	B	SHSS02	SRM	LT	16392	3.120E+18	5.290E+10	556	47.	124.	98.	105.	51.	19.	0.217	1.478	0.011	0.015	0.225	0.640	0.095	0.502	0.170
A5082	OC3	D	FOC301	F	TL	68443	1.450E+19	5.950E+10	556	-2.	141.	21.	124.	22.	17.	0.240	0.720	0.014	0.012	0.210	0.760	0.340	0.620	0.020
A5082	OC3	D	FOC302	F	TL	68443	1.450E+19	5.950E+10	556	1.	110.	39.	92.	38.	19.	0.210	0.580	0.011	0.015	0.240	0.730	0.300	0.600	0.010
A533B1	OC3	D	SHSS02	SRM	LT	68443	1.450E+19	5.950E+10	556	47.	124.	150.	100.	103.	24.	0.217	1.478	0.011	0.015	0.225	0.640	0.095	0.502	0.170
A302B1	OYS	210D	POYS01	P	LT	71400	7.460E+17	2.900E+09	525	16.	93.	93.	89.	78.	4.	0.200	1.400	0.011	0.022	0.024	0.107	-999.000	0.510	0.173
A302BM	PAL	A240	PPAL01	P	LT	19806	6.000E+19	-9.990E+02	524	3.	159.	204.	99.	201.	61.	0.115	1.368	0.012	0.011	0.180	0.530	0.085	0.501	0.250
A302BM	PAL	A240	PPAL01	P	TL	19806	6.000E+19	-9.990E+02	524	18.	102.	212.	74.	195.	28.	0.115	1.368	0.012	0.011	0.180	0.530	0.085	0.501	0.250
A302BM	PAL	T330	PPAL01	P	LT	43611	1.000E+13	-9.990E+02	-999	3.	159.	11.	173.	9.	-14.	0.115	1.368	0.012	0.011	0.180	0.530	0.085	0.501	0.250
A302BM	PAL	T330	PPAL01	P	TL	43611	1.000E+13	-9.990E+02	-999	18.	102.	21.	108.	3.	-5.	0.115	1.368	0.012	0.011	0.180	0.530	0.085	0.501	0.250
A302BM	PAL	W110	PPAL01	P	LT	87167	1.779E+19	5.668E+10	533	3.	159.	175.	107.	172.	52.	0.115	1.368	0.012	0.011	0.180	0.530	0.085	0.501	0.250
A533B1	PAL	W110	SHSS01	SRM	LT	87167	1.779E+19	5.668E+10	533	24.	138.	167.	103.	143.	35.	0.219	1.465	0.010	0.015	0.186	0.665	0.103	0.548	0.174
A302BM	PAL	W290	PPAL01	P	LT	43611	1.090E+19	6.940E+10	530	3.	159.	174.	116.	172.	44.	0.115	1.368	0.012	0.011	0.180	0.530	0.085	0.501	0.250
A302BM	PAL	W290	PPAL01	P	TL	43611	1.090E+19	6.940E+10	530	18.	102.	174.	88.	156.	14.	0.115	1.368	0.012	0.011	0.180	0.530	0.085	0.501	0.250
A302B	PB1	R	PPB101	P	LT	44722	2.320E+19	1.470E+11	542	-35.	109.	58.	104.	93.	5.	0.190	1.460	0.010	0.020	0.250	0.056	0.057	0.480	0.200
A302B	PB1	R	PPB102	P	LT	44722	2.320E+19	1.470E+11	542	-26.	121.	2.	143.	28.	-22.	0.210	1.460	0.014	0.019	0.250	0.067	0.062	0.470	0.120
A302B	PB1	R	SASTM	SRM	LT	44722	2.320E+19	1.470E+11	542	37.	-999.	149.	-999.	112.	-999.	0.240	1.340	0.014	0.023	0.230	0.180	0.110	0.510	0.200
A302B	PB1	S	PPB101	P	LT	31667	7.870E+18	7.000E+10	542	-35.	109.	52.	93.	87.	16.	0.190	1.460	0.010	0.020	0.250	0.056	0.057	0.480	0.200
A302B	PB1	S	PPB102	P	LT	31667	7.870E+18	7.000E+10	542	-26.	121.	17.	145.	43.	-24.	0.210	1.460	0.014	0.019	0.250	0.067	0.062	0.470	0.120

Embrittlement Analysis Data Base

Material ID	Plant ID	Capsule	Heat ID	Product ID	Specimen Orientation	Irradiation time hr	Fluence n/cm^2	Flux n/cm^2/s	Tcoolant F	TTu30 F	USEu ft-lb	TTi30 F	USEi ft-lb	dTT30 F	dUSE ft-lb	C wt%	Mn wt%	P wt%	S wt%	Si wt%	Ni wt%	Cr wt%	Mo wt%	Cu wt%
A302B	PB1	S	SASTM	SRM	LT	31667	7.870E+18	7.000E+10	542	37.	-999.	129.	78.	92.	-999.	0.240	1.340	0.014	0.023	0.230	0.180	0.110	0.510	0.200
A302B	PB1	T	PPB101	P	LT	81389	2.290E+19	8.100E+10	535	-35.	109.	47.	97.	82.	12.	0.190	1.460	0.010	0.020	0.250	0.056	0.057	0.480	0.200
A302B	PB1	T	PPB102	P	LT	81389	2.290E+19	8.100E+10	535	-26.	121.	19.	139.	45.	-18.	0.210	1.460	0.014	0.019	0.250	0.067	0.062	0.470	0.120
A302B	PB1	T	SASTM	SRM	LT	81389	2.290E+19	8.100E+10	535	37.	-999.	112.	69.	75.	-999.	0.240	1.340	0.014	0.023	0.230	0.180	0.110	0.510	0.200
A302B	PB1	V	PPB101	P	LT	13028	4.970E+18	1.120E+11	542	-35.	109.	46.	92.	81.	17.	0.190	1.460	0.010	0.020	0.250	0.056	0.057	0.480	0.200
A302B	PB1	V	PPB102	P	LT	13028	4.970E+18	1.120E+11	542	-26.	121.	15.	122.	41.	0.	0.210	1.460	0.014	0.019	0.250	0.067	0.062	0.470	0.120
A302B	PB1	V	SASTM	SRM	LT	13028	4.970E+18	1.120E+11	542	37.	-999.	132.	84.	95.	-999.	0.240	1.340	0.014	0.023	0.230	0.180	0.110	0.510	0.200
A5082	PB2	R	FPB201	F	LT	45556	2.200E+19	1.540E+11	542	-55.	153.	-4.	136.	50.	16.	0.220	0.590	0.010	0.008	0.230	0.700	0.330	0.600	0.051
A5082	PB2	R	FPB202	F	LT	45556	2.200E+19	1.540E+11	542	-87.	173.	0.	190.	88.	-17.	0.200	0.650	0.009	0.009	0.240	0.710	0.350	0.590	0.088
A533B1	PB2	R	SHSS02	SRM	LT	45556	2.200E+19	1.540E+11	542	47.	124.	200.	103.	153.	21.	0.217	1.478	0.011	0.015	0.225	0.640	0.095	0.502	0.170
A5082	PB2	S	FPB201	F	LT	129444	3.100E+19	8.060E+10	542	-55.	153.	7.	137.	61.	16.	0.220	0.590	0.010	0.008	0.230	0.700	0.330	0.600	0.051
A5082	PB2	S	FPB202	F	LT	129444	3.100E+19	8.060E+10	542	-87.	173.	13.	162.	101.	11.	0.200	0.650	0.009	0.009	0.240	0.710	0.350	0.590	0.088
A533B1	PB2	S	SHSS02	SRM	LT	129444	3.100E+19	8.060E+10	542	47.	124.	197.	85.	150.	39.	0.217	1.478	0.011	0.015	0.225	0.640	0.095	0.502	0.170
A5082	PB2	T	FPB201	F	LT	30278	8.610E+18	9.220E+10	542	-55.	153.	-20.	154.	35.	-1.	0.220	0.590	0.010	0.008	0.230	0.700	0.330	0.600	0.051
A5082	PB2	T	FPB202	F	LT	30278	8.610E+18	9.220E+10	542	-87.	173.	-25.	205.	62.	-32.	0.200	0.650	0.009	0.009	0.240	0.710	0.350	0.590	0.088
A533B1	PB2	T	SHSS02	SRM	LT	30278	8.610E+18	9.220E+10	542	47.	124.	166.	116.	119.	8.	0.217	1.478	0.011	0.015	0.225	0.640	0.095	0.502	0.170
A5082	PB2	V	FPB201	F	LT	13361	5.850E+18	1.220E+11	542	-55.	153.	-15.	145.	39.	8.	0.220	0.590	0.010	0.008	0.230	0.700	0.330	0.600	0.051
A5082	PB2	V	FPB202	F	LT	13361	5.850E+18	1.220E+11	542	-87.	173.	-48.	195.	39.	-22.	0.200	0.650	0.009	0.009	0.240	0.710	0.350	0.590	0.088
A533B1	PB2	V	SHSS02	SRM	LT	13361	5.850E+18	1.220E+11	542	47.	124.	140.	95.	93.	29.	0.217	1.478	0.011	0.015	0.225	0.640	0.095	0.502	0.170
A302BM	PH3	1	PPH301	P	LT	66359	1.600E+17	6.800E+08	528	-11.	137.	1.	123.	12.	14.	0.210	1.427	0.008	0.016	0.233	0.620	-999.000	0.497	0.133
A5083	PI1	P	FPI101	F	LT	50278	1.460E+19	8.090E+10	527	-35.	162.	-14.	143.	21.	19.	0.170	1.410	0.013	0.005	0.280	0.720	0.170	0.480	0.060
A5083	PI1	P	FPI101	F	TL	50278	1.460E+19	8.090E+10	527	-26.	145.	4.	139.	31.	6.	0.170	1.410	0.013	0.005	0.280	0.720	0.170	0.480	0.060
A533B1	PI1	P	SHSS02	SRM	LT	50278	1.460E+19	8.090E+10	527	47.	124.	207.	85.	161.	39.	0.217	1.478	0.011	0.015	0.225	0.640	0.095	0.502	0.170
A5083	PI1	R	FPI101	F	LT	75000	3.950E+19	1.460E+11	527	-35.	162.	57.	151.	92.	11.	0.170	1.410	0.013	0.005	0.280	0.720	0.170	0.480	0.060
A5083	PI1	R	FPI101	F	TL	75000	3.950E+19	1.460E+11	527	-26.	145.	55.	141.	81.	4.	0.170	1.410	0.013	0.005	0.280	0.720	0.170	0.480	0.060
A533B1	PI1	R	SHSS02	SRM	LT	75000	3.950E+19	1.460E+11	527	47.	124.	239.	92.	193.	32.	0.217	1.478	0.011	0.015	0.225	0.640	0.095	0.502	0.170
A5083	PI1	V	FPI101	F	LT	11722	5.400E+18	1.280E+11	527	-35.	162.	0.	160.	35.	2.	0.170	1.410	0.013	0.005	0.280	0.720	0.170	0.480	0.060
A5083	PI1	V	FPI101	F	TL	11722	5.400E+18	1.280E+11	527	-26.	145.	18.	145.	44.	-1.	0.170	1.410	0.013	0.005	0.280	0.720	0.170	0.480	0.060
A533B1	PI1	V	SHSS02	SRM	LT	11722	5.400E+18	1.280E+11	527	47.	124.	149.	106.	102.	18.	0.217	1.478	0.011	0.015	0.225	0.640	0.095	0.502	0.170
A5083	PI2	R	FPI201	F	LT	77222	4.050E+19	1.460E+11	527	-24.	147.	62.	131.	86.	16.	0.174	1.215	0.011	0.012	0.272	0.697	0.144	0.458	0.077
A5083	PI2	R	FPI201	F	TL	77222	4.050E+19	1.460E+11	527	-1.	107.	83.	105.	83.	2.	0.174	1.215	0.011	0.012	0.272	0.697	0.144	0.458	0.077
A533B1	PI2	R	SHSS02	SRM	LT	77222	4.050E+19	1.460E+11	527	47.	124.	230.	87.	183.	37.	0.217	1.478	0.011	0.015	0.225	0.640	0.095	0.502	0.170
A5083	PI2	T	FPI201	F	LT	36111	1.090E+19	8.380E+10	527	-24.	147.	28.	139.	51.	8.	0.174	1.215	0.011	0.012	0.272	0.697	0.144	0.458	0.077
A5083	PI2	T	FPI201	F	TL	36111	1.090E+19	8.380E+10	527	-1.	107.	29.	99.	29.	8.	0.174	1.215	0.011	0.012	0.272	0.697	0.144	0.458	0.077
A533B1	PI2	T	SHSS02	SRM	LT	36111	1.090E+19	8.380E+10	527	47.	124.	207.	89.	160.	35.	0.217	1.478	0.011	0.015	0.225	0.640	0.095	0.502	0.170
A5083	PI2	V	FPI201	F	LT	12222	5.780E+18	1.310E+11	527	-24.	147.	14.	163.	38.	-16.	0.174	1.215	0.011	0.012	0.272	0.697	0.144	0.458	0.077
A5083	PI2	V	FPI201	F	TL	12222	5.780E+18	1.310E+11	527	-1.	107.	36.	118.	36.	-11.	0.174	1.215	0.011	0.012	0.272	0.697	0.144	0.458	0.077
A533B1	PI2	V	SHSS02	SRM	LT	12222	5.780E+18	1.310E+11	527	47.	124.	169.	105.	122.	19.	0.217	1.478	0.011	0.015	0.225	0.640	0.095	0.502	0.170
A533B1	PL1	1	PPL101	P	LT	36582	2.300E+17	1.740E+09	529	6.	132.	35.	120.	29.	12.	0.231	1.337	0.015	0.014	0.175	0.634	0.135	0.596	0.134
A533B1	PV1	W137	PPV1J2	P	LT	-999	3.450E+18	-9.990E+02	552	12.	151.	41.	131.	29.	20.	-999.000	-999.000	-999.000	-999.000	-999.000	-999.000	-999.000	-999.000	-999.000
A533B1	PV1	W137	PPV1J2	P	TL	-999	3.450E+18	-9.990E+02	552	28.	109.	43.	89.	15.	21.	-999.000	-999.000	-999.000	-999.000	-999.000	-999.000	-999.000	-999.000	-999.000
A533B1	PV1	W137	SHSS01	SRM	LT	-999	3.450E+18	-9.990E+02	552	24.	138.	122.	109.	98.	29.	0.219	1.465	0.010	0.015	0.186	0.665	0.103	0.548	0.174
A533B1	PV2	W137	PPV201	P	LT	39806	4.071E+18	2.842E+10	552	0.	132.	8.	142.	8.	-11.	0.240	1.540	0.006	0.009	0.210	0.680	0.030	0.520	0.040
A533B1	PV2	W137	PPV201	P	TL	39806	4.071E+18	2.842E+10	552	3.	145.	9.	125.	6.	20.	0.240	1.540	0.006	0.009	0.210	0.680	0.030	0.520	0.040
A533B1	PV2	W137	SHSS01	SRM	LT	39806	4.071E+18	2.842E+10	552	24.	138.	120.	127.	96.	11.	0.219	1.465	0.010	0.015	0.186	0.665	0.103	0.548	0.174
	PV3	W137	PPV3JW	P	TL	-999	3.640E+18	-9.990E+02	552	-30.	-999.	-13.	129.	17.	-999.	-999.000	-999.000	-999.000	-999.000	-999.000	-999.000	-999.000	-999.000	-999.000
A302BM	QC1	1	PQC101	P	LT	10800	8.200E+18	2.110E+11	546	-28.	107.	79.	93.	107.	14.	0.238	1.520	0.010	0.017	0.224	0.520	0.110	0.490	0.212
A302BM	QC1	2	PQC101	P	LT	10800	1.025E+16	2.635E+08	530	-28.	107.	-37.	118.	-8.	-11.	0.238	1.520	0.010	0.017	0.224	0.520	0.110	0.490	0.212
A302BM	QC1	3	PQC101	P	LT	34528	4.230E+19	-9.990E+02	546	-28.	107.	137.	73.	165.	34.	0.238	1.520	0.010	0.017	0.224	0.520	0.110	0.490	0.212
A302BM	QC1	8	PQC101	P	LT	58206	5.500E+16	2.610E+08	530	-28.	107.	-25.	108.	3.	-1.	0.238	1.520	0.010	0.017	0.224	0.520	0.110	0.490	0.212
A302BM	QC2	12	PQC201	P	LT	14316	9.750E+18	-9.990E+02	546	-12.	138.	25.	124.	37.	14.	0.268	1.640	0.008	0.016	0.283	0.522	0.130	0.474	0.095
A302BM	QC2	13	PQC201	P	LT	14316	1.730E+16	-9.990E+02	530	-12.	138.	-10.	135.	2.	3.	0.268	1.640	0.008	0.016	0.283	0.522	0.130	0.474	0.095
A302BM	QC2	18	PQC201	P	LT	49353	6.560E+16	3.690E+08	530	-12.	138.	-11.	150.	1.	-12.	0.268	1.640	0.008	0.016	0.283	0.522	0.130	0.474	0.095
A302BM	QC2	3	PQC201	P	LT	39500	4.280E+19	-9.990E+02	546	-12.	138.	41.	123.	53.	15.	0.268	1.640	0.008	0.016	0.283	0.522	0.130	0.474	0.095
A5082	RI2	X	FRI201	F	LT	15886	-9.990E+02	-9.990E+02	547	-49.	139.	17.	123.	67.	16.	0.190	0.660	0.012	0.009	0.300	0.740	0.310	0.660	0.100
A5082	RI2	X	FRI201	F	TL	15886	-9.990E+02	-9.990E+02	547	16.	78.	52.	99.	36.	-21.	0.190	0.660	0.012	0.009	0.300	0.740	0.310	0.660	0.100
A533B1	RS1	B	PRS101	P	TL	13068	3.990E+18	8.470E+10	556	5.	91.	40.	92.	34.	-1.	0.200	1.260	0.013	0.017	0.150	0.600	0.140	0.550	0.120
A533B1	RS1	D	PRS101	P	TL	20172	6.600E+18	9.080E+10	556	5.	91.	63.	84.	57.	7.	0.200	1.260	0.013	0.017	0.150	0.600	0.140	0.550	0.120
A533B1	RS1	F	PRS101	P	TL	42720	1.420E+19	9.240E+10	556	5.	91.	75.	79.	69.	12.	0.200	1.260	0.013	0.017	0.150	0.600	0.140	0.550	0.120
A533B1	SA1	T	PSA101	P	LT	9639	2.560E+18	7.380E+10	539	-22.	135.	87.	98.	109.	37.	0.235	1.497	0.013	0.017	0.285	0.528	0.185	0.480	0.241
A533B1	SA1	T	PSA102	P	LT	9639	2.560E+18	7.380E+10	539	-21.	143.	68.	117.	89.	26.	0.220	1.467	0.016	0.018	0.305	0.525	0.175	0.473	0.235
A533B1	SA1	T	PSA103	P	LT	9639	2.560E+18	7.380E+10	539	-43.	137.	25.	137.	68.	0.	0.200	1.220	0.012	0.026	0.270	0.508	0.110	0.437	0.220
A533B1	SA1	T	SHSS02	SRM	LT	9639	2.560E+18	7.380E+10	539	47.	124.	114.	-999.	67.	-999.	0.217	1.478	0.011	0.015	0.225	0.640	0.095	0.502	0.170
A533B1	SA1	Y	PSA103	P	LT	31389	9.300E+18	8.260E+10	539	-43.	137.	71.	120.	114.	18.	0.200	1.220	0.012	0.026	0.270	0.508	0.110	0.437	0.220
A533B1	SA1	Y	SHSS02	SRM	LT	31389	9.300E+18	8.260E+10	539	47.	124.	178.	105.	132.	19.	0.217	1.478	0.011	0.015	0.225	0.640	0.095	0.502	0.170
A533B1	SA1	Z	PSA101	P	LT	53056	1.230E+19	6.460E+10	539	-22.	135.	159.	96.	181.	38.	0.235	1.497	0.013	0.017	0.285	0.528	0.185	0.480	0.241
A533B1	SA1	Z	PSA102	P	LT	53056	1.230E+19	6.460E+10	539	-21.	143.	137.	109.	158.	34.	0.220	1.467	0.016	0.018	0.305	0.525	0.175	0.473	0.235
A533B1	SA1	Z	PSA103	P	LT	53056	1.230E+19	6.460E+10	539	-43.	137.	64.	112.	107.	25.	0.200	1.220	0.012	0.026	0.270	0.508	0.110	0.437	0.220
A533B1	SA1	Z	SHSS02	SRM	LT	53056	1.230E+19	6.460E+10	539	47.	124.	182.	99.	135.	25.	0.217	1.478	0.011	0.015	0.225	0.640	0.095	0.502	0.170
A533B1	SA2	T	PSA201	P	LT	10444	2.750E+18	7.320E+10	539	28.	124.	84.	125.	56.	-1.	0.235	1.359	0.010	0.009	0.275	0.617	0.105	0.563	0.117
A533B1	SA2	T	PSA201	P	TL	10444	2.750E+18	7.320E+10	539	11.	103.	87.	99.	76.	4.	0.235	1.359	0.010	0.009	0.275	0.617	0.105	0.563	0.117
A533B1	SA2	U	PSA201	P	LT	23667	5.500E+18	6.450E+10	539	28.	124.	92.	122.	65.	2.	0.235	1.359	0.010	0.009	0.275	0.617	0.105	0.563	0.117
A533B1	SA2	U	PSA201	P	TL	23667	5.500E+18	6.450E+10	539	11.	103.	111.	86.	99.	17.	0.235	1.359	0.010	0.009	0.275	0.617	0.105	0.563	0.117
A533B1	SA2	X	PSA201	P	LT	54444	1.070E+19	5.500E+10	539	28.	124.	116.	-999.	88.	-999.	0.235	1.359	0.010	0.009	0.275	0.617	0.105	0.563	0.117
A533B1	SA2	X	PSA201	P	TL	54444	1.070E+19	5.500E+10	539	11.	103.	138.	-999.	127.	-999.	0.235	1.359	0.010	0.009	0.275	0.617	0.105	0.563	0.117
A533B1	SB1	U	PSB101	P	LT	8001	3.360E+18	1.170E+11	558	-24.	124.	15.	120.	39.	5.	0.200	1.450	0.007	0.010	0.240	0.570	0.060	0.550	0.060
A533B1	SB1	U	PSB101	P	TL	8001	3.360E+18	1.170E+11	558	9.	84.	37.	75.	29.	9.	0.200	1.450	0.007	0.010	0.240	0.570	0.060	0.550	0.060
A533B1	SH1	30D	PSH101	P	LT	58531	1.400E+17	6.600E+08	528	10.	136.	28.	142.	18.	-6.	0.180	1.313	0.009	0.015	0.177	0.613	-999.000	0.567	0.093
A533B1	SH2	30D	PSH201	P	LT	54619	1.300E+17	6.700E+08	528	-9.	132.	0.	134.	9.	-2.	0.200	1.300	0.008	0.015	0.240	0.633	-999.000	0.573	0.123
A533B1	SL1	W104	PSL101	P	LT	83408	7.160E+18	2.380E+10	545	6.	148.	86.	124.	80.	24.	0.250	1.300	0.007	0.017	0.201	0.575	0.070	0.629	0.141
A533B1	SL1	W104	SHSS01	SRM	LT	83408	7.160E+18	2.380E+10	545	30.	138.	159.	-999.	129.	-999.	0.219	1.465	0.010	0.015	0.186	0.665	0.103	0.548	0.174
A533B1	SL1	W97	PSL101	P	LT	40917	5.500E+18	-9.990E+02	541	6.	148.	76.	108.	69.	40.	0.250	1.300	0.007	0.017	0.201	0.575	0.070	0.629	0.141

Material ID	Plant ID	Capsule	Heat ID	Product ID	Specimen Orientation	Irradiation time hr	Fluence n/cm^2	Flux n/cm^2/s	Tcoolant F	TTu30 F	USEu ft-lb	TTi30 F	USEi ft-lb	dTT30 F	dUSE ft-lb	C wt%	Mn wt%	P wt%	S wt%	Si wt%	Ni wt%	Cr wt%	Mo wt%	Cu wt%
A533B1	SL1	W97	PSL101	P	TL	40917	5.500E+18	-9.990E+02	541	19.	103.	79.	82.	60.	21.	0.250	1.300	0.007	0.017	0.201	0.575	0.070	0.629	0.141
A533B1	SL2	W83	PSL201	P	LT	9773	1.600E+18	4.540E+10	548	12.	135.	39.	120.	27.	15.	0.275	1.335	0.005	0.010	0.270	0.565	0.095	0.535	0.101
A533B1	SL2	W83	PSL201	P	TL	9773	1.600E+18	4.540E+10	548	31.	105.	60.	103.	29.	1.	0.275	1.335	0.005	0.010	0.270	0.565	0.095	0.535	0.101
A336	SMG	190D	FSMGJW	F	LT	139116	1.260E+18	2.510E+09	528	-9.	146.	-12.	138.	-4.	9.	0.180	0.590	0.012	-999.000	0.320	0.720	0.350	0.600	0.079
A302B	SO1	A	PSO103	P	LT	16278	1.750E+19	2.990E+11	-999	27.	106.	121.	72.	94.	34.	0.205	1.437	0.011	0.023	0.245	0.200	-999.000	0.467	0.180
A302B	SO1	A	SASTM	SRM	LT	16278	1.750E+19	2.990E+11	-999	37.	-999.	147.	57.	110.	-999.	0.240	1.340	0.014	0.023	0.230	0.180	0.110	0.510	0.200
A302B	SO1	D	PSO101	P	LT	24722	3.480E+19	3.910E+11	-999	31.	98.	150.	63.	118.	35.	0.235	1.403	0.013	0.021	0.270	0.200	-999.000	0.453	0.170
A302B	SO1	D	PSO102	P	LT	24722	3.480E+19	3.910E+11	-999	14.	112.	119.	70.	104.	42.	0.210	1.360	0.011	0.019	0.230	0.200	-999.000	0.470	0.180
A302B	SO1	D	PSO103	P	LT	24722	3.480E+19	3.910E+11	-999	27.	106.	145.	73.	118.	33.	0.205	1.437	0.011	0.023	0.245	0.200	-999.000	0.467	0.180
A302B	SO1	D	SASTM	SRM	LT	24722	3.480E+19	3.910E+11	-999	37.	-999.	185.	59.	148.	-999.	0.240	1.340	0.014	0.023	0.230	0.180	0.110	0.510	0.200
A302B	SO1	F	PSO102	P	LT	67500	3.850E+19	1.590E+11	-999	14.	112.	123.	85.	108.	26.	0.210	1.360	0.011	0.019	0.230	0.200	-999.000	0.470	0.180
A302B	SO1	F	SASTM	SRM	LT	67500	3.850E+19	1.590E+11	-999	37.	-999.	161.	63.	124.	-999.	0.240	1.340	0.014	0.023	0.230	0.180	0.110	0.510	0.200
	SO2	W97	PSO2JW	P	LT	23620	5.070E+18	5.960E+10	553	23.	151.	73.	135.	51.	17.	-999.000	-999.000	-999.000	-999.000	-999.000	-999.000	-999.000	-999.000	-999.000
	SO2	W97	PSO2JW	P	TL	23620	5.070E+18	5.960E+10	553	26.	133.	67.	106.	41.	26.	-999.000	-999.000	-999.000	-999.000	-999.000	-999.000	-999.000	-999.000	-999.000
A533B1	SO3	W97	PSO301	P	LT	37957	8.000E+18	5.860E+10	553	82.	102.	138.	-999.	56.	-999.	0.238	1.343	0.009	0.014	0.139	0.573	0.086	0.555	0.054
A533B1	SO3	W97	PSO301	P	TL	37957	8.000E+18	5.860E+10	553	43.	93.	111.	-999.	68.	-999.	0.238	1.343	0.009	0.014	0.139	0.573	0.086	0.555	0.054
A5082	SQ1	T	FSQ101	F	LT	9361	2.880E+18	8.540E+10	545	-31.	119.	32.	101.	63.	18.	0.170	0.620	0.020	0.016	0.220	0.760	0.370	0.560	0.130
A5082	SQ1	T	FSQ101	F	TL	9361	2.880E+18	8.540E+10	545	40.	67.	93.	75.	53.	-8.	0.170	0.620	0.020	0.016	0.220	0.760	0.370	0.560	0.130
A5082	SQ1	U	FSQ101	F	LT	25139	9.550E+18	1.060E+11	545	-31.	119.	78.	98.	109.	21.	0.170	0.620	0.020	0.016	0.220	0.760	0.370	0.560	0.130
A5082	SQ1	U	FSQ101	F	TL	25139	9.550E+18	1.060E+11	545	40.	67.	114.	60.	74.	7.	0.170	0.620	0.020	0.016	0.220	0.760	0.370	0.560	0.130
A5082	SQ1	X	FSQ101	F	LT	46111	1.390E+19	8.340E+10	545	-31.	119.	106.	113.	138.	6.	0.170	0.620	0.020	0.016	0.220	0.760	0.370	0.560	0.130
A5082	SQ1	X	FSQ101	F	TL	46111	1.390E+19	8.340E+10	545	40.	67.	147.	62.	106.	5.	0.170	0.620	0.020	0.016	0.220	0.760	0.370	0.560	0.130
A5082	SQ2	T	FSQ201	F	LT	9333	2.420E+18	7.190E+10	545	-54.	138.	2.	123.	55.	15.	0.185	0.710	0.018	0.015	0.245	0.740	0.335	0.605	0.130
A5082	SQ2	T	FSQ201	F	TL	9333	2.420E+18	7.190E+10	545	-14.	97.	36.	88.	50.	9.	0.185	0.710	0.018	0.015	0.245	0.740	0.335	0.605	0.130
A5082	SQ2	U	FSQ201	F	LT	25528	6.080E+18	6.610E+10	545	-54.	138.	15.	114.	68.	24.	0.185	0.710	0.018	0.015	0.245	0.740	0.335	0.605	0.130
A5082	SQ2	U	FSQ201	F	TL	25528	6.080E+18	6.610E+10	545	-14.	97.	54.	84.	68.	13.	0.185	0.710	0.018	0.015	0.245	0.740	0.335	0.605	0.130
A5082	SQ2	X	FSQ201	F	LT	46944	1.030E+19	6.070E+10	545	-54.	138.	24.	124.	78.	15.	0.185	0.710	0.018	0.015	0.245	0.740	0.335	0.605	0.130
A5082	SQ2	X	FSQ201	F	TL	46944	1.030E+19	6.070E+10	545	-14.	97.	99.	101.	113.	-4.	0.185	0.710	0.018	0.015	0.245	0.740	0.335	0.605	0.130
A533B1	SR1	U	PSR101	P	LT	9583	6.120E+18	1.780E+11	557	52.	91.	82.	96.	29.	-4.	0.220	1.340	0.014	0.016	0.370	0.490	0.095	0.500	0.073
A533B1	SR1	U	PSR101	P	TL	9583	6.120E+18	1.780E+11	557	74.	77.	110.	70.	36.	8.	0.220	1.340	0.014	0.016	0.370	0.490	0.095	0.500	0.073
A533B1	SR1	V	PSR101	P	LT	26722	1.520E+19	1.580E+11	557	52.	91.	94.	86.	42.	5.	0.220	1.340	0.014	0.016	0.370	0.490	0.095	0.500	0.073
A533B1	SR1	V	PSR101	P	TL	26722	1.520E+19	1.580E+11	557	74.	77.	106.	64.	33.	13.	0.220	1.340	0.014	0.016	0.370	0.490	0.095	0.500	0.073
A533B1	ST1	U	PST101	P	LT	6861	2.830E+18	1.140E+11	560	-46.	137.	-34.	134.	12.	4.	0.190	1.180	0.012	0.013	0.190	0.650	0.030	0.530	0.060
A533B1	ST1	U	PST101	P	TL	6861	2.830E+18	1.140E+11	560	-6.	121.	16.	108.	21.	13.	0.190	1.180	0.012	0.013	0.190	0.650	0.030	0.530	0.060
A533B1	ST2	V	PST2JW	P	LT	7889	2.540E+18	8.970E+10	560	-34.	131.	-23.	141.	11.	-10.	-999.000	-999.000	0.006	-999.000	-999.000	0.650	-999.000	-999.000	0.040
A533B1	ST2	V	PST2JW	P	TL	7889	2.540E+18	8.970E+10	560	-18.	103.	-10.	126.	8.	-23.	-999.000	-999.000	0.006	-999.000	-999.000	0.650	-999.000	-999.000	0.040
A533B1	SU1	T	PSU101	P	LT	9389	2.820E+18	8.340E+10	534	-7.	128.	42.	123.	49.	5.	0.232	1.395	0.013	0.015	0.325	0.500	0.091	0.584	0.110
A533B1	SU1	T	SHSS02	SRM	LT	9389	2.820E+18	8.340E+10	534	47.	124.	119.	110.	72.	14.	0.217	1.478	0.011	0.015	0.225	0.640	0.095	0.502	0.170
A533B1	SU1	V	PSU101	P	LT	70278	1.970E+19	7.790E+10	538	-7.	128.	105.	122.	112.	6.	0.232	1.395	0.013	0.015	0.325	0.500	0.091	0.584	0.110
A533B1	SU1	V	SHSS02	SRM	LT	70278	1.970E+19	7.790E+10	538	47.	124.	186.	101.	139.	23.	0.217	1.478	0.011	0.015	0.225	0.640	0.095	0.502	0.170
A533B1	SU2	V	PSU201	P	LT	73333	1.750E+19	6.640E+10	540	-2.	134.	77.	126.	80.	8.	0.244	1.340	0.011	0.014	0.244	0.540	0.083	0.536	0.110
A533B1	SU2	V	PSU201	P	TL	73333	1.750E+19	6.640E+10	540	11.	113.	76.	95.	65.	18.	0.244	1.340	0.011	0.014	0.244	0.540	0.083	0.536	0.110
A533B1	SU2	V	SHSS02	SRM	LT	73333	1.750E+19	6.640E+10	540	47.	124.	162.	106.	115.	18.	0.217	1.478	0.011	0.015	0.225	0.640	0.095	0.502	0.170
A533B1	SU2	X	PSU201	P	LT	10250	2.940E+18	7.970E+10	535	-2.	134.	56.	125.	58.	9.	0.244	1.340	0.011	0.014	0.244	0.540	0.083	0.536	0.110
A533B1	SU2	X	PSU201	P	TL	10250	2.940E+18	7.970E+10	535	11.	113.	59.	98.	49.	15.	0.244	1.340	0.011	0.014	0.244	0.540	0.083	0.536	0.110
A533B1	SU2	X	SHSS02	SRM	LT	10250	2.940E+18	7.970E+10	535	47.	124.	108.	112.	61.	12.	0.217	1.478	0.011	0.015	0.225	0.640	0.095	0.502	0.170
A302B	TM1	C	PTM101	P	LT	38371	8.660E+18	6.260E+10	556	-11.	129.	2.	117.	14.	12.	0.240	1.360	0.010	0.017	0.230	0.570	0.190	0.510	0.090
A302B	TM1	C	PTM101	P	TL	38371	8.660E+18	6.260E+10	556	25.	98.	41.	83.	15.	15.	0.240	1.360	0.010	0.017	0.230	0.570	0.190	0.510	0.090
A533B1	TM1	C	SHSS02	SRM	LT	38371	8.660E+18	6.260E+10	556	47.	124.	124.	99.	77.	25.	0.217	1.478	0.011	0.015	0.225	0.640	0.095	0.502	0.170
A302B	TM1	E	PTM101	P	LT	11211	1.090E+18	-9.990E+02	556	-11.	129.	14.	121.	26.	7.	0.240	1.360	0.010	0.017	0.230	0.570	0.190	0.510	0.090
A302B	TM1	E	PTM101	P	TL	11211	1.090E+18	-9.990E+02	556	25.	98.	-999.	-999.	-999.	-999.	0.240	1.360	0.010	0.017	0.230	0.570	0.190	0.510	0.090
A533B1	TM1	E	SHSS02	SRM	LT	11211	1.090E+18	-9.990E+02	556	47.	124.	88.	113.	41.	11.	0.217	1.478	0.011	0.015	0.225	0.640	0.095	0.502	0.170
A5082	TP3	S	FTP301	F	LT	30278	1.720E+19	1.570E+11	547	-45.	147.	-32.	129.	13.	19.	0.200	0.640	0.010	0.010	0.260	0.700	0.400	0.620	0.060
A5082	TP3	S	FTP302	F	LT	30278	1.720E+19	1.570E+11	547	-58.	152.	-16.	124.	42.	28.	0.190	0.610	0.010	0.008	0.200	0.670	0.380	0.580	0.080
A302B	TP3	S	SASTM	SRM	LT	30278	1.720E+19	1.570E+11	547	37.	-999.	137.	54.	100.	-999.	0.240	1.340	0.014	0.023	0.230	0.180	0.110	0.510	0.200
A5082	TP3	T	FTP301	F	LT	10056	7.390E+18	2.040E+11	547	-45.	147.	-27.	153.	18.	-6.	0.200	0.640	0.010	0.010	0.260	0.700	0.400	0.620	0.060
A302B	TP3	T	SASTM	SRM	LT	10056	7.390E+18	2.040E+11	547	37.	-999.	117.	83.	80.	-999.	0.240	1.340	0.014	0.023	0.230	0.180	0.110	0.510	0.200
A5082	TP3	V	FTP302	F	LT	70556	1.530E+19	6.000E+10	547	-58.	152.	-2.	171.	55.	-19.	0.190	0.610	0.010	0.008	0.200	0.670	0.380	0.580	0.080
A302B	TP3	V	SASTM	SRM	LT	70556	1.530E+19	6.000E+10	547	37.	-999.	131.	73.	94.	-999.	0.240	1.340	0.014	0.023	0.230	0.180	0.110	0.510	0.200
A5082	TP4	S	FTP401	F	LT	30000	1.430E+19	1.330E+11	547	-26.	130.	-44.	125.	-18.	5.	0.210	0.670	0.011	0.009	0.230	0.700	0.310	0.560	0.060
A5082	TP4	S	FTP402	F	LT	30000	1.430E+19	1.330E+11	547	-14.	143.	34.	124.	48.	19.	0.220	0.670	0.010	0.009	0.200	0.710	0.330	0.560	0.050
A533B1	TP4	S	SHSS02	SRM	LT	30000	1.430E+19	1.330E+11	547	47.	124.	150.	100.	103.	24.	0.217	1.478	0.011	0.015	0.225	0.640	0.095	0.502	0.170
A5082	TP4	T	FTP401	F	LT	10278	7.080E+18	1.920E+11	547	-26.	130.	-14.	134.	12.	-4.	0.210	0.670	0.011	0.009	0.230	0.700	0.310	0.560	0.060
A533B1	TP4	T	SHSS02	SRM	LT	10278	7.080E+18	1.920E+11	547	47.	124.	134.	96.	87.	28.	0.217	1.478	0.011	0.015	0.225	0.640	0.095	0.502	0.170
A533B1	TRO	U	PTRO01	P	LT	10139	4.110E+18	1.130E+11	554	-17.	119.	45.	118.	62.	1.	0.210	1.270	0.011	0.016	0.200	0.600	0.048	0.530	0.150
A533B1	TRO	U	PTRO01	P	TL	10139	4.110E+18	1.130E+11	554	-6.	87.	60.	92.	66.	-5.	0.210	1.270	0.011	0.016	0.200	0.600	0.048	0.530	0.150
A533B1	TRO	V	PTRO01	P	LT	70278	2.340E+19	9.250E+10	554	-17.	119.	72.	-999.	89.	-999.	0.210	1.270	0.011	0.016	0.200	0.600	0.048	0.530	0.150
A533B1	TRO	V	PTRO01	P	TL	70278	2.340E+19	9.250E+10	554	-6.	87.	94.	87.	99.	-1.	0.210	1.270	0.011	0.016	0.200	0.600	0.048	0.530	0.150
A533B1	TRO	X	PTRO01	P	LT	38333	1.770E+19	1.290E+11	554	-17.	119.	69.	110.	86.	8.	0.210	1.270	0.011	0.016	0.200	0.600	0.048	0.530	0.150
A533B1	TRO	X	PTRO01	P	TL	38333	1.770E+19	1.290E+11	554	-6.	87.	102.	78.	108.	9.	0.210	1.270	0.011	0.016	0.200	0.600	0.048	0.530	0.150
A533B1	VO1	Y	PVO101	P	LT	40556	1.310E+19	8.930E+10	560	-14.	127.	24.	135.	38.	-8.	0.235	1.301	0.014	0.010	0.270	0.593	0.049	0.510	0.057
A533B1	VO1	Y	PVO101	P	TL	40556	1.310E+19	8.930E+10	560	17.	102.	27.	131.	10.	-29.	0.235	1.301	0.014	0.010	0.270	0.593	0.049	0.510	0.057
A533B1	VO2	JW	PVO201	P	LT	-999	1.130E+19	-9.990E+02	-999	8.	93.	14.	104.	6.	-11.	0.217	1.280	0.008	0.013	0.227	0.594	0.050	0.545	0.052
A533B1	VO2	JW	PVO201	P	TL	-999	1.130E+19	-9.990E+02	-999	27.	71.	30.	78.	3.	-7.	0.217	1.280	0.008	0.013	0.227	0.594	0.050	0.545	0.052
A533B1	VO2	U	PVO201	P	LT	10361	4.030E+18	1.080E+11	-999	8.	93.	11.	107.	2.	-13.	0.217	1.280	0.008	0.013	0.227	0.594	0.050	0.545	0.052
A533B1	VO2	U	PVO201	P	TL	10361	4.030E+18	1.080E+11	-999	27.	71.	21.	82.	-7.	-11.	0.217	1.280	0.008	0.013	0.227	0.594	0.050	0.545	0.052
A533B1	VS1	U	PVS101	P	LT	9861	6.550E+18	1.850E+11	555	-19.	135.	21.	132.	40.	3.	0.220	1.300	0.009	0.015	0.240	0.510	0.080	0.490	0.100
A533B1	VS1	U	PVS101	P	TL	9861	6.550E+18	1.850E+11	555	28.	78.	43.	77.	15.	1.	0.220	1.300	0.009	0.015	0.240	0.510	0.080	0.490	0.100
A533B1	VS1	V	PVS101	P	LT	25639	1.550E+19	1.680E+11	555	-19.	135.	40.	126.	58.	9.	0.220	1.300	0.009	0.015	0.240	0.510	0.080	0.490	0.100
A533B1	VS1	V	PVS101	P	TL	25639	1.550E+19	1.680E+11	555	28.	78.	60.	81.	32.	-3.	0.220	1.300	0.009	0.015	0.240	0.510	0.080	0.490	0.100
A533B1	VS1	X	PVS101	P	LT	44167	2.620E+19	1.650E+11	555	-19.	135.	16.	134.	35.	1.	0.220	1.300	0.009	0.015	0.240	0.510	0.080	0.490	0.100
A533B1	VS1	X	PVS101	P	TL	44167	2.620E+19	1.650E+11	555	28.	78.	56.	85.	28.	-7.	0.220	1.300	0.009	0.015	0.240	0.510	0.080	0.490	0.100

Embrittlement Analysis Data Base

Material ID	Plant ID	Capsule	Heat ID	Product ID	Specimen Orientation	Irradiation time hr	Fluence n/cm^2	Flux n/cm^2/s	Tcoolant F	TTu30 F	USEu ft-lb	TTi30 F	USEi ft-lb	dTT30 F	dUSE ft-lb	C wt%	Mn wt%	P wt%	S wt%	Si wt%	Ni wt%	Cr wt%	Mo wt%	Cu wt%
A533B1	VY	30D	PVY_01	P	LT	66120	4.300E+16	1.804E+08	527	8.	148.	27.	129.	19.	19.	-999.000	-999.000	0.015	-999.000	-999.000	0.679	-999.000	-999.000	0.104
A533B1	WC1	U	PWC101	P	LT	9417	3.530E+18	1.040E+11	560	-18.	149.	15.	144.	32.	5.	0.200	1.450	0.008	0.010	0.200	0.620	0.050	0.550	0.070
A533B1	WC1	U	PWC101	P	TL	9417	3.530E+18	1.040E+11	560	2.	97.	26.	97.	24.	0.	0.200	1.450	0.008	0.010	0.200	0.620	0.050	0.550	0.070
A533B1	WC1	Y	PWC101	P	LT	41944	1.270E+19	8.360E+10	561	-18.	149.	-7.	129.	11.	20.	0.200	1.450	0.008	0.010	0.200	0.620	0.050	0.550	0.070
A533B1	WC1	Y	PWC101	P	TL	41944	1.270E+19	8.360E+10	561	2.	97.	38.	102.	36.	-5.	0.200	1.450	0.008	0.010	0.200	0.620	0.050	0.550	0.070
A533B1	WF3	W97	PWF301	P	LT	38921	6.470E+18	4.620E+10	553	-7.	173.	-2.	158.	5.	14.	0.230	1.380	0.005	0.005	0.230	0.580	0.010	0.570	0.030
A533B1	WF3	W97	PWF301	P	TL	38921	6.470E+18	4.620E+10	553	-25.	146.	6.	125.	31.	20.	0.230	1.380	0.005	0.005	0.230	0.580	0.010	0.570	0.030
A533B1	ZN1	T	PZN101	P	LT	10667	3.100E+18	8.460E+10	529	-3.	140.	50.	132.	53.	8.	0.239	1.375	0.010	0.015	0.202	0.490	0.082	0.467	0.110
A533B1	ZN1	T	PZN101	P	TL	10667	3.100E+18	8.460E+10	529	21.	118.	53.	117.	32.	0.	0.239	1.375	0.010	0.015	0.202	0.490	0.082	0.467	0.110
A533B1	ZN1	T	SHSS02	SRM	LT	10667	3.100E+18	8.460E+10	529	47.	124.	113.	106.	67.	18.	0.217	1.478	0.011	0.015	0.225	0.640	0.095	0.502	0.170
A533B1	ZN1	U	PZN101	P	LT	31389	1.020E+19	8.550E+10	529	-3.	140.	87.	128.	90.	12.	0.239	1.375	0.010	0.015	0.202	0.490	0.082	0.467	0.110
A533B1	ZN1	U	PZN101	P	TL	31389	1.020E+19	8.550E+10	529	21.	118.	87.	117.	65.	0.	0.239	1.375	0.010	0.015	0.202	0.490	0.082	0.467	0.110
A533B1	ZN1	U	SHSS02	SRM	LT	31389	1.020E+19	8.550E+10	529	47.	124.	171.	94.	124.	30.	0.217	1.478	0.011	0.015	0.225	0.640	0.095	0.502	0.170
A533B1	ZN1	X	PZN101	P	LT	45278	1.260E+19	8.170E+10	529	-3.	140.	91.	117.	94.	23.	0.239	1.375	0.010	0.015	0.202	0.490	0.082	0.467	0.110
A533B1	ZN1	X	PZN101	P	TL	45278	1.260E+19	8.170E+10	529	21.	118.	94.	98.	73.	20.	0.239	1.375	0.010	0.015	0.202	0.490	0.082	0.467	0.110
A533B1	ZN1	X	SHSS02	SRM	LT	45278	1.260E+19	8.170E+10	529	47.	124.	165.	93.	118.	31.	0.217	1.478	0.011	0.015	0.225	0.640	0.095	0.502	0.170
A533B1	ZN1	Y	PZN101	P	LT	75278	1.560E+19	6.560E+10	529	-3.	140.	96.	117.	99.	24.	0.239	1.375	0.010	0.015	0.202	0.490	0.082	0.467	0.110
A533B1	ZN1	Y	PZN101	P	TL	75278	1.560E+19	6.560E+10	529	21.	118.	121.	95.	100.	22.	0.239	1.375	0.010	0.015	0.202	0.490	0.082	0.467	0.110
A533B1	ZN1	Y	SHSS02	SRM	LT	75278	1.560E+19	6.560E+10	529	47.	124.	168.	98.	121.	26.	0.217	1.478	0.011	0.015	0.225	0.640	0.095	0.502	0.170
A533B1	ZN2	T	PZN201	P	LT	31389	7.790E+18	7.450E+10	528	31.	126.	102.	105.	71.	22.	0.160	1.315	0.007	0.013	0.235	0.530	0.065	0.495	0.120
A533B1	ZN2	T	PZN201	P	TL	31389	7.790E+18	7.450E+10	528	47.	95.	130.	84.	83.	12.	0.160	1.315	0.007	0.013	0.235	0.530	0.065	0.495	0.120
A533B1	ZN2	T	SHSS02	SRM	LT	31389	7.790E+18	7.450E+10	528	47.	124.	146.	89.	99.	35.	0.217	1.478	0.011	0.015	0.225	0.640	0.095	0.502	0.170
A533B1	ZN2	U	PZN201	P	LT	11583	2.700E+18	6.760E+10	528	31.	126.	73.	121.	42.	5.	0.160	1.315	0.007	0.013	0.235	0.530	0.065	0.495	0.120
A533B1	ZN2	U	PZN201	P	TL	11583	2.700E+18	6.760E+10	528	47.	95.	100.	97.	53.	-2.	0.160	1.315	0.007	0.013	0.235	0.530	0.065	0.495	0.120
A533B1	ZN2	U	SHSS02	SRM	LT	11583	2.700E+18	6.760E+10	528	47.	124.	97.	108.	50.	16.	0.217	1.478	0.011	0.015	0.225	0.640	0.095	0.502	0.170
A533B1	ZN2	Y	PZN201	P	LT	80556	1.460E+19	5.750E+10	528	31.	126.	126.	114.	94.	12.	0.160	1.315	0.007	0.013	0.235	0.530	0.065	0.495	0.120
A533B1	ZN2	Y	PZN201	P	TL	80556	1.460E+19	5.750E+10	528	47.	95.	168.	95.	121.	0.	0.160	1.315	0.007	0.013	0.235	0.530	0.065	0.495	0.120
A533B1	ZN2	Y	SHSS02	SRM	LT	80556	1.460E+19	5.750E+10	528	47.	124.	181.	113.	134.	11.	0.217	1.478	0.011	0.015	0.225	0.640	0.095	0.502	0.170
A5082	AD1	V	WAD101	W	TL	8607	4.580E+18	-9.990E+02	-999	-75.	170.	-67.	154.	7.	16.	0.130	1.400	0.005	0.005	0.310	0.560	0.150	0.490	0.030
A533B1	AN1	A	WAN101	W	TL	-999	1.030E+19	8.980E+10	556	8.	75.	153.	45.	145.	30.	0.077	1.495	0.016	0.012	0.465	0.590	0.060	0.375	0.280
A533B1	AN1	C	WAN101	W	TL	-999	1.460E+19	8.630E+10	556	8.	75.	182.	46.	174.	29.	0.077	1.495	0.016	0.012	0.465	0.590	0.060	0.375	0.280
A533B1	AN1	E	WAN101	W	TL	8281	7.270E+17	-9.990E+02	556	8.	75.	108.	58.	100.	17.	0.077	1.495	0.016	0.012	0.465	0.590	0.060	0.375	0.280
A533B1	AN2	W97	WAN201	W	TL	14815	3.340E+18	6.400E+10	553	-2.	149.	12.	142.	14.	7.	0.130	1.330	0.007	0.009	0.140	0.083	0.020	0.620	0.044
A5083	BD1	U	WBD101	W	TL	9639	3.700E+18	1.070E+11	551	-28.	70.	-9.	73.	18.	-3.	0.065	1.467	0.017	0.013	0.488	0.657	0.090	0.443	0.032
A5083	BD1	X	WBD101	W	TL	37080	1.144E+19	-9.990E+02	551	-28.	70.	4.	76.	32.	-6.	0.065	1.467	0.017	0.013	0.488	0.657	0.090	0.443	0.032
A5083	BD2	U	WBD201	W	TL	10056	3.850E+18	1.060E+11	558	-19.	73.	-19.	65.	-1.	8.	0.068	1.445	0.015	0.013	0.505	0.718	0.091	0.450	0.033
A5083	BD2	X	WBD201	W	TL	-999	1.126E+19	-9.990E+02	558	-19.	73.	6.	69.	24.	4.	0.068	1.445	0.015	0.013	0.505	0.718	0.091	0.450	0.033
A302BM	BF2	30D	WBF2JW	W		79299	1.520E+17	5.890E+08	528	-48.	119.	-20.	116.	28.	3.	0.150	1.490	0.010	0.011	0.090	0.330	-999.000	0.490	0.200
A302B	BR	119	WBR_01	W	TS	6578	1.500E+18	6.100E+10	570	-72.	101.	-23.	69.	49.	32.	0.120	1.250	0.014	0.012	0.280	0.100	0.190	0.530	0.270
A302B	BR	122	WBR_01	W	TS	6578	2.300E+19	9.600E+11	570	-72.	101.	-999.	-999.	-999.	-999.	0.120	1.250	0.014	0.012	0.280	0.100	0.190	0.530	0.270
A302B	BR	124	WBR_01	W	TS	18290	1.070E+20	1.600E+12	570	-72.	101.	-999.	-999.	-999.	-999.	0.120	1.250	0.014	0.012	0.280	0.100	0.190	0.530	0.270
A302B	BR	125	WBR_01	W	TS	75556	2.270E+19	8.380E+10	570	-72.	101.	51.	82.	123.	19.	0.120	1.250	0.014	0.012	0.280	0.100	0.190	0.530	0.270
A302B	BR	127	WBR_01	W	TS	26114	7.100E+18	7.500E+10	570	-72.	101.	69.	-999.	141.	-999.	0.120	1.250	0.014	0.012	0.280	0.100	0.190	0.530	0.270
A533B1	BV1	U	WBV101	W	TL	31389	6.530E+18	5.770E+10	547	-63.	109.	98.	92.	161.	18.	0.117	1.395	0.013	0.005	0.274	0.629	0.022	0.480	0.245
A533B1	BV1	V	WBV101	W	TL	10167	2.810E+18	7.660E+10	547	-63.	109.	92.	89.	154.	20.	0.117	1.395	0.013	0.005	0.274	0.629	0.022	0.480	0.245
A533B1	BV1	W	WBV101	W	TL	51667	9.130E+18	4.910E+10	547	-63.	109.	119.	83.	182.	27.	0.117	1.395	0.013	0.005	0.274	0.629	0.022	0.480	0.245
A5082	BY1	U	WBY101	W	TL	10083	3.720E+18	1.020E+11	551	-30.	78.	-26.	72.	4.	6.	0.080	1.443	0.011	0.014	0.535	0.690	0.099	0.417	0.022
A5082	BY1	X	WBY101	W	TL	49444	1.390E+19	7.810E+10	551	-30.	78.	10.	69.	40.	9.	0.080	1.443	0.011	0.014	0.535	0.690	0.099	0.417	0.022
A5083	BY2	U	WBY201	W	TL	10111	3.930E+18	1.080E+11	551	-71.	70.	-64.	83.	8.	-13.	0.083	1.417	0.012	0.013	0.520	0.708	0.086	0.433	0.028
A5083	BY2	W	WBY201	W	TL	40587	1.211E+19	-9.990E+02	551	-71.	70.	-42.	77.	29.	-7.	0.083	1.417	0.012	0.013	0.520	0.708	0.086	0.433	0.028
A533B1	CAB	K	WCAB01	W	TL	36730	1.400E+19	-9.990E+02	-999	-31.	103.	106.	-999.	137.	-999.	0.170	1.380	0.018	0.011	0.282	0.086	-999.000	0.370	0.225
A533B1	CAB	N	WCAB01	W	TL	64722	3.680E+19	1.580E+11	-999	-31.	103.	184.	66.	216.	37.	0.170	1.380	0.018	0.011	0.282	0.086	-999.000	0.370	0.225
A5082	CB1	Y	WCB101	W	TL	43611	1.350E+19	8.600E+10	-999	-37.	129.	-19.	125.	18.	4.	0.059	1.850	0.012	0.007	0.239	0.725	0.021	0.570	0.049
A5082	CB1	Z	WCB101	W	TL	6944	3.320E+18	1.320E+11	562	-37.	129.	-37.	129.	0.	0.	0.059	1.850	0.012	0.007	0.239	0.725	0.021	0.570	0.049
A533B1	CB2	X	WCB201	W	TL	39722	1.220E+19	8.580E+10	562	-51.	149.	-19.	130.	32.	19.	0.140	1.163	0.008	0.010	0.133	0.153	0.043	0.568	0.042
A533B1	CB2	Z	WCB201	W	TL	0	3.380E+18	1.250E+11	-999	-51.	149.	-84.	148.	-32.	1.	0.140	1.163	0.008	0.010	0.133	0.153	0.043	0.568	0.042
A533B1	CC1	W263	WCC101	W	TL	25760	6.100E+18	6.490E+10	545	-53.	157.	-10.	120.	43.	37.	0.150	1.254	0.009	0.028	0.291	0.150	0.036	0.470	0.175
A533B1	CC1	W97	WCC101	W	TL	-999	2.180E+19	-9.990E+02	545	-53.	157.	43.	106.	96.	51.	0.150	1.254	0.009	0.028	0.291	0.150	0.036	0.470	0.175
A533B1	CC2	W263	WCC201	W	TL	40114	8.060E+18	5.580E+10	545	-49.	142.	18.	107.	67.	34.	0.115	1.167	0.013	0.008	0.143	0.182	0.050	0.480	0.262
A533B1	CC2	W97	WCC201	W	TL	-999	1.850E+19	-9.990E+02	545	-49.	142.	30.	101.	78.	41.	0.115	1.167	0.013	0.008	0.143	0.182	0.050	0.480	0.262
A533B1	CK1	T	WCK101	W		11111	2.690E+18	6.720E+10	537	-97.	113.	-27.	82.	70.	31.	0.260	1.330	0.023	0.014	0.180	0.740	0.022	0.440	0.270
A533B1	CK1	U	WCK101	W		80556	1.770E+19	6.110E+10	537	-97.	113.	11.	-999.	109.	-999.	0.260	1.330	0.023	0.014	0.180	0.740	0.022	0.440	0.270
A533B1	CK1	Y	WCK101	W		43333	1.230E+19	7.860E+10	537	-97.	113.	86.	72.	184.	41.	0.260	1.330	0.023	0.014	0.180	0.740	0.022	0.440	0.270
A533B1	CK2	T	WCK201	W	TL	9444	2.180E+18	6.400E+10	542	2.	77.	44.	74.	41.	3.	0.095	1.375	0.020	0.014	0.400	0.965	0.069	0.540	0.053
A533B1	CK2	U	WCK201	W	TL	75833	1.500E+19	5.490E+10	542	2.	77.	54.	87.	51.	-9.	0.095	1.375	0.020	0.014	0.400	0.965	0.069	0.540	0.053
A533B1	CK2	X	WCK201	W	TL	46111	1.030E+19	6.220E+10	542	2.	77.	69.	71.	67.	6.	0.095	1.375	0.020	0.014	0.400	0.965	0.069	0.540	0.053
A533B1	CK2	Y	WCK201	W	TL	28333	6.620E+18	6.510E+10	542	2.	77.	47.	72.	45.	5.	0.095	1.375	0.020	0.014	0.400	0.965	0.069	0.540	0.053
A533B1	CL1	U	WCL101	W	TL	9222	3.470E+18	1.050E+11	558	-55.	115.	13.	103.	68.	12.	0.130	1.325	0.005	0.012	0.455	0.065	0.040	0.520	0.045
A533B1	CL1	Y	WCL101	W	TL	40278	1.300E+19	8.970E+10	558	-55.	115.	-16.	93.	39.	22.	0.130	1.325	0.005	0.012	0.455	0.065	0.040	0.520	0.045
A533B1	COF	3D	WCOFJW	W		49646	8.400E+17	4.700E+09	533	-36.	169.	-64.	170.	-28.	-1.	-999.000	1.700	0.012	-999.000	0.240	0.760	-999.000	0.510	0.072
A533B1	CP1	U	WCP1JW	W		7972	3.530E+18	1.230E+11	-999	-65.	131.	-81.	131.	-16.	0.	-999.000	-999.000	0.004	-999.000	-999.000	0.220	-999.000	-999.000	0.040
A533B1	CP2	U	WCP201	W		7924	3.280E+18	-9.990E+02	-999	-50.	97.	-48.	85.	2.	12.	0.110	1.370	0.011	0.014	0.490	0.072	0.058	0.590	0.030
A533B1	CR3	B	WCR301	W	TL	6451	1.050E+18	4.510E+10	556	38.	92.	70.	73.	32.	19.	0.087	1.623	0.020	0.012	0.847	0.100	0.080	0.443	0.410
A533B1	CR3	C	WCR301	W	TL	35568	6.560E+18	5.120E+10	556	38.	92.	151.	70.	114.	22.	0.087	1.623	0.020	0.012	0.847	0.100	0.080	0.443	0.410
A5082	CR3	C1	WHSS63	W		-999	7.790E+18	-9.990E+02	556	-18.	83.	187.	48.	205.	35.	0.090	1.580	0.015	0.016	0.540	0.700	0.090	0.420	0.350
A5082	CR3	C1	WHSS65	W		-999	5.100E+18	-9.990E+02	556	-13.	82.	116.	56.	129.	26.	0.080	1.450	0.016	0.016	0.510	0.590	0.090	0.380	0.210
A5082	CR3	C1	WHSSCR	W		-999	6.090E+18	-9.990E+02	556	-1.	75.	167.	56.	168.	19.	0.080	1.550	0.021	0.016	0.580	0.600	0.100	0.400	0.220
A5082	CR3	C2	WHSS65	W		-999	1.670E+19	-9.990E+02	556	-26.	83.	144.	52.	170.	30.	0.080	1.450	0.016	0.016	0.510	0.590	0.090	0.380	0.210
A5082	CR3	C2	WHSSCR	W		-999	1.950E+19	-9.990E+02	556	-1.	75.	137.	50.	138.	25.	0.080	1.550	0.021	0.016	0.580	0.600	0.100	0.400	0.220
A533B1	CR3	D	WCR301	W	TL	41592	7.500E+18	4.960E+10	556	38.	92.	136.	75.	99.	17.	0.087	1.623	0.020	0.012	0.847	0.100	0.080	0.443	0.410
A533B1	CR3	F	WCR301	W	TL	45024	1.080E+19	6.580E+10	556	38.	92.	156.	69.	118.	23.	0.087	1.623	0.020	0.012	0.847	0.100	0.080	0.443	0.410
A302B	CTY	A	WCTY01	W	TL	14806	2.590E+18	4.870E+10	537	-49.	108.	52.	79.	100.	29.	0.047	1.304	0.018	0.019	0.325	0.044	0.061	0.516	0.205

Material ID	Plant ID	Capsule	Heat ID	Product ID	Specimen Orientation	Irradiation time hr	Fluence n/cm^2	Flux n/cm^2/s	Tcoolant F	TTu30 F	USEu ft-lb	TTi30 F	USEi ft-lb	dTT30 F	dUSE ft-lb	C wt%	Mn wt%	P wt%	S wt%	Si wt%	Ni wt%	Cr wt%	Mo wt%	Cu wt%
A302B	CTY	D	WCTY01	W	TL	95278	2.280E+19	6.660E+10	537	-49.	108.	64.	85.	112.	23.	0.047	1.304	0.018	0.019	0.325	0.044	0.061	0.516	0.205
A533B1	DAC	1	WDAC01	W	LT	52000	4.900E+17	2.600E+09	532	-45.	99.	-41.	102.	4.	-3.	-999.000	1.250	0.012	-999.000	0.325	0.973	0.035	0.490	0.023
A5082	DB1	A	WDB101	W	TL	29146	1.290E+19	1.230E+11	556	-6.	70.	157.	67.	163.	4.	0.089	1.705	0.014	0.014	0.422	0.630	0.150	0.415	0.210
A5082	DB1	B	WDB101	W	TL	22632	5.920E+18	-9.990E+02	556	-6.	70.	103.	53.	109.	17.	0.089	1.705	0.014	0.014	0.422	0.630	0.150	0.415	0.210
A5082	DB1	D	WDB101	W	TL	47755	9.620E+18	5.600E+10	556	-6.	70.	136.	55.	142.	15.	0.089	1.705	0.014	0.014	0.422	0.630	0.150	0.415	0.210
A5082	DB1	D1	WHSS66	W		-999	6.630E+18	-9.990E+02	556	44.	59.	181.	43.	138.	16.	0.090	1.630	0.018	0.009	0.540	0.590	0.110	0.400	0.420
A5082	DB1	D1	WHSS67	W		-999	1.030E+19	-9.990E+02	556	-33.	75.	105.	55.	138.	20.	0.080	1.450	0.011	0.013	0.490	0.590	0.080	0.380	0.270
A5082	DB1	D1	WHSSDB	W		-999	8.210E+18	-9.990E+02	556	-46.	82.	144.	52.	189.	30.	0.080	1.470	0.016	0.015	0.540	0.590	0.070	0.400	0.320
A5082	DB1	F	WDB101	W	TL	8976	1.960E+18	6.080E+10	556	-6.	70.	101.	66.	107.	4.	0.089	1.705	0.014	0.014	0.422	0.630	0.150	0.415	0.210
A533B1	DC1	S	WDC101	W	TL	11056	2.840E+18	7.150E+10	539	-68.	98.	45.	87.	113.	11.	0.097	1.347	0.013	0.016	0.214	1.000	0.113	0.501	0.196
A533B1	DC1	Y	WDC101	W	TL	51389	9.410E+18	5.090E+10	540	-68.	98.	166.	67.	233.	32.	0.097	1.347	0.013	0.016	0.214	1.000	0.113	0.501	0.196
A533B1	DC2	U	WDC201	W	TL	8694	3.650E+18	1.160E+11	542	-13.	121.	160.	85.	173.	36.	0.127	1.403	0.015	0.007	0.158	0.871	0.049	0.493	0.219
A533B1	DC2	X	WDC201	W	TL	27250	9.160E+18	9.340E+10	541	-13.	121.	190.	74.	203.	47.	0.127	1.403	0.015	0.007	0.158	0.871	0.049	0.493	0.219
A533B1	DC2	Y	WDC201	W	TL	61362	1.320E+19	-9.990E+02	540	-13.	121.	198.	78.	211.	44.	0.127	1.403	0.015	0.007	0.158	0.871	0.049	0.493	0.219
A302B	DR2	2	WDR202	W	TL	20136	2.000E+19	2.760E+11	546	-16.	70.	89.	80.	104.	-10.	-999.000	1.540	-999.000	0.020	0.110	0.500	0.020	0.320	0.310
A302B	DR2	4	WDR202	W	TL	-999	6.400E+18	3.100E+11	546	-16.	70.	56.	48.	72.	22.	-999.000	1.540	-999.000	0.020	0.110	0.500	0.020	0.320	0.310
A302B	DR2	5	WDR202	W	TL	33984	4.290E+19	3.510E+11	546	-16.	70.	201.	-999.	217.	-999.	-999.000	1.540	-999.000	0.020	0.110	0.500	0.020	0.320	0.310
A302BM	DR3	12	WDR301	W	TL	13200	1.360E+19	2.860E+11	546	45.	74.	146.	60.	101.	14.	0.209	1.780	0.009	0.017	0.213	0.345	0.065	0.522	0.212
A302B	DR3	12	WDR302	W	TL	13200	1.360E+19	2.860E+11	546	-47.	77.	155.	42.	201.	36.	0.090	1.750	0.013	0.013	0.540	0.730	0.100	0.420	0.350
A302BM	DR3	13	WDR301	W	TL	8460	0.926E+16	3.040E+08	529	45.	74.	35.	83.	-10.	-10.	0.209	1.780	0.009	0.017	0.213	0.345	0.065	0.522	0.212
A302BM	DR3	14	WDR301	W	TL	8460	7.110E+18	2.340E+11	546	45.	74.	181.	70.	136.	4.	0.209	1.780	0.009	0.017	0.213	0.345	0.065	0.522	0.212
A302B	DR3	14	WDR302	W	TL	8460	7.110E+18	2.340E+11	546	-47.	77.	151.	47.	198.	30.	0.090	1.750	0.013	0.013	0.540	0.730	0.100	0.420	0.350
A302BM	DR3	18	WDR301	W	TL	52421	7.100E+16	3.760E+08	529	45.	74.	37.	73.	-8.	1.	0.209	1.780	0.009	0.017	0.213	0.345	0.065	0.522	0.212
A302BM	DR3	4	WDR301	W	TL	23564	1.605E+19	-9.990E+02	546	45.	74.	184.	64.	139.	10.	0.209	1.780	0.009	0.017	0.213	0.345	0.065	0.522	0.212
A302B	DR3	4	WDR302	W	TL	23564	1.080E+19	-9.990E+02	546	-47.	77.	212.	44.	259.	34.	0.090	1.750	0.013	0.013	0.540	0.730	0.100	0.420	0.350
A533B1	FA1	U	WFA101	W	TL	27056	1.750E+19	1.800E+11	-999	-73.	148.	-2.	108.	72.	41.	0.130	1.060	0.016	0.009	0.270	0.190	0.063	0.500	0.140
A533B1	FA1	W	WFA101	W	TL	108961	4.040E+19	-9.990E+02	-999	-73.	148.	23.	108.	96.	40.	0.130	1.060	0.016	0.009	0.270	0.190	0.063	0.500	0.140
A533B1	FA1	X	WFA101	W	TL	53611	2.990E+19	1.550E+11	-999	-73.	148.	14.	117.	87.	31.	0.130	1.060	0.016	0.009	0.270	0.190	0.063	0.500	0.140
A533B1	FA1	Y	WFA101	W	TL	10111	5.730E+18	1.580E+11	-999	-73.	148.	1.	125.	74.	23.	0.130	1.060	0.016	0.009	0.270	0.190	0.063	0.500	0.140
A533B1	FA2	U	WFA201	W	TL	9750	6.120E+18	1.750E+11	-999	-28.	147.	-44.	134.	-16.	13.	0.139	0.937	0.004	0.014	0.324	0.900	0.027	0.234	0.030
A533B1	FA2	W	WFA201	W	TL	34722	1.670E+19	1.340E+11	-999	-28.	147.	-29.	147.	-1.	-1.	0.139	0.937	0.004	0.014	0.324	0.900	0.027	0.234	0.030
A533B1	FA2	X	WFA201	W	TL	56389	3.020E+19	1.490E+11	-999	-28.	147.	-47.	157.	-19.	-10.	0.139	0.937	0.004	0.014	0.324	0.900	0.027	0.234	0.030
A533B1	FC1	W225	WFC101	W	TL	22753	5.530E+18	-9.990E+02	527	-32.	111.	178.	78.	210.	33.	0.140	1.563	0.013	0.012	0.202	0.600	0.030	0.527	0.301
A533B1	FC1	W265	WFC101	W	TL	51895	7.710E+18	-9.990E+02	534	-32.	111.	193.	65.	225.	46.	0.140	1.563	0.013	0.012	0.202	0.600	0.030	0.527	0.301
A533B1	FC1	W275	WFC101	W	TL	-999	1.280E+19	-9.990E+02	538	-32.	111.	187.	66.	219.	46.	0.140	1.563	0.013	0.012	0.202	0.600	0.030	0.527	0.301
A5082	GIN	R	WGIN01	W	TL	22333	1.100E+19	1.360E+11	550	-36.	80.	122.	50.	158.	30.	0.072	1.337	0.010	0.017	0.530	0.560	0.228	0.313	0.230
A5082	GIN	S	WGIN01	W	TL	149167	3.510E+19	6.550E+10	-999	-36.	80.	184.	64.	221.	16.	0.072	1.337	0.010	0.017	0.530	0.560	0.228	0.313	0.230
A5082	GIN	T	WGIN01	W	TL	60278	1.910E+19	8.810E+10	548	-36.	80.	129.	59.	165.	22.	0.072	1.337	0.010	0.017	0.530	0.560	0.228	0.313	0.230
A5082	GIN	V	WGIN01	W	TL	12361	5.850E+18	1.310E+11	552	-36.	80.	111.	55.	148.	25.	0.072	1.337	0.010	0.017	0.530	0.560	0.228	0.313	0.230
A533B1	HA2	30D	WHA2JW	W		57692	2.300E+17	1.100E+09	532	-18.	122.	-17.	122.	1.	0.	-999.000	1.190	0.014	-999.000	-999.000	0.095	-999.000	0.570	0.125
A302B	HB2	T	WHB201	W	TL	63611	4.420E+19	1.930E+11	546	-88.	118.	210.	-999.	298.	-999.	0.117	1.170	0.024	0.024	0.275	0.660	0.022	0.350	0.340
A302B	HB2	V	WHB201	W	TL	28056	6.010E+18	5.980E+10	546	-88.	118.	123.	81.	211.	37.	0.117	1.170	0.024	0.024	0.275	0.660	0.022	0.350	0.340
A533B1	HOP	30D	WHOPJW	W		52646	1.420E+17	7.500E+08	532	-55.	176.	-6.	166.	49.	9.	-999.000	1.480	0.014	-999.000	-999.000	0.590	0.011	0.400	0.080
A302B	IP2	V	WIP201	W	TL	75833	5.060E+18	1.860E+10	524	-68.	120.	128.	91.	196.	29.	-999.000	-999.000	0.019	-999.000	-999.000	1.150	-999.000	-999.000	0.200
A302B	IP2	Y	WIP201	W	TL	20833	4.530E+18	6.150E+10	529	-68.	120.	128.	69.	196.	51.	-999.000	-999.000	0.019	-999.000	-999.000	1.150	-999.000	-999.000	0.200
A302B	IP3	T	WIP301	W	TL	12000	3.120E+18	7.220E+10	540	-70.	122.	85.	94.	155.	28.	0.080	1.180	0.019	0.016	0.170	1.080	0.040	0.530	0.155
A302B	IP3	Y	WIP301	W	TL	29167	7.240E+18	6.920E+10	540	-70.	122.	106.	72.	176.	49.	0.080	1.180	0.019	0.016	0.170	1.080	0.040	0.530	0.155
A302B	IP3	Z	WIP301	W	TL	48889	1.040E+19	5.930E+10	540	-70.	122.	165.	82.	235.	40.	0.080	1.180	0.019	0.016	0.170	1.080	0.040	0.530	0.155
A533B1	KU1	177D	WKU1JW	W		59968	9.600E+17	4.400E+09	533	-31.	95.	-15.	88.	15.	7.	0.096	1.300	0.009	0.012	0.370	0.880	0.083	0.450	0.080
A533B1	KU2	3D	WKU2JW	W		61223	1.100E+18	4.900E+09	533	-38.	86.	-4.	89.	34.	-3.	0.086	1.430	0.010	0.016	0.400	0.870	0.092	0.440	0.050
A5082	KWE	P	WKWE01	W	TL	97500	2.840E+19	8.090E+10	532	-69.	138.	180.	78.	248.	60.	0.120	1.370	0.016	0.011	0.200	0.724	0.090	0.480	0.218
A5082	KWE	R	WKWE01	W	TL	40556	1.900E+19	1.300E+11	532	-69.	138.	180.	85.	249.	53.	0.120	1.370	0.016	0.011	0.200	0.724	0.090	0.480	0.218
A5082	KWE	S	WKWE01	W	TL	142009	3.450E+19	-9.990E+02	532	-69.	138.	180.	68.	249.	70.	0.120	1.370	0.016	0.011	0.200	0.724	0.090	0.480	0.218
A5082	KWE	V	WKWE01	W	TL	11278	6.080E+18	1.500E+11	532	-69.	138.	126.	85.	194.	53.	0.120	1.370	0.016	0.011	0.200	0.724	0.090	0.480	0.218
A302B	LAC	1A	WLAC01	W	TL	12472	4.580E+18	1.020E+11	-999	-34.	55.	41.	95.	74.	-40.	0.100	1.390	0.016	0.006	0.430	0.120	0.030	0.550	0.180
A302B	LAC	1B	WLAC01	W	TL	12472	4.130E+18	9.200E+10	-999	-34.	55.	81.	52.	115.	3.	0.100	1.390	0.016	0.006	0.430	0.120	0.030	0.550	0.180
A302B	LAC	2A	WLAC01	W	TL	26912	1.100E+19	1.140E+11	-999	-34.	55.	59.	41.	93.	14.	0.100	1.390	0.016	0.006	0.430	0.120	0.030	0.550	0.180
A302B	LAC	3A	WLAC01	W	TL	49087	1.080E+19	6.150E+10	-999	-34.	55.	74.	-999.	108.	-999.	0.100	1.390	0.016	0.006	0.430	0.120	0.030	0.550	0.180
A302B	LAC	3B	WLAC01	W	TL	49087	1.080E+19	5.900E+10	-999	-34.	55.	77.	52.	110.	3.	0.100	1.390	0.016	0.006	0.430	0.120	0.030	0.550	0.180
A302B	LAC	7B	WLAC01	W	TL	26912	1.020E+19	1.050E+11	-999	-34.	55.	38.	43.	72.	13.	0.100	1.390	0.016	0.006	0.430	0.120	0.030	0.550	0.180
A302B	LAC	8A	WLAC01	W	TL	49087	1.080E+19	6.010E+10	-999	-34.	55.	76.	57.	109.	-2.	0.100	1.390	0.016	0.006	0.430	0.120	0.030	0.550	0.180
A302B	LAC	8B	WLAC01	W	TL	49087	1.080E+19	6.320E+10	-999	-34.	55.	66.	55.	100.	0.	0.100	1.390	0.016	0.006	0.430	0.120	0.030	0.550	0.180
A302B	LAC	9A	WLAC01	W	TL	26912	6.550E+18	6.760E+10	-999	-34.	55.	72.	-999.	106.	-999.	0.100	1.390	0.016	0.006	0.430	0.120	0.030	0.550	0.180
A302B	LAC	9B	WLAC01	W	TL	26912	6.640E+18	6.850E+10	-999	-34.	55.	-999.	68.	-999.	-13.	0.100	1.390	0.016	0.006	0.430	0.120	0.030	0.550	0.180
A533B1	LS1	300D	WLS1JW	W		56979	9.000E+16	4.400E+08	533	-69.	138.	-12.	108.	56.	30.	-999.000	1.490	0.016	-999.000	-999.000	0.780	0.080	0.520	0.210
A533B1	LS2	300D	WLS2JW	W	LT	61217	1.150E+17	5.220E+08	533	-60.	83.	-40.	87.	20.	-4.	-999.000	1.470	0.010	-999.000	0.370	0.890	0.080	0.470	0.040
A533B1	MC1	U	WMC101	W	TL	9556	4.430E+18	1.290E+11	558	-11.	113.	146.	80.	157.	33.	0.100	1.275	0.013	0.008	0.235	0.874	0.045	0.545	0.198
A533B1	MC1	X	WMC101	W	TL	37778	1.460E+19	1.070E+11	557	-11.	113.	155.	86.	167.	27.	0.100	1.275	0.013	0.008	0.235	0.874	0.045	0.545	0.198
A5082	MC2	U	WMC201	W	TL	53056	2.000E+19	1.050E+11	558	-52.	137.	-31.	137.	21.	0.	0.059	1.830	0.013	0.009	0.200	0.736	0.035	0.575	0.036
A5082	MC2	V	WMC201	W	TL	9000	3.330E+18	1.030E+11	558	-52.	137.	-13.	141.	39.	-4.	0.059	1.830	0.013	0.009	0.200	0.736	0.035	0.575	0.036
A5082	MC2	X	WMC201	W	TL	36389	1.460E+19	1.110E+11	558	-52.	137.	-19.	144.	33.	-6.	0.059	1.830	0.013	0.009	0.200	0.736	0.035	0.575	0.036
A302BM	ML1	210D	WML101	W	TS	78470	3.300E+17	1.150E+09	531	-42.	111.	-21.	110.	22.	0.	0.110	1.280	0.019	0.016	0.170	1.050	-999.000	0.550	0.200
A302BM	ML1	300D	WML101	W	TS	129823	6.600E+17	2.000E+09	531	-42.	111.	26.	92.	68.	19.	0.110	1.280	0.019	0.016	0.170	1.050	-999.000	0.550	0.200
A533B1	ML2	W104	WML201	W	TL	87149	8.840E+18	-9.990E+02	549	-34.	135.	25.	108.	59.	27.	0.120	1.104	0.013	0.015	0.247	0.059	0.040	0.536	0.279
A533B1	MY	A25	WMY_01	W	TL	7714	1.760E+19	-9.990E+02	522	-34.	110.	238.	58.	272.	51.	0.176	1.418	0.013	0.011	0.180	0.780	0.036	0.489	0.360
A533B1	MY	A35	WMY_01	W	TL	40167	7.130E+19	-9.990E+02	533	-34.	110.	311.	55.	345.	54.	0.176	1.418	0.013	0.011	0.180	0.780	0.036	0.489	0.360
A533B1	MY	W253	WMY_01	W	TL	102562	1.250E+19	3.410E+10	542	-34.	110.	221.	69.	255.	41.	0.176	1.418	0.013	0.011	0.180	0.780	0.036	0.489	0.360
A533B1	MY	W263	WMY_01	W	TL	40167	5.670E+18	-9.990E+02	533	-34.	110.	188.	64.	222.	46.	0.176	1.418	0.013	0.011	0.180	0.780	0.036	0.489	0.360
A5082	NA1	U	WNA101	W	TL	49722	8.720E+18	4.880E+10	553	-40.	98.	-13.	107.	27.	-9.	0.060	1.370	0.020	0.012	0.350	0.110	0.041	0.514	0.086
A5082	NA1	V	WNA101	W	TL	9444	2.630E+18	7.720E+10	550	-40.	98.	45.	96.	84.	2.	0.060	1.370	0.020	0.012	0.350	0.110	0.041	0.514	0.086
A5082	NA2	U	WNA201	W	TL	53333	9.800E+18	5.090E+10	554	-35.	110.	-23.	126.	13.	-16.	0.080	1.820	0.017	0.011	0.250	0.084	0.042	0.490	0.088
A5082	NA2	V	WNA201	W	TL	8722	2.460E+18	7.820E+10	550	-35.	110.	-20.	99.	15.	11.	0.080	1.820	0.017	0.011	0.250	0.084	0.042	0.490	0.088

Embrittlement Analysis Data Base

Material ID	Plant ID	Capsule	Heat ID	Product ID	Specimen Orientation	Irradiation time hr	Fluence n/cm^2	Flux n/cm^2/s	Tcoolant F	TTu30 F	USEu ft-lb	TTi30 F	USEi ft-lb	dTT30 F	dUSE ft-lb	C wt%	Mn wt%	P wt%	S wt%	Si wt%	Ni wt%	Cr wt%	Mo wt%	Cu wt%
A302B	OC1	A	WOC101	W	TL	38093	8.950E+18	6.530E+10	556	-9.	65.	163.	53.	172.	12.	0.079	1.482	0.018	0.011	0.564	0.590	0.069	0.444	0.320
A302B	OC1	C	WOC101	W	TL	51888	9.860E+18	5.270E+10	556	-9.	65.	180.	49.	189.	16.	0.079	1.482	0.018	0.011	0.564	0.590	0.069	0.444	0.320
A302B	OC1	E	WOC101	W	TL	14406	1.500E+18	-9.990E+02	556	-9.	65.	73.	56.	82.	10.	0.079	1.482	0.018	0.011	0.564	0.590	0.069	0.444	0.320
A5082	OC2	A	WOC201	W	TL	18672	3.370E+18	5.030E+10	556	5.	67.	111.	47.	107.	20.	0.088	1.565	0.021	0.007	0.605	0.580	0.090	0.360	0.360
A5082	OC2	C	WOC201	W	TL	10561	1.020E+18	-9.990E+02	556	5.	67.	51.	54.	46.	13.	0.088	1.565	0.021	0.007	0.605	0.580	0.090	0.360	0.360
A5082	OC2	E	WOC201	W	TL	55584	1.210E+19	6.030E+10	556	5.	67.	179.	44.	174.	23.	0.088	1.565	0.021	0.007	0.605	0.580	0.090	0.360	0.360
A5082	OC3	A	WOC301	W	TL	8286	8.050E+17	-9.990E+02	556	29.	65.	45.	63.	16.	3.	0.077	1.613	0.018	0.010	0.593	0.580	0.098	0.370	0.390
A5082	OC3	B	WOC301	W	TL	16392	3.120E+18	5.290E+10	556	29.	65.	98.	52.	70.	13.	0.077	1.613	0.018	0.010	0.593	0.580	0.098	0.370	0.390
A5082	OC3	D	WOC301	W	TL	68443	1.450E+19	5.950E+10	556	29.	65.	174.	43.	145.	22.	0.077	1.613	0.018	0.010	0.593	0.580	0.098	0.370	0.390
A302BM	PAL	A240	WPAL01	W	TL	19806	6.000E+19	-9.990E+02	524	-86.	118.	272.	51.	358.	67.	0.134	1.230	0.012	0.011	0.199	1.200	0.068	0.507	0.230
A302BM	PAL	T330	WPAL01	W	TL	43611	1.000E+13	-9.990E+02	-999	-86.	118.	-58.	137.	28.	-19.	0.134	1.230	0.012	0.011	0.199	1.200	0.068	0.507	0.230
A302BM	PAL	W110	WPAL01	W	TL	87167	1.779E+19	5.668E+10	533	-86.	118.	219.	65.	305.	53.	0.134	1.230	0.012	0.011	0.199	1.200	0.068	0.507	0.230
A302BM	PAL	W290	WPAL01	W	TL	43611	1.090E+19	6.940E+10	530	-86.	118.	199.	65.	285.	53.	0.134	1.230	0.012	0.011	0.199	1.200	0.068	0.507	0.230
A302B	PB1	R	WPB101	W	TL	44722	2.320E+19	1.470E+11	542	-42.	65.	112.	56.	154.	10.	0.090	1.575	0.019	0.024	0.490	0.570	0.140	0.385	0.220
A302B	PB1	S	WPB101	W	TL	31667	7.870E+18	7.000E+10	542	-42.	65.	123.	54.	165.	12.	0.090	1.575	0.019	0.024	0.490	0.570	0.140	0.385	0.220
A302B	PB1	T	WPB101	W	TL	81389	2.290E+19	8.100E+10	535	-42.	65.	137.	57.	179.	9.	0.090	1.575	0.019	0.024	0.490	0.570	0.140	0.385	0.220
A302B	PB1	V	WPB101	W	TL	13028	4.970E+18	1.120E+11	542	-42.	65.	54.	54.	108.	11.	0.090	1.575	0.019	0.024	0.490	0.570	0.140	0.385	0.220
A5082	PB2	R	WPB201	W	TL	45556	2.200E+19	1.540E+11	542	-10.	69.	214.	51.	223.	18.	0.079	1.400	0.014	0.013	0.550	0.590	0.070	0.390	0.250
A5082	PB2	S	WPB201	W	TL	129444	3.100E+19	8.060E+10	542	-10.	69.	215.	42.	224.	27.	0.079	1.400	0.014	0.013	0.550	0.590	0.070	0.390	0.250
A5082	PB2	T	WPB201	W	TL	30278	8.610E+18	9.220E+10	542	-10.	69.	145.	66.	154.	3.	0.079	1.400	0.014	0.013	0.550	0.590	0.070	0.390	0.250
A5082	PB2	V	WPB201	W	TL	13361	6.500E+18	1.220E+11	542	-10.	69.	157.	43.	167.	26.	0.079	1.400	0.014	0.013	0.550	0.590	0.070	0.390	0.250
A302BM	PH3	1	WPH301	W	LT	66359	1.600E+17	6.800E+08	528	3.	111.	17.	101.	14.	10.	-999.000	1.560	0.009	-999.000	0.190	0.407	-999.000	0.507	0.110
A5083	PI1	P	WPI101	W	TL	50278	1.460E+19	8.090E+10	527	-62.	80.	-22.	93.	40.	-13.	0.052	1.290	0.017	0.013	0.173	0.090	0.013	0.520	0.130
A5083	PI1	R	WPI101	W	TL	75000	3.950E+19	1.460E+11	527	-62.	80.	59.	83.	121.	-3.	0.052	1.290	0.017	0.013	0.173	0.090	0.013	0.520	0.130
A5083	PI1	V	WPI101	W	TL	11722	5.400E+18	1.280E+11	527	-62.	80.	-33.	96.	29.	-16.	0.052	1.290	0.017	0.013	0.173	0.090	0.013	0.520	0.130
A5083	PI2	R	WPI201	W	TL	77222	4.050E+19	1.460E+11	527	-74.	105.	24.	95.	98.	9.	0.046	1.280	0.019	0.014	0.445	0.071	0.015	0.505	0.082
A5083	PI2	T	WPI201	W	TL	36111	1.090E+19	8.380E+10	527	-74.	105.	-18.	93.	56.	11.	0.046	1.280	0.019	0.014	0.445	0.071	0.015	0.505	0.082
A5083	PI2	V	WPI201	W	TL	12222	5.780E+18	1.310E+11	527	-74.	105.	-6.	97.	67.	7.	0.046	1.280	0.019	0.014	0.445	0.071	0.015	0.505	0.082
A533B1	PL1	1	WPL101	W	TL	36582	2.300E+17	1.740E+09	529	-112.	114.	-83.	102.	29.	13.	0.122	1.122	0.014	0.009	0.245	0.794	0.099	0.618	0.161
A533B1	PV1	W137	WPV1JW	W		-999	3.450E+18	-9.990E+02	552	-53.	161.	-51.	163.	2.	-2.	-999.000	-999.000	-999.000	-999.000	-999.000	-999.000	-999.000	-999.000	-999.000
A533B1	PV2	W137	WPV201	W	TL	39806	4.071E+18	2.842E+10	552	-38.	113.	-42.	112.	-4.	1.	0.120	1.460	0.010	0.011	0.470	0.090	0.100	0.510	0.070
A302BM	QC1	1	WQC101	W	TL	10800	8.200E+18	2.110E+11	546	14.	103.	96.	86.	83.	17.	0.203	1.560	0.012	0.009	0.153	0.315	0.061	0.450	0.188
A302B	QC1	1	WQC102	W	TL	10800	8.200E+18	2.110E+11	546	-38.	70.	120.	46.	158.	25.	0.090	1.800	0.010	0.014	0.550	0.650	0.080	0.390	0.310
A302BM	QC1	2	WQC101	W	TL	10800	1.025E+16	2.635E+08	530	14.	103.	1.	102.	-12.	1.	0.203	1.560	0.012	0.009	0.153	0.315	0.061	0.450	0.188
A302BM	QC1	3	WQC101	W	TL	34528	3.675E+19	-9.990E+02	546	14.	103.	169.	83.	155.	20.	0.203	1.560	0.012	0.009	0.153	0.315	0.061	0.450	0.188
A302B	QC1	3	WQC102	W	TL	34806	2.470E+19	-9.990E+02	546	-38.	70.	224.	52.	262.	18.	0.090	1.800	0.010	0.014	0.550	0.650	0.080	0.390	0.310
A302BM	QC1	8	WQC101	W	TL	58206	5.500E+16	2.610E+08	530	14.	103.	-18.	90.	-32.	13.	0.203	1.560	0.012	0.009	0.153	0.315	0.061	0.450	0.188
A302BM	QC2	12	WQC201	W	TL	14316	9.750E+18	-9.990E+02	546	-26.	136.	67.	95.	93.	41.	0.202	1.750	0.009	0.016	0.145	0.338	0.087	0.501	0.158
A302B1	QC2	12	WQC202	W	TL	14316	9.750E+18	-9.990E+02	546	9.	91.	192.	-999.	182.	-999.	0.090	1.880	0.013	0.014	0.300	0.600	0.070	0.390	0.260
A302BM	QC2	13	WQC201	W	TL	14316	1.730E+16	-9.990E+02	530	-26.	136.	7.	107.	33.	29.	0.202	1.750	0.009	0.016	0.145	0.338	0.087	0.501	0.158
A302BM	QC2	18	WQC201	W	TL	49353	6.560E+16	3.690E+08	530	-26.	136.	6.	89.	32.	47.	0.202	1.750	0.009	0.016	0.145	0.338	0.087	0.501	0.158
A302BM	QC2	3	WQC201	W	TL	39500	3.940E+19	-9.990E+02	546	-26.	136.	124.	84.	150.	52.	0.202	1.750	0.009	0.016	0.145	0.338	0.087	0.501	0.158
A302B1	QC2	3	WQC202	W	TL	39500	2.520E+19	-9.990E+02	546	9.	91.	224.	42.	214.	49.	0.090	1.880	0.013	0.014	0.300	0.600	0.070	0.390	0.260
A5082	RI2	X	WRI201	W		15886	-9.990E+02	-9.990E+02	547	-55.	124.	-18.	120.	37.	4.	0.070	1.570	0.017	0.007	0.460	0.084	0.045	0.530	0.100
A533B1	RS1	B	WRS101	W	TL	13068	3.990E+18	8.470E+10	556	-20.	71.	95.	49.	114.	22.	0.085	1.492	0.016	0.014	0.496	0.590	0.063	0.388	0.280
A533B1	RS1	D	WRS101	W	TL	20172	6.600E+18	9.080E+10	556	-20.	71.	129.	52.	148.	19.	0.085	1.492	0.016	0.014	0.496	0.590	0.063	0.388	0.280
A533B1	RS1	F	WRS101	W	TL	42720	1.420E+19	9.240E+10	556	-20.	71.	145.	47.	164.	24.	0.085	1.492	0.016	0.014	0.496	0.590	0.063	0.388	0.280
A533B1	SA1	Y	WSA101	W	TL	31389	9.300E+18	8.260E+10	539	-150.	-999.	36.	83.	186.	-999.	0.150	1.210	0.019	0.015	0.165	1.260	0.040	0.510	0.160
A533B1	SA2	T	WSA201	W	TL	10444	2.750E+18	7.320E+10	539	-33.	112.	112.	-999.	145.	-999.	0.103	1.285	0.015	0.010	0.247	0.726	0.025	0.459	0.254
A533B1	SA2	U	WSA201	W	TL	23667	5.500E+18	6.450E+10	539	-33.	112.	147.	80.	180.	32.	0.103	1.285	0.015	0.010	0.247	0.726	0.025	0.459	0.254
A533B1	SA2	X	WSA201	W	TL	54444	1.070E+19	5.500E+10	539	-33.	112.	155.	-999.	188.	-999.	0.103	1.285	0.015	0.010	0.247	0.726	0.025	0.459	0.254
A533B1	SB1	U	WSB101	W	TL	8001	3.360E+18	1.170E+11	558	-64.	160.	-47.	147.	18.	13.	0.140	1.267	0.009	0.007	0.133	0.075	0.022	0.510	0.020
A533B1	SH1	30D	WSH101	W	TL	58531	1.400E+17	6.600E+08	528	-41.	109.	-16.	112.	25.	-3.	0.055	1.182	0.014	0.018	0.392	0.950	-999.000	0.532	0.025
A533B1	SH2	30D	WSH201	W	TL	54619	1.300E+17	6.700E+08	528	-7.	115.	-38.	122.	-31.	-7.	0.050	1.172	0.014	0.015	0.430	0.965	-999.000	0.532	0.025
A533B1	SL1	W104	WSL101	W	TL	83408	7.160E+18	2.380E+10	545	-55.	149.	11.	117.	66.	32.	0.120	1.069	0.015	0.012	0.205	0.061	0.060	0.530	0.247
A533B1	SL1	W97	WSL101	W	TL	40917	5.500E+18	-9.990E+02	541	-55.	149.	18.	101.	73.	48.	0.120	1.069	0.015	0.012	0.205	0.061	0.060	0.530	0.247
A533B1	SL2	W83	WSL201	W	TL	9773	1.600E+18	4.540E+10	548	-44.	115.	-33.	103.	11.	11.	0.160	1.525	0.005	0.012	0.375	0.067	0.056	0.555	0.048
A336	SMG	190D	WSMGJW	W		139116	1.260E+18	2.510E+09	528	-89.	112.	-4.	84.	86.	28.	0.070	1.430	0.016	-999.000	0.380	0.092	0.042	0.500	0.330
A302B	SO1	A	WSO101	W	TL	16278	1.750E+19	2.990E+11	-999	-23.	100.	62.	65.	85.	35.	-999.000	1.260	-999.000	-999.000	-999.000	0.080	-999.000	0.430	0.190
A302B	SO1	F	WSO101	W	TL	67500	3.850E+19	1.590E+11	-999	-23.	100.	114.	100.	137.	0.	-999.000	1.260	-999.000	-999.000	-999.000	0.080	-999.000	0.430	0.190
A533B1	SO2	W97	WSO201	W		23620	5.070E+18	5.960E+10	553	-58.	153.	-50.	144.	9.	9.	-999.000	1.400	0.003	-999.000	-999.000	0.133	0.107	0.514	0.028
A533B1	SO3	W97	WSO301	W	TL	37957	8.000E+18	5.860E+10	553	-28.	82.	2.	74.	30.	8.	0.116	1.478	0.010	0.008	0.379	0.094	0.058	0.552	0.032
A5082	SQ1	T	WSQ101	W	TL	9361	2.880E+18	8.540E+10	545	-80.	115.	47.	82.	128.	33.	0.058	1.400	0.021	0.009	0.420	0.125	0.068	0.530	0.370
A5082	SQ1	U	WSQ101	W	TL	25139	9.550E+18	1.060E+11	545	-80.	115.	65.	87.	145.	29.	0.058	1.400	0.021	0.009	0.420	0.125	0.068	0.530	0.370
A5082	SQ1	X	WSQ101	W	TL	46111	1.390E+19	8.340E+10	545	-80.	115.	77.	113.	157.	2.	0.058	1.400	0.021	0.009	0.420	0.125	0.068	0.530	0.370
A5082	SQ2	T	WSQ201	W	TL	9333	2.420E+18	7.190E+10	545	-82.	108.	-1.	116.	81.	-8.	0.095	1.500	0.016	0.013	0.410	0.110	0.085	0.530	0.130
A5082	SQ2	U	WSQ201	W	TL	25528	6.080E+18	6.610E+10	545	-82.	108.	72.	113.	154.	-4.	0.095	1.500	0.016	0.013	0.410	0.110	0.085	0.530	0.130
A5082	SQ2	X	WSQ201	W	TL	46944	1.030E+19	6.070E+10	545	-82.	108.	-53.	61.	30.	47.	0.095	1.500	0.016	0.013	0.410	0.110	0.085	0.530	0.130
A533B1	SR1	U	WSR101	W	TL	9583	6.120E+18	1.780E+11	557	-34.	95.	-15.	84.	18.	12.	0.040	1.230	0.006	0.006	0.410	0.958	0.068	0.480	0.024
A533B1	ST1	U	WST101	W	TL	6861	2.830E+18	1.140E+11	560	-54.	87.	-23.	87.	31.	0.	0.120	1.360	0.009	0.010	0.420	0.090	0.020	0.530	0.020
A533B1	ST2	V	WST2JW	W		7889	2.540E+18	8.970E+10	560	-15.	99.	-23.	99.	-8.	1.	-999.000	-999.000	0.010	-999.000	-999.000	0.150	-999.000	-999.000	0.010
A533B1	SU1	T	WSU101	W	TL	9389	2.820E+18	8.340E+10	534	-25.	74.	146.	55.	171.	19.	0.125	1.497	0.011	0.015	0.443	0.680	0.078	0.428	0.350
A533B1	SU1	V	WSU101	W	TL	70278	1.970E+19	7.790E+10	538	-25.	74.	225.	51.	250.	23.	0.125	1.497	0.011	0.015	0.443	0.680	0.078	0.428	0.350
A533B1	SU2	V	WSU201	W	TL	73333	1.750E+19	6.640E+10	540	-20.	85.	121.	66.	141.	19.	0.093	1.535	0.018	0.014	0.454	0.560	0.108	0.410	0.190
A533B1	SU2	X	WSU201	W	TL	10250	2.940E+18	7.970E+10	535	-20.	85.	75.	73.	95.	12.	0.093	1.535	0.018	0.014	0.454	0.560	0.108	0.410	0.190
A302B	TM1	C	WTM101	W	TL	38371	8.660E+18	6.260E+10	556	-25.	83.	140.	50.	165.	32.	0.089	1.560	0.017	0.013	0.455	0.680	0.100	0.365	0.330
A302B	TM1	E	WTM101	W	TL	11211	1.090E+18	-9.990E+02	556	-25.	83.	50.	64.	75.	19.	0.089	1.560	0.017	0.013	0.455	0.680	0.100	0.365	0.330
A5082	TM2	T1	WTM2J1	W		-999	8.300E+18	-9.990E+02	556	-25.	84.	201.	54.	226.	29.	0.090	1.530	0.013	0.017	0.530	0.700	0.080	0.420	0.380
A5082	TM2	T1	WTM2J2	W		-999	9.680E+18	-9.990E+02	556	15.	75.	262.	51.	247.	24.	0.090	1.580	0.015	0.016	0.540	0.670	0.090	0.420	0.400
A5082	TM2	T1	WTM2J3	W		-999	5.850E+18	-9.990E+02	556	44.	59.	166.	45.	122.	14.	0.090	1.630	0.018	0.009	0.540	0.590	0.110	0.400	0.400
A5082	TP3	T	WTP301	W	TL	10056	7.390E+18	2.040E+11	547	0.	69.	166.	67.	166.	1.	0.078	1.410	0.011	0.013	0.625	0.570	0.150	0.400	0.310
A5082	TP3	V	WTP301	W	TL	70556	1.530E+19	6.000E+10	547	0.	69.	180.	48.	180.	20.	0.078	1.410	0.011	0.013	0.625	0.570	0.150	0.400	0.310

Embrittlement Analysis Data Base

Material ID	Plant ID	Capsule	Heat ID	Product ID	Specimen Orientation	Irradiation time hr	Fluence n/cm^2	Flux n/cm^2/s	Tcoolant F	TTu30 F	USEu ft-lb	TTi30 F	USEi ft-lb	dTT30 F	dUSE ft-lb	C wt%	Mn wt%	P wt%	S wt%	Si wt%	Ni wt%	Cr wt%	Mo wt%	Cu wt%
A5082	TP4	T	WTP401	W		10278	7.080E+18	1.920E+11	547	-4.	66.	207.	46.	211.	20.	0.098	1.440	0.014	0.011	0.500	0.600	0.140	0.360	0.300
A533B1	TRO	U	WTRO01	W	TL	10139	4.110E+18	1.130E+11	554	-10.	83.	22.	89.	33.	-6.	0.185	1.390	0.020	0.013	0.445	0.957	0.074	0.505	0.055
A533B1	TRO	V	WTRO01	W	TL	70278	2.340E+19	9.250E+10	554	-10.	83.	32.	68.	42.	15.	0.185	1.390	0.020	0.013	0.445	0.957	0.074	0.505	0.055
A533B1	TRO	X	WTRO01	W	TL	38333	1.770E+19	1.290E+11	554	-10.	83.	37.	87.	47.	-3.	0.185	1.390	0.020	0.013	0.445	0.957	0.074	0.505	0.055
A533B1	VO1	Y	WVO101	W	TL	40556	1.310E+19	8.930E+10	560	-49.	145.	-28.	129.	21.	16.	0.133	1.130	0.012	0.010	0.153	0.102	0.051	0.562	0.040
A533B1	VO2	JW	WVO201	W	TL	-999	1.130E+19	-9.990E+02	-999	-19.	91.	-32.	96.	-13.	-6.	0.083	1.210	0.010	0.011	0.471	0.131	0.064	0.506	0.043
A533B1	VO2	JW	WVO201	W	TL	-999	1.130E+19	-9.990E+02	-999	-19.	91.	0.	84.	19.	7.	0.083	1.210	0.010	0.011	0.471	0.131	0.064	0.506	0.043
A533B1	VS1	U	WVS101	W	TL	9861	6.550E+18	1.850E+11	555	-53.	93.	-31.	91.	23.	2.	0.085	1.410	0.009	0.009	0.450	0.950	0.130	0.475	0.040
A533B1	VS1	V	WVS101	W	TL	25639	1.550E+19	1.680E+11	555	-53.	93.	-6.	87.	47.	6.	0.085	1.410	0.009	0.009	0.450	0.950	0.130	0.475	0.040
A533B1	VS1	X	WVS101	W	TL	44167	2.620E+19	1.650E+11	555	-53.	93.	-30.	84.	23.	9.	0.085	1.410	0.009	0.009	0.450	0.950	0.130	0.475	0.040
A533B1	VY	30D	WVY_01	W	TL	66120	4.300E+16	1.804E+08	527	-56.	123.	-46.	122.	10.	1.	-999.000	-999.000	0.013	-999.000	-999.000	0.941	-999.000	-999.000	0.026
A533B1	WC1	U	WWC101	W	TL	9417	3.530E+18	1.040E+11	560	-55.	99.	-31.	92.	24.	8.	0.110	1.460	0.005	0.011	0.480	0.090	0.090	0.560	0.040
A533B1	WC1	Y	WWC101	W	TL	41944	1.270E+19	8.360E+10	561	-55.	99.	-12.	94.	43.	5.	0.110	1.460	0.005	0.011	0.480	0.090	0.090	0.560	0.040
A533B1	WF3	W97	WWF301	W		38921	6.470E+18	4.620E+10	553	-81.	156.	8.	125.	88.	31.	0.230	1.350	0.008	0.006	0.160	0.220	0.050	0.570	0.040
A533B1	ZN1	T	WZN101	W	TL	10667	3.100E+18	8.460E+10	529	5.	65.	113.	56.	108.	8.	0.100	1.500	0.020	0.011	0.688	0.570	0.077	0.385	0.280
A533B1	ZN1	U	WZN101	W	TL	31389	1.020E+19	8.550E+10	529	5.	65.	194.	52.	190.	12.	0.100	1.500	0.020	0.011	0.688	0.570	0.077	0.385	0.280
A533B1	ZN1	X	WZN101	W	TL	45278	1.260E+19	8.170E+10	529	5.	65.	199.	48.	194.	16.	0.100	1.500	0.020	0.011	0.688	0.570	0.077	0.385	0.280
A533B1	ZN1	Y	WZN101	W	TL	75278	1.560E+19	6.560E+10	529	5.	65.	205.	46.	200.	18.	0.100	1.500	0.020	0.011	0.688	0.570	0.077	0.385	0.280
A533B1	ZN2	T	WZN201	W	LT	31389	7.790E+18	7.450E+10	528	-23.	69.	151.	42.	174.	27.	0.087	1.581	0.019	0.010	0.460	0.550	0.075	0.389	0.260
A533B1	ZN2	U	WZN201	W	LT	11583	2.700E+18	6.760E+10	528	-23.	69.	115.	49.	138.	19.	0.087	1.581	0.019	0.010	0.460	0.550	0.075	0.389	0.260
A533B1	ZN2	Y	WZN201	W	LT	80556	1.460E+19	5.750E+10	528	-23.	69.	202.	55.	225.	14.	0.087	1.581	0.019	0.010	0.460	0.550	0.075	0.389	0.260

Embrittlement Analysis Data Base

Material ID	Plant ID	Capsule	Heat ID	Product ID	Specimen Orientation	Reactor Type	Vessel Manufacturer	Plant Designer	Weld Wire Heat	Weld Flux
A5082	AD1	V	FAD101	F	LT	PWR	Babcock & Wilcox	Westinghouse/EBE		
A5082	AD1	V	FAD101	F	TL	PWR	Babcock & Wilcox	Westinghouse/EBE		
A533B1	AN1	A	PAN101	P	LT	PWR	Babcock & Wilcox	Babcock & Wilcox		
A533B1	AN1	A	PAN101	P	TL	PWR	Babcock & Wilcox	Babcock & Wilcox		
A533B1	AN1	A	SHSS02	SRM	LT	PWR	Babcock & Wilcox	Babcock & Wilcox		
A533B1	AN1	B	PAN102	P	LT	PWR	Babcock & Wilcox	Babcock & Wilcox		
A533B1	AN1	B	PAN102	P	TL	PWR	Babcock & Wilcox	Babcock & Wilcox		
A533B1	AN1	B	SHSS02	SRM	LT	PWR	Babcock & Wilcox	Babcock & Wilcox		
A533B1	AN1	C	PAN101	P	LT	PWR	Babcock & Wilcox	Babcock & Wilcox		
A533B1	AN1	C	PAN101	P	TL	PWR	Babcock & Wilcox	Babcock & Wilcox		
A533B1	AN1	C	SHSS02	SRM	LT	PWR	Babcock & Wilcox	Babcock & Wilcox		
A533B1	AN1	E	PAN101	P	LT	PWR	Babcock & Wilcox	Babcock & Wilcox		
A533B1	AN1	E	PAN101	P	TL	PWR	Babcock & Wilcox	Babcock & Wilcox		
A533B1	AN1	E	SHSS02	SRM	LT	PWR	Babcock & Wilcox	Babcock & Wilcox		
A533B1	AN2	W97	PAN201	P	LT	PWR	Combustion Engineering	Combustion Engineering		
A533B1	AN2	W97	PAN201	P	TL	PWR	Combustion Engineering	Combustion Engineering		
A5083	BD1	U	FBD1JW	F	LT	PWR		Westinghouse		
A5083	BD1	U	FBD1JW	F	TL	PWR		Westinghouse		
A5083	BD1	X	FBD1JW	F	LT	PWR		Westinghouse		
A5083	BD1	X	FBD1JW	F	TL	PWR		Westinghouse		
A5083	BD2	U	FBD201	F	LT	PWR		Westinghouse		
A5083	BD2	U	FBD201	F	TL	PWR		Westinghouse		
A5083	BD2	X	FBD201	F	LT	PWR		Westinghouse		
A5083	BD2	X	FBD201	F	TL	PWR		Westinghouse		
A302BM	BF2	30D	PBF2JW	P	LT	BWR	Babcock & Wilcox/IHI	General Electric		
A302B	BR	119	PBR_01	P	TL	BWa	Combustion Engineering	General Electric		
A302B	BR	122	PBR_01	P	TL	BWa	Combustion Engineering	General Electric		
A302B	BR	124	PBR_01	P	TL	BWa	Combustion Engineering	General Electric		
A302B	BR	125	PBR_01	P	TL	BWa	Combustion Engineering	General Electric		
A302B	BR	127	PBR_01	P	TL	BWa	Combustion Engineering	General Electric		
A533B1	BV1	U	PBV101	P	LT	PWR	Combustion Engineering	Westinghouse		
A533B1	BV1	U	PBV101	P	TL	PWR	Combustion Engineering	Westinghouse		
A533B1	BV1	V	PBV101	P	LT	PWR	Combustion Engineering	Westinghouse		
A533B1	BV1	V	PBV101	P	TL	PWR	Combustion Engineering	Westinghouse		
A533B1	BV1	W	PBV101	P	LT	PWR	Combustion Engineering	Westinghouse		
A533B1	BV1	W	PBV101	P	TL	PWR	Combustion Engineering	Westinghouse		
A5082	BY1	U	FBY101	F	LT	PWR		Westinghouse		
A5082	BY1	U	FBY101	F	TL	PWR		Westinghouse		
A5082	BY1	X	FBY101	F	LT	PWR		Westinghouse		
A5082	BY1	X	FBY101	F	TL	PWR		Westinghouse		
A5083	BY2	U	FBY201	F	LT	PWR		Westinghouse		
A5083	BY2	U	FBY201	F	TL	PWR		Westinghouse		
A5083	BY2	W	FBY201	F	LT	PWR		Westinghouse		
A5083	BY2	W	FBY201	F	TL	PWR		Westinghouse		
A302B	BZ1	R	SASTM	SRM	LT	PWR	Societe des Forges et Ateliers du Creusot	Westinghouse		
A302B	BZ1	V	SASTM	SRM	LT	PWR	Societe des Forges et Ateliers du Creusot	Westinghouse		
A533B1	CAB	K	PCAB01	P	LT	PWR	Combustion Engineering	Westinghouse		
A302B	CAB	K	SASTM	SRM	LT	PWR	Combustion Engineering	Westinghouse		
A533B1	CAB	N	PCAB01	P	LT	PWR	Combustion Engineering	Westinghouse		
A302B	CAB	N	SASTM	SRM	LT	PWR	Combustion Engineering	Westinghouse		
A533B1	CAB	P	PCAB01	P	LT	PWR	Combustion Engineering	Westinghouse		
A533B1	CAB	P	PCAB02	P	LT	PWR	Combustion Engineering	Westinghouse		
A302B	CAB	P	SASTM	SRM	LT	PWR	Combustion Engineering	Westinghouse		
A5082	CB1	Y	FCB101	F	LT	PWR	Rotterdamse Droogdok Madtdschappij (Netherlands)	Westinghouse		
A5082	CB1	Y	FCB101	F	TL	PWR	Rotterdamse Droogdok Madtdschappij (Netherlands)	Westinghouse		
A5082	CB1	Z	FCB101	F	LT	PWR	Rotterdamse Droogdok Madtdschappij (Netherlands)	Westinghouse		
A5082	CB1	Z	FCB101	F	TL	PWR	Rotterdamse Droogdok Madtdschappij (Netherlands)	Westinghouse		
A533B1	CB2	X	PCB201	P	LT	PWR		Westinghouse		
A533B1	CB2	X	PCB201	P	TL	PWR		Westinghouse		
A533B1	CB2	Z	PCB201	P	LT	PWR		Westinghouse		
A533B1	CB2	Z	PCB201	P	TL	PWR		Westinghouse		
A533B1	CC1	W263	PCC103	P	LT	PWR	Combustion Engineering	Combustion Engineering		
A533B1	CC1	W263	SHSS01	SRM	LT	PWR	Combustion Engineering	Combustion Engineering		
A533B1	CC1	W97	PCC103	P	LT	PWR	Combustion Engineering	Combustion Engineering		
A533B1	CC1	W97	PCC103	P	TL	PWR	Combustion Engineering	Combustion Engineering		
A533B1	CC2	W263	PCC202	P	LT	PWR	Combustion Engineering	Combustion Engineering		
A533B1	CC2	W263	SHSS01	SRM	LT	PWR	Combustion Engineering	Combustion Engineering		
A533B1	CC2	W97	PCC202	P	LT	PWR	Combustion Engineering	Combustion Engineering		
A533B1	CC2	W97	PCC202	P	TL	PWR	Combustion Engineering	Combustion Engineering		
A533B1	CH1	30D	PCH1JW	P	LT	BWR		General Electric		
A533B1	CK1	T	PCK101	P	LT	PWR	Combustion Engineering	Westinghouse		
A533B1	CK1	T	PCK101	P	TL	PWR	Combustion Engineering	Westinghouse		
A533B1	CK1	T	SHSS02	SRM	LT	PWR	Combustion Engineering	Westinghouse		
A533B1	CK1	U	PCK101	P	LT	PWR	Combustion Engineering	Westinghouse		
A533B1	CK1	U	PCK101	P	TL	PWR	Combustion Engineering	Westinghouse		
A533B1	CK1	U	SHSS02	SRM	LT	PWR	Combustion Engineering	Westinghouse		
A533B1	CK1	X	PCK101	P	LT	PWR	Combustion Engineering	Westinghouse		
A533B1	CK1	X	PCK101	P	TL	PWR	Combustion Engineering	Westinghouse		
A533B1	CK1	X	SHSS02	SRM	LT	PWR	Combustion Engineering	Westinghouse		
A533B1	CK1	Y	PCK101	P	LT	PWR	Combustion Engineering	Westinghouse		
A533B1	CK1	Y	PCK101	P	TL	PWR	Combustion Engineering	Westinghouse		
A533B1	CK1	Y	SHSS02	SRM	LT	PWR	Combustion Engineering	Westinghouse		

Material ID	Plant ID	Capsule	Heat ID	Product ID	Specimen Orientation	Reactor Type	Vessel Manufacturer	Plant Designer	Weld Wire Heat	Weld Flux
A533B1	CK2	T	PCK201	P	LT	PWR	Chicago Bridge and Iron	Westinghouse		
A533B1	CK2	T	PCK201	P	TL	PWR	Chicago Bridge and Iron	Westinghouse		
A533B1	CK2	U	PCK201	P	LT	PWR	Chicago Bridge and Iron	Westinghouse		
A533B1	CK2	U	PCK201	P	TL	PWR	Chicago Bridge and Iron	Westinghouse		
A533B1	CK2	X	PCK201	P	LT	PWR	Chicago Bridge and Iron	Westinghouse		
A533B1	CK2	X	PCK201	P	TL	PWR	Chicago Bridge and Iron	Westinghouse		
A533B1	CK2	Y	PCK201	P	LT	PWR	Chicago Bridge and Iron	Westinghouse		
A533B1	CK2	Y	PCK201	P	TL	PWR	Chicago Bridge and Iron	Westinghouse		
A533B1	CL1	U	PCL101	P	LT	PWR	Combustion Engineering	Westinghouse		
A533B1	CL1	U	PCL101	P	TL	PWR	Combustion Engineering	Westinghouse		
A533B1	CL1	Y	PCL101	P	LT	PWR	Combustion Engineering	Westinghouse		
A533B1	CL1	Y	PCL101	P	TL	PWR	Combustion Engineering	Westinghouse		
A533B1	COF	3D	PCOFJW	P	TL	BWR		General Electric		
A533B1	CP1	U	PCP1JW	P	LT	PWR		Westinghouse Corporation		
A533B1	CP1	U	PCP1JW	P	TL	PWR		Westinghouse Corporation		
A533B1	CP2	U	PCP201	P	LT	PWR		Westinghouse Corporation		
A533B1	CP2	U	PCP201	P	TL	PWR		Westinghouse Corporation		
A533B1	CPR	30D	PCPR01	P	LT	BWR	Combustion Engineering	General Electric		
A533B1	CPR	300D	PCPR01	P	LT	BWR	Combustion Engineering	General Electric		
A533B1	CR3	B	PCR301	P	TL	PWR	Babcock & Wilcox	Babcock & Wilcox		
A533B1	CR3	C	PCR301	P	TL	PWR	Babcock & Wilcox	Babcock & Wilcox		
A533B1	CR3	C	SHSS02	SRM	LT	PWR	Babcock & Wilcox	Babcock & Wilcox		
A533B1	CR3	D	PCR301	P	TL	PWR	Babcock & Wilcox	Babcock & Wilcox		
A533B1	CR3	F	PCR301	P	TL	PWR	Babcock & Wilcox	Babcock & Wilcox		
A302B	CTY	A	PCTY02	P	LT	PWR	Combustion Engineering	Westinghouse		
A302B	CTY	A	SASTM	SRM	LT	PWR	Combustion Engineering	Westinghouse		
A302B	CTY	D	PCTY04	P	LT	PWR	Combustion Engineering	Westinghouse		
A302B	CTY	D	SASTM	SRM	LT	PWR	Combustion Engineering	Westinghouse		
A302B	CTY	F	PCTY02	P	LT	PWR	Combustion Engineering	Westinghouse		
A302B	CTY	F	PCTY04	P	LT	PWR	Combustion Engineering	Westinghouse		
A302B	CTY	F	PCTY07	P	LT	PWR	Combustion Engineering	Westinghouse		
A302B	CTY	F	SASTM	SRM	LT	PWR	Combustion Engineering	Westinghouse		
A302B	CTY	H	PCTY02	P	LT	PWR	Combustion Engineering	Westinghouse		
A302B	CTY	H	PCTY04	P	LT	PWR	Combustion Engineering	Westinghouse		
A302B	CTY	H	PCTY07	P	LT	PWR	Combustion Engineering	Westinghouse		
A302B	CTY	H	SASTM	SRM	LT	PWR	Combustion Engineering	Westinghouse		
A533B1	DAC	1	PDAC01	P	LT	BWR	Chicago Bridge and Iron	General Electric		
A5082	DB1	A	FDB101	F	TL	PWR	Babcock & Wilcox	Babcock & Wilcox		
A5082	DB1	A	FDB102	F	TL	PWR	Babcock & Wilcox	Babcock & Wilcox		
A533B1	DB1	A	SHSS02	SRM	LT	PWR	Babcock & Wilcox	Babcock & Wilcox		
A5082	DB1	B	FDB102	F	TL	PWR	Babcock & Wilcox	Babcock & Wilcox		
A5082	DB1	D	FDB102	F	TL	PWR	Babcock & Wilcox	Babcock & Wilcox		
A5082	DB1	F	FDB102	F	TL	PWR	Babcock & Wilcox	Babcock & Wilcox		
A533B1	DC1	S	PDC103	P	LT	PWR	Combustion Engineering	Westinghouse		
A533B1	DC1	S	SHSS02	SRM	LT	PWR	Combustion Engineering	Westinghouse		
A533B1	DC1	Y	PDC103	P	LT	PWR	Combustion Engineering	Westinghouse		
A533B1	DC1	Y	SHSS02	SRM	LT	PWR	Combustion Engineering	Westinghouse		
A533B1	DC2	U	PDC201	P	LT	PWR	Combustion Engineering	Westinghouse		
A533B1	DC2	U	PDC201	P	TL	PWR	Combustion Engineering	Westinghouse		
A533B1	DC2	X	PDC201	P	LT	PWR	Combustion Engineering	Westinghouse		
A533B1	DC2	X	PDC201	P	TL	PWR	Combustion Engineering	Westinghouse		
A533B1	DC2	Y	PDC201	P	LT	PWR	Combustion Engineering	Westinghouse		
A533B1	DC2	Y	PDC201	P	TL	PWR	Combustion Engineering	Westinghouse		
A302BM	DR2	2	PDR201	P	LT	BWb	Babcock and Wilcox	General Electric		
A302BM	DR2	3	PDR201	P	LT	BWb	Babcock and Wilcox	General Electric		
A302BM	DR2	4	PDR201	P	LT	BWb	Babcock and Wilcox	General Electric		
A302BM	DR2	5	PDR201	P	LT	BWb	Babcock and Wilcox	General Electric		
A302BM	DR2	8	PDR201	P	LT	BWR	Babcock and Wilcox	General Electric		
A302BM	DR3	12	PDR301	P	LT	BWb	Babcock and Wilcox	General Electric		
A302BM	DR3	13	PDR301	P	LT	BWR	Babcock and Wilcox	General Electric		
A302BM	DR3	14	PDR301	P	LT	BWb	Babcock and Wilcox	General Electric		
A302BM	DR3	18	PDR301	P	LT	BWR	Babcock and Wilcox	General Electric		
A302BM	DR3	4	PDR301	P	LT	BWb	Babcock and Wilcox	General Electric		
A302BM	DR3	6	PDR301	P	LT	BWR	Babcock and Wilcox	General Electric		
A533B1	FA1	U	PFA101	P	LT	PWR	Combustion Engineering	Westinghouse		
A533B1	FA1	U	PFA101	P	TL	PWR	Combustion Engineering	Westinghouse		
A533B1	FA1	W	PFA101	P	LT	PWR	Combustion Engineering	Westinghouse		
A533B1	FA1	W	PFA101	P	TL	PWR	Combustion Engineering	Westinghouse		
A533B1	FA1	X	PFA101	P	LT	PWR	Combustion Engineering	Westinghouse		
A533B1	FA1	X	PFA101	P	TL	PWR	Combustion Engineering	Westinghouse		
A533B1	FA1	Y	PFA101	P	LT	PWR	Combustion Engineering	Westinghouse		
A533B1	FA1	Y	PFA101	P	TL	PWR	Combustion Engineering	Westinghouse		
A533B1	FA2	U	PFA201	P	LT	PWR	Combustion Engineering	Westinghouse		
A533B1	FA2	U	PFA201	P	TL	PWR	Combustion Engineering	Westinghouse		
A533B1	FA2	W	PFA201	P	LT	PWR	Combustion Engineering	Westinghouse		
A533B1	FA2	W	PFA201	P	TL	PWR	Combustion Engineering	Westinghouse		
A533B1	FA2	X	PFA201	P	LT	PWR	Combustion Engineering	Westinghouse		
A533B1	FA2	X	PFA201	P	TL	PWR	Combustion Engineering	Westinghouse		
A533B1	FC1	W225	PFC101	P	LT	PWR	Combustion Engineering	Combustion Engineering		
A533B1	FC1	W225	SHSS01	SRM	LT	PWR	Combustion Engineering	Combustion Engineering		
A533B1	FC1	W265	PFC101	P	LT	PWR	Combustion Engineering	Combustion Engineering		
A533B1	FC1	W265	PFC101	P	TL	PWR	Combustion Engineering	Combustion Engineering		

Embrittlement Analysis Data Base

Material ID	Plant ID	Capsule	Heat ID	Product ID	Specimen Orientation	Reactor Type	Vessel Manufacturer	Plant Designer	Weld Wire Heat	Weld Flux
A533B1	FC1	W275	PFC101	P	LT	PWR	Combustion Engineering	Combustion Engineering		
A533B1	FC1	W275	PFC101	P	TL	PWR	Combustion Engineering	Combustion Engineering		
A533B1	FC1	W275	SHSS01	SRM	LT	PWR	Combustion Engineering	Combustion Engineering		
A533B1	FTZ	30D	PFTZ01	P	LT	BWR	Combustion Engineering	General Electric		
A5082	GIN	R	FGIN01	F	LT	PWR	Babcock & Wilcox	Westinghouse		
A5082	GIN	R	FGIN02	F	LT	PWR	Babcock & Wilcox	Westinghouse		
A302B	GIN	R	SASTM	SRM	LT	PWR	Babcock & Wilcox	Westinghouse		
A5082	GIN	S	FGIN01	F	LT	PWR	Babcock & Wilcox	Westinghouse		
A5082	GIN	S	FGIN02	F	LT	PWR	Babcock & Wilcox	Westinghouse		
A5082	GIN	T	FGIN01	F	LT	PWR	Babcock & Wilcox	Westinghouse		
A5082	GIN	T	FGIN02	F	LT	PWR	Babcock & Wilcox	Westinghouse		
A302B	GIN	T	SASTM	SRM	LT	PWR	Babcock & Wilcox	Westinghouse		
A5082	GIN	V	FGIN01	F	LT	PWR	Babcock & Wilcox	Westinghouse		
A5082	GIN	V	FGIN02	F	LT	PWR	Babcock & Wilcox	Westinghouse		
A302B	GIN	V	SASTM	SRM	LT	PWR	Babcock & Wilcox	Westinghouse		
A533B1	HA1	30D	PHA101	P	LT	BWR	Combustion Engineering	General Electric		
A533B1	HA2	30D	PHA2JW	P	LT	BWR	Combustion Engineering	General Electric		
A302B	HB2	S	PHB201	P	LT	PWR	Combustion Engineering	Westinghouse		
A302B	HB2	S	PHB202	P	LT	PWR	Combustion Engineering	Westinghouse		
A302B	HB2	S	PHB203	P	LT	PWR	Combustion Engineering	Westinghouse		
A302B	HB2	S	SASTM	SRM	TL	PWR	Combustion Engineering	Westinghouse		
A302B	HB2	T	PHB203	P	LT	PWR	Combustion Engineering	Westinghouse		
A302B	HB2	T	SASTM	SRM	TL	PWR	Combustion Engineering	Westinghouse		
A302B	HB2	V	PHB202	P	LT	PWR	Combustion Engineering	Westinghouse		
A302B	HB2	V	SASTM	SRM	TL	PWR	Combustion Engineering	Westinghouse		
A302B	HM3	01	SHM3	SRM	LT	BWa	Combustion Engineering	General Electric		
A302B	HM3	4	SHM3	SRM	LT	BWa	Combustion Engineering	General Electric		
A533B1	HOP	30D	PHOPJW	P	LT	BWR		General Electric		
A302B	IP2	T	PIP201	P	LT	PWR	Combustion Engineering	Westinghouse		
A302B	IP2	T	PIP202	P	LT	PWR	Combustion Engineering	Westinghouse		
A302B	IP2	T	PIP203	P	LT	PWR	Combustion Engineering	Westinghouse		
A302B	IP2	T	SASTM	SRM	LT	PWR	Combustion Engineering	Westinghouse		
A302B	IP2	V	PIP202	P	LT	PWR	Combustion Engineering	Westinghouse		
A302B	IP2	V	SASTM	SRM	LT	PWR	Combustion Engineering	Westinghouse		
A302B	IP2	Y	PIP203	P	LT	PWR	Combustion Engineering	Westinghouse		
A302B	IP2	Y	SASTM	SRM	LT	PWR	Combustion Engineering	Westinghouse		
A302B	IP2	Z	PIP201	P	LT	PWR	Combustion Engineering	Westinghouse		
A302B	IP2	Z	PIP202	P	LT	PWR	Combustion Engineering	Westinghouse		
A302B	IP2	Z	PIP203	P	LT	PWR	Combustion Engineering	Westinghouse		
A302B	IP2	Z	SASTM	SRM	LT	PWR	Combustion Engineering	Westinghouse		
A302BM	IP3	T	PIP301	P	LT	PWR	Combustion Engineering	Westinghouse		
A302BM	IP3	T	PIP304	P	LT	PWR	Combustion Engineering	Westinghouse		
A302BM	IP3	T	PIP304	P	TL	PWR	Combustion Engineering	Westinghouse		
A302BM	IP3	Y	PIP304	P	TL	PWR	Combustion Engineering	Westinghouse		
A533B1	IP3	Y	SHSS02	SRM	LT	PWR	Combustion Engineering	Westinghouse		
A302BM	IP3	Z	PIP303	P	LT	PWR	Combustion Engineering	Westinghouse		
A302BM	IP3	Z	PIP304	P	LT	PWR	Combustion Engineering	Westinghouse		
A302BM	IP3	Z	PIP304	P	TL	PWR	Combustion Engineering	Westinghouse		
A533B1	KU1	177D	PKU1JW	P	TL	BWR		General Electric		
A533B1	KU2	3D	PKU2JW	P	TL	BWR		General Electric		
A5082	KWE	P	FKWE01	F	LT	PWR	Combustion Engineering	Westinghouse		
A5082	KWE	P	FKWE02	F	LT	PWR	Combustion Engineering	Westinghouse		
A533B1	KWE	P	SHSS02	SRM	LT	PWR	Combustion Engineering	Westinghouse		
A5082	KWE	R	FKWE01	F	LT	PWR	Combustion Engineering	Westinghouse		
A5082	KWE	R	FKWE02	F	LT	PWR	Combustion Engineering	Westinghouse		
A533B1	KWE	R	SHSS02	SRM	LT	PWR	Combustion Engineering	Westinghouse		
A5082	KWE	S	FKWE01	F	LT	PWR	Combustion Engineering	Westinghouse		
A5082	KWE	S	FKWE02	F	LT	PWR	Combustion Engineering	Westinghouse		
A533B1	KWE	S	SHSS02	SRM	LT	PWR	Combustion Engineering	Westinghouse		
A5082	KWE	V	FKWE01	F	LT	PWR	Combustion Engineering	Westinghouse		
A5082	KWE	V	FKWE02	F	LT	PWR	Combustion Engineering	Westinghouse		
A533B1	KWE	V	SHSS02	SRM	LT	PWR	Combustion Engineering	Westinghouse		
A302B	LAC	1A	PLAC02	P	LT	BWa	Combustion Engineering	Allis-Chalmers		
A302B	LAC	1A	SLAC01	SRM	LT	BWa	Combustion Engineering	Allis-Chalmers		
A302B	LAC	1B	PLAC02	P	LT	BWa	Combustion Engineering	Allis-Chalmers		
A302B	LAC	1B	PLAC03	P	LT	BWa	Combustion Engineering	Allis-Chalmers		
A302B	LAC	1B	SLAC01	SRM	LT	BWa	Combustion Engineering	Allis-Chalmers		
A302B	LAC	2A	PLAC02	P	LT	BWa	Combustion Engineering	Allis-Chalmers		
A302B	LAC	2A	SLAC01	SRM	LT	BWa	Combustion Engineering	Allis-Chalmers		
A302B	LAC	3A	PLAC02	P	LT	BWa	Combustion Engineering	Allis-Chalmers		
A302B	LAC	3A	SLAC01	SRM	LT	BWa	Combustion Engineering	Allis-Chalmers		
A302B	LAC	3B	PLAC02	P	LT	BWa	Combustion Engineering	Allis-Chalmers		
A302B	LAC	3B	PLAC03	P	LT	BWa	Combustion Engineering	Allis-Chalmers		
A302B	LAC	3B	SLAC01	SRM	LT	BWa	Combustion Engineering	Allis-Chalmers		
A302B	LAC	7B	PLAC02	P	LT	BWa	Combustion Engineering	Allis-Chalmers		
A302B	LAC	7B	PLAC03	P	LT	BWa	Combustion Engineering	Allis-Chalmers		
A302B	LAC	7B	SLAC01	SRM	LT	BWa	Combustion Engineering	Allis-Chalmers		
A302B	LAC	8A	PLAC02	P	LT	BWa	Combustion Engineering	Allis-Chalmers		
A302B	LAC	8A	SLAC01	SRM	LT	BWa	Combustion Engineering	Allis-Chalmers		
A302B	LAC	8B	PLAC02	P	LT	BWa	Combustion Engineering	Allis-Chalmers		
A302B	LAC	8B	PLAC03	P	LT	BWa	Combustion Engineering	Allis-Chalmers		
A302B	LAC	8B	SLAC01	SRM	LT	BWa	Combustion Engineering	Allis-Chalmers		

Material ID	Plant ID	Capsule	Heat ID	Product ID	Specimen Orientation	Reactor Type	Vessel Manufacturer	Plant Designer	Weld Wire Heat	Weld Flux
A302B	LAC	9A	PLAC02	P	LT	BWa	Combustion Engineering	Allis-Chalmers		
A302B	LAC	9A	SLAC01	SRM	LT	BWa	Combustion Engineering	Allis-Chalmers		
A302B	LAC	9B	PLAC02	P	LT	BWa	Combustion Engineering	Allis-Chalmers		
A302B	LAC	9B	PLAC03	P	LT	BWa	Combustion Engineering	Allis-Chalmers		
A302B	LAC	9B	SLAC01	SRM	LT	BWa	Combustion Engineering	Allis-Chalmers		
A533B1	LS1	300D	PLS1JW	P	LT	BWR		General Electric		
A533B1	MC1	U	PMC101	P	LT	PWR	Combustion Engineering	Westinghouse		
A533B1	MC1	U	PMC101	P	TL	PWR	Combustion Engineering	Westinghouse		
A533B1	MC1	X	PMC101	P	LT	PWR	Combustion Engineering	Westinghouse		
A533B1	MC1	X	PMC101	P	TL	PWR	Combustion Engineering	Westinghouse		
A5082	MC2	U	FMC201	F	LT	PWR	Rotterdamse Droogdok Madtdschappij (Netherlands)	Westinghouse		
A5082	MC2	U	FMC201	F	TL	PWR	Rotterdamse Droogdok Madtdschappij (Netherlands)	Westinghouse		
A5082	MC2	V	FMC201	F	LT	PWR	Rotterdamse Droogdok Madtdschappij (Netherlands)	Westinghouse		
A5082	MC2	V	FMC201	F	TL	PWR	Rotterdamse Droogdok Madtdschappij (Netherlands)	Westinghouse		
A5082	MC2	X	FMC201	F	LT	PWR	Rotterdamse Droogdok Madtdschappij (Netherlands)	Westinghouse		
A5082	MC2	X	FMC201	F	TL	PWR	Rotterdamse Droogdok Madtdschappij (Netherlands)	Westinghouse		
A302BM	ML1	210D	PML101	P	LT	BWR	Combustion Engineering	General Electric		
A302BM	ML1	300D	PML101	P	LT	BWR	Combustion Engineering	General Electric		
A533B1	ML2	W104	PML201	P	LT	PWR	Combustion Engineering	Combustion Engineering		
A533B1	ML2	W104	SHSS01	SRM	LT	PWR	Combustion Engineering	Combustion Engineering		
A533B1	ML2	W97	PML201	P	LT	PWR	Combustion Engineering	Combustion Engineering		
A533B1	ML2	W97	PML201	P	TL	PWR	Combustion Engineering	Combustion Engineering		
A533B1	MY	A25	PMY_01	P	LT	PWR	Combustion Engineering	Combustion Engineering		
A533B1	MY	A25	SHSS01	SRM	LT	PWR	Combustion Engineering	Combustion Engineering		
A533B1	MY	A35	PMY_01	P	LT	PWR	Combustion Engineering	Combustion Engineering		
A533B1	MY	A35	PMY_01	P	TL	PWR	Combustion Engineering	Combustion Engineering		
A533B1	MY	W253	PMY_01	P	LT	PWR	Combustion Engineering	Combustion Engineering		
A533B1	MY	W253	SHSS01	SRM	LT	PWR	Combustion Engineering	Combustion Engineering		
A533B1	MY	W263	PMY_01	P	LT	PWR	Combustion Engineering	Combustion Engineering		
A533B1	MY	W263	PMY_01	P	TL	PWR	Combustion Engineering	Combustion Engineering		
A5082	NA1	U	FNA101	F	LT	PWR	Rotterdamse Droogdok Madtdschappij (Netherlands)	Westinghouse		
A5082	NA1	U	FNA101	F	TL	PWR	Rotterdamse Droogdok Madtdschappij (Netherlands)	Westinghouse		
A5082	NA1	V	FNA101	F	LT	PWR	Rotterdamse Droogdok Madtdschappij (Netherlands)	Westinghouse		
A5082	NA1	V	FNA101	F	TL	PWR	Rotterdamse Droogdok Madtdschappij (Netherlands)	Westinghouse		
A5082	NA2	U	FNA201	F	LT	PWR	Rotterdamse Droogdok Madtdschappij (Netherlands)	Westinghouse		
A5082	NA2	U	FNA201	F	TL	PWR	Rotterdamse Droogdok Madtdschappij (Netherlands)	Westinghouse		
A5082	NA2	V	FNA201	F	LT	PWR	Rotterdamse Droogdok Madtdschappij (Netherlands)	Westinghouse		
A5082	NA2	V	FNA201	F	TL	PWR	Rotterdamse Droogdok Madtdschappij (Netherlands)	Westinghouse		
A302B	OC1	A	POC102	P	LT	PWR	Babcock & Wilcox	Babcock & Wilcox		
A302B	OC1	A	POC102	P	TL	PWR	Babcock & Wilcox	Babcock & Wilcox		
A533B1	OC1	A	SHSS02	SRM	LT	PWR	Babcock & Wilcox	Babcock & Wilcox		
A302B	OC1	C	POC102	P	LT	PWR	Babcock & Wilcox	Babcock & Wilcox		
A302B	OC1	C	POC102	P	TL	PWR	Babcock & Wilcox	Babcock & Wilcox		
A533B1	OC1	C	SHSS02	SRM	LT	PWR	Babcock & Wilcox	Babcock & Wilcox		
A302B	OC1	E	POC102	P	LT	PWR	Babcock & Wilcox	Babcock & Wilcox		
A302B	OC1	E	POC102	P	TL	PWR	Babcock & Wilcox	Babcock & Wilcox		
A533B1	OC1	E	SHSS02	SRM	LT	PWR	Babcock & Wilcox	Babcock & Wilcox		
A302B	OC1	F	POC101	P	LT	PWR	Babcock & Wilcox	Babcock & Wilcox		
A302B	OC1	F	POC101	P	TL	PWR	Babcock & Wilcox	Babcock & Wilcox		
A533B1	OC1	F	SHSS02	SRM	LT	PWR	Babcock & Wilcox	Babcock & Wilcox		
A5082	OC2	A	FOC201	F	LT	PWR	Babcock & Wilcox	Babcock & Wilcox		
A5082	OC2	A	FOC201	F	TL	PWR	Babcock & Wilcox	Babcock & Wilcox		
A533B1	OC2	A	SHSS02	SRM	LT	PWR	Babcock & Wilcox	Babcock & Wilcox		
A5082	OC2	C	FOC201	F	LT	PWR	Babcock & Wilcox	Babcock & Wilcox		
A5082	OC2	C	FOC201	F	TL	PWR	Babcock & Wilcox	Babcock & Wilcox		
A533B1	OC2	C	SHSS02	SRM	LT	PWR	Babcock & Wilcox	Babcock & Wilcox		
A5082	OC2	E	FOC201	F	LT	PWR	Babcock & Wilcox	Babcock & Wilcox		
A5082	OC2	E	FOC201	F	TL	PWR	Babcock & Wilcox	Babcock & Wilcox		
A533B1	OC2	E	SHSS02	SRM	LT	PWR	Babcock & Wilcox	Babcock & Wilcox		
A5082	OC3	A	FOC301	F	LT	PWR	Babcock & Wilcox	Babcock & Wilcox		
A5082	OC3	A	FOC301	F	TL	PWR	Babcock & Wilcox	Babcock & Wilcox		
A5082	OC3	A	FOC302	F	TL	PWR	Babcock & Wilcox	Babcock & Wilcox		
A5082	OC3	B	FOC301	F	TL	PWR	Babcock & Wilcox	Babcock & Wilcox		
A5082	OC3	B	FOC302	F	TL	PWR	Babcock & Wilcox	Babcock & Wilcox		
A533B1	OC3	B	SHSS02	SRM	LT	PWR	Babcock & Wilcox	Babcock & Wilcox		
A5082	OC3	D	FOC301	F	TL	PWR	Babcock & Wilcox	Babcock & Wilcox		
A5082	OC3	D	FOC302	F	TL	PWR	Babcock & Wilcox	Babcock & Wilcox		
A533B1	OC3	D	SHSS02	SRM	LT	PWR	Babcock & Wilcox	Babcock & Wilcox		
A302B1	OYS	210D	POYS01	P	LT	BWR	Combustion Engineering	General Electric		
A302BM	PAL	A240	PPAL01	P	LT	PWR	Combustion Engineering	Combustion Engineering		
A302BM	PAL	A240	PPAL01	P	TL	PWR	Combustion Engineering	Combustion Engineering		
A302BM	PAL	T330	PPAL01	P	LT	PWR	Combustion Engineering	Combustion Engineering		
A302BM	PAL	T330	PPAL01	P	TL	PWR	Combustion Engineering	Combustion Engineering		
A302BM	PAL	W110	PPAL01	P	LT	PWR	Combustion Engineering	Combustion Engineering		
A533B1	PAL	W110	SHSS01	SRM	LT	PWR	Combustion Engineering	Combustion Engineering		
A302BM	PAL	W290	PPAL01	P	LT	PWR	Combustion Engineering	Combustion Engineering		
A302BM	PAL	W290	PPAL01	P	TL	PWR	Combustion Engineering	Combustion Engineering		
A302B	PB1	R	PPB101	P	LT	PWR	Babcock & Wilcox	Westinghouse		
A302B	PB1	R	PPB102	P	LT	PWR	Babcock & Wilcox	Westinghouse		
A302B	PB1	R	SASTM	SRM	LT	PWR	Babcock & Wilcox	Westinghouse		
A302B	PB1	S	PPB101	P	LT	PWR	Babcock & Wilcox	Westinghouse		
A302B	PB1	S	PPB102	P	LT	PWR	Babcock & Wilcox	Westinghouse		

Embrittlement Analysis Data Base

Material ID	Plant ID	Capsule	Heat ID	Product ID	Specimen Orientation	Reactor Type	Vessel Manufacturer	Plant Designer	Weld Wire Heat	Weld Flux
A302B	PB1	S	SASTM	SRM	LT	PWR	Babcock & Wilcox	Westinghouse		
A302B	PB1	T	PPB101	P	LT	PWR	Babcock & Wilcox	Westinghouse		
A302B	PB1	T	PPB102	P	LT	PWR	Babcock & Wilcox	Westinghouse		
A302B	PB1	T	SASTM	SRM	LT	PWR	Babcock & Wilcox	Westinghouse		
A302B	PB1	V	PPB101	P	LT	PWR	Babcock & Wilcox	Westinghouse		
A302B	PB1	V	PPB102	P	LT	PWR	Babcock & Wilcox	Westinghouse		
A302B	PB1	V	SASTM	SRM	LT	PWR	Babcock & Wilcox	Westinghouse		
A5082	PB2	R	FPB201	F	LT	PWR	Combustion Engineering	Westinghouse		
A5082	PB2	R	FPB202	F	LT	PWR	Combustion Engineering	Westinghouse		
A533B1	PB2	R	SHSS02	SRM	LT	PWR	Combustion Engineering	Westinghouse		
A5082	PB2	S	FPB201	F	LT	PWR	Combustion Engineering	Westinghouse		
A5082	PB2	S	FPB202	F	LT	PWR	Combustion Engineering	Westinghouse		
A533B1	PB2	S	SHSS02	SRM	LT	PWR	Combustion Engineering	Westinghouse		
A5082	PB2	T	FPB201	F	LT	PWR	Combustion Engineering	Westinghouse		
A5082	PB2	T	FPB202	F	LT	PWR	Combustion Engineering	Westinghouse		
A533B1	PB2	T	SHSS02	SRM	LT	PWR	Combustion Engineering	Westinghouse		
A5082	PB2	V	FPB201	F	LT	PWR	Combustion Engineering	Westinghouse		
A5082	PB2	V	FPB202	F	LT	PWR	Combustion Engineering	Westinghouse		
A533B1	PB2	V	SHSS02	SRM	LT	PWR	Combustion Engineering	Westinghouse		
A302BM	PH3	1	PPH301	P	LT	BWR	Babcock & Wilcox/Chicago Bridge & Iron Company	General Electric		
A5083	PI1	P	FPI101	F	LT	PWR	Societe des Forges et Ateliers du Creusot	Westinghouse		
A5083	PI1	P	FPI101	F	TL	PWR	Societe des Forges et Ateliers du Creusot	Westinghouse		
A533B1	PI1	P	SHSS02	SRM	LT	PWR	Societe des Forges et Ateliers du Creusot	Westinghouse		
A5083	PI1	R	FPI101	F	LT	PWR	Societe des Forges et Ateliers du Creusot	Westinghouse		
A5083	PI1	R	FPI101	F	TL	PWR	Societe des Forges et Ateliers du Creusot	Westinghouse		
A533B1	PI1	R	SHSS02	SRM	LT	PWR	Societe des Forges et Ateliers du Creusot	Westinghouse		
A5083	PI1	V	FPI101	F	LT	PWR	Societe des Forges et Ateliers du Creusot	Westinghouse		
A5083	PI1	V	FPI101	F	TL	PWR	Societe des Forges et Ateliers du Creusot	Westinghouse		
A533B1	PI1	V	SHSS02	SRM	LT	PWR	Societe des Forges et Ateliers du Creusot	Westinghouse		
A5083	PI2	R	FPI201	F	LT	PWR	Societe des Forges et Ateliers du Creusot	Westinghouse		
A5083	PI2	R	FPI201	F	TL	PWR	Societe des Forges et Ateliers du Creusot	Westinghouse		
A533B1	PI2	R	SHSS02	SRM	LT	PWR	Societe des Forges et Ateliers du Creusot	Westinghouse		
A5083	PI2	T	FPI201	F	LT	PWR	Societe des Forges et Ateliers du Creusot	Westinghouse		
A5083	PI2	T	FPI201	F	TL	PWR	Societe des Forges et Ateliers du Creusot	Westinghouse		
A533B1	PI2	T	SHSS02	SRM	LT	PWR	Societe des Forges et Ateliers du Creusot	Westinghouse		
A5083	PI2	V	FPI201	F	LT	PWR	Societe des Forges et Ateliers du Creusot	Westinghouse		
A5083	PI2	V	FPI201	F	TL	PWR	Societe des Forges et Ateliers du Creusot	Westinghouse		
A533B1	PI2	V	SHSS02	SRM	LT	PWR	Societe des Forges et Ateliers du Creusot	Westinghouse		
A533B1	PL1	1	PPL101	P	LT	BWR	Combustion Engineering	General Electric		
A533B1	PV1	W137	PPV1J2	P	LT	PWR		Combustion Engineering		
A533B1	PV1	W137	PPV1J2	P	TL	PWR		Combustion Engineering		
A533B1	PV1	W137	SHSS01	SRM	LT	PWR		Combustion Engineering		
A533B1	PV2	W137	PPV201	P	LT	PWR		Combustion Engineering		
A533B1	PV2	W137	PPV201	P	TL	PWR		Combustion Engineering		
A533B1	PV2	W137	SHSS01	SRM	LT	PWR		Combustion Engineering		
	PV3	W137	PPV3JW	P	TL	PWR		Combustion Engineering		
A302BM	QC1	1	PQC101	P	LT	BWb	Babcock and Wilcox	General Electric		
A302BM	QC1	2	PQC101	P	LT	BWR	Babcock and Wilcox	General Electric		
A302BM	QC1	3	PQC101	P	LT	BWb	Babcock and Wilcox	General Electric		
A302BM	QC1	8	PQC101	P	LT	BWR	Babcock and Wilcox	General Electric		
A302BM	QC2	12	PQC201	P	LT	BWb	Babcock and Wilcox/Chicago Bridge and Iron	General Electric		
A302BM	QC2	13	PQC201	P	LT	BWR	Babcock and Wilcox/Chicago Bridge and Iron	General Electric		
A302BM	QC2	18	PQC201	P	LT	BWR	Babcock and Wilcox/Chicago Bridge and Iron	General Electric		
A302BM	QC2	3	PQC201	P	LT	BWb	Babcock and Wilcox/Chicago Bridge and Iron	General Electric		
A5082	RI2	X	FRI201	F	LT	PWR	Rotterdamse Droogdok Madtdschappij (Netherlands)	Westinghouse		
A5082	RI2	X	FRI201	F	TL	PWR	Rotterdamse Droogdok Madtdschappij (Netherlands)	Westinghouse		
A533B1	RS1	B	PRS101	P	TL	PWR	Babcock & Wilcox	Babcock & Wilcox		
A533B1	RS1	D	PRS101	P	TL	PWR	Babcock & Wilcox	Babcock & Wilcox		
A533B1	RS1	F	PRS101	P	TL	PWR	Babcock & Wilcox	Babcock & Wilcox		
A533B1	SA1	T	PSA101	P	LT	PWR	Combustion Engineering	Westinghouse		
A533B1	SA1	T	PSA102	P	LT	PWR	Combustion Engineering	Westinghouse		
A533B1	SA1	T	PSA103	P	LT	PWR	Combustion Engineering	Westinghouse		
A533B1	SA1	T	SHSS02	SRM	LT	PWR	Combustion Engineering	Westinghouse		
A533B1	SA1	Y	PSA103	P	LT	PWR	Combustion Engineering	Westinghouse		
A533B1	SA1	Y	SHSS02	SRM	LT	PWR	Combustion Engineering	Westinghouse		
A533B1	SA1	Z	PSA101	P	LT	PWR	Combustion Engineering	Westinghouse		
A533B1	SA1	Z	PSA102	P	LT	PWR	Combustion Engineering	Westinghouse		
A533B1	SA1	Z	PSA103	P	LT	PWR	Combustion Engineering	Westinghouse		
A533B1	SA1	Z	SHSS02	SRM	LT	PWR	Combustion Engineering	Westinghouse		
A533B1	SA2	T	PSA201	P	LT	PWR	Combustion Engineering	Westinghouse		
A533B1	SA2	T	PSA201	P	TL	PWR	Combustion Engineering	Westinghouse		
A533B1	SA2	U	PSA201	P	LT	PWR	Combustion Engineering	Westinghouse		
A533B1	SA2	U	PSA201	P	TL	PWR	Combustion Engineering	Westinghouse		
A533B1	SA2	X	PSA201	P	LT	PWR	Combustion Engineering	Westinghouse		
A533B1	SA2	X	PSA201	P	TL	PWR	Combustion Engineering	Westinghouse		
A533B1	SB1	U	PSB101	P	LT	PWR	Westinghouse	Westinghouse		
A533B1	SB1	U	PSB101	P	TL	PWR	Westinghouse	Westinghouse		
A533B1	SH1	30D	PSH101	P	LT	BWR	Chicago Bridge and Iron	General Electric		
A533B1	SH2	30D	PSH201	P	LT	BWR	Chicago Bridge and Iron	General Electric		
A533B1	SL1	W104	PSL101	P	LT	PWR	Combustion Engineering	Combustion Engineering		
A533B1	SL1	W104	SHSS01	SRM	LT	PWR	Combustion Engineering	Combustion Engineering		
A533B1	SL1	W97	PSL101	P	LT	PWR	Combustion Engineering	Combustion Engineering		

Material ID	Plant ID	Capsule	Heat ID	Product ID	Specimen Orientation	Reactor Type	Vessel Manufacturer	Plant Designer	Weld Wire Heat	Weld Flux
A533B1	SL1	W97	PSL101	P	TL	PWR	Combustion Engineering	Combustion Engineering		
A533B1	SL2	W83	PSL201	P	LT	PWR	Combustion Engineering	Combustion Engineering		
A533B1	SL2	W83	PSL201	P	TL	PWR	Combustion Engineering	Combustion Engineering		
A336	SMG	190D	FSMGJW	F	LT	BWR		General Electric		
A302B	SO1	A	PSO103	P	LT	PWR	Combustion Engineering	Westinghouse		
A302B	SO1	A	SASTM	SRM	LT	PWR	Combustion Engineering	Westinghouse		
A302B	SO1	D	PSO101	P	LT	PWR	Combustion Engineering	Westinghouse		
A302B	SO1	D	PSO102	P	LT	PWR	Combustion Engineering	Westinghouse		
A302B	SO1	D	PSO103	P	LT	PWR	Combustion Engineering	Westinghouse		
A302B	SO1	D	SASTM	SRM	LT	PWR	Combustion Engineering	Westinghouse		
A302B	SO1	F	PSO102	P	LT	PWR	Combustion Engineering	Westinghouse		
A302B	SO1	F	SASTM	SRM	LT	PWR	Combustion Engineering	Westinghouse		
	SO2	W97	PSO2JW	P	LT	PWR	Combustion Engineering	Combustion Engineering		
	SO2	W97	PSO2JW	P	TL	PWR	Combustion Engineering	Combustion Engineering		
A533B1	SO3	W97	PSO301	P	LT	PWR	Combustion Engineering	Combustion Engineering		
A533B1	SO3	W97	PSO301	P	TL	PWR	Combustion Engineering	Combustion Engineering		
A5082	SQ1	T	FSQ101	F	LT	PWR	Rotterdamse Droogdok Madtdschappij (Netherlands)	Westinghouse		
A5082	SQ1	T	FSQ101	F	TL	PWR	Rotterdamse Droogdok Madtdschappij (Netherlands)	Westinghouse		
A5082	SQ1	U	FSQ101	F	LT	PWR	Rotterdamse Droogdok Madtdschappij (Netherlands)	Westinghouse		
A5082	SQ1	U	FSQ101	F	TL	PWR	Rotterdamse Droogdok Madtdschappij (Netherlands)	Westinghouse		
A5082	SQ1	X	FSQ101	F	LT	PWR	Rotterdamse Droogdok Madtdschappij (Netherlands)	Westinghouse		
A5082	SQ1	X	FSQ101	F	TL	PWR	Rotterdamse Droogdok Madtdschappij (Netherlands)	Westinghouse		
A5082	SQ2	T	FSQ201	F	LT	PWR	Rotterdamse Droogdok Madtdschappij (Netherlands)	Westinghouse		
A5082	SQ2	T	FSQ201	F	TL	PWR	Rotterdamse Droogdok Madtdschappij (Netherlands)	Westinghouse		
A5082	SQ2	U	FSQ201	F	LT	PWR	Rotterdamse Droogdok Madtdschappij (Netherlands)	Westinghouse		
A5082	SQ2	U	FSQ201	F	TL	PWR	Rotterdamse Droogdok Madtdschappij (Netherlands)	Westinghouse		
A5082	SQ2	X	FSQ201	F	LT	PWR	Rotterdamse Droogdok Madtdschappij (Netherlands)	Westinghouse		
A5082	SQ2	X	FSQ201	F	TL	PWR	Rotterdamse Droogdok Madtdschappij (Netherlands)	Westinghouse		
A533B1	SR1	U	PSR101	P	LT	PWR		Westinghouse		
A533B1	SR1	U	PSR101	P	TL	PWR		Westinghouse		
A533B1	SR1	V	PSR101	P	LT	PWR		Westinghouse		
A533B1	SR1	V	PSR101	P	TL	PWR		Westinghouse		
A533B1	ST1	U	PST101	P	LT	PWR		Westinghouse		
A533B1	ST1	U	PST101	P	TL	PWR		Westinghouse		
A533B1	ST2	V	PST2JW	P	LT	PWR		Westinghouse		
A533B1	ST2	V	PST2JW	P	TL	PWR		Westinghouse		
A533B1	SU1	T	PSU101	P	LT	PWR	Rotterdamse Droogdok Madtdschappij (Netherlands)	Westinghouse		
A533B1	SU1	T	SHSS02	SRM	LT	PWR	Rotterdamse Droogdok Madtdschappij (Netherlands)	Westinghouse		
A533B1	SU1	V	PSU101	P	LT	PWR	Rotterdamse Droogdok Madtdschappij (Netherlands)	Westinghouse		
A533B1	SU1	V	SHSS02	SRM	LT	PWR	Rotterdamse Droogdok Madtdschappij (Netherlands)	Westinghouse		
A533B1	SU2	V	PSU201	P	LT	PWR	Rotterdamse Droogdok Madtdschappij (Netherlands)	Westinghouse		
A533B1	SU2	V	PSU201	P	TL	PWR	Rotterdamse Droogdok Madtdschappij (Netherlands)	Westinghouse		
A533B1	SU2	V	SHSS02	SRM	LT	PWR	Rotterdamse Droogdok Madtdschappij (Netherlands)	Westinghouse		
A533B1	SU2	X	PSU201	P	LT	PWR	Rotterdamse Droogdok Madtdschappij (Netherlands)	Westinghouse		
A533B1	SU2	X	PSU201	P	TL	PWR	Rotterdamse Droogdok Madtdschappij (Netherlands)	Westinghouse		
A533B1	SU2	X	SHSS02	SRM	LT	PWR	Rotterdamse Droogdok Madtdschappij (Netherlands)	Westinghouse		
A302B	TM1	C	PTM101	P	LT	PWR	Babcock & Wilcox	Babcock & Wilcox		
A302B	TM1	C	PTM101	P	TL	PWR	Babcock & Wilcox	Babcock & Wilcox		
A533B1	TM1	C	SHSS02	SRM	LT	PWR	Babcock & Wilcox	Babcock & Wilcox		
A302B	TM1	E	PTM101	P	LT	PWR	Babcock & Wilcox	Babcock & Wilcox		
A302B	TM1	E	PTM101	P	TL	PWR	Babcock & Wilcox	Babcock & Wilcox		
A533B1	TM1	E	SHSS02	SRM	LT	PWR	Babcock & Wilcox	Babcock & Wilcox		
A5082	TP3	S	FTP301	F	LT	PWR	Babcock & Wilcox	Westinghouse		
A5082	TP3	S	FTP302	F	LT	PWR	Babcock & Wilcox	Westinghouse		
A302B	TP3	S	SASTM	SRM	LT	PWR	Babcock & Wilcox	Westinghouse		
A5082	TP3	T	FTP301	F	LT	PWR	Babcock & Wilcox	Westinghouse		
A302B	TP3	T	SASTM	SRM	LT	PWR	Babcock & Wilcox	Westinghouse		
A5082	TP3	V	FTP302	F	LT	PWR	Babcock & Wilcox	Westinghouse		
A302B	TP3	V	SASTM	SRM	LT	PWR	Babcock & Wilcox	Westinghouse		
A5082	TP4	S	FTP401	F	LT	PWR	Babcock & Wilcox	Westinghouse		
A5082	TP4	S	FTP402	F	LT	PWR	Babcock & Wilcox	Westinghouse		
A533B1	TP4	S	SHSS02	SRM	LT	PWR	Babcock & Wilcox	Westinghouse		
A5082	TP4	T	FTP401	F	LT	PWR	Babcock & Wilcox	Westinghouse		
A533B1	TP4	T	SHSS02	SRM	LT	PWR	Babcock & Wilcox	Westinghouse		
A533B1	TRO	U	PTRO01	P	LT	PWR	Chicago Bridge and Iron	Westinghouse		
A533B1	TRO	U	PTRO01	P	TL	PWR	Chicago Bridge and Iron	Westinghouse		
A533B1	TRO	V	PTRO01	P	LT	PWR	Chicago Bridge and Iron	Westinghouse		
A533B1	TRO	V	PTRO01	P	TL	PWR	Chicago Bridge and Iron	Westinghouse		
A533B1	TRO	X	PTRO01	P	LT	PWR	Chicago Bridge and Iron	Westinghouse		
A533B1	TRO	X	PTRO01	P	TL	PWR	Chicago Bridge and Iron	Westinghouse		
A533B1	VO1	Y	PVO101	P	LT	PWR		Westinghouse		
A533B1	VO1	Y	PVO101	P	TL	PWR		Westinghouse		
A533B1	VO2	JW	PVO201	P	LT	PWR		Westinghouse		
A533B1	VO2	JW	PVO201	P	TL	PWR		Westinghouse		
A533B1	VO2	U	PVO201	P	LT	PWR		Westinghouse		
A533B1	VO2	U	PVO201	P	TL	PWR		Westinghouse		
A533B1	VS1	U	PVS101	P	LT	PWR	Chicago Bridge and Iron	Westinghouse		
A533B1	VS1	U	PVS101	P	TL	PWR	Chicago Bridge and Iron	Westinghouse		
A533B1	VS1	V	PVS101	P	LT	PWR	Chicago Bridge and Iron	Westinghouse		
A533B1	VS1	V	PVS101	P	TL	PWR	Chicago Bridge and Iron	Westinghouse		
A533B1	VS1	X	PVS101	P	LT	PWR	Chicago Bridge and Iron	Westinghouse		
A533B1	VS1	X	PVS101	P	TL	PWR	Chicago Bridge and Iron	Westinghouse		

Embrittlement Analysis Data Base

Material ID	Plant ID	Capsule	Heat ID	Product ID	Specimen Orientation	Reactor Type	Vessel Manufacturer	Plant Designer	Weld Wire Heat	Weld Flux
A533B1	VY	30D	PVY_01	P	LT	BWR	Chicago Bridge and Iron	General Electric		
A533B1	WC1	U	PWC101	P	LT	PWR	Combustion Engineering	Westinghouse		
A533B1	WC1	U	PWC101	P	TL	PWR	Combustion Engineering	Westinghouse		
A533B1	WC1	Y	PWC101	P	LT	PWR	Combustion Engineering	Westinghouse		
A533B1	WC1	Y	PWC101	P	TL	PWR	Combustion Engineering	Westinghouse		
A533B1	WF3	W97	PWF301	P	LT	PWR	Combustion Engineering	Combustion Engineering		
A533B1	WF3	W97	PWF301	P	TL	PWR	Combustion Engineering	Combustion Engineering		
A533B1	ZN1	T	PZN101	P	LT	PWR	Babcock & Wilcox	Westinghouse		
A533B1	ZN1	T	PZN101	P	TL	PWR	Babcock & Wilcox	Westinghouse		
A533B1	ZN1	T	SHSS02	SRM	LT	PWR	Babcock & Wilcox	Westinghouse		
A533B1	ZN1	U	PZN101	P	LT	PWR	Babcock & Wilcox	Westinghouse		
A533B1	ZN1	U	PZN101	P	TL	PWR	Babcock & Wilcox	Westinghouse		
A533B1	ZN1	U	SHSS02	SRM	LT	PWR	Babcock & Wilcox	Westinghouse		
A533B1	ZN1	X	PZN101	P	LT	PWR	Babcock & Wilcox	Westinghouse		
A533B1	ZN1	X	PZN101	P	TL	PWR	Babcock & Wilcox	Westinghouse		
A533B1	ZN1	X	SHSS02	SRM	LT	PWR	Babcock & Wilcox	Westinghouse		
A533B1	ZN1	Y	PZN101	P	LT	PWR	Babcock & Wilcox	Westinghouse		
A533B1	ZN1	Y	PZN101	P	TL	PWR	Babcock & Wilcox	Westinghouse		
A533B1	ZN1	Y	SHSS02	SRM	LT	PWR	Babcock & Wilcox	Westinghouse		
A533B1	ZN2	T	PZN201	P	LT	PWR	Babcock & Wilcox	Westinghouse		
A533B1	ZN2	T	PZN201	P	TL	PWR	Babcock & Wilcox	Westinghouse		
A533B1	ZN2	T	SHSS02	SRM	LT	PWR	Babcock & Wilcox	Westinghouse		
A533B1	ZN2	U	PZN201	P	LT	PWR	Babcock & Wilcox	Westinghouse		
A533B1	ZN2	U	PZN201	P	TL	PWR	Babcock & Wilcox	Westinghouse		
A533B1	ZN2	U	SHSS02	SRM	LT	PWR	Babcock & Wilcox	Westinghouse		
A533B1	ZN2	Y	PZN201	P	LT	PWR	Babcock & Wilcox	Westinghouse		
A533B1	ZN2	Y	PZN201	P	TL	PWR	Babcock & Wilcox	Westinghouse		
A533B1	ZN2	Y	SHSS02	SRM	LT	PWR	Babcock & Wilcox	Westinghouse		
A5082	AD1	V	WAD101	W	TL	PWR	Babcock & Wilcox	Westinghouse/EBE	82912	L0091
A533B1	AN1	A	WAN101	W	TL	PWR	Babcock & Wilcox	Babcock & Wilcox	406L44	L80
A533B1	AN1	C	WAN101	W	TL	PWR	Babcock & Wilcox	Babcock & Wilcox	406L44	L80
A533B1	AN1	E	WAN101	W	TL	PWR	Babcock & Wilcox	Babcock & Wilcox	406L44	L80
A533B1	AN2	W97	WAN201	W	TL	PWR	Combustion Engineering	Combustion Engineering	83650	L0091
A5083	BD1	U	WBD101	W	TL	PWR		Westinghouse		
A5083	BD1	X	WBD101	W	TL	PWR		Westinghouse		
A5083	BD2	U	WBD201	W	TL	PWR		Westinghouse	442011	L80
A5083	BD2	X	WBD201	W	TL	PWR		Westinghouse	442011	L80
A302BM	BF2	30D	WBF2JW	W		BWR	Babcock & Wilcox/IHI	General Electric		
A302B	BR	119	WBR_01	W	TS	BWa	Combustion Engineering	General Electric		
A302B	BR	122	WBR_01	W	TS	BWa	Combustion Engineering	General Electric		
A302B	BR	124	WBR_01	W	TS	BWa	Combustion Engineering	General Electric		
A302B	BR	125	WBR_01	W	TS	BWa	Combustion Engineering	General Electric		
A302B	BR	127	WBR_01	W	TS	BWa	Combustion Engineering	General Electric		
A533B1	BV1	U	WBV101	W	TL	PWR	Combustion Engineering	Westinghouse	305424	L1092
A533B1	BV1	V	WBV101	W	TL	PWR	Combustion Engineering	Westinghouse	305424	L1092
A533B1	BV1	W	WBV101	W	TL	PWR	Combustion Engineering	Westinghouse	305424	L1092
A5082	BY1	U	WBY101	W	TL	PWR		Westinghouse	442002	L80
A5082	BY1	X	WBY101	W	TL	PWR		Westinghouse	442002	L80
A5083	BY2	U	WBY201	W	TL	PWR		Westinghouse	442002	L80
A5083	BY2	W	WBY201	W	TL	PWR		Westinghouse	442002	L80
A533B1	CAB	K	WCAB01	W	TL	PWR	Combustion Engineering	Westinghouse	1248	
A533B1	CAB	N	WCAB01	W	TL	PWR	Combustion Engineering	Westinghouse	1248	
A5082	CB1	Y	WCB101	W	TL	PWR	Rotterdamse Droogdok Madtdschappij (Netherlands)	Westinghouse	895075	LW320
A5082	CB1	Z	WCB101	W	TL	PWR	Rotterdamse Droogdok Madtdschappij (Netherlands)	Westinghouse	895075	LW320
A533B1	CB2	X	WCB201	W	TL	PWR		Westinghouse	83648	L0091
A533B1	CB2	Z	WCB201	W	TL	PWR		Westinghouse	83648	L0091
A533B1	CC1	W263	WCC101	W	TL	PWR	Combustion Engineering	Combustion Engineering	33A277	L0091
A533B1	CC1	W97	WCC101	W	TL	PWR	Combustion Engineering	Combustion Engineering	33A277	L0091
A533B1	CC2	W263	WCC201	W	TL	PWR	Combustion Engineering	Combustion Engineering	10137	L0091
A533B1	CC2	W97	WCC201	W	TL	PWR	Combustion Engineering	Combustion Engineering	10137	L0091
A533B1	CK1	T	WCK101	W		PWR	Combustion Engineering	Westinghouse	13253	L1092
A533B1	CK1	U	WCK101	W		PWR	Combustion Engineering	Westinghouse	13253	L1092
A533B1	CK1	Y	WCK101	W		PWR	Combustion Engineering	Westinghouse	13253	L1092
A533B1	CK2	T	WCK201	W	TL	PWR	Chicago Bridge and Iron	Westinghouse	S3986	L124
A533B1	CK2	U	WCK201	W	TL	PWR	Chicago Bridge and Iron	Westinghouse	S3986	L124
A533B1	CK2	X	WCK201	W	TL	PWR	Chicago Bridge and Iron	Westinghouse	S3986	L124
A533B1	CK2	Y	WCK201	W	TL	PWR	Chicago Bridge and Iron	Westinghouse	S3986	L124
A533B1	CL1	U	WCL101	W	TL	PWR	Combustion Engineering	Westinghouse	90077	L124
A533B1	CL1	Y	WCL101	W	TL	PWR	Combustion Engineering	Westinghouse	90077	L124
A533B1	COF	3D	WCOFJW	W		BWR		General Electric		
A533B1	CP1	U	WCP1JW	W		PWR		Westinghouse Corporation		
A533B1	CP2	U	WCP201	W		PWR		Westinghouse Corporation	89833	L124
A533B1	CR3	B	WCR301	W	TL	PWR	Babcock & Wilcox	Babcock & Wilcox		L80
A533B1	CR3	C	WCR301	W	TL	PWR	Babcock & Wilcox	Babcock & Wilcox		L80
A5082	CR3	C1	WHSS63	W		PWR	Babcock & Wilcox	Babcock & Wilcox	299L44	L80
A5082	CR3	C1	WHSS65	W		PWR	Babcock & Wilcox	Babcock & Wilcox	72445	L80
A5082	CR3	C1	WHSSCR	W		PWR	Babcock & Wilcox	Babcock & Wilcox	72442	L80
A5082	CR3	C2	WHSS65	W		PWR	Babcock & Wilcox	Babcock & Wilcox	72445	L80
A5082	CR3	C2	WHSSCR	W		PWR	Babcock & Wilcox	Babcock & Wilcox	72442	L80
A533B1	CR3	D	WCR301	W	TL	PWR	Babcock & Wilcox	Babcock & Wilcox		L80
A533B1	CR3	F	WCR301	W	TL	PWR	Babcock & Wilcox	Babcock & Wilcox		L80
A302B	CTY	A	WCTY01	W	TL	PWR	Combustion Engineering	Westinghouse	86054B	ARCO B5

Material ID	Plant ID	Capsule	Heat ID	Product ID	Specimen Orientation	Reactor Type	Vessel Manufacturer	Plant Designer	Weld Wire Heat	Weld Flux
A302B	CTY	D	WCTY01	W	TL	PWR	Combustion Engineering	Westinghouse	86054B	ARCO B5
A533B1	DAC	1	WDAC01	W	LT	BWR	Chicago Bridge and Iron	General Electric		
A5082	DB1	A	WDB101	W	TL	PWR	Babcock & Wilcox	Babcock & Wilcox	821T44	L80
A5082	DB1	B	WDB101	W	TL	PWR	Babcock & Wilcox	Babcock & Wilcox	821T44	L80
A5082	DB1	D	WDB101	W	TL	PWR	Babcock & Wilcox	Babcock & Wilcox	821T44	L80
A5082	DB1	D1	WHSS66	W		PWR	Babcock & Wilcox	Babcock & Wilcox	72105	L80
A5082	DB1	D1	WHSS67	W		PWR	Babcock & Wilcox	Babcock & Wilcox	61782	L80
A5082	DB1	D1	WHSSDB	W		PWR	Babcock & Wilcox	Babcock & Wilcox	406L44	L80
A5082	DB1	F	WDB101	W	TL	PWR	Babcock & Wilcox	Babcock & Wilcox	821T44	L80
A533B1	DC1	S	WDC101	W	TL	PWR	Combustion Engineering	Westinghouse	27204	L1092
A533B1	DC1	Y	WDC101	W	TL	PWR	Combustion Engineering	Westinghouse	27204	L1092
A533B1	DC2	U	WDC201	W	TL	PWR	Combustion Engineering	Westinghouse	21935	L1092
A533B1	DC2	X	WDC201	W	TL	PWR	Combustion Engineering	Westinghouse	21935	L1092
A533B1	DC2	Y	WDC201	W	TL	PWR	Combustion Engineering	Westinghouse	21935	L1092
A302B	DR2	2	WDR202	W	TL	BWb	Babcock and Wilcox	General Electric		
A302B	DR2	4	WDR202	W	TL	BWb	Babcock and Wilcox	General Electric		
A302B	DR2	5	WDR202	W	TL	BWb	Babcock and Wilcox	General Electric		
A302BM	DR3	12	WDR301	W	TL	BWb	Babcock and Wilcox	General Electric		
A302B	DR3	12	WDR302	W	TL	BWb	Babcock and Wilcox	General Electric		
A302BM	DR3	13	WDR301	W	TL	BWR	Babcock and Wilcox	General Electric		
A302BM	DR3	14	WDR301	W	TL	BWb	Babcock and Wilcox	General Electric		
A302B	DR3	14	WDR302	W	TL	BWb	Babcock and Wilcox	General Electric		
A302BM	DR3	18	WDR301	W	TL	BWR	Babcock and Wilcox	General Electric		
A302BM	DR3	4	WDR301	W	TL	BWb	Babcock and Wilcox	General Electric		
A302B	DR3	4	WDR302	W	TL	BWb	Babcock and Wilcox	General Electric		
A533B1	FA1	U	WFA101	W	TL	PWR	Combustion Engineering	Westinghouse	33A277	L0091
A533B1	FA1	W	WFA101	W	TL	PWR	Combustion Engineering	Westinghouse	33A277	L0091
A533B1	FA1	X	WFA101	W	TL	PWR	Combustion Engineering	Westinghouse	33A277	L0091
A533B1	FA1	Y	WFA101	W	TL	PWR	Combustion Engineering	Westinghouse	33A277	L0091
A533B1	FA2	U	WFA201	W	TL	PWR	Combustion Engineering	Westinghouse	BOLA	
A533B1	FA2	W	WFA201	W	TL	PWR	Combustion Engineering	Westinghouse	BOLA	
A533B1	FA2	X	WFA201	W	TL	PWR	Combustion Engineering	Westinghouse	BOLA	
A533B1	FC1	W225	WFC101	W	TL	PWR	Combustion Engineering	Combustion Engineering	305414	L1092
A533B1	FC1	W265	WFC101	W	TL	PWR	Combustion Engineering	Combustion Engineering	305414	L1092
A533B1	FC1	W275	WFC101	W	TL	PWR	Combustion Engineering	Combustion Engineering	305414	L1092
A5082	GIN	R	WGIN01	W	TL	PWR	Babcock & Wilcox	Westinghouse	61782	L80
A5082	GIN	S	WGIN01	W	TL	PWR	Babcock & Wilcox	Westinghouse	61782	L80
A5082	GIN	T	WGIN01	W	TL	PWR	Babcock & Wilcox	Westinghouse	61782	L80
A5082	GIN	V	WGIN01	W	TL	PWR	Babcock & Wilcox	Westinghouse	61782	L80
A533B1	HA2	30D	WHA2JW	W		BWR	Combustion Engineering	General Electric		
A302B	HB2	T	WHB201	W	TL	PWR	Combustion Engineering	Westinghouse	W5214	L1092
A302B	HB2	V	WHB201	W	TL	PWR	Combustion Engineering	Westinghouse	W5214	L1092
A533B1	HOP	30D	WHOPJW	W		BWR		General Electric		
A302B	IP2	V	WIP201	W	TL	PWR	Combustion Engineering	Westinghouse	W5214	L1092
A302B	IP2	Y	WIP201	W	TL	PWR	Combustion Engineering	Westinghouse	W5214	L1092
A302B	IP3	T	WIP301	W	TL	PWR	Combustion Engineering	Westinghouse	W5214	L1092
A302B	IP3	Y	WIP301	W	TL	PWR	Combustion Engineering	Westinghouse	W5214	L1092
A302B	IP3	Z	WIP301	W	TL	PWR	Combustion Engineering	Westinghouse	W5214	L1092
A533B1	KU1	177D	WKU1JW	W		BWR		General Electric		
A533B1	KU2	3D	WKU2JW	W		BWR		General Electric		
A5082	KWE	P	WKWE01	W	TL	PWR	Combustion Engineering	Westinghouse	1P3571	L1092
A5082	KWE	R	WKWE01	W	TL	PWR	Combustion Engineering	Westinghouse	1P3571	L1092
A5082	KWE	S	WKWE01	W	TL	PWR	Combustion Engineering	Westinghouse	1P3571	L1092
A5082	KWE	V	WKWE01	W	TL	PWR	Combustion Engineering	Westinghouse	1P3571	L1092
A302B	LAC	1A	WLAC01	W	TL	BWa	Combustion Engineering	Allis-Chalmers		
A302B	LAC	1B	WLAC01	W	TL	BWa	Combustion Engineering	Allis-Chalmers		
A302B	LAC	2A	WLAC01	W	TL	BWa	Combustion Engineering	Allis-Chalmers		
A302B	LAC	3A	WLAC01	W	TL	BWa	Combustion Engineering	Allis-Chalmers		
A302B	LAC	3B	WLAC01	W	TL	BWa	Combustion Engineering	Allis-Chalmers		
A302B	LAC	7B	WLAC01	W	TL	BWa	Combustion Engineering	Allis-Chalmers		
A302B	LAC	8A	WLAC01	W	TL	BWa	Combustion Engineering	Allis-Chalmers		
A302B	LAC	8B	WLAC01	W	TL	BWa	Combustion Engineering	Allis-Chalmers		
A302B	LAC	9A	WLAC01	W	TL	BWa	Combustion Engineering	Allis-Chalmers		
A302B	LAC	9B	WLAC01	W	TL	BWa	Combustion Engineering	Allis-Chalmers		
A533B1	LS1	300D	WLS1JW	W		BWR		General Electric		
A533B1	LS2	300D	WLS2JW	W	LT	BWR		General Electric		
A533B1	MC1	U	WMC101	W	TL	PWR	Combustion Engineering	Westinghouse	20291	L1092
A533B1	MC1	X	WMC101	W	TL	PWR	Combustion Engineering	Westinghouse	20291	L1092
A5082	MC2	U	WMC201	W	TL	PWR	Rotterdamse Droogdok Madtdschappij (Netherlands)	Westinghouse	895075	LW320
A5082	MC2	V	WMC201	W	TL	PWR	Rotterdamse Droogdok Madtdschappij (Netherlands)	Westinghouse	895075	LW320
A5082	MC2	X	WMC201	W	TL	PWR	Rotterdamse Droogdok Madtdschappij (Netherlands)	Westinghouse	895075	LW320
A302BM	ML1	210D	WML101	W	TS	BWR	Combustion Engineering	General Electric	34B009	L1092
A302BM	ML1	300D	WML101	W	TS	BWR	Combustion Engineering	General Electric	34B009	L1092
A533B1	ML2	W104	WML201	W	TL	PWR	Combustion Engineering	Combustion Engineering	90136	L0091
A533B1	MY	A25	WMY_01	W	TL	PWR	Combustion Engineering	Combustion Engineering	IP3571	L1092
A533B1	MY	A35	WMY_01	W	TL	PWR	Combustion Engineering	Combustion Engineering	IP3571	L1092
A533B1	MY	W253	WMY_01	W	TL	PWR	Combustion Engineering	Combustion Engineering	IP3571	L1092
A533B1	MY	W263	WMY_01	W	TL	PWR	Combustion Engineering	Combustion Engineering	IP3571	L1092
A5082	NA1	U	WNA101	W	TL	PWR	Rotterdamse Droogdok Madtdschappij (Netherlands)	Westinghouse	25531	SMIT 89
A5082	NA1	V	WNA101	W	TL	PWR	Rotterdamse Droogdok Madtdschappij (Netherlands)	Westinghouse	25531	SMIT 89
A5082	NA2	U	WNA201	W	TL	PWR	Rotterdamse Droogdok Madtdschappij (Netherlands)	Westinghouse	716126	LW320
A5082	NA2	V	WNA201	W	TL	PWR	Rotterdamse Droogdok Madtdschappij (Netherlands)	Westinghouse	716126	LW320

Material ID	Plant ID	Capsule	Heat ID	Product ID	Specimen Orientation	Reactor Type	Vessel Manufacturer	Plant Designer	Weld Wire Heat	Weld Flux
A302B	OC1	A	WOC101	W	TL	PWR	Babcock & Wilcox	Babcock & Wilcox	406L44	L80
A302B	OC1	C	WOC101	W	TL	PWR	Babcock & Wilcox	Babcock & Wilcox	406L44	L80
A302B	OC1	E	WOC101	W	TL	PWR	Babcock & Wilcox	Babcock & Wilcox	406L44	L80
A5082	OC2	A	WOC201	W	TL	PWR	Babcock & Wilcox	Babcock & Wilcox	72105	L80
A5082	OC2	C	WOC201	W	TL	PWR	Babcock & Wilcox	Babcock & Wilcox	72105	L80
A5082	OC2	E	WOC201	W	TL	PWR	Babcock & Wilcox	Babcock & Wilcox	72105	L80
A5082	OC3	A	WOC301	W	TL	PWR	Babcock & Wilcox	Babcock & Wilcox	72105	L80
A5082	OC3	B	WOC301	W	TL	PWR	Babcock & Wilcox	Babcock & Wilcox	72105	L80
A5082	OC3	D	WOC301	W	TL	PWR	Babcock & Wilcox	Babcock & Wilcox	72105	L80
A302BM	PAL	A240	WPAL01	W	TL	PWR	Combustion Engineering	Combustion Engineering	3277	L1092
A302BM	PAL	T330	WPAL01	W	TL	PWR	Combustion Engineering	Combustion Engineering	3277	L1092
A302BM	PAL	W110	WPAL01	W	TL	PWR	Combustion Engineering	Combustion Engineering	3277	L1092
A302BM	PAL	W290	WPAL01	W	TL	PWR	Combustion Engineering	Combustion Engineering	3277	L1092
A302B	PB1	R	WPB101	W	TL	PWR	Babcock & Wilcox	Westinghouse	72445	L80
A302B	PB1	S	WPB101	W	TL	PWR	Babcock & Wilcox	Westinghouse	72445	L80
A302B	PB1	T	WPB101	W	TL	PWR	Babcock & Wilcox	Westinghouse	72445	L80
A302B	PB1	V	WPB101	W	TL	PWR	Babcock & Wilcox	Westinghouse	72445	L80
A5082	PB2	R	WPB201	W	TL	PWR	Combustion Engineering	Westinghouse	406L44	L80
A5082	PB2	S	WPB201	W	TL	PWR	Combustion Engineering	Westinghouse	406L44	L80
A5082	PB2	T	WPB201	W	TL	PWR	Combustion Engineering	Westinghouse	406L44	L80
A5082	PB2	V	WPB201	W	TL	PWR	Combustion Engineering	Westinghouse	406L44	L80
A302BM	PH3	1	WPH301	W	LT	BWR	Babcock & Wilcox/Chicago Bridge & Iron Company	General Electric		
A5083	PI1	P	WPI101	W	TL	PWR	Societe des Forges et Ateliers du Creusot	Westinghouse	1752	UM89
A5083	PI1	R	WPI101	W	TL	PWR	Societe des Forges et Ateliers du Creusot	Westinghouse	1752	UM89
A5083	PI1	V	WPI101	W	TL	PWR	Societe des Forges et Ateliers du Creusot	Westinghouse	1752	UM89
A5083	PI2	R	WPI201	W	TL	PWR	Societe des Forges et Ateliers du Creusot	Westinghouse	2721	UM89
A5083	PI2	T	WPI201	W	TL	PWR	Societe des Forges et Ateliers du Creusot	Westinghouse	2721	UM89
A5083	PI2	V	WPI201	W	TL	PWR	Societe des Forges et Ateliers du Creusot	Westinghouse	2721	UM89
A533B1	PL1	1	WPL101	W	TL	BWR	Combustion Engineering	General Electric		
A533B1	PV1	W137	WPV1JW	W		PWR		Combustion Engineering		
A533B1	PV2	W137	WPV201	W	TL	PWR		Combustion Engineering		
A302BM	QC1	1	WQC101	W	TL	BWb	Babcock and Wilcox	General Electric		
A302B	QC1	1	WQC102	W	TL	BWb	Babcock and Wilcox	General Electric		
A302BM	QC1	2	WQC101	W	TL	BWR	Babcock and Wilcox	General Electric		
A302BM	QC1	3	WQC101	W	TL	BWb	Babcock and Wilcox	General Electric		
A302B	QC1	3	WQC102	W	TL	BWb	Babcock and Wilcox	General Electric		
A302BM	QC1	8	WQC101	W	TL	BWR	Babcock and Wilcox	General Electric		
A302BM	QC2	12	WQC201	W	TL	BWb	Babcock and Wilcox/Chicago Bridge and Iron	General Electric		
A302B1	QC2	12	WQC202	W	TL	BWb	Babcock and Wilcox/Chicago Bridge and Iron	General Electric		
A302BM	QC2	13	WQC201	W	TL	BWR	Babcock and Wilcox/Chicago Bridge and Iron	General Electric		
A302BM	QC2	18	WQC201	W	TL	BWR	Babcock and Wilcox/Chicago Bridge and Iron	General Electric		
A302BM	QC2	3	WQC201	W	TL	BWb	Babcock and Wilcox/Chicago Bridge and Iron	General Electric		
A302B1	QC2	3	WQC202	W	TL	BWb	Babcock and Wilcox/Chicago Bridge and Iron	General Electric		
A5082	RI2	X	WRI201	W		PWR	Rotterdamse Droogdok Madtdschappij (Netherlands)	Westinghouse	1725	SMIT 89
A533B1	RS1	B	WRS101	W	TL	PWR	Babcock & Wilcox	Babcock & Wilcox	406L44	L80
A533B1	RS1	D	WRS101	W	TL	PWR	Babcock & Wilcox	Babcock & Wilcox	406L44	L80
A533B1	RS1	F	WRS101	W	TL	PWR	Babcock & Wilcox	Babcock & Wilcox	406L44	L80
A533B1	SA1	Y	WSA101	W	TL	PWR	Combustion Engineering	Westinghouse	39B196	L1092
A533B1	SA2	T	WSA201	W	TL	PWR	Combustion Engineering	Westinghouse	13253	L1092
A533B1	SA2	U	WSA201	W	TL	PWR	Combustion Engineering	Westinghouse	13253	L1092
A533B1	SA2	X	WSA201	W	TL	PWR	Combustion Engineering	Westinghouse	13253	L1092
A533B1	SB1	U	WSB101	W	TL	PWR	Westinghouse	Westinghouse	4P6052	L0091
A533B1	SH1	30D	WSH101	W	TL	BWR	Chicago Bridge and Iron	General Electric	411L3071	L311A27AF
A533B1	SH2	30D	WSH201	W	TL	BWR	Chicago Bridge and Iron	General Electric	411L3071	
A533B1	SL1	W104	WSL101	W	TL	PWR	Combustion Engineering	Combustion Engineering	90136	L0091
A533B1	SL1	W97	WSL101	W	TL	PWR	Combustion Engineering	Combustion Engineering	90136	L0091
A533B1	SL2	W83	WSL201	W	TL	PWR	Combustion Engineering	Combustion Engineering	83637	L0124
A336	SMG	190D	WSMGJW	W		BWR		General Electric		
A302B	SO1	A	WSO101	W	TL	PWR	Combustion Engineering	Westinghouse		
A302B	SO1	F	WSO101	W	TL	PWR	Combustion Engineering	Westinghouse		
A533B1	SO2	W97	WSO201	W		PWR	Combustion Engineering	Combustion Engineering		
A533B1	SO3	W97	WSO301	W	TL	PWR	Combustion Engineering	Combustion Engineering		L124
A5082	SQ1	T	WSQ101	W	TL	PWR	Rotterdamse Droogdok Madtdschappij (Netherlands)	Westinghouse	25295	SMIT 89
A5082	SQ1	U	WSQ101	W	TL	PWR	Rotterdamse Droogdok Madtdschappij (Netherlands)	Westinghouse	25295	SMIT 89
A5082	SQ1	X	WSQ101	W	TL	PWR	Rotterdamse Droogdok Madtdschappij (Netherlands)	Westinghouse	25295	SMIT 89
A5082	SQ2	T	WSQ201	W	TL	PWR	Rotterdamse Droogdok Madtdschappij (Netherlands)	Westinghouse	4278	SMIT 89
A5082	SQ2	U	WSQ201	W	TL	PWR	Rotterdamse Droogdok Madtdschappij (Netherlands)	Westinghouse	4278	SMIT 89
A5082	SQ2	X	WSQ201	W	TL	PWR	Rotterdamse Droogdok Madtdschappij (Netherlands)	Westinghouse	4278	SMIT 89
A533B1	SR1	U	WSR101	W	TL	PWR		Westinghouse	5P6771	L124
A533B1	ST1	U	WST101	W	TL	PWR		Westinghouse	V89476	L124
A533B1	ST2	V	WST2JW	W		PWR		Westinghouse		
A533B1	SU1	T	WSU101	W	TL	PWR	Rotterdamse Droogdok Madtdschappij (Netherlands)	Westinghouse	299L44	L80
A533B1	SU1	V	WSU101	W	TL	PWR	Rotterdamse Droogdok Madtdschappij (Netherlands)	Westinghouse	299L44	L80
A533B1	SU2	V	WSU201	W	TL	PWR	Rotterdamse Droogdok Madtdschappij (Netherlands)	Westinghouse	0227	GRAU LO
A533B1	SU2	X	WSU201	W	TL	PWR	Rotterdamse Droogdok Madtdschappij (Netherlands)	Westinghouse	0227	GRAU LO
A302B	TM1	C	WTM101	W	TL	PWR	Babcock & Wilcox	Babcock & Wilcox	299L44	L80
A302B	TM1	E	WTM101	W	TL	PWR	Babcock & Wilcox	Babcock & Wilcox	299L44	L80
A5082	TM2	T1	WTM2J1	W		PWR	Babcock & Wilcox	Babcock & Wilcox	299L44	L80
A5082	TM2	T1	WTM2J2	W		PWR	Babcock & Wilcox	Babcock & Wilcox	299L44	L80
A5082	TM2	T1	WTM2J3	W		PWR	Babcock & Wilcox	Babcock & Wilcox	72105	L80
A5082	TP3	T	WTP301	W	TL	PWR	Babcock & Wilcox	Westinghouse	71249	L80
A5082	TP3	V	WTP301	W	TL	PWR	Babcock & Wilcox	Westinghouse	71249	L80

Material ID	Plant ID	Capsule	Heat ID	Product ID	Specimen Orientation	Reactor Type	Vessel Manufacturer	Plant Designer	Weld Wire Heat	Weld Flux
A5082	TP4	T	WTP401	W		PWR	Babcock & Wilcox	Westinghouse	71249	L80
A533B1	TRO	U	WTRO01	W	TL	PWR	Chicago Bridge and Iron	Westinghouse	S3986	L124
A533B1	TRO	V	WTRO01	W	TL	PWR	Chicago Bridge and Iron	Westinghouse	S3986	L124
A533B1	TRO	X	WTRO01	W	TL	PWR	Chicago Bridge and Iron	Westinghouse	S3986	L124
A533B1	VO1	Y	WVO101	W	TL	PWR		Westinghouse	83653	L0091
A533B1	VO2	JW	WVO201	W	TL	PWR		Westinghouse	87005	L124
A533B1	VO2	JW	WVO201	W	TL	PWR		Westinghouse	87005	L124
A533B1	VS1	U	WVS101	W	TL	PWR	Chicago Bridge and Iron	Westinghouse	4P4784	L124
A533B1	VS1	V	WVS101	W	TL	PWR	Chicago Bridge and Iron	Westinghouse	4P4784	L124
A533B1	VS1	X	WVS101	W	TL	PWR	Chicago Bridge and Iron	Westinghouse	4P4784	L124
A533B1	VY	30D	WVY_01	W	TL	BWR	Chicago Bridge and Iron	General Electric		
A533B1	WC1	U	WWC101	W	TL	PWR	Combustion Engineering	Westinghouse	90146	L124
A533B1	WC1	Y	WWC101	W	TL	PWR	Combustion Engineering	Westinghouse	90146	L124
A533B1	WF3	W97	WWF301	W		PWR	Combustion Engineering	Combustion Engineering	88114	L0091
A533B1	ZN1	T	WZN101	W	TL	PWR	Babcock & Wilcox	Westinghouse	72105	L80
A533B1	ZN1	U	WZN101	W	TL	PWR	Babcock & Wilcox	Westinghouse	72105	L80
A533B1	ZN1	X	WZN101	W	TL	PWR	Babcock & Wilcox	Westinghouse	72105	L80
A533B1	ZN1	Y	WZN101	W	TL	PWR	Babcock & Wilcox	Westinghouse	72105	L80
A533B1	ZN2	T	WZN201	W	LT	PWR	Babcock & Wilcox	Westinghouse	72105	L80
A533B1	ZN2	U	WZN201	W	LT	PWR	Babcock & Wilcox	Westinghouse	72105	L80
A533B1	ZN2	Y	WZN201	W	LT	PWR	Babcock & Wilcox	Westinghouse	72105	L80

APPENDIX B
DETERMINATION OF FIXED LOWER SHELF ENERGY FOR CHARPY *tanh* FITS

During the development of the embrittlement analysis data base, raw Charpy data from the Power Reactor Embrittlement Data Base (PR-EDB: NUREG/CR-4816) were fitted to a hyperbolic tangent curve, wherever possible; if inadequate data were available to establish an upper shelf, the data were fitted using an exponential curve. Since the PR-EDB primarily focused on transition temperature and upper shelf energy, the raw Charpy data sets did not contain sufficient points to establish lower shelves for the individual curve fits. For this reason, it was necessary to establish a fixed value (or values) of lower shelf energy (LSE) to be assumed during fitting.

Raw Charpy data from the Test Reactor Embrittlement Data Base (TR-EDB: NUREG/CR-6076) were used to help establish the fixed LSE. Inspection of the TR-EDB revealed 11 Charpy data sets with well-defined lower shelves. The selection process involved plotting all raw Charpy data sets from the TR-EDB and then looking at each plot. To be considered "well-defined," the lower shelf had to include points below 10 ft-lb at several different temperatures and to exhibit a levelling-off trend with decreasing temperature. This approach, though labor-intensive and somewhat subjective, was more successful than attempts to automate the screening. Midland weld data (NUREG/CR-5914) provided a twelfth set of Charpy data exhibiting lower shelf behavior. Of the 12 Charpy data sets, all except two sets consisted of unirradiated data; half of the sets were from longitudinal specimens, and half were from transverse specimens; two sets were from welds, and the rest were from plates. See Table B.1 for descriptions of the data sets.

To determine the asymptotic lower shelf energy for each raw Charpy data set, an exponential function was fitted to the lower shelf and transition data (below 50 ft-lb) using nonlinear least squares (SURFIT). The function had the form:

$$C_v = a\exp(bT^c) \qquad \textbf{(B-1)}$$

where T is the temperature in absolute units (°R), and C_v is the Charpy V-notch impact energy (ft-lb). The values for the fitting parameters a, b, and c are shown on the plots in Figure B.1, which also show the exponential fit with the raw data. Data weighting was utilized where necessary to obtain reasonable fits to the lower shelf data.

The asymptotic lower shelf energy is given directly by the fitting parameter a; by definition, this is the estimated Charpy energy at absolute zero.

Using Chauvenet's criterion, it was determined that the LSE value for data set lse08 (C_v = 0.00184 ft-lb) could be excluded based on its low probability of occurrence. Chauvenet's criterion allows deletion of a point if it is more than t_α standard deviations from the mean or expected value, where $\alpha = 1/2N$, and $N = 12$ is the number of points, as described in Appendix C (Young, 1962; Taylor, 1982). On this basis, the outlier (lse08) is 2.8 standard deviations from the mean (in $\log_{10}C_v$ units), so the point can be deleted with a probability of error of less than 1%.

The remaining LSE values were averaged to determine the fixed estimate of LSE. The distribution of lower shelf data was assumed to be lognormal, so logarithmic averages were computed. The lognormal distribution assumption was based on a) the fact that Charpy energy is strictly positive and b) histograms and cumulative distribution plots of the data. Various statistical analyses were performed to verify that the remaining data could be considered together despite the various test conditions. For example, comparisons were made between:

- irradiated versus unirradiated sets
- transverse versus longitudinal specimen orientation
- weld versus plate
- different heats

None of these conditions produced statistically significant differences in the asymptotic lower shelf energy, based on the analyses conducted. Thus, a single value of asymptotic lower shelf energy was used for all Charpy curves, regardless of orientation, irradiation, and weld versus plate. The logarithmic average for the 11 points (excluding lse08) was 1.28 ft-lb. Note that this is somewhat lower than the value of 2.2 ft-lb (3 J) (attributed to Oldfield) that has been used in other work. The difference in fitted transition temperature at 30 ft-lb using 1.28 instead of 2.2 ft-lb for the lower shelf energy is small, and there is no discernable difference in fitted upper shelf energy.

Table B.1 Charpy lower shelf data sets

Source	Product Form	Orientation	Irradiated or Unirradiated	Plot ID	LSE (ft-lb)
ORNL-6740	Weld	Longitudinal	Unirradiated	Midland	1.41
TR-EDB	Plate	LT	Unirradiated	lse02	0.464
TR-EDB	Plate	TL	Unirradiated	lse04	1.74
TR-EDB	Plate	TL	Unirradiated	lse06	2.58
TR-EDB	Plate	LT	Unirradiated	lse08	0.00184
TR-EDB	Plate	TL	Unirradiated	lse09	1.52
TR-EDB	Plate	TL	Unirradiated	lse10	4.21
TR-EDB	Plate	LT	Unirradiated	lse12	1.70
TR-EDB	Plate	LT	Unirradiated	lse13	1.13
TR-EDB	Plate	TL	Unirradiated	lse14	2.22
TR-EDB	Weld	TL	Irradiated	lse15	0.0781
TR-EDB	Plate	LT	Irradiated	lse17	2.37

REFERENCES

Oldfield, W., et al., *Nuclear Plant Irradiated Steel Handbook,* EPRI NP-4797, Sept. 1986.

Taylor, J. R., *An Introduction to Error Analysis,* University Science Books, Mill Valley, CA 1982.

Young, H. D., *Statistical Treatment of Experimental Data,* McGraw-Hill Book Company, Inc., New York, 1962.

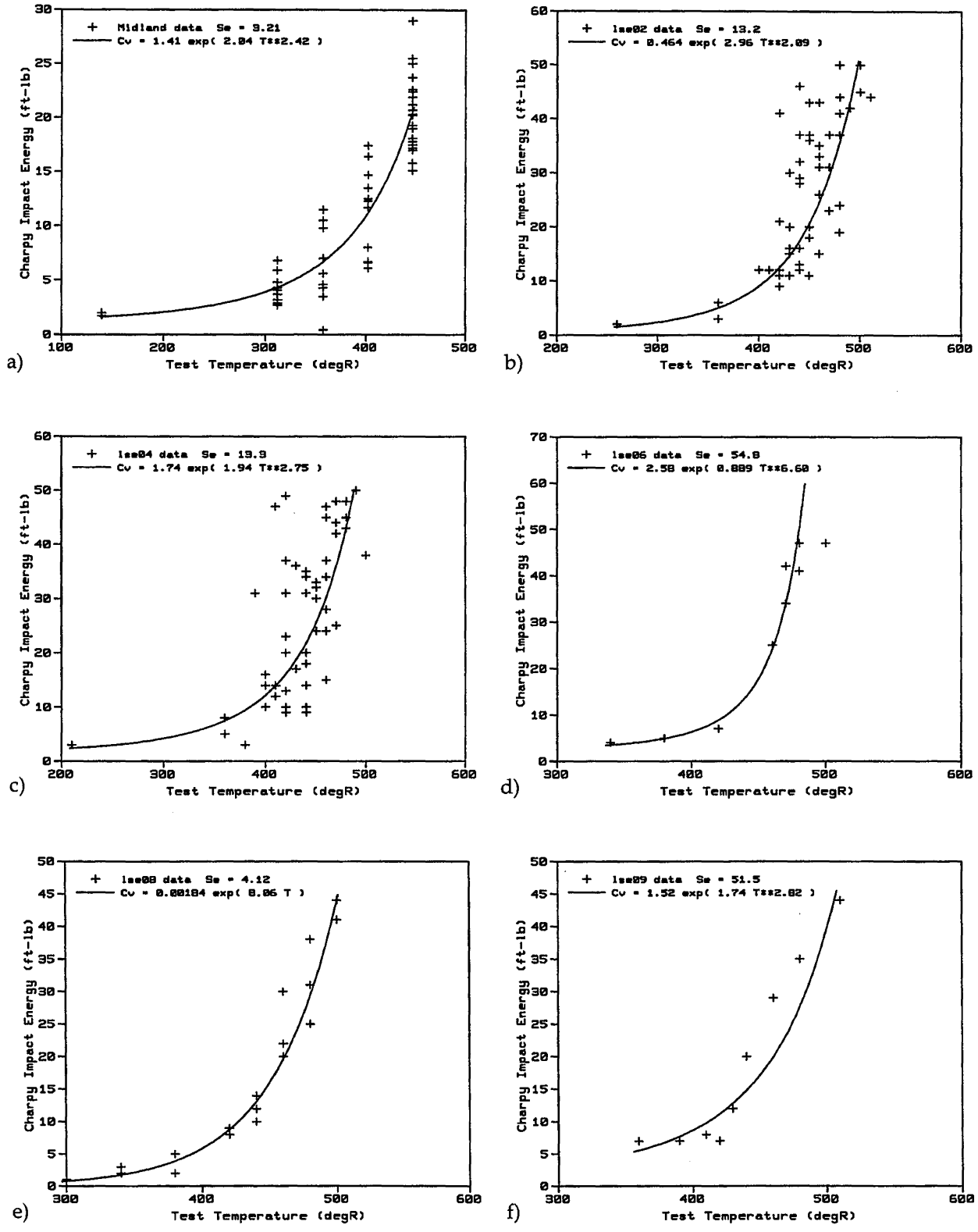

Figure B.1 Data and exponential fits used to determine fixed LSE

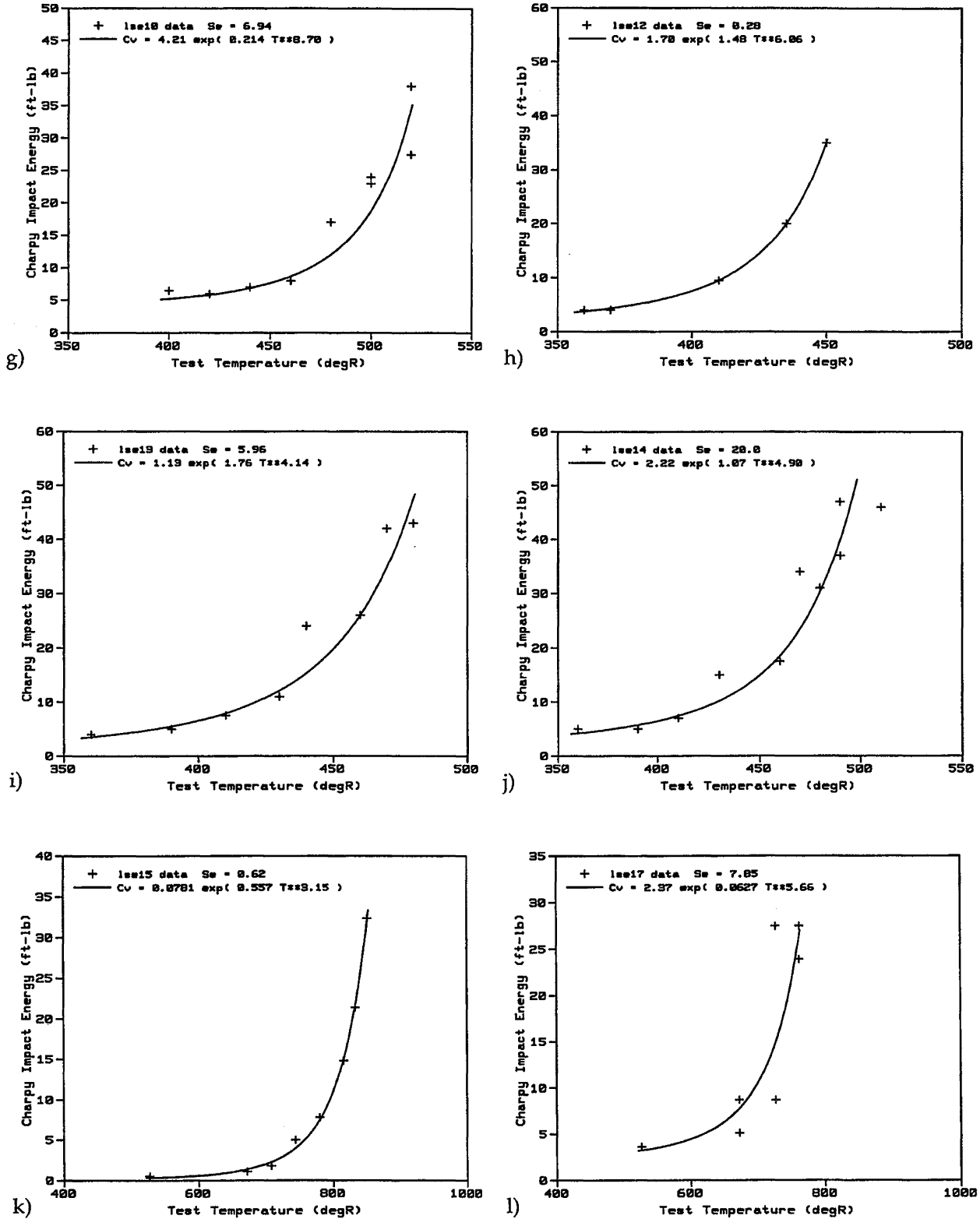

Figure B.1 Data and exponential fits used to determine fixed LSE, cont'd

APPENDIX C
OUTLIERS REMOVED USING CHAUVENET'S CRITERION

The issue of discarding outlier points during model calibration is a controversial subject, on which reasonable analysts can and do disagree. The question is whether or not an outlier is enough different from the bulk of the data to suggest that the point is in error. The risk in using such a point for model calibration can be substantial, because large outliers can have a disproportionate effect on the sum of squares that is minimized in a least squares fit, so that a single outlier can create a large bias in model calibration. The risk in not using such points is the possibility that they are valid, hence by omitting them the fitted model or the standard error could be unrealistic. In the authors' experience, the risk of a biased fit from leaving outliers in a calibration set is the greater risk, particularly in large datasets as analyzed here.

The procedure followed in this analysis was to calibrate a preliminary model, then apply an objective statistical criterion (Chauvenet's, discussed below) to identify potential outliers among the residuals. These outlier points were investigated to the extent possible with the documentation available to the authors in an attempt to determine if there were obvious physical causes for the anomalous behavior, or if the points were extreme in their test or irradiation conditions or composition. The residuals about the preliminary model appeared to be reasonably normally distributed, thus satisfying the basic assumption of both Chauvenet's criterion and the least squares fitting procedure. Then the models were re-calibrated without the identified outliers, producing the results presented in this report.

Chauvenet's criterion is a rule-of-thumb that provides a quantitative means of deciding whether or not an outlier point may be discarded (Young, 1962; Taylor, 1982). Chauvenet's criterion calls for rejection of an outlier if the probability of obtaining it is less than 1/(2N), where N is the total number of points. In other words, an outlier is rejected if the expected number of points that far from the model is less than ½. So the critical multiple of S_e from the model, beyond which the data are suspect, can be calculated from the normal distribution. For example, where only 100 points are used for calibration, an outlier might be rejected if further than $2.8S_e$ from the model, whereas an outlier must be further than about $3.4S_e$ from the model to be considered for rejection if more than 500 points are used for calibration.

In the present application, there are enough data points so that only the most extreme outliers, greater than about four standard deviations from the model, are identified by Chauvenet's criterion. In addition, the dataset is so large that the effect of including the outliers or not including them is reasonably small. Thus, the main effect of excluding outliers in this case is to enhance the reliability of the least squares procedure by eliminating a few points that appear to deviate from the normal distribution assumption that is implicit in least squares.

Chauvenet's criterion was used to justify removal of two (2) out of 611 points for calibration of the TTS model and three (3) out of 665 points for calibration of the USE_i model. The removed outliers are shown in Tables C.1 and C.2. They do not appear to be unusual in their values of independent variables, only in their observed values of the dependent variables. Further investigation of detailed records on these data points is recommended.

REFERENCES

Taylor, J. R., *An Introduction to Error Analysis*, University Science Books, Mill Valley, CA 1982.

Young, H. D., *Statistical Treatment of Experimental Data*, McGraw-Hill Book Company, Inc., New York, 1962.

Table C.1 Outliers removed during TTS model calibration

Heat	Material	TTS (°F)	Cu (wt%)	Ni (wt%)	P (wt%)	ϕt (n/cm^2)	t_i (hr)	T_c (°F)
WCK101	A533B1	109	0.270	0.740	0.023	1.77×10^{19}	80556	537
WSQ201	A5082	154	0.130	0.110	0.016	6.08×10^{18}	25528	545

Table C.2 Outliers removed during USE_i model calibration

Heat	Material	USE_i (ft-lb)	Cu (wt%)	Ni (wt%)	P (wt%)	ϕt (n/cm^2)	USE_u (ft-lb)
PCH1JW	A533B1	154	0.165	0.530	0.016	1.30×10^{17}	110
PMY_01	A533B1	87	0.100	0.528	0.013	7.13×10^{19}	158
FPB202	A5082	205	0.088	0.710	0.009	8.61×10^{18}	173

APPENDIX D
ALTERNATIVE TTS MODELS

Many variations of the final embrittlement model (Eq. 4-1) were investigated to varying degrees, a few of which are presented in this Appendix. Caution is advised if considering simplifying the form given in Equation 4-1. In cases where all the predictive variables needed for Equation 4-1 are known (i.e., Cu, Ni, P, ϕt, ϕ, and T_c), it is strongly recommended that Equation 4-1 be used. This recommendation is based on several considerations. First, the simpler alternative models have not been evaluated to the same degree as Equation 4-1. Second, even a simplification that does not increase the standard error by a statistically significant amount may cause unconservative changes in the quality of fit for some subsets of the data base and/or in some regime(s) of the variables. Third, seemingly minor changes in the models also caused marked degradation in the agreement between the model and data from other sources, discussed in Section 5.1.

The alternative TTS models shown in Table D.1 are provided primarily to show the effects of simplifying or increasing the complexity of Equation 4-1. All models were calibrated to the same 609 data points used to calibrate Equation 4-1, even though additional points could have been included in some cases (e.g., additional points which have missing values of flux and irradiation time become useable when irradiation time is not in the model). This approach facilitates comparisons among models. Table D.1 shows the models, standard errors, and corresponding figure numbers for residual plots; for the model without product form, predicted versus actual plots for subsets of data are also provided. The ranges of Cu given for each entry in Table D.1 indicate the threshold and upper limit values; e.g. when using Equation 4-1 for Cu < 0.072 wt%, 0.072 is used in the model, and for Cu > 0.3 wt%, 0.3 is used.

In the subsections below, the alternative models presented in Table D.1 are discussed, presenting potential reasons for considering them and reasons why they were not selected as the baseline model. The regions in the data base where the alternatives did not fit well are described, with reference to the associated residual plots. The reader should keep in mind that the authors considered statistical, mechanistic, and engineering criteria, with the goal of characterizing all trends that could be technically justified by these criteria. Degree of complexity was not the major consideration in the selection of Equation 4-1. None of these alternatives is significantly different from Equation 4-1 on a statistical basis, considering F tests on the overall standard errors, S_e.

Based on experience with various alternative models, including many more than are reported here, the authors would consider the Ni term inside the fluence *tanh* as the most promising addition to the baseline model. The simplification with the least effect on the quality of predictions would be deletion of the irradiation time term.

As was noted above, simplifying the model by simply dropping out terms is not recommended. There are two safer alternative approaches. The first approach is to use a model that has been recalibrated without the particular term. That approach distributes the effect of the missing terms over all other terms in the model. Thus, a missing phosphorous term might cause the fluence, temperature, copper, and nickel terms all to be a little different. This approach can only be justified if the effect of the missing variable is negligible. The second approach, which can be used for both small and large variable effects, is to hold the term fixed at a bounding value of the variable. Thus, the phosphorous term (1+57.7P) in Equation 4-1 could be conservatively replaced by 2.38, the result of evaluating the term with the maximum value in the database, P = 0.024 wt%. This second approach is the only recommended approach for terms that are not negligible.

Ni term in fluence *tanh*

This alternative gives a slightly lower standard error (22.8 versus 23.0°F) than the recommended Equation 4-1. The motivation for the extra Ni term is the observation in the literature that the fluence at which the CRP mechanism initiates and saturates depends on Cu (higher value shifts the saturation to lower fluence) and Ni (higher value shifts the saturation to higher fluence) (Williams and Phythian, 1996). Terms involving Cu in the *tanh* function could not be calibrated (the effect was contrary to other observations). The Ni term in this alternative did produce a small effect in the right direction. But the Ni (and Cu) term inside the *tanh* function tended to trade off numerically with the Cu and Ni terms outside the *tanh* function (note the change in powers on Cu and Ni), reducing the confidence in the calibrated values. Further, there were insufficient independent data over a wide range of fluence to validate the calibration of the model with Ni in the fluence function. Consequently, the Ni-dependent fluence model was considered a potential improvement, but one that is not sufficiently established at this time.

No phosphorous term

The reason for considering this alternative is that the phosphorous effect is relatively weak, so it is a likely candidate for elimination in order to simplify the model. The standard error is adversely affected by a small amount if the P term is deleted, and all other terms recalibrate to somewhat different values. Because the effect is relatively small, the unmodeled trend in the phosphorous residuals is difficult to see (they are sloping downward to the right in Figure D.2d). The justifications for leaving phosphorous in the model are (1) it does slightly improve the quality of the fit and (2) the existence of the P-effect is considered clearly demonstrated by controlled experiments and microstructural studies and by many other data correlations. There was no numerical difficulty calibrating a phosphorous effect when included in the matrix defect term, with various forms for SMD and CRP terms.

No irradiation time term

The irradiation time term is another relatively weak effect that is a potential candidate for elimination in order to simplify the model. The irradiation time term is small to negligible for flux greater than about 10^{10} n/cm^2/s; it has an effect similar to doubling the fluence below fluences of about 5.5×10^{17} n/cm^2, for times of about 100,000 hours. The reasons for including the irradiation time term are: (1) it improves the fit slightly, (2) there is corroborating evidence of time-dependent effects in other studies, and (3) ignoring the effect would be unconservative at low flux. The latter two reasons were given the greatest weight in recommending the model that includes an irradiation time term. This is an engineering judgement; from a statistical point of view the term is not significant either overall or in the low-flux region where it is most noticeable.

The benefit of the irradiation term does not show up in the residual plots (i.e., Figure 4.6f versus Figure D.3f), both because the low flux points are not identified and because the effect is small. Since the effect is only noticeable at combinations of fluence and time that imply low flux, the more relevant plot for assessing this effect is Figure 4.13. The standard error is slightly lower overall (0.07°F) with the irradiation time term, though the result looks the same when rounded in Table D.1.

There are no data beyond 139,000 hr to support the irradiation time term, but reactor pressure vessels may exceed that time during their service life. Unfortunately, this means that the model probably will be used for extrapolation in time. Expressing the time effect as a flux effect does not avoid the problem - there are no data with low flux and high fluence. Additional data at low flux and longer time are not expected from surveillance programs, so the proof of this term may have to wait until vessels are decommissioned after long service lives. Until then, it is probably conservative to use the calibrated term for extrapolation.

No irradiation time term and constant fluence power

The comments about irradiation time given above also apply here. In addition, a simple power on fluence rather than a function of fluence would appear to be a potential simplification. The problem is that the best-fit power on fluence over the data base (with or without the irradiation time term) is about 0.25-0.50, and with such a power, the fluence residuals above about 5×10^{19} are biased in the negative (unconservative) direction (compare Figure D.4a with Figure 4.6a). Some of the most unconservative predictions ($\geq$ 60°F below observed) are at the highest fluences in the data base when a model with a constant power is used. Even greater discrepancy at high fluence is noted between models with a constant power and French surveillance data (which may be caused in part by the different index level). The constant power does produce smaller residuals at low fluence ($< 10^{17}$ n/cm^2), but on an engineering basis it was considered much more important to reduce the nonconservative predictions at high fluence, where the shifts are large, at the expense of greater conservatism at low fluence, where the shifts are very small. In the mid-range fluences, where most of the data lie (3×10^{18} - 2×10^{19} n/cm^2), the constant and variable powers give similar results.

To further investigate the constant power on fluence in the SMD term, a subset of low-Cu data was analyzed in detail. The criteria for selecting data for this task were: (1) Cu $\leq$ 0.1 wt%, (2) at least three points for the same heat in the same plant, and (3) at least two different fluences for the same heat. Points with negative shifts were omitted. The selected data consisted of 143 points from 37 different heats. The fluence power p was fitted to all points in this subset of the low-Cu data, such that $TTS = C(\phi t)^p$, while the coefficient C was fitted separately to each heat/plant to account for differences in material composition and environment. Least squares was used to fit the curve shown in Figure D.5. The resulting power was $p = 0.34$, somewhat lower than expected but consistent with French FIS and FIM models, where the power is $p = 0.35$, and with the overall constant exponent fit in the present data base. Statistical analysis indicated 99.5% confidence that the power should be less than 0.44 for the low-Cu data.

As mentioned earlier in the report, the reasons for the relatively low fitted power, when others have obtained a power near 0.5 (and the higher power is needed for good fits to the high fluence data) are worthy of additional

investigation. The baseline model avoids the issue by allowing the power to vary with fluence, which may prove to be the correct approach if features that only appear at high fluence are responsible for the behavior.

No P-term, no t_i term, and constant power on ϕt

The comments given above on the corresponding variations apply to this alternative, which combines three variations already discussed.

Decreasing P effect with increasing Cu, Ni in *tanh* term

This alternative should be compared with the first alternative in this appendix; the only difference is the decreasing effect of phosphorous as Cu increases. The comments given above about the effect of Ni in the *tanh* term apply here as well.

The $C_1 P \cdot \exp(-C_2 Cu)$ term was introduced in the SMD term to account for the decreasing effect of phosphorous with increasing copper. This decaying P effect is evident in the raw data, was confirmed in the analysis of low Cu data, and is supported by other studies (Jones and Buswell, 1988). However, attempts to calibrate a model including the Cu-P effect in the SMD term caused numerical trade-offs to occur between the Cu effects in the SMD and CRP terms. The C_1 coefficient increased as expected (151 versus about 50-70), so that the P effect was greater at low Cu. However, when a reasonable C_2 was calibrated the upper saturation value for Cu in the CRP term decreased to 0.26 wt%, a change toward less conservatism. Based on engineering considerations, it is undesirable to have potentially unconservative results at high Cu, where the greatest shifts are expected. In addition, the fact that the upper Cu cut-off value in the CRP term was affected by introducing this Cu effect in the SMD term is a cause for concern about the numerical stability of this model form. These two concerns were judged to outweigh the small benefit to capturing the expected interaction between P and Cu.

No product form dependence

This alternative is applicable to all product forms but has no explicit product form dependence. The standard error is quite a bit larger in this case (23.8 versus 23.0°F), but the difference is still not large enough to be statistically significant at the $p = 0.05$ level in an F test. It is worth noting that the trends in the other modeling variables are similar across all product forms, whether product form is considered or not (compare Figures D.8 and D.9 without product form and Figures 4.6 and 4.9 with product form). It is also noteworthy that welds and plates are reasonably well characterized without considering product form, but the non-product form model is biased high relative to the actual forging data (see Figure D.9a - D.9c). The reasons for including the product form are to avoid this unnecessary conservatism for forging data, to slightly improve the weld and plate results, and improve the overall quality of fit. The improvement in the standard deviation of residuals for the forging subset of data by considering product form was significant, though the overall improvement in standard error was not.

Different upper limit on Cu for Linde 80 welds versus all other welds

Equation 4-1 is conservative with respect to the Linde 80 data subset, as indicated by a bias in the residuals of 6.2°F. An alternative model that eliminates this conservatism can be developed by recalibrating the upper limit on Cu in Equation 4-1 to obtain different values for Linde 80 welds and for all other welds. This model was fitted while holding all other parameters fixed to the values in Equation 4-1, so no additional model equation appears in Table D.1 for this alternative. Note that the upper Cu limit originally fitted to the entire data base (0.30 wt%) was actually determined by weld data, since there are no forging or plate data in the calibration set with Cu above 0.25 wt%. When fitting Linde 80 and all other welds separately, the fitted value of the upper Cu limit for Linde 80 welds is 0.26 wt%, and the limit for all other welds is 0.32 wt%. The upper limit on Cu for plates and forgings can not be determined from the data base; it is sufficient for this discussion to continue to assume the overall weld value of 0.30 wt%.

Residual plots are shown for all weld data together, using the two upper Cu limits given above, in Figure D.10. These can be compared to Figure 4.12 where the single upper Cu limit of 0.30 wt% was used. The recalibration improves the fit to the Linde 80 subset, from S_d = 23.5°F in Table 4.1 to S_d = 21.6°F in this alternative, but the bias becomes slightly unconservative (-0.7°F). The quality of fit to all other (non-Linde 80) welds is about the same as before: S_d = 25.4°F for all other welds in this alternative versus S_d = 25.6°F for all other welds using Equation 4-1; the fits to forgings and plates are unaffected. Figures D.11 and D.12 show the normalized Cu effect for Equation 4-1 and the model with two separate upper Cu limits, respectively. For both Linde 80 welds and all other welds, the data at high Cu are better centered about the model when two separate limits are used. The same approach could, in principle, be used to recalibrate upper Cu limits for weld subsets other than Linde 80 welds, but in some cases there are not enough high Cu points to establish saturation. Before adopting separate values, further investigation is clearly warranted to establish whether or not these separate upper limits are reasonable relative to factors such as differences in Ni content and details of the actual post-weld heat treatment procedures.

These unresolved issues, the question of how many data points are needed to establish saturation with confidence, and the slightly unconservative bias of the separate Linde 80 model are the reasons for not adopting separate upper limits on Cu. Additional research may make it feasible to replace the fitted value of the upper Cu limit by a Cu-in-solution submodel.

Equation 4-1 with flux term in place of irradiation time term and calibrated to data set with negative shifts set to zero

As discussed in Section 4.2, the data set used for calibration of the models presented here included some negative shifts, despite the belief that the Charpy transition temperature for reactor pressure vessel steels does not decrease during irradiation. In fact, the mathematical form of the models presented here actually precludes the prediction of negative shifts. Under the alternative approach presented in Section 4.2, Equation 4-1 has also been calibrated with the negative shift values set to zero; this model is shown in Table D.1, with residual plots shown in Figure D.13. This model also has been presented elsewhere (Eason, et al., 1997). Note that the irradiation time term in Equation 4-1 has been replaced by an equivalent flux term, since this is the form of the model presented in the Reference. The improvement in standard error - 22.1°F compared to 23.0°F - is solely due to setting the negative shifts to zero.

Figures D.14 and D.15 present the same information for the model with negative shifts set to zero as is presented in Figures 4.7 and 4.8 using negative shifts as computed. If the corresponding figures are overlaid, the difference is less than the line width of the curves above 10^{18} n/cm^2. Below that fluence, there is a small but evident difference, with the estimated shift being higher for the case with negative shifts set to zero.

REFERENCE

Eason, E. D., J. E. Wright, and G. R. Odette, "An Improved Embrittlement Correlation for Reactor Pressure Vessel Steels," *8th International Symposium on Environmental Degradation of Materials in Nuclear Power Systems - Water Reactors*, NACE International, August 1997, pp 889-896.

Table D.1 Alternative TTS models

Model	S_e, °F
Equation 4-1 (shown for reference, see Figure 4.6) $TTS = \begin{Bmatrix} 1.23\times10^{-7}, \text{p} \\ 8.98\times10^{-8}, \text{f} \\ 1.10\times10^{-7}, \text{w} \end{Bmatrix} \exp\left(\frac{1.906\times10^{4}}{T_c+460}\right)(1+57.7P)\left(\frac{\phi t}{10^{19}}\right)^{\left[0.4449+0.0597\log\left(\frac{\phi t}{10^{19}}\right)\right]}$ $+\begin{Bmatrix} 172, \text{p} \\ 135, \text{f} \\ 209, \text{w} \end{Bmatrix}(Cu-0.072)^{0.678}(1+2.56Ni^{1.358})\left\{\frac{1}{2}+\frac{1}{2}\tanh\left[\frac{\log(\phi t+5.48\times10^{12}t_i)-18.290}{0.600}\right]\right\}$ $0.072 \le Cu \le 0.300$ wt%	23.0
Ni term in fluence *tanh* (Figure D.1) $TTS = \begin{Bmatrix} 2.06\times10^{-7}, \text{p} \\ 1.50\times10^{-7}, \text{f} \\ 1.82\times10^{-7}, \text{w} \end{Bmatrix} \exp\left(\frac{1.849\times10^{4}}{T_c+460}\right)(1+65.5P)\left(\frac{\phi t}{10^{19}}\right)^{\left[0.4669+0.0594\log\left(\frac{\phi t}{10^{19}}\right)\right]}$ $+\begin{Bmatrix} 155, \text{p} \\ 121, \text{f} \\ 189, \text{w} \end{Bmatrix}(Cu-0.073)^{0.662}(1+2.89Ni^{1.474})\left\{\frac{1}{2}+\frac{1}{2}\tanh\left[\frac{\log(\phi t+8.42\times10^{12}t_i)-0.391Ni-18.033}{0.506}\right]\right\}$ $0.073 \le Cu \le 0.300$ wt%	22.8
No phosphorous term (Figure D.2) $TTS = \begin{Bmatrix} 4.92\times10^{-8}, \text{p} \\ 3.52\times10^{-8}, \text{f} \\ 5.26\times10^{-8}, \text{w} \end{Bmatrix} \exp\left(\frac{2.045\times10^{4}}{T_c+460}\right)\left(\frac{\phi t}{10^{19}}\right)^{\left[0.4602+0.0573\log\left(\frac{\phi t}{10^{19}}\right)\right]}$ $+\begin{Bmatrix} 181, \text{p} \\ 156, \text{f} \\ 216, \text{w} \end{Bmatrix}(Cu-0.072)^{0.682}(1+2.36Ni^{1.368})\left\{\frac{1}{2}+\frac{1}{2}\tanh\left[\frac{\log(\phi t+5.73\times10^{12}t_i)-18.269}{0.578}\right]\right\}$ $0.072 \le Cu \le 0.300$ wt%	23.1

Model	S_e, °F
No irradiation time term (Figure D.3) $TTS = \begin{Bmatrix} 7.22\times10^{-8}, \text{p} \\ 5.17\times10^{-8}, \text{f} \\ 6.11\times10^{-8}, \text{w} \end{Bmatrix} \exp\left(\frac{1.961\times10^{4}}{T_c+460}\right)(1+62.0P)\left(\frac{\phi t}{10^{19}}\right)^{\left[0.4132+0.0595\log\left(\frac{\phi t}{10^{19}}\right)\right]}$ $+\begin{Bmatrix} 172, \text{p} \\ 136, \text{f} \\ 215, \text{w} \end{Bmatrix}(Cu-0.074)^{0.661}(1+2.56Ni^{1.359})\left\{\frac{1}{2}+\frac{1}{2}\tanh\left[\frac{\log(\phi t)-18.288}{0.759}\right]\right\}$ $0.074 \le Cu \le 0.300$ wt%	23.0
No irradiation time term and constant fluence power (Figure D.4) $TTS = \begin{Bmatrix} 3.85\times10^{-8}, \text{p} \\ 2.69\times10^{-8}, \text{f} \\ 3.19\times10^{-8}, \text{w} \end{Bmatrix} \exp\left(\frac{2.030\times10^{4}}{T_c+460}\right)(1+60.6P)\left(\frac{\phi t}{10^{19}}\right)^{0.3982}$ $+\begin{Bmatrix} 177, \text{p} \\ 142, \text{f} \\ 225, \text{w} \end{Bmatrix}(Cu-0.074)^{0.667}(1+2.59Ni^{1.360})\left\{\frac{1}{2}+\frac{1}{2}\tanh\left[\frac{\log(\phi t)-18.308}{0.885}\right]\right\}$ $0.074 \le Cu \le 0.300$ wt%	23.1
No phosphorous term, no irradiation time term, and constant fluence power (Figure D.6) $TTS = \begin{Bmatrix} 1.04\times10^{-8}, \text{p} \\ 7.27\times10^{-9}, \text{f} \\ 1.07\times10^{-8}, \text{w} \end{Bmatrix} \exp\left(\frac{2.207\times10^{4}}{T_c+460}\right)\left(\frac{\phi t}{10^{19}}\right)^{0.4132}$ $+\begin{Bmatrix} 192, \text{p} \\ 168, \text{f} \\ 235, \text{w} \end{Bmatrix}(Cu-0.072)^{0.683}(1+2.35Ni^{1.381})\left\{\frac{1}{2}+\frac{1}{2}\tanh\left[\frac{\log(\phi t)-18.270}{0.849}\right]\right\}$ $0.072 \le Cu \le 0.300$ wt%	23.3

Model	S_e, °F
Decreasing phosphorous effect with increasing copper content and nickel in fluence *tanh* (Figure D.7) Note: lower limit on Cu applies only in the second term; upper limit applies in both terms. $$TTS = \begin{Bmatrix} 2.70\times10^{-8}, \text{p} \\ 1.76\times10^{-8}, \text{f} \\ 2.10\times10^{-8}, \text{w} \end{Bmatrix} \exp\left(\frac{2.030\times10^{4}}{T_c+460}\right)\left[1+151P\exp(-3.31\,Cu)\right]\left(\frac{\phi t}{10^{19}}\right)^{\left[0.4741+0.0689\log\left(\frac{\phi t}{10^{19}}\right)\right]}$$ $$+\begin{Bmatrix} 224, \text{p} \\ 190, \text{f} \\ 284, \text{w} \end{Bmatrix}(Cu-0.072)^{0.777}(1+2.62Ni^{1.402})\left\{\frac{1}{2}+\frac{1}{2}\tanh\left[\frac{\log(\phi t+7.23\times10^{12}t_i)-0.392Ni-18.045}{0.575}\right]\right\}$$ $$0.072 \le Cu \le 0.259 \text{ wt\%}$$	22.8
No dependence on product form (Figures D.8 and D.9) $$TTS = 6.36\times10^{-8}\exp\left(\frac{1.958\times10^{4}}{T_c+460}\right)(1+54.7P)\left(\frac{\phi t}{10^{19}}\right)^{\left[0.4702+0.0739\log\left(\frac{\phi t}{10^{19}}\right)\right]}$$ $$+296(Cu-0.070)^{0.831}(1+2.21\,Ni^{1.556})\left\{\frac{1}{2}+\frac{1}{2}\tanh\left[\frac{\log(\phi t+6.83\times10^{12}t_i)-18.298}{0.576}\right]\right\}$$ $$0.070 \le Cu \le 0.300 \text{ wt\%}$$	23.8
Equation 4-1 with flux term in place of irradiation time term and calibrated to data set with negative shifts set to zero (Figure D.13) $$TTS = \begin{Bmatrix} 2.43\times10^{-7}, \text{p} \\ 1.82\times10^{-7}, \text{f} \\ 2.18\times10^{-7}, \text{w} \end{Bmatrix} \exp\left(\frac{1.843\times10^{4}}{T_c+460}\right)(1+54.3P)\left(\frac{\phi t}{10^{19}}\right)^{\left[0.4265+0.0761\log\left(\frac{\phi t}{10^{19}}\right)\right]}$$ $$+\begin{Bmatrix} 167, \text{p} \\ 130, \text{f} \\ 203, \text{w} \end{Bmatrix}(Cu-0.074)^{0.673}(1+2.62Ni^{1.356})\left(\frac{1}{2}+\frac{1}{2}\tanh\left\{\frac{\log\left[\phi t\left(1+\frac{1.77\times10^{9}}{\phi}\right)\right]-18.304}{0.584}\right\}\right)$$ $$0.074 \le Cu \le 0.300 \text{ wt\%}$$	22.1

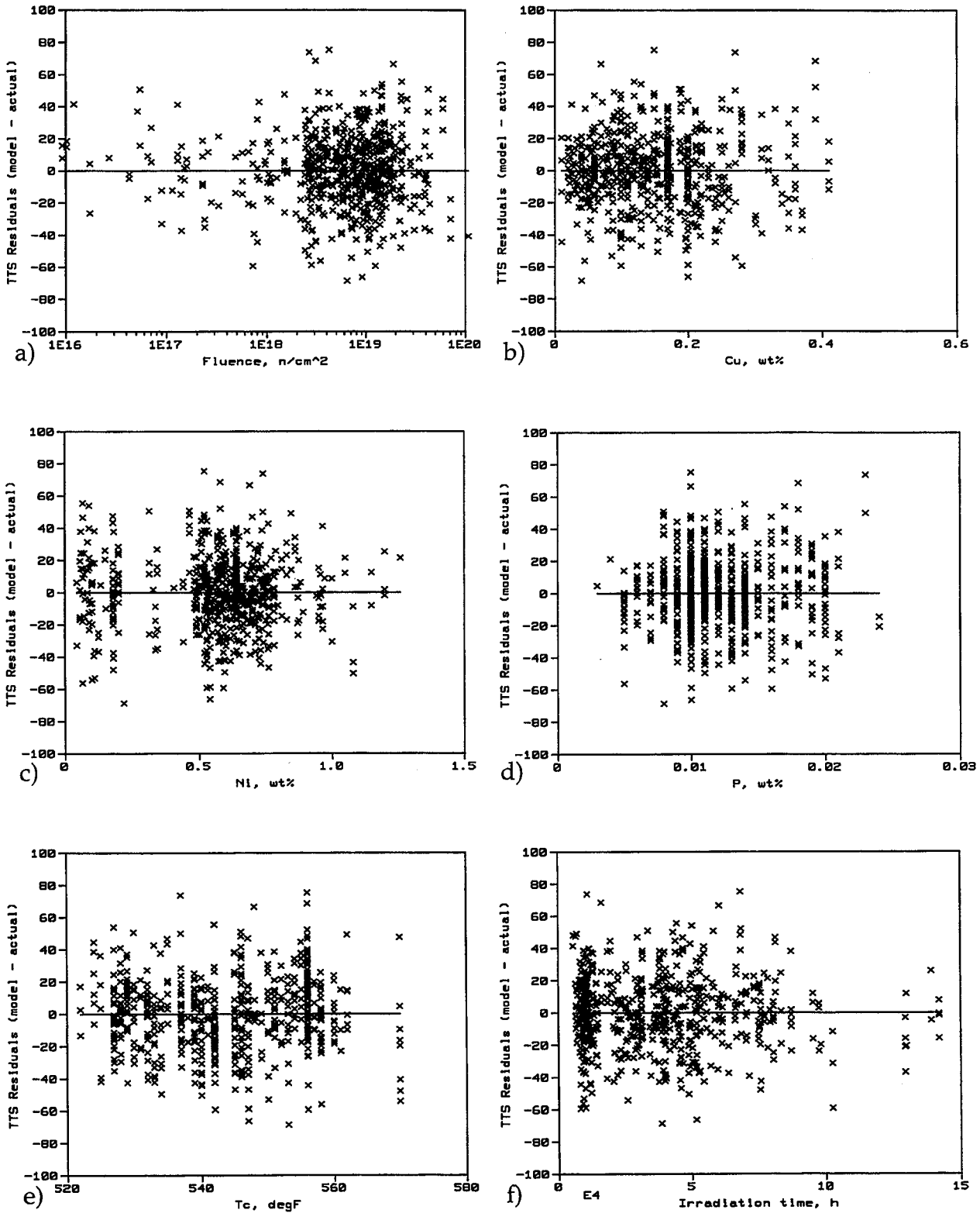

Figure D.1 Residual plots for TTS model with Ni term in fluence *tanh*

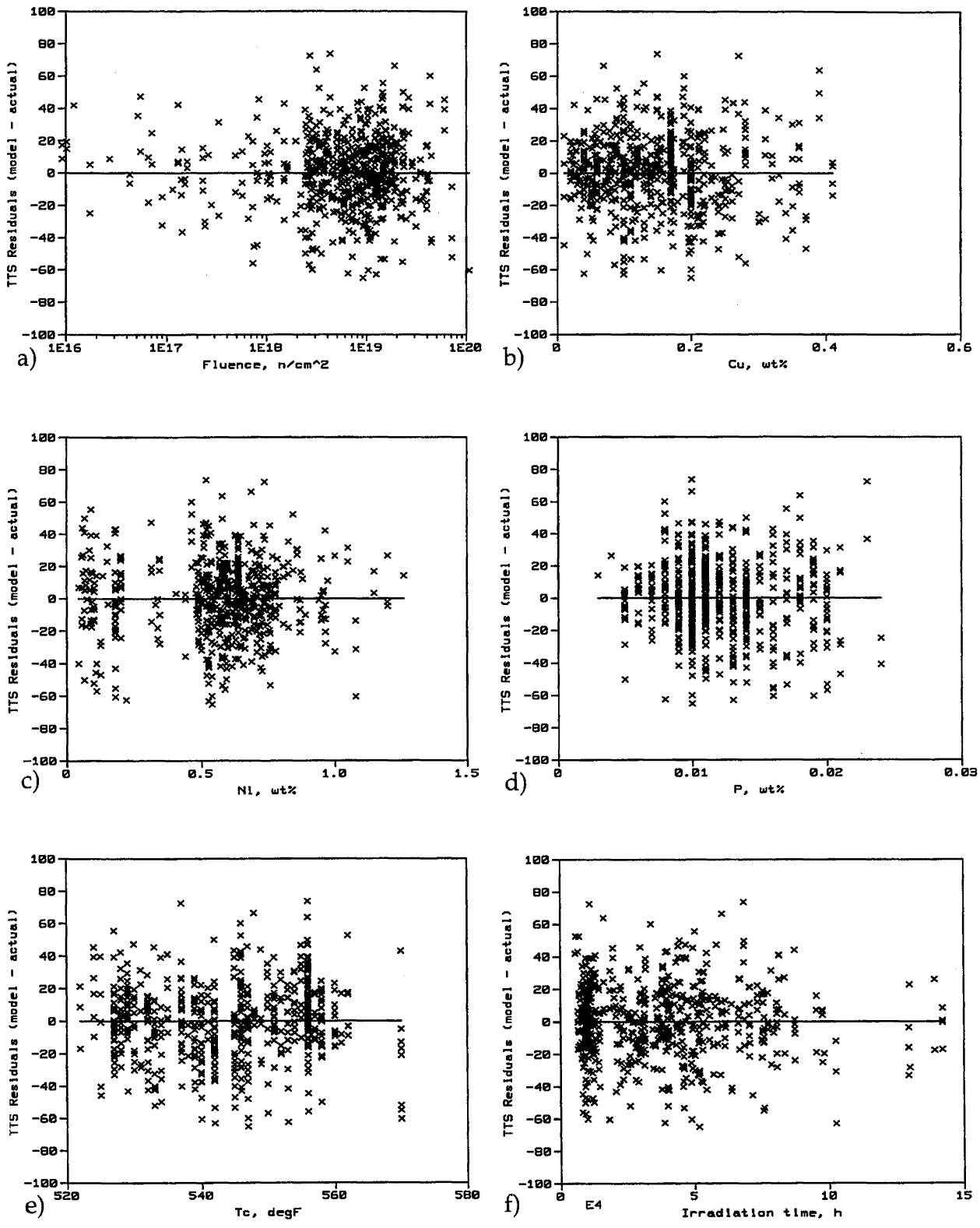

Figure D.2 Residual plots for TTS model without phosphorous

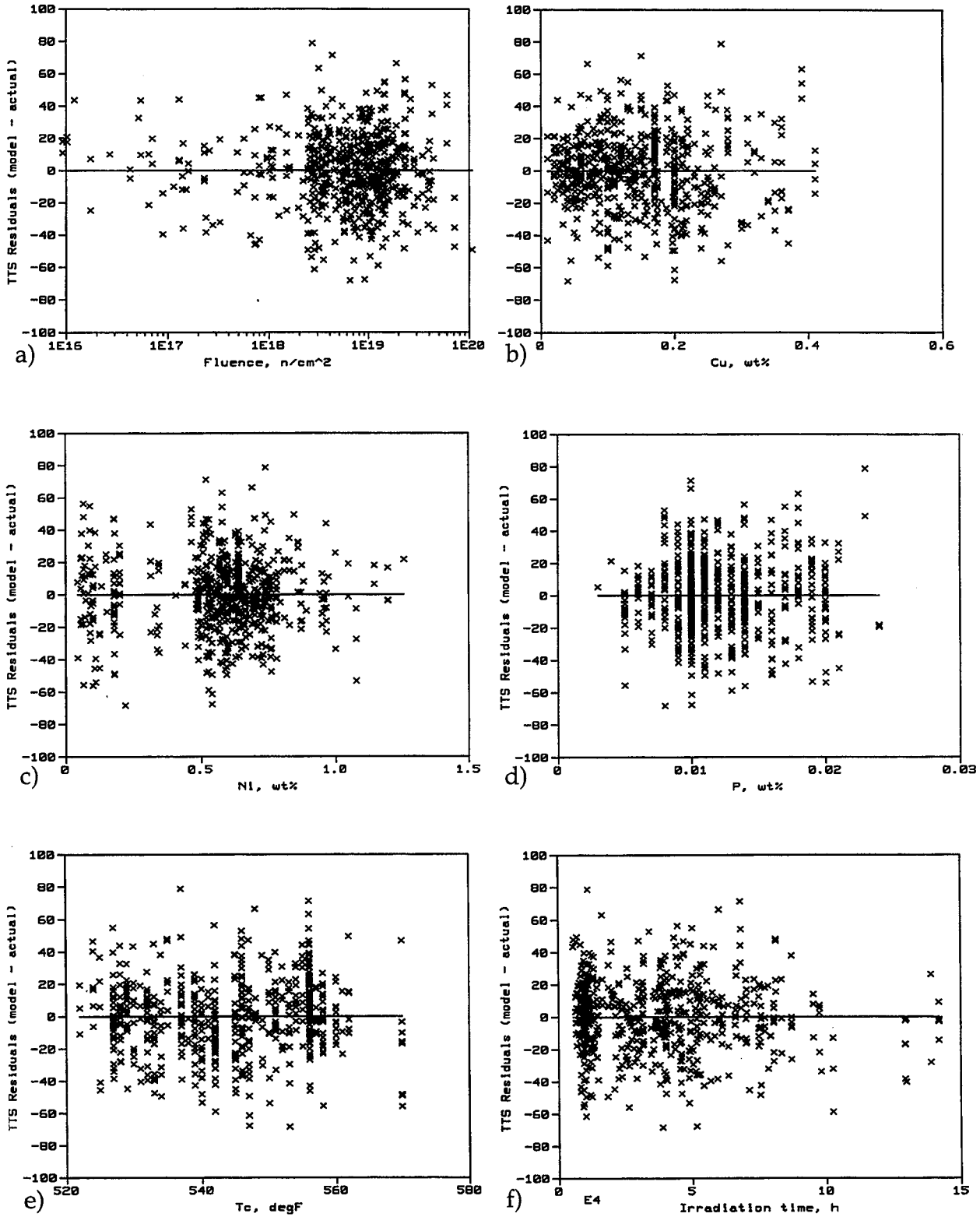

Figure D.3 Residual plots for TTS model without irradiation time

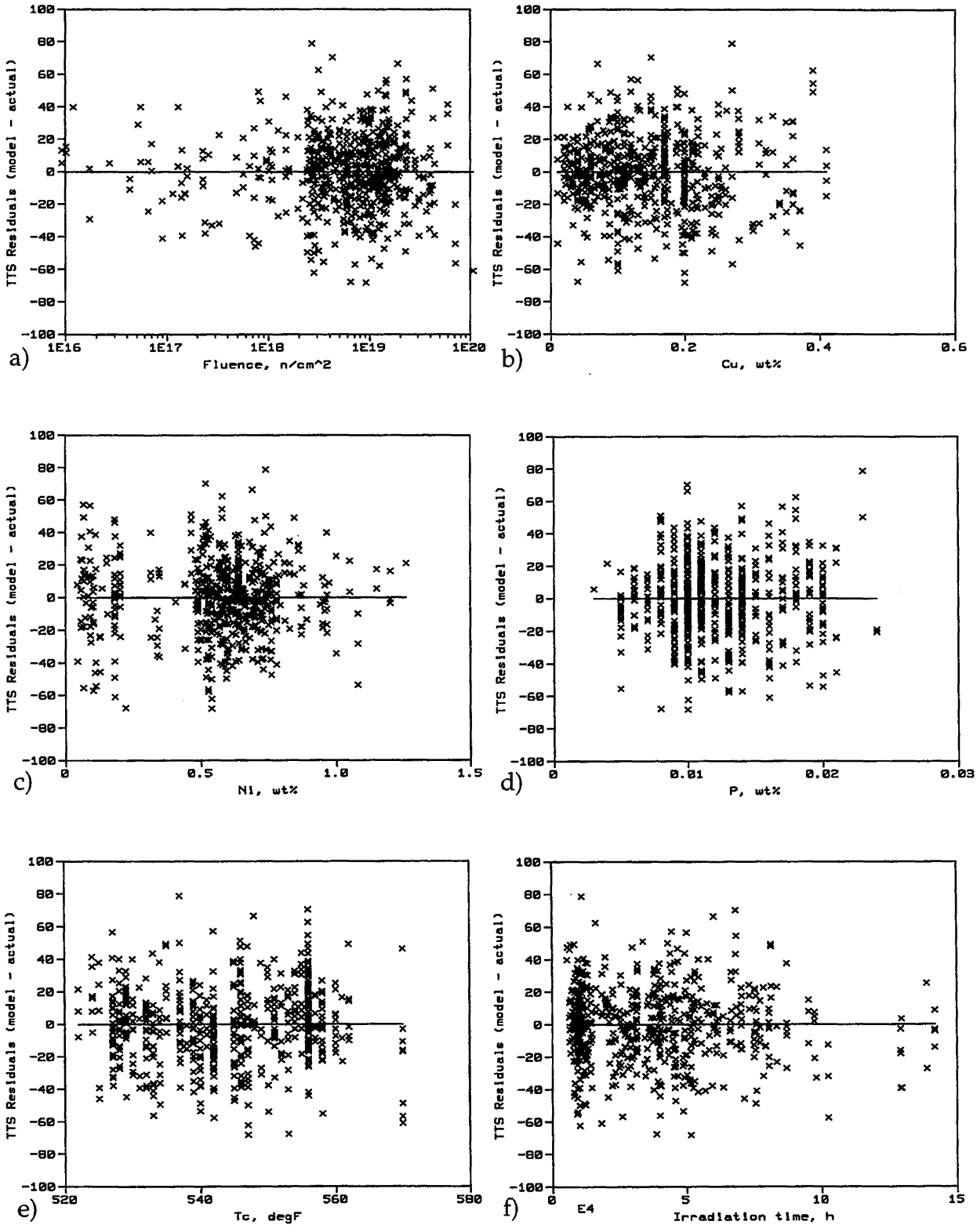

Figure D.4 Residual plots for TTS model without irradiation time and with constant power on fluence in SMD term

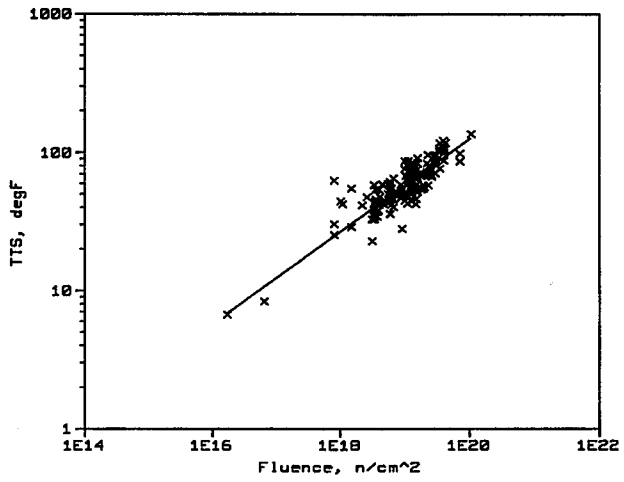

Figure D.5 Low Cu data fitted for power on fluence in matrix defect term of TTS model

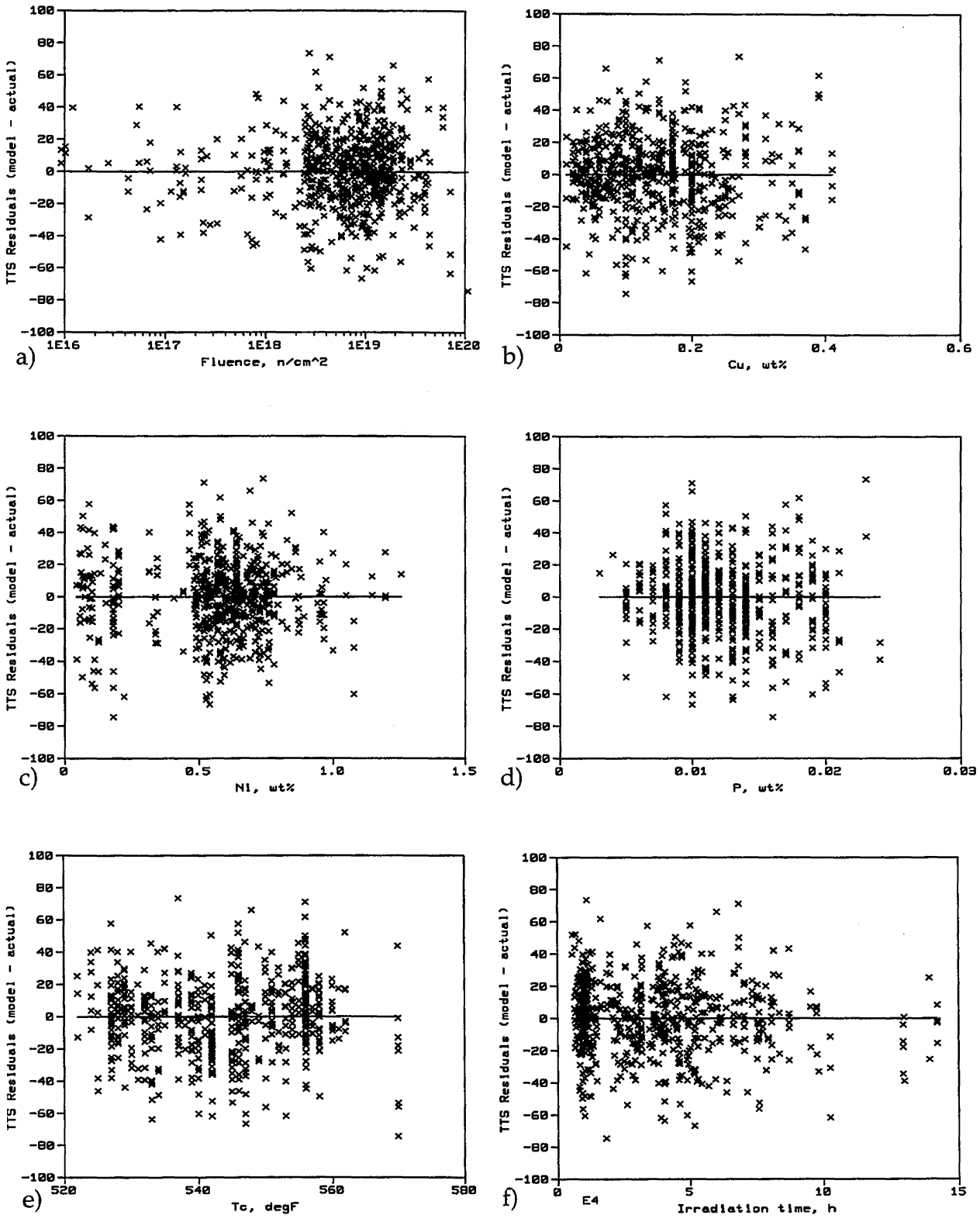

Figure D.6 Residual plots for TTS model without phosphorous or irradiation time and with constant power on fluence in SMD term

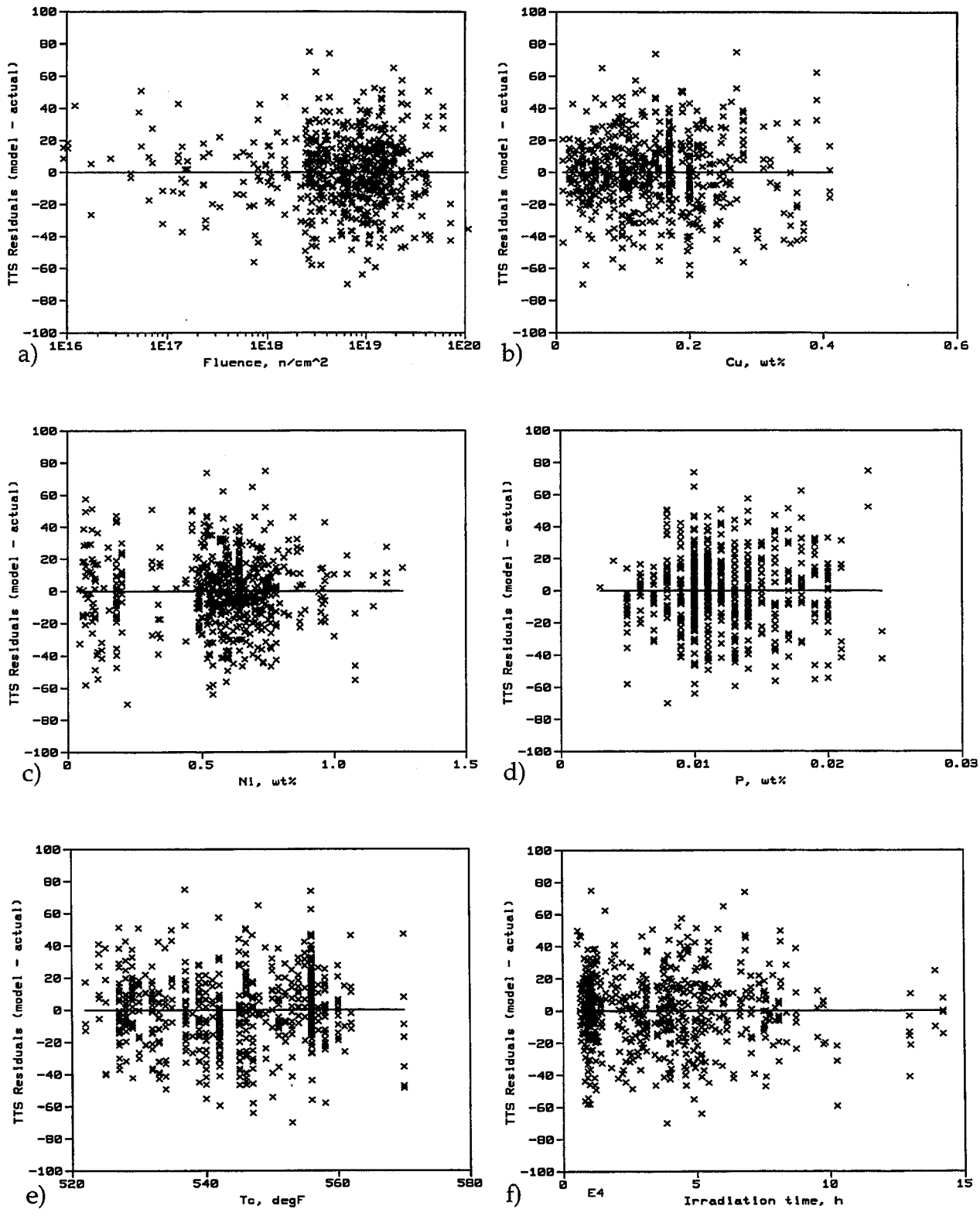

Figure D.7 Residual plots for TTS model with decaying phosphorous term and Ni in fluence *tanh*

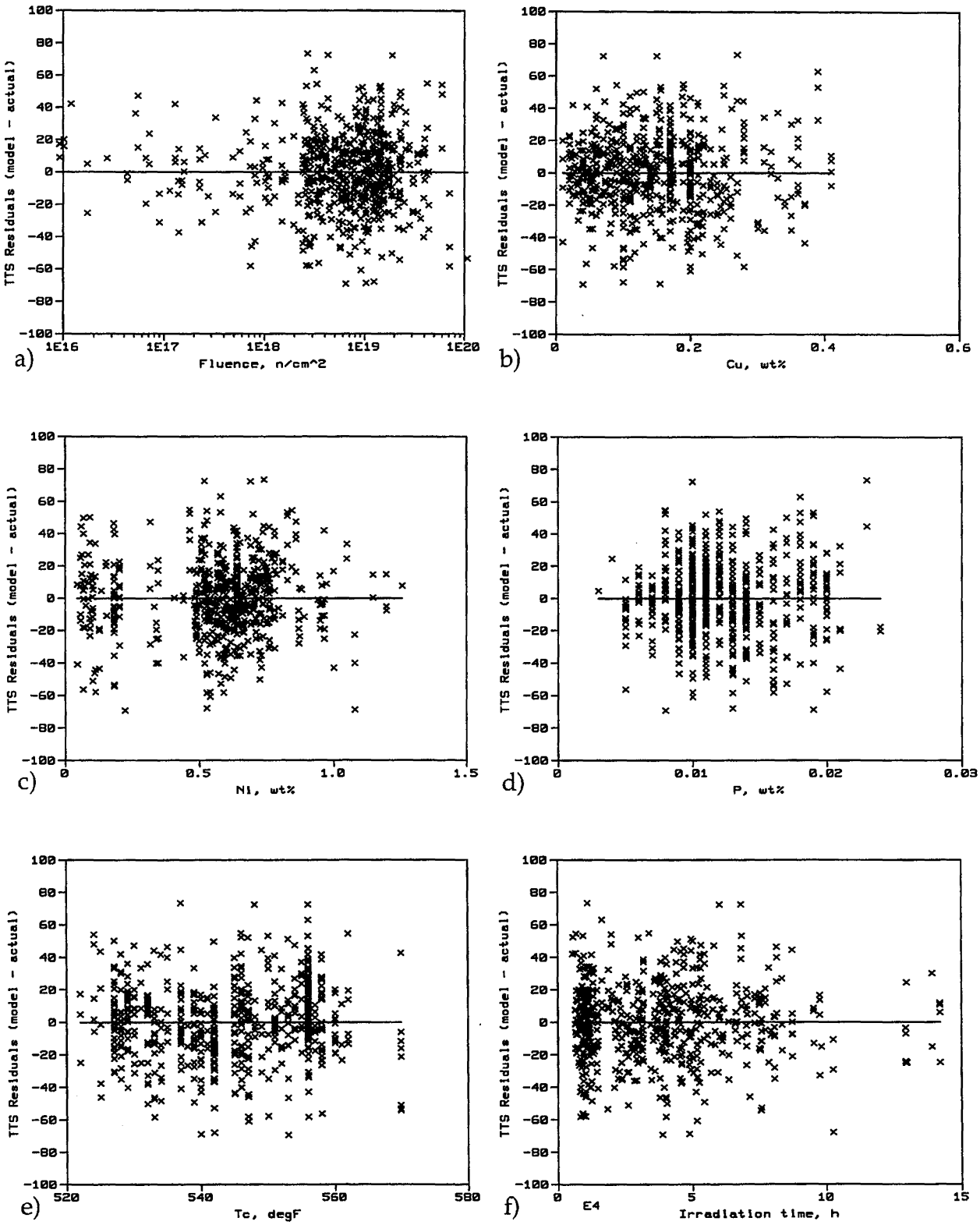

Figure D.8 Residual plots for TTS model without product form

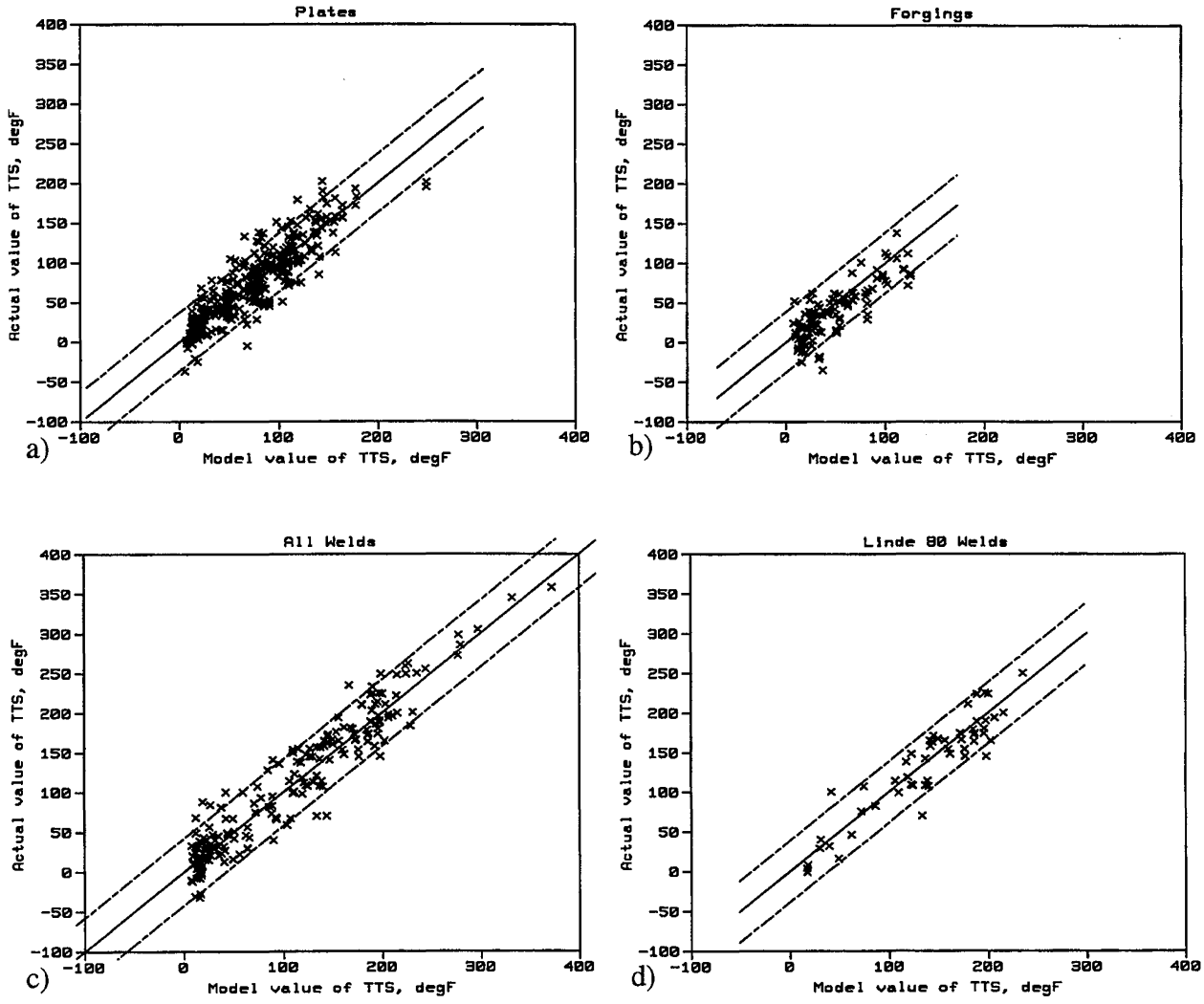

Figure D.9 Predicted versus actual plots for subsets of data for TTS model without product form

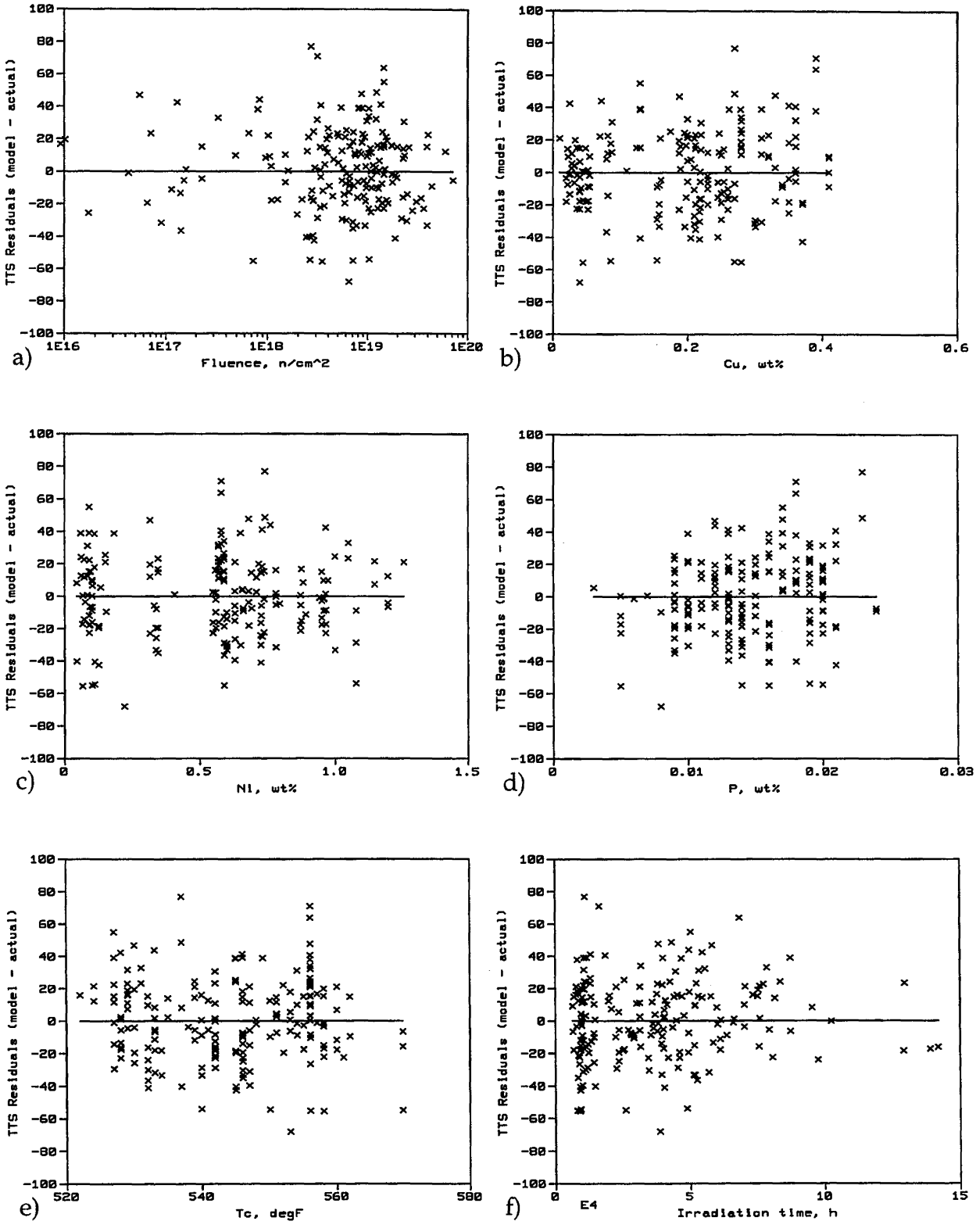

Figure D.10 Residuals of weld data about TTS model with different Cu saturation values for Linde 80 welds versus other welds

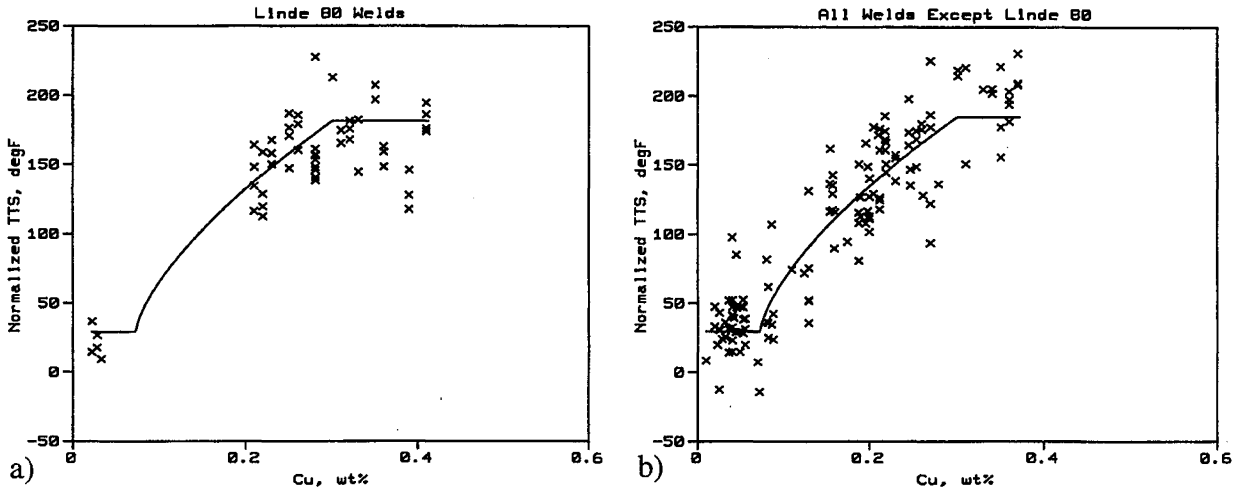

Figure D.11 Normalized plots for Equation 4-1 showing data from Linde 80 welds and all other welds (upper Cu limit = 0.30 wt%)

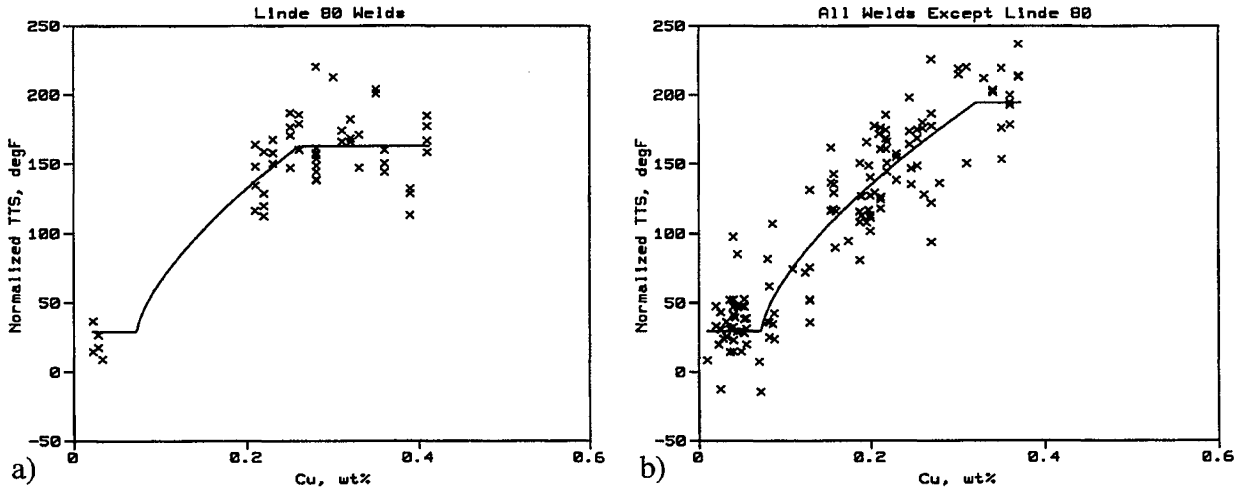

Figure D.12 Normalized plots for TTS model with different Cu saturation values showing data from Linde 80 welds (upper Cu limit = 0.26 wt%) and all other welds (upper Cu limit = 0.32 wt%)

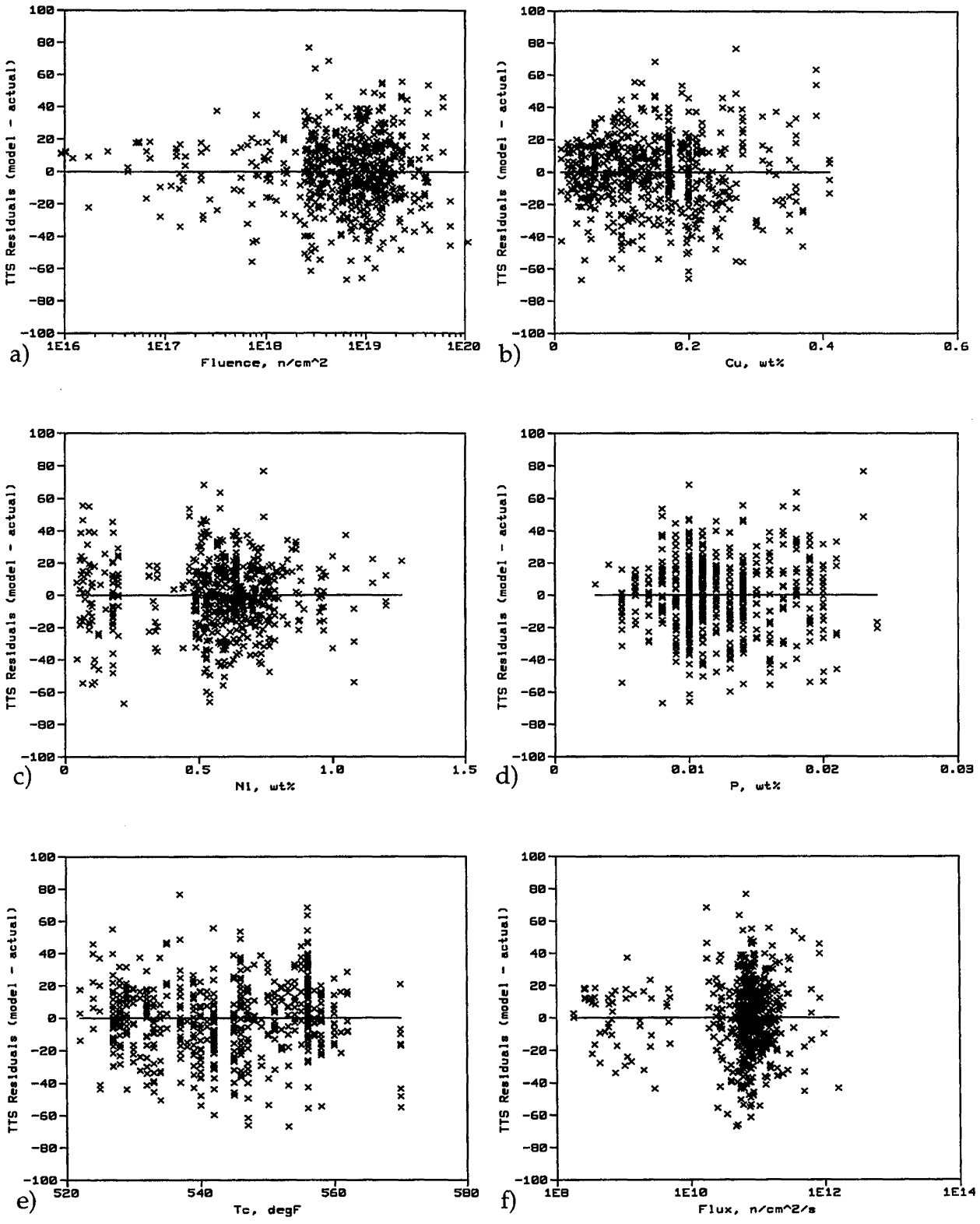

Figure D.13 Residual plots for TTS model with flux term instead of irradiation time term and calibrated to data set with negative shifts set to zero

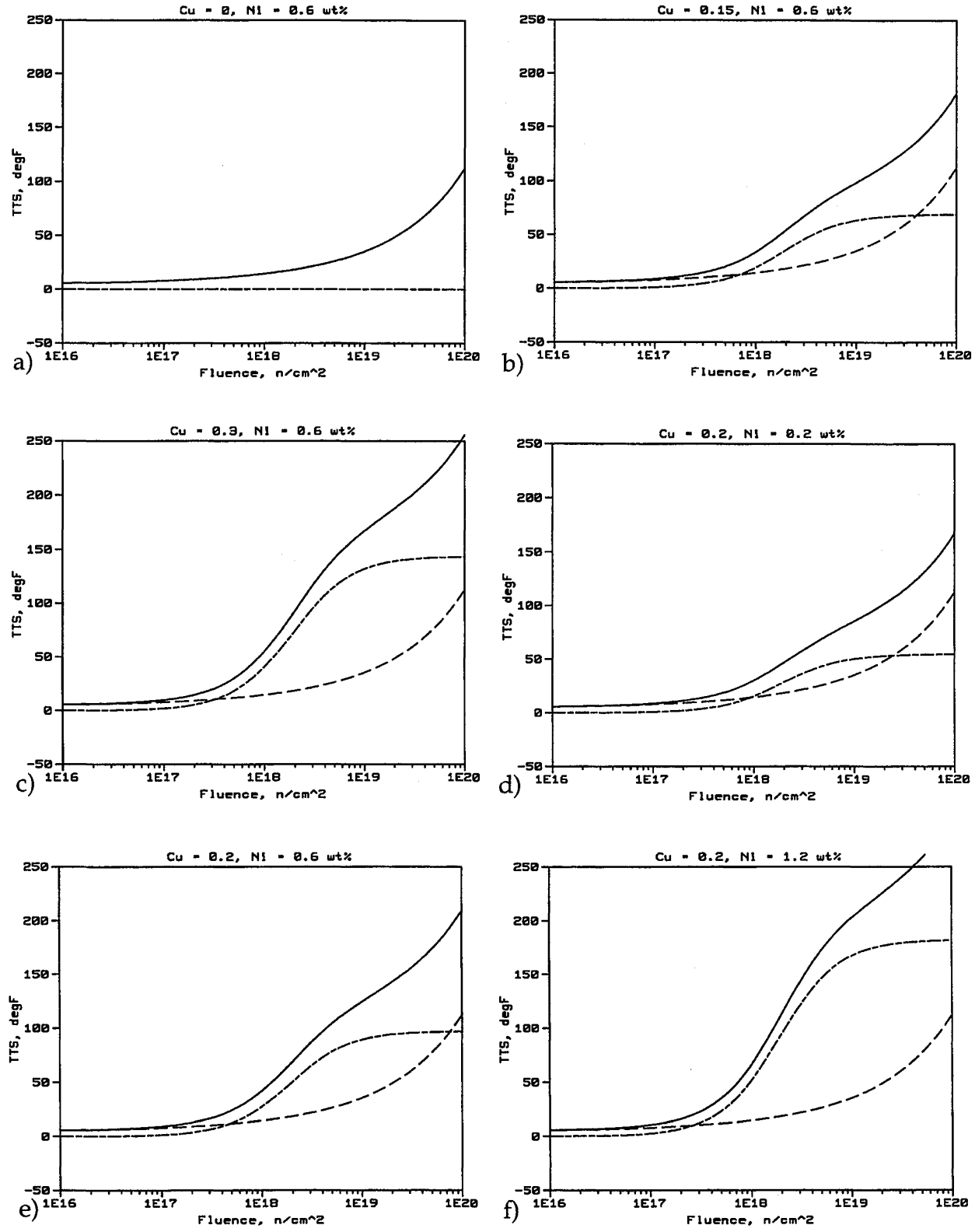

Figure D.14 Contributions of SMD and CRP terms of TTS model (with ϕ instead of t_i and calibrated to data set with zeroed negative shifts) to overall embrittlement for various Cu and Ni values

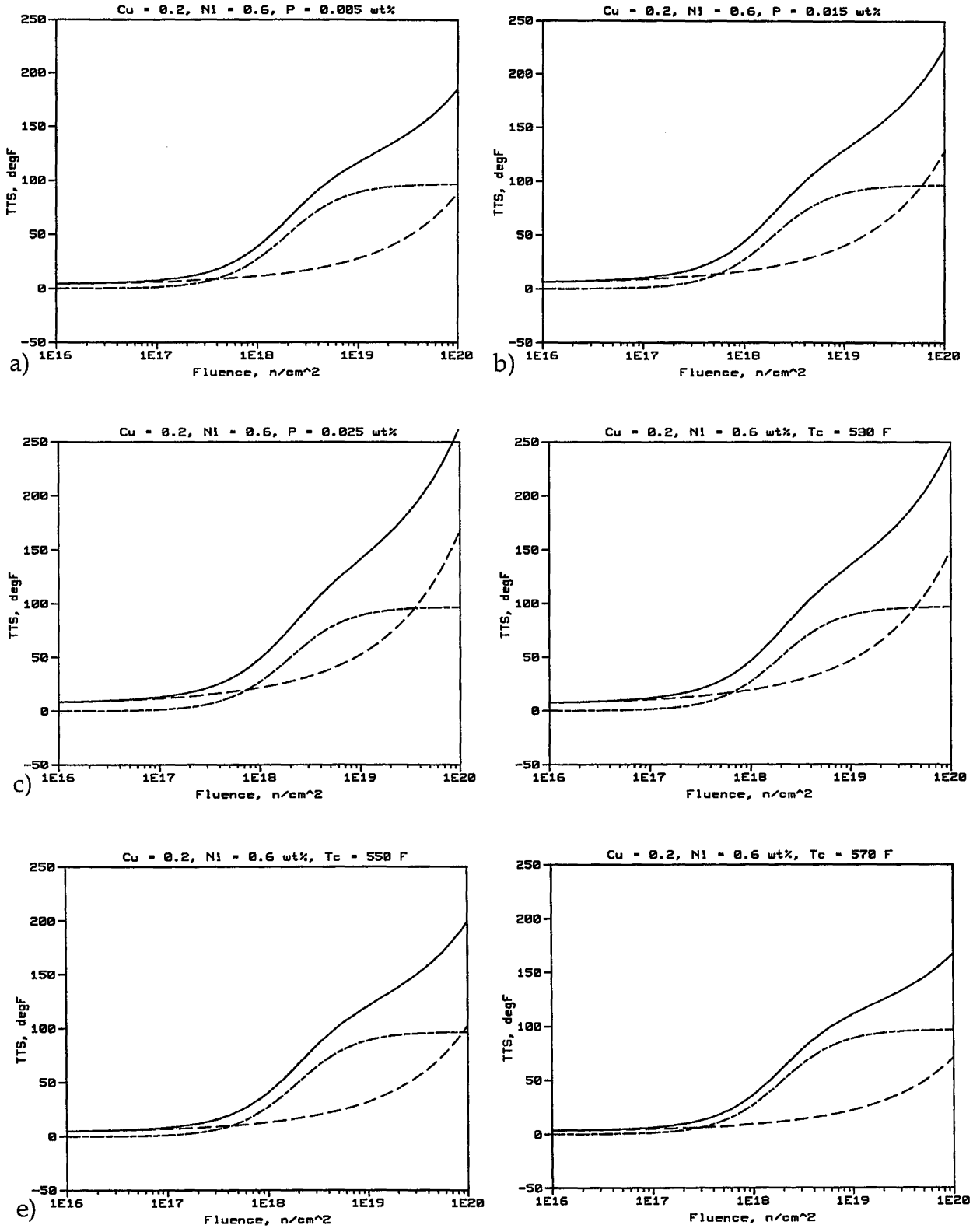

Figure D.15 Contributions of SMD and CRP terms of TTS model (with ϕ instead of t_1 and calibrated to data set with zeroed negative shifts) to overall embrittlement for various P and T_c values

APPENDIX E
M&CS QUALITY ASSURANCE PROCEDURES

1 Guiding Principles

The quality assurance (QA) program at Modeling & Computing Services (M&CS) is made up of guiding principles and policy. Specific policies are discussed in subsequent subsections. The guiding principles are as follows:

1.1 All M&CS work product related to a final result shall be independently checked by a second engineer. This includes, but is not limited to, hand calculations, computer programs and subroutines, the transference of data from the output of one program to the input of another, and the transcription of results from computer programs or other documents to reports.

1.2 All computer programs used for M&CS work product, whether publicly available or internally generated, shall be checked for correctness.

1.3 All results presented in final reports shall be supported by a written QA package. This package must contain a copy of the report and back-up material. The back-up material is organized in such a way that another experienced engineer could duplicate all the calculations.

1.4 Subcontractors to M&CS shall follow their own quality assurance procedures on all work performed for M&CS.

2 General Policy

Subsequent subsections describe quality assurance policy related to data files, software, models, and reports. This subsection describes more general policy.

2.1 The QA package for all work product shall be maintained for a minimum of three years past the end of the project. This package includes both written and electronic forms sufficient to reproduce the original work.

2.2 The QA procedures described in this document are considered the minimum acceptable for any M&CS work. For contracts requiring additional QA, the additional requirements for retention period, acceptance criteria, verification, or documentation will be defined as a part of the job scope. Such additional QA requirements should be appended to a copy of this document.

2.3 Every employee of M&CS is responsible for carrying out the letter and intent of this quality assurance policy. Ernest Eason has primary responsibility for the development, implementation, and maintenance of the QA program.

2.4 Major software development projects shall divide the work into phases and identify the verification procedures to be carried out at the end of each phase. The verification results should be recorded and checked when the actions are completed.

3 Database Policy

3.1 When a database arrives at M&CS, a copy of the raw database is archived.

3.2 Data are often edited or keyed into a data file by hand at M&CS. Before such data are used, each entry is checked by a second staff person, who initials a printout of the data entered.

3.3 When a database is analyzed at M&CS, one or more of the following steps are taken to identify and resolve discrepancies:

3.3.1 The database is screened to:

a. determine ranges of variables
b. compute statistics for each variable (mean, median, standard deviation, etc.)
c. produce histograms showing data distributions for all variables

3.3.2 Appropriate residual plots with respect to calibrated models are generated for the

database and relevant subsets of the data, noting all outliers and tracing their sources.

3.3.3 Outliers are dispositioned by technical considerations where possible (e.g., known problems with experiments), by objective statistical approaches, or based on documented engineering judgment.

3.3.4 When data are missing or appear suspicious, the originator of the data is contacted to resolve the discrepancy. Written records of such contacts and the originator's response are maintained in the project file.

Note: Which of the above steps are taken generally depends on project scope and schedule.

3.4 The final database used for calibrating models shall be archived.

4 Software Policy

4.1 Software QA may include one or more of the following, as appropriate:

4.1.1 The software demonstrates the ability to correctly solve one or more problems with known solutions.

4.1.2 Results on one or more test problems are compared to results from other software products that are intended to solve the same problem and that are believed to be reliable.

4.1.3 The software results are compared to bounding cases developed with asymptotic estimates or other hand calculations to ensure reasonableness.

4.1.4 The software is exercised via parametric studies to assure reasonableness over a range of conditions.

Note: Compliance with procedures 4.1.1, 4.1.2, and/or 4.1.3 is preferred whenever possible. Procedure 4.1.4 should only be used for those codes that are unique and for which no problems with known solutions or software intended to solve the same problem are available.

4.2 Some problems are simple enough that one can check the software definitively by solving a handful of basic problems. Such cases include without limitation linear equation solvers. When such simple checks are possible, they shall be performed.

4.3 For more complicated nonlinear problems, a simple definitive check is often impossible. The convergence of nonlinear codes is often strongly dependent on the problem and the initial solution estimate. The algorithm may not converge on any particular problem, and if it does, there may not be a unique solution. Steps to be taken to check such software shall include:

4.3.1 The calculated results and convergence monitoring information are evaluated in view of the input data and the expected nature of the solution.

4.3.2 The software results are compared to bounding cases developed with asymptotic estimates or other hand calculations to ensure reasonableness, where possible.

4.3.3 For all iterative techniques, more than one initial estimate shall be employed to learn a) whether the algorithm converges to multiple solutions and b) which solution is most reasonable.

4.4 Each software verification is documented in writing, including the input and output files and hand calculations, if any. Later, as the software is modified, the old verification problems are re-run to confirm that the new modifications have not affected the code's ability to solve earlier problems.

4.5 When a piece of software arrives at M&CS: a) a copy of the software is saved permanently, and b) an initial check of the software is performed.

4.6 Some software is to be used on only one project. QA documentation is then stored with the project files.

4.7 Some software is intended for use on multiple projects. QA documentation is then stored in a software file, which will contain solved verification problems, records of software changes, etc.

5 Correlation Model Policy

5.1 When correlations and physically-motivated models are developed by fitting to data, the reasonableness of the model shall be assessed by plotting the effects of each variable in the model and the data, normalized to common conditions of the variables not plotted.

5.2 The model shall be plotted over the intended range of application to understand how it interpolates and extrapolates. The limits of applicability shall be stated in the report on the model.

5.3 The quality of fit of the model to the calibration data shall be assessed by two or more of the following methods, as appropriate.

5.3.1 The standard error of estimate, defined as the square root of (sum of squared residuals divided by number of degrees of freedom).

5.3.2 Plot(s) of predicted versus measured values of the dependent variable.

5.3.3 Residual plots for each independent variable in the model and potential model variables.

5.3.4 Plots such as 5.3.2 and 5.3.3 for appropriate subsets of the database.

5.4 Where curve-fit models are intended to predict results for conditions different from the data on which they are calibrated, it is M&CS policy for one or more of the following validations to be performed, as appropriate:

5.4.1 The model shall be compared to data not used for calibration.

5.4.2 The predictions of the model shall be compared to predictions of other models developed using other data.

5.4.3 Predictions of the model shall be confirmed by other generally-accepted engineering techniques, including (without limitation) detailed analysis and testing.

Note: The preferred method for validating the predictive capability of a model is 5.4.1. This validity check can be implemented in more than one way. One approach is to use all available data for calibrating the model, in anticipation of additional experimental data becoming available during the course of the project. Then the new data can be used as an independent validation set. A second approach is to set aside a portion of the currently-available data, say 20%, and perform the calibration on the other 80%. Then the data that were reserved may be used to verify the predictive capability. A third approach is to compare the results of fitting to several subsets of the available data.

6 Report Policy

6.1 All results presented in final reports shall be supported by a written QA package. This package must contain a copy of the report and the following items in a neat and organized manner.

6.2 A Report QA Summary, which shows that each section of the report was checked for technical content, calculations and other results, and editorial style.

6.3 All hand calculations that directly support the results in the report shall be preserved in written form, in enough detail so that another experienced engineer could duplicate the calculation. Each such calculation must be checked by an independent checker who shall initial and date the calculation document to indicate acceptability.

6.4 All computer calculations shall be preserved both in electronic and printed form where possible, including program listings or the revision level of commercial codes, as appropriate, output files, and input files. Where multiple versions exist, documentation of which version of input file and program was used for the particular run must be recorded for each result appearing in the report. Each of these documents and their relationship to each other shall be checked by an independent reviewer who shall initial and date the documents to indicate their acceptability.

6.5 All databases used in analysis shall be maintained in their original form, as well as the

form used for producing the results presented in the report. The differences between the original databases and the final form used in the report shall be documented, either on database documents or as notes in database or "README" files, and in the report. Where multiple versions or subsets of a database are used, each such subset of data shall be identified, e.g., with a version number, so that any result in the report can be traced to the version or subset of the database that was used to produce it.

7 Configuration Management

Configuration management provides a mechanism for identifying, controlling, and tracking the versions of software developed or used at M&CS. In many cases older versions still in use must also be maintained and controlled. Configuration management at M&CS contains the following procedures:

7.1 Each version of each software item is identified by a unique name and/or version number.

7.2 Each software item is identified with a particular prime developer.

7.3 The prime developer a) controls all updates of that software item, b) tracks the resolution of any problems reported for that item, and c) maintains a copy of all versions that remain in use.

7.4 Software item versions to be stored include: versions received by M&CS, versions used for major verification efforts, and versions sent out by M&CS.

7.5 Minimum retention period for QA materials is three years past the completion of the project (see Section 2.1). Materials that may be used for other projects are retained indefinitely.

7.6 Before a disk is read into a M&CS computer or sent to a client, a virus check using commercial software is performed.

8 Supplement for NRC Contract 04-92-048

This section customizes M&CS's general QA procedure, described earlier, to the referenced NRC project. The section provides comments specific to the NRC project and specifies some policies that go beyond the normal policy. The section numbers given below refer to the corresponding section numbers in the basic M&CS QA procedure given above. These QA procedures shall apply to all project tasks.

PR-EDB Database Comments

The PR-EDB has been subjected to an extensive QA effort by ORNL, EPRI, vendors, and selected utilities. Additional checking is expected during the course of this project, because most discrepancies and problems in a database are usually found during the analysis of the database. M&CS will cooperate with efforts by ORNL, NRC, ASTM committees and others to check, expand, and correct the PR-EDB during this project, but the primary responsibility for PR-EDB QA remains with its developers at ORNL. The version and revision level of PR-EDB used for the final analysis database shall be documented in the final report.

Database Policy

3.1 When the PR-EDB database or database update arrives at M&CS a copy of the raw database and any associated documentation shall be archived.

3.2 (No supplement.)

3.3 The procedure for selecting data from the PR-EDB for analysis shall be described in the final report, including details on any points identified as outliers. The analysis database derived from the PR-EDB shall be made available for comment prior to calibration of final models.

3.4 The final version of the analysis database used to develop calibrated models shall be archived at M&CS, delivered to the NRC, and reproduced in the final report.

Software Comments

The M&CS software QA procedure described above was applied to the M&CS proprietary software TAC, TACMVS, and SURFIT prior to this contract. These codes were all able to solve problems with known results. They have also been checked against each other, against other software on problems that both can solve (e.g., linear least squares), and by comparing the models they produce to the original raw data on many problems over a period of several years. No additional QA of these codes is anticipated under this

project.

The orthogonal distance regression code (ODR) was developed at the U.S. National Institute of Standards and Technology (NIST) and was extensively QA'd by the developers. It has been used for many studies over a period of several years and compared with problems with known solutions, both at NIST and in papers published in the open literature. In addition, M&CS compared the results of the ODR code to the SURFIT code previously QA'd at M&CS, on hundreds of Charpy datasets in the course of the project.

The FITCV code was developed specifically for this project to analyze raw Charpy data as described in the final report. The software calls SURFIT and ODR, discussed above, fits several models by both methods, and plots the raw data and the best of the fitted models from both SURFIT and ODR for inspection. FITCV was checked by an independent reviewer, by solving problems with known solutions, as well as by reviewing the hundreds of plots produced under this project which present raw data and fitted results. Each of these plots was individually examined as described in the report.

Model Validation Strategy

The methods used for validation include all those given above in sections 5.1-5.3 plus 5.4.1 and 5.4.2 of this Appendix. The results are described in detail in the report.

Retention Period

For the present project, the retention period will be longer than the minimum three-year period in the M&CS QA procedure. Project technical records will be archived for at least ten (10) years. Subcontractors shall maintain their project files for at least ten (10) years. Key results and the final calibration database will be doubly archived, by delivering an electronic copy to the NRC Project Officer.

APPENDIX F
SAMPLE CALCULATIONS

For the convenience of some readers, sample calculations are provided in Table F.1. These are provided simply to give the reader who has programmed Equations 3-2 (to estimate irradiated USE) and/or 4-1 (to estimate TTS) a means of verifying his/her program. Results in the table were computed directly from Equations 3-2 and 4-1 using the number of digits in those equations for each constant (i.e., without the enhanced precision used for some results in the body of the report), so that the readers' results should match exactly. The entries in Table F.1 are not intended to represent any known materials. While some variations in the input variables are shown, no attempt has been made to provide sample calculations for all classes of materials that may be of interest. The stated purpose of the table - providing sample calculations for checking programmed equations - can be achieved with only a few calculations.

Table F.1 Sample calculations

Product Form	Cu wt%	Ni wt%	P wt%	T_c °F	ϕt n/cm^2	t_i h	USE_u ft-lb	USE_i ft-lb (Eq. 3-2)	TTS °F (Eq. 4-1)
Plate	0.2	0.5	0.010	550	2.5×10^{18}	10000	135	113.8	68.3
Plate	0.2	0.5	0.010	550	1.5×10^{19}	75000	135	104.3	118.1
Plate	0.03	0.6	0.005	540	2.5×10^{18}	10000	140	134.2	17.2
Plate	0.03	0.6	0.005	540	1.5×10^{19}	75000	140	132.9	36.4
Forging	0.04	0.7	0.010	530	1.5×10^{19}	75000	130	128.0	39.1
Forging	0.04	0.7	0.010	520	2.5×10^{18}	10000	130	130.1	22.5
Forging	0.17	0.6	0.010	520	1.5×10^{19}	75000	120	100.9	108.3
Forging	0.17	0.6	0.010	530	2.5×10^{18}	10000	120	109.5	56.5
Weld	0.3	0.6	0.015	550	1.5×10^{19}	75000	110	71.2	205.2
Weld	0.3	0.6	0.015	550	2.5×10^{18}	10000	110	83.6	122.6
Weld	0.2	1.0	0.015	540	1.5×10^{19}	75000	145	96.6	222.6
Weld	0.2	1.0	0.015	540	2.5×10^{18}	10000	145	109.3	132.2

NRC FORM 335 (2-89) NRCM 1102, 3201, 3202

U.S. NUCLEAR REGULATORY COMMISSION

BIBLIOGRAPHIC DATA SHEET

(See instructions on the reverse)

1. REPORT NUMBER (Assigned by NRC, Add Vol., Supp., Rev., and Addendum Numbers, if any.)

NUREG/CR-6551
MCS 970501

2. TITLE AND SUBTITLE

Improved Embrittlement Correlations for Reactor Pressure Vessel Steels

3. DATE REPORT PUBLISHED

MONTH	YEAR
November	1998

4. FIN OR GRANT NUMBER

W6878

5. AUTHOR(S)

Ernest D. Eason, Joyce E. Wright, Modeling and Computing Services
G. Robert Odette, University of California

6. TYPE OF REPORT

Technical

7. PERIOD COVERED *(Inclusive Dates)*

8. PERFORMING ORGANIZATION - NAME AND ADDRESS *(If NRC, provide Division, Office or Region, U.S. Nuclear Regulatory Commission, and mailing address; if contractor, provide name and mailing address.)*

Modeling and Computing Services
6560 Gunpark Drive, Suite B
Boulder, CO 80301

University of California
Santa Barbara, CA 93106

9. SPONSORING ORGANIZATION - NAME AND ADDRESS *(If NRC, type "Same as above"; if contractor, provide NRC Division, Office or Region, U.S. Nuclear Regulatory Commission, and mailing address.)*

Division of Engineering Technology
Office of Nuclear Regulatory Research
U. S. Nuclear Regulatory Commission
Washington, D.C. 20555-0001

10. SUPPLEMENTARY NOTES

A. L. Lund, NRC Project Manager

11. ABSTRACT *(200 words or less)*

The reactor pressure vessels of commercial nuclear power plants are subject to embrittlement due to exposure to high energy neutrons from the core. The purpose of the reported work was to improve on the correlation models in the current Regulatory Guide 1.99 Revision 2 (RG1.99/2) using the broader data base now available. The embrittlement data base used for this analysis was derived primarily from the Power Reactor Embrittlement Data Base developed at Oak Ridge National Laboratory. Shifts in transition temperature and drops in upper shelf energy were calculated on a consistent basis from individual fits to unirradiated and irradiated raw Charpy data. The final transition temperature shift (TTS) and upper shelf energy (USE) models include fluence, copper, nickel, phosphorous content, and product form; the TTS model also includes coolant temperature and neutron flux. The models were developed using multivariable surface-fitting techniques, based on pattern recognition, understanding of the TTS mechanisms, and engineering judgement. The key variable trends, such as the copper-nickel dependence in the new TTS model, are much improved over RG1.99/2 and are well supported by independent data and current understanding of embrittlement mechanisms. The improved TTS model reduces scatter significantly relative to RG1.99/2 on the currently-available data base for plates, forgings, and welds.

12. KEY WORDS/DESCRIPTORS *(List words or phrases that will assist researchers in locating the report.)*

Reactor Pressure Vessel, Embrittlement, Charpy Upper Shelf Energy, Charpy Transition Temperature, Statistical and Physical Models, Pattern Recognition, Correlations, Transition Temperature Shift Model, Embrittlement Mechanisms

13. AVAILABILITY STATEMENT

unlimited

14. SECURITY CLASSIFICATION

(This Page) unclassified

(This Report) unclassified

15. NUMBER OF PAGES

16. PRICE

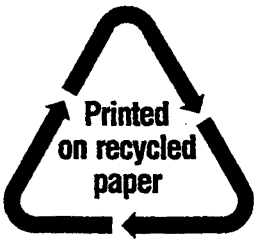

Federal Recycling Program